INTEGRATED IN-WHEEL MOTORS FOR LOW POWER TRACTION APPLICATIONS

PRAKASHRAJ KASINATHAN

Department of Electric Power Engineering

CHALMERS UNIVERSITY OF TECHNOLOGY

Gothenburg, Sweden,

2003

THESIS FOR THE DEGREE OF DOCTOR OF PHILOSOPHY

INTEGRATED IN-WHEEL MOTORS FOR LOW POWER TRACTION APPLICATIONS

PRAKASHRAJ KASINATHAN

Department of Electric Power Engineering

CHALMERS UNIVERSITY OF TECHNOLOGY

Gothenburg, Sweden

2003

INTEGRATED IN-WHEEL MOTORS FOR LOW POWER TRACTION APPLICATIONS

PRAKASHRAJ KASINATHAN
ISBN 91-7291-268-5

Technical report No. 445
School of Electrical Engineering
Electrical Machine and Drive Systems Group
Chalmers University of Technology
Ny serie nr 1950
ISSN 1651-498X

Department of Electric Power Engineering
Electrical Machines and Drive Systems Group
Chalmers University of Technology
SE-41296 Göteborg
Sweden

FRONT COVER: REPRODUCE COURTESY OF SUNRISE MEDICAL

Chalmers Bibliotek, Reproservice
Göteborg, Sweden 2003

1.1. ABSTRACT

This thesis is primarily concerned with the practical limits, imposed by magnetic saturation and thermal considerations, of the force density in low-speed permanent-magnet electric machines. The practical force density values obtainable in integral- and fractional-slot machines are determined. The achievable force density for machines utilizing slot per pole per phase of 0.375, 0.5, 0.75 and 1 are determined. The theoretical investigation covered a large range of machine sizes.

For saturation reasons, shallow slots are more favourable for achieving high force densities. However for thermal reasons deeper slots become favourable. An optimum slot depth that maximises the force density for each current density level therefore exists and is determined in this thesis for a range of machines. In particular, the maximum allowable slot depth range for four low-speed applications are identified for a given maximum motor diameter.

Plots of the force density against slot depth for various current densities for fixed pole pitches enabled a useful database to be established. These curves would enable one to determine if the demanding specification can be meet within a given restricted space. The slot depth required can be determined instantly for the practical allowable current density.

The results presented will help the design engineer to determine if the surface mounted permanent magnet machine configuration is suitable to fulfil one's specification. If the configuration is not suitable, then other topologies must be considered.

An experimental in-wheel motor, intended for wheelchair applications, was built and tested, and is shown to meet the design specifications. When assembled into the wheelchair the results were

promising and showed a remarkable increase in performance compared to the existing conventional geared drive.

1.2. KEYWORDS

- Traction motors
- Force density
- Direct-drive
- Low speed machines
- Flux-linkage
- Integral-slot
- Fractional-slot
- Electric wheelchairs/Power wheelchairs
- Electric golf cart
- Forklift trucks

Acknowledgements

The author is very grateful to the UK's Centre For Advanced Electronically Controlled Drives for financing his work while at Cardiff University and acknowledges the centre members for building the electric wheelchair prototype. The author is extremely grateful to the Rector of Chalmers, Professor Jan-Eric Sundgren for making available the necessary finance that enabled completion of the PhD work in Sweden.

The author is very grateful to his examiner and supervisor Professor Essam Hamdi for providing an enjoyable work environment and for invaluable help and guidance throughout his University study. The author wishes to applaud the abilities of Professor Hamdi as an academic and tutor.

The author wishes to express his heartfelt thanks to his supervisor at Chalmers, Dr Anders Grauers, with whom the collaboration throughout this thesis was extremely valuable.

The author wishes to thank his former colleague at Cardiff University, Dr John Dolan with whom views were exchanged on many topics. Thanks are also due to Paul Farrugia for assisting in many computing, software and other technical matters.

Finally, the author wishes to thank all his fellow PhD students at Chalmers. In particular, he wishes to give a special acknowledgement to his colleagues at the Machines and Drive Systems Group and regrets to inform them that his name will, hopefully, be removed from the Monday Lunch *rota soon.*

Table of Content

Chapter 1: Introduction

Chapter 2: Permanent Magnet Motors

Chapter 3: Force Density Limits In Integral Slot Machines

CHAPTER I

INTRODUCTION

1.3. BACKGROUND AND MOTIVATION

For traction applications, the short-term rating, which governs acceleration and hill-climbing ability, is possibly as important as the continuous rating. By virtue of its overload capacity, the electric motor is superior to the petrol engine in performance because the latter cannot utilise its full rated power at all times. For this reason, a 11kW electric motor is able to replace a 30 kW petrol engine, giving almost the same performance [1].

One of the main objectives of the development of traction motors is reduction of specific weight, which is somewhat high at about 6 to 9 kg/kW for continuous rating, improving to about half these values for peak rating. Traditionally, the dc motor has been widely used as the main propulsion motor for battery-powered road and industrial electric vehicles. While the series-wound type yield the ideal torque versus speeds characteristics for the majority of applications, the dc compound motor has found a niche in some industrial trucks where electric braking is required.

The main drawback of dc motors is of course their maintenance requirements. Consequently, constant efforts are being made to develop alternative type of drive systems with equally or almost as good characteristics, but without commutator or brushgear. Continuous development of semiconductor switching devices and power electronic converters has made it possible to meet the traction requirements for many applications by an induction motor drive system.

It should be noted that ac motors would give higher specific output than the dc motor. The possible weight-to-power ratios, including the gearbox, inverter and cooling arrangements, of a high-speed squirrel-cage induction motor (10,000 to 20,000 rev/min) could be about 2 kg/kW at continuous rating [1].

In recent years, attention has been focused on further reducing the maintenance requirements, especially in low-power traction applications. Removal of the gearbox is seen by a number of manufacturers of wheelchairs and forklift trucks as the next step in reducing maintenance requirements and increasing system reliability. This is of course no mean challenge. The motor would be either directly coupled to the wheel shaft or incorporated within the wheel itself. Either way, the motor speed would be much lower than that of a geared drive and this would require the designer to aim for much higher power-to-weight ratios than hitherto been required. In fact, the designer would be working on the edge of present technology; i.e. the system would need to be designed as close to the theoretical limits of achievable force density as is practically possible. To this end, the work presented here provides a database giving the maximum achievable force density for a range of current densities and pole-pitches. It enables the designer to readily establish

whether or not certain traction requirements can be met, at least theoretically, with present day technologies and materials.

In order to demonstrate the practical significance of research work, the force density limits are used to design integrated in-wheel drives for a number of low power traction applications. The work also includes experimental evaluation for one such drive intended for wheelchair applications.

1.4. BATTERY POWERED ELECTRIC VEHICLES

There are many types of totally battery powered electric vehicles currently available in the market. They can be divided into 3 broad categories: light electric vehicles, medium electric vehicle and heavy electric vehicles. Within each category there are sub categories consisting of many different models with their own advantage and disadvantages. Figure 1.1 lists some of the applications that fall into these sub categories. The electric drive technology based on the motorised wheels can be used in different types of vehicles (with one or two drive wheels, or with full drive). Although there are many suitable applications, in this thesis only the electric wheelchairs, golf carts and forklift trucks are considered.

At present a typical propulsion system for an electric wheelchair consists of a pair of brushed dc internally rotating permanent magnet motors; one for each drive wheel. The shunt and series motors have been the prime candidates for the forklift truck and golf carts as their torque and power characteristic meet the application requirements as the speed can be easily controlled with these motors. Each motor is coupled to the rear wheel through a reduction gearbox and a break unit.

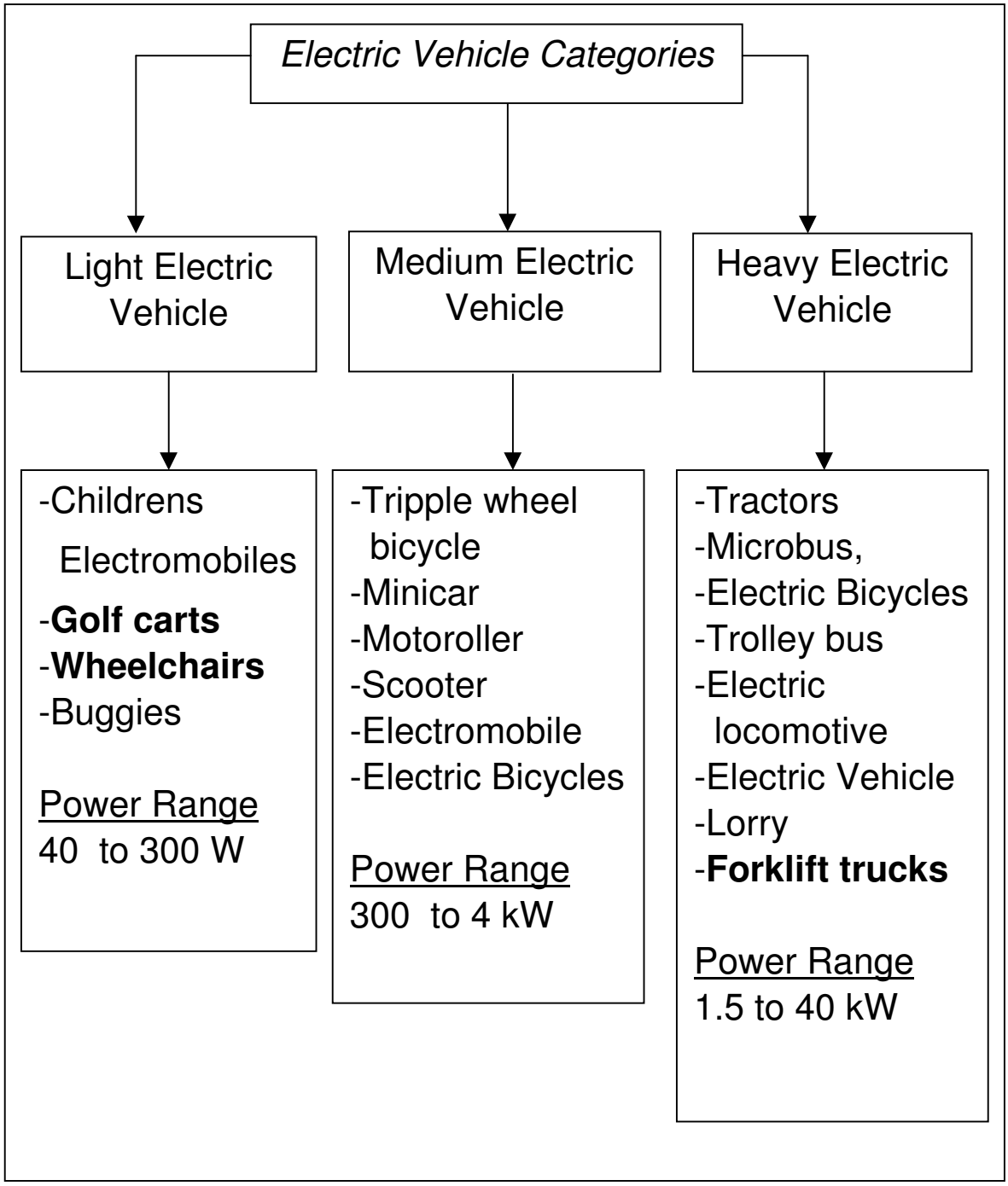

Figure 1.1: Classification of battery-powered electrical vehicles.

The gear train, apart from being a shock absorber when the drive wheels are stuck or under heavy load, serve to reduce the motor speed while proportionally increasing motor torque. This result in a significant reduction of required motor volume leading to a lower manufacturing cost.

However, useful as they are, the conventional dc electric motors used in the present propulsion system for these applications have a number of limitations. The available conventional dc motors operate with mechanical systems of gears and brushes. As a consequence, these mechanical systems are the weakest link of the electric vehicle and are too expensive to maintain. The chatter and swiping of gears and the friction associated with motor and idler bearings are potential sources of vibration and noise. As with any mechanical system, parts wear, break and need to be serviced. Brushes and gears wear due to friction and the grease used to overcome friction problems is prone to leaking and can lead to expensive clean up costs. The failure of these component results in the vehicle being returned to the manufacturer for regular inspection and replacement resulting in the users paying high maintenance costs. Hence many users operate their motor until failure and purchase a replacement motor unit in preference to being both inconvenienced and paying high maintenance costs.

In order to overcome these problems and replace the mechanical system of the conventional dc motor of these vehicles the system needs to have no gears, brushes or grease. Hence the system has to have no touching parts. The brushless motor technology would make it possible to achieve these requirements.

1.5. MOTOR RATING AND SYSTEM VOLTAGE

The nominal kilowatt rating for traction drive motors is usually related to a one-hour operating period plus an overload of 200% full-load torque for a period in the order of 5 minutes, with temperatures of the windings remaining within the limits prescribed in the relevant standards for the insulation system used.

High-voltage systems obviously require less current, for the same output, than low-voltage systems. This is advantageous as far as the controller is concerned. Also, as the system voltage is increased, electrical power loss throughout the entire circuit from the battery to the motor armature will be reduced. Clearly, one of the most important factors in designing battery-operated vehicles, in general, is the system efficiency, or more accurately losses. Typically, 1 kWh of lost energy requires the carriage of an additional lead-acid battery weight of some 25 to 30 kg. For example, it is expected that there would be a reduction in power losses of about 10 to 15% when a truck is changed from 24 to 36 V [1]

For a given motor peak power requirement there exists a range of possible voltages which would provide for a satisfactory battery pack. However, sensible values of maximum currents tend to limit this range to some extent. Also, safety considerations tend to limit maximum voltage especially in applications such as wheelchairs. Hence some sort of compromise has to be arrived at.

The nominal voltages most used in low power traction systems are 12, 24, 36, 48, 72 and 80. High voltages of several hundreds of volts are possible in road vehicles, such as buses and passenger cars. This is because such vehicles are serviced by skilled personnel who will be aware of the dangers associated with such systems.

Wheelchairs normally operate on 24 V systems while most golf carts and similar vehicles operate on 36 or 48 V. Within the sphere of industrial electric trucks the trend is towards high-voltage drive systems. Here, the term *high-voltage* applies to the high side of the available voltage spectrum for a particular truck type. Rider-operated forklift trucks normally operate on 48 or 72 V systems. It should be noted that some rider operated trucks and most pedestrian-operated trucks operate on lower voltages than 48 V.

1.6. REQUIREMENTS OF LOW POWER TRACTION

The proposed electric motor replacing the existing conventional dc motors currently used must be powerful enough to satisfy the traction requirements, but this is not the only criterion. The following lists some of the main requirements that must be fulfilled to enable the widespread use of proposed electric motors for all these applications.

1. The motor should be small and lightweight.
2. High economical efficiency.
3. Durable and easy to maintain.
4. Low noise.
5. Low cost.
6. Must be able to be used under various conditions and humidity.
7. Regenerative braking.

1.7. TRANSMISSION OPTIONS

The drive train is a mechanical system that transfers power from the motor to the drive-wheels. The conventional drive train is composed of gears, belts, chains and other mechanical elements that serve to reduce motor speed while proportionally increasing the motor

torque. Motor and drive train efficiency impacts battery performance and the overall performance of the system. Weather these vehicles are suitable for the appropriate tasks are determined by the characteristics of its motor, drive train, battery and power management system.

Figure 1.2 illustrates different possible ways that can be adopted to transfer power from the motor to the wheels. Some are easier and cheaper to build then the others. Each type presents advantages and disadvantages. Deciding which is the most appropriate configuration for traction purposes depends on the specific application requirements.

Belt drive configurations require specific belt tension and alignment to ensure smooth operation. If the belt tension is not set properly, this will cause slippage. Overtime, belts tend to stretch and will eventually slip around the pulley's circumference. The fatigue of belts and bearings can reduce tension, requiring re-tensioning. In order to avoid these, frequent checks must be made and this will become too cumbersome. On the other hand, extensive tension leads to bearing failure and inconsistent *gear* reduction. The effects will manifest itself in the drive system non-repeatability, low efficiency, shorter machine life and performance problems. Chain drives are similar to belt drives configuration. The following lists their advantages over belt drive.

1. Longer life.
2. No slippage between chain and sprocket due to the sprocket tooth.
3. Ability to operate in high temperatures, moisture, oil and dirt environments.
4. They only require a few sprocket teeth for effective engagement.

5. The tendency to stretch over time not possible due to the high tensile strength of the steel chain and sprocket.
6. They allow higher reduction ratios than belts, translating to higher output torque and increased load carrying capabilities.

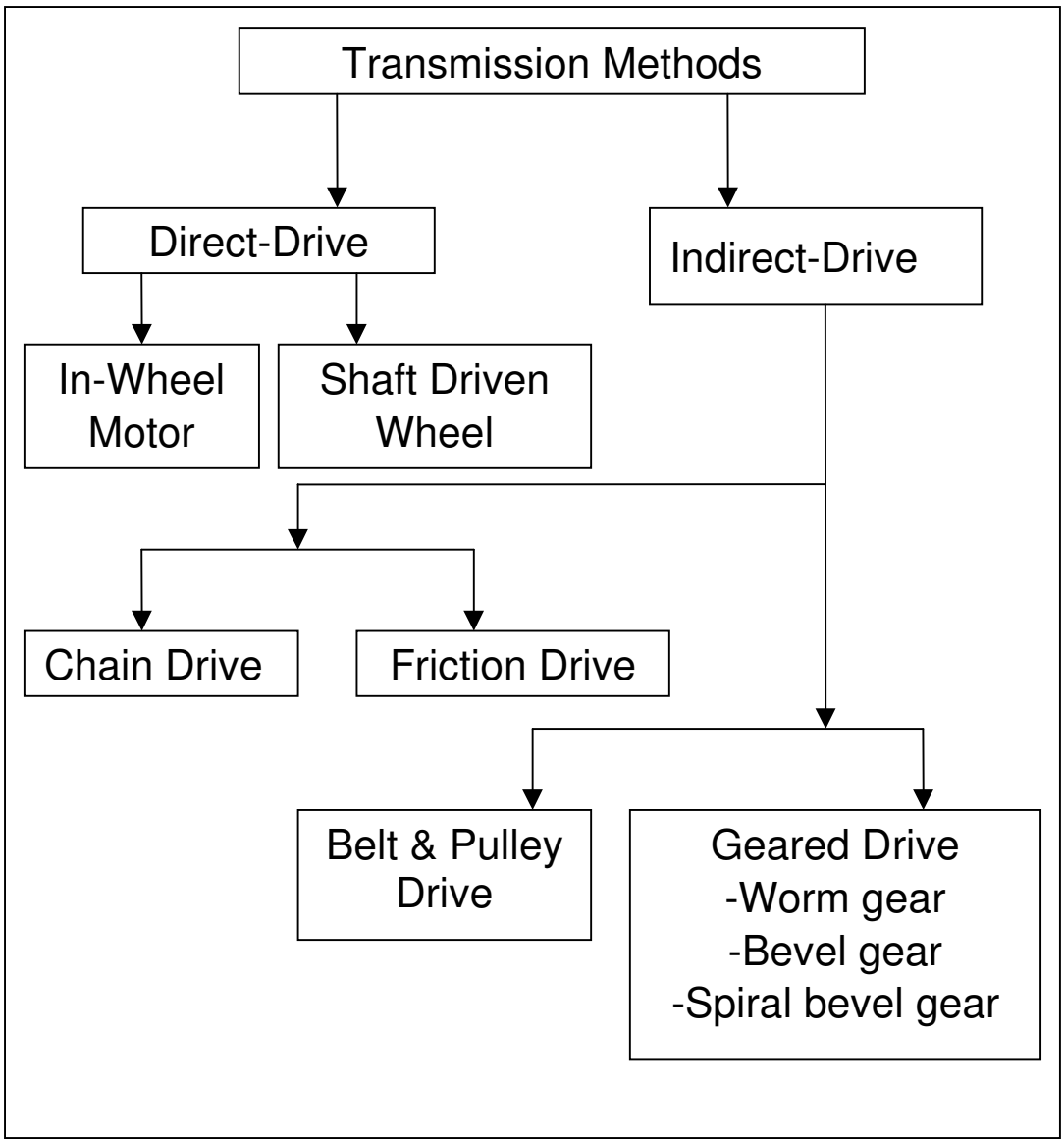

Figure 1.2: Power transfer options.

However apart from being limited to a single plane, chain drives operate at considerably much higher noise levels compared to belts or geared sets. Usually when the worn chains are replaced, the

sprocket also needs to be replaced. The belt sheaves usually exhibit very little wear and usually do not require replacement. Both chain and belt drives requires frequent oiling and are also hard to install. Thus the long term cost on both of these drives are high.

Friction drives are usually not used in any of the electric vehicle categories. Friction losses generate heat and a non-efficient and non-economical drive system will result. The most common type of transmission used in wheelchairs, golf carts and forklift trucks are the geared and direct-drive design with the earlier still dominating. However among the six mentioned the simplest type of transmission is the direct-drive design. The last few years have seen many developments in direct-drive technology. Although direct-drive are not suitable for every application, their attractive inherent properties have made them a prime candidate for traction purposes. An increasing need exist for such drives in many industrial processes as the elimination of transmission mechanisms have proven to improve raggedness, efficiency and control precision. Overall, all mentioned advantage listed in the next section together with the simple construction of the motor-wheel make the drive exceptionally profitable and competitive industrial product in relation to manufacturing expenses and unit costs.

1.8. ASSESSMENT OF BRUSHLESS DIRECT-DRIVE DESIGN

The advantages offered by a direct-drive employing a brushless system over the conventional geared drive design are summarised as follows:

1. With direct-drive the motor is connected directly to the axle of the driven wheel resulting in both motor and wheel speed being equal.

2. There is no mechanical power transfer by friction wheels or belts. Thus mechanical wear and tear is eliminated. Since the wheel is rigidly coupled to the motor there are no transmission errors such as backlash, belt stretch and gear tooth error. Since there is no mechanical friction, less power is consumed. Thus a high economical efficiency is achieved due to the low power consumption. There will not be error in the speed feedback system due to gear slippage. Internal stresses between bearings are also eliminated.

3. With fewer moving parts, they offer reduced audible noise. Zero maintenance is required, as the bearings are the only wearing component.

4. The relatively high friction, high compliance transmission components that commonly cause stick-slip in traditionally mechanical transmissions are eliminated in direct-drive systems.

5. Since the coupling between the load and motor is stiff, problems associated with mechanical resonance are eliminated. In direct drive systems the load inertia can be many times greater than the motor inertia without degrading the system performance.

5. The usage of the motorised wheel, apart from enabling the complete elimination of the transmission components, reduces the current during the start and acceleration.

6. The controller becomes much simplified in direct-drive systems as the movement regime does not need optimisation.

Of course, as with most engineering problems, the advantages offered by direct-drive systems are offset by certain disadvantages. These are summarised in the following:

1. Since direct-drive systems have no transmission components, they must provide more torque at a lower speed compared to the geared version. This will require more expensive magnetic material with higher number of poles and coils which makes it larger in diameter.

2. They are usually much expensive than traditional transmission systems especially in applications requiring high torque. The cost penalty has to be weighed against improvement in overall system performance in deciding the viability of direct-drives for a given application.

1.9. SCOPE OF THIS THESIS

The thesis deals with the design of brushless dc geared and direct-drive design for electric wheelchairs, electric golf carts and forklift trucks. Various slot and pole combinations are investigated and a number of designs fulfilling industrial specification are provided. The thesis presents a design and an experimental evaluation of a direct-drive in-wheel motor for a wheelchair application. The comparison between fractional and integral slot design are made and the suitability of a fractional-slot machines for these applications is evaluated.

The thesis is organised into six chapters. Following this introduction, chapter 2 reviews and critically assesses different machines topologies which may be suitable for traction applications. Upon considering the forklift truck requirements, it became obvious that such an application requires extremely high force density. To enable the designer to establish if the traction requirements can be met within available space envelope, the force density achieved for various machine designs are determined. The effect that magnetic saturation has on the achievable force density is investigated. Various current densities are assumed and the slot depths above which any increase in slot current does not yield an increase in force density, due to saturation, is determined for various pole-pitches. The investigation includes both integral-slot and fractional-slot designs. Both surface and inset magnet rotor configurations are considered. In the fractional-slot design slot per pole per phase of 0.375, 0.5 and 0.75 are considered. In the inset rotor configuration, the computation included pole arcs of 120, 150 and 170 electrical degrees. This work is presented in Chapters 3 and 4 for the integral-slot and fractional slot designs, respectively.

Chapter 5 deals with direct-drive design for electric wheelchairs, golf carts and forklift trucks. Various design having different slot and pole combinations that meet the performance requirements are presented and an experimental wheelchair drive is developed and evaluated.

The conclusions of the present work and recommendation of further investigations are given in Chapter 6.

CHAPTER II

PERMANENT MAGNET MOTORS

1.10. INTRODUCTION

One area in which important technical advances have been made in recent years is that of magnetism. The properties of magnetic materials have been profoundly improved and permanent magnets have become a vital part of present day life.

Unlike soft magnetic materials, magnets are able to hold their *magnetic charge* after being removed from the magnetizing device. This feature, have made permanent magnets very attractive for a large number of applications [6-10]. These applications can be classified as follows:

1. Electro-mechanical energy conversion: in these applications electrical energy at the input causes relative movement of the magnets resulting in the desired mechanical output. Alternatively, the relative movement of the magnets, with respect to an electric circuit, produces an electrical output.
2. Magnets can be used to lift and hold magnetic objects, and/or apply a repulsive force.

3. Magnetic field can be used to control, shape or direct an object or substance.

By replacing the electromagnets with permanent magnets, to produce the air-gap flux for example, significant performance improvements and benefits, such as higher efficiency and power density, lower electromechanical time constant, less assembling problems, improved heat dissipation and increased reliability of overall drive system can be achieved in the Power Electric Wheelchair and other demanding industries [11-12]. Figure 2.1 broadly lists the three major groups of permanent magnet materials used in electric motors that are commercially available.

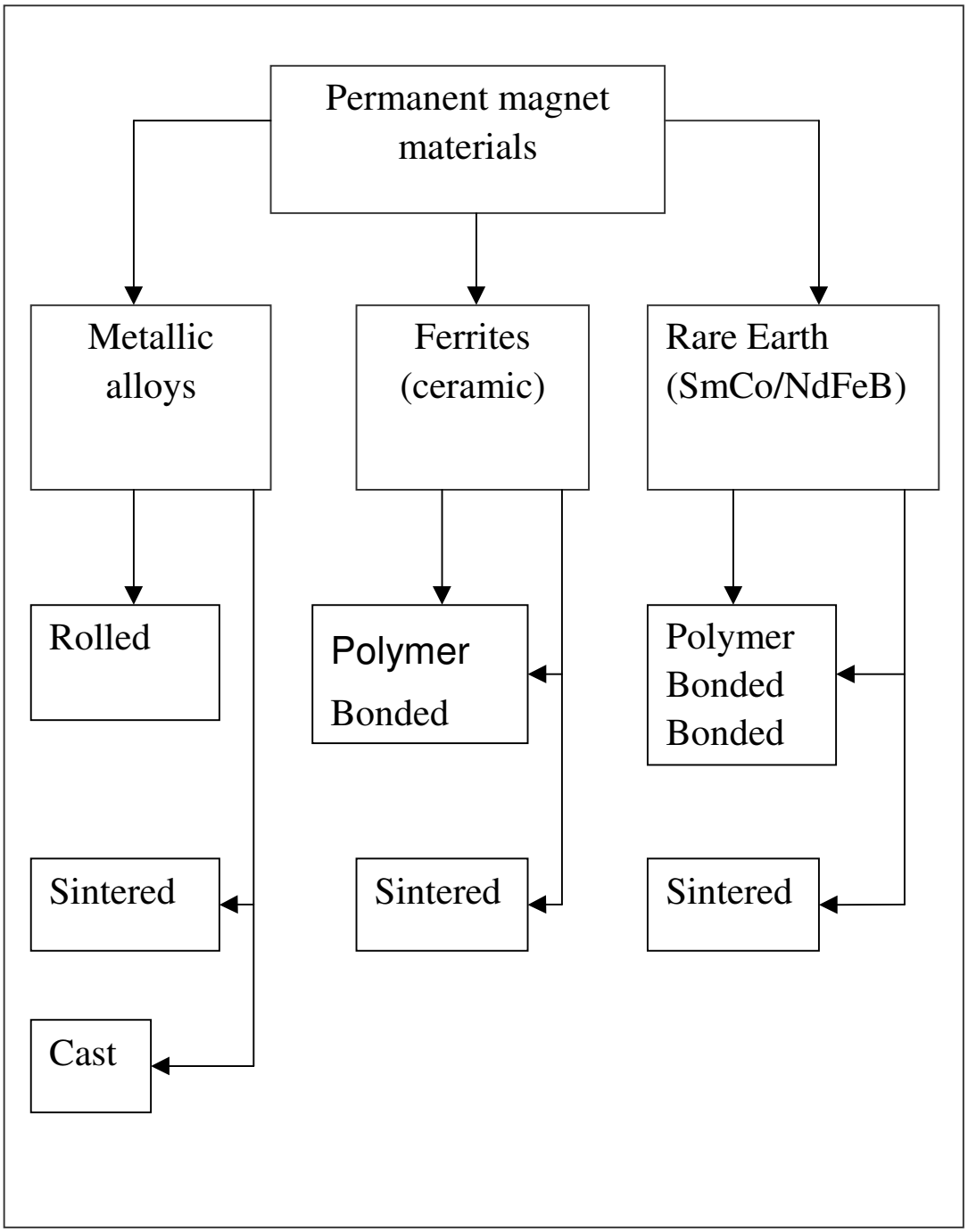

Figure 2.1: Permanent magnet materials used in electric motors.

The well-known Ferrite, and Alnico magnets, have been used widely in rotating machines for the past 60 years while the advent of rare-earth magnets have made many existing motor design constraints relaxed. Each family of materials have several grades with range of magnetic properties. Either type of magnets may be preferred dependent upon the design or performance criteria being applied. The choice of the material is affected by the maximum operating temperature, size and weight, and most important the required magnetic energy to produce the short-term torque. Thus before evaluating any materials for its suitability for a particular design some basic design equations and criteria are reviewed.

1.11. PERMANENT MAGNETS [1,2,38,39]

Although essentially a bulk material property, magnetism is often explained using a model of the atomic structure of matter. In the classical atomic model, spinning negatively charged electrons revolve around a positively charged nucleus. The motion of these electrons can be regarded as a current loop which gives rise to a magnetic dipole, in the same way as a current flowing through a conductor produces a magnetic field.

In a non-magnetic material, these magnetic dipoles are randomly oriented, and produce no net magnetic moment in the bulk material. In a magnetic material, however, the dipoles align themselves locally, in regions called *domains*. These domains are usually aligned randomly throughout the material and so produce no net magnetic moment. In the presence of an external magnetic field, domains already aligned with the field grow at the expense of non-aligned domains. The bulk material then has a net magnetic moment and is said to be *polarised* in the field direction. As field strength

increases, the aligned domains expand until, finally, no non-aligned domains remain. The material is then said to be *saturated*.

The ease with which a magnetic material can be polarised (or, as an engineer would say, magnetised) depends upon its microstructure. Likewise, this affects its behaviour when the magnetising field is removed; the domains then resist returning to the previous disorganised state and a residual polarisation (magnetisation) remains known as the *remanence*. To reduce the polarisation to zero, a field in the reverse direction must be applied; the magnitude of this field is known as the *coercivity* of the material. This is an important property of a magnetic material, as its value indicates the material's magnetic *hardness*. Soft magnetic materials, used, for example, in transformers and motor cores, have coercivities of only a few Ampere per meter. Permanent magnets are produced from hard magnetic material, which is the general term for materials with coercivities exceeding 1 kA/m. This is the lower limit for hard magnetic materials; in general, the coercivities of such materials considerably higher.

The most appropriate single parameter for characterising the quality of a magnet is the maximum energy product $(BH)_{max}$ of its induction and magnetic field; as it represents the maximum energy available from the magnet. The size of the permanent magnet is at a minimum when the magnet is operating at its maximum energy product point, $(BH)_{max}$.

Normally, a magnet is an integral part of the device. Therefore mechanical as well as electrical properties have to be considered. Moreover, each application has its own special requirements, so a range of materials must be available if the users are to find one that

fully satisfies their needs. These are reviewed in the following sections.

2.2.1. Alnico magnets

Alnico magnets became available from the late 1930s. They have been employed in electrical machines, and the high remanence types offered, prior to the introduction of rare-earth magnets, the greatest flux. However, their demagnetisation characteristic is non-linear and the coercivity value is very low. Thus to prevent demagnetisation, a large magnet thickness will be required when operating at high current levels. Furthermore, the knee point occurs slightly below the remanence point and somewhat above the maximum energy product point, as is illustrated in Figure 2.2.

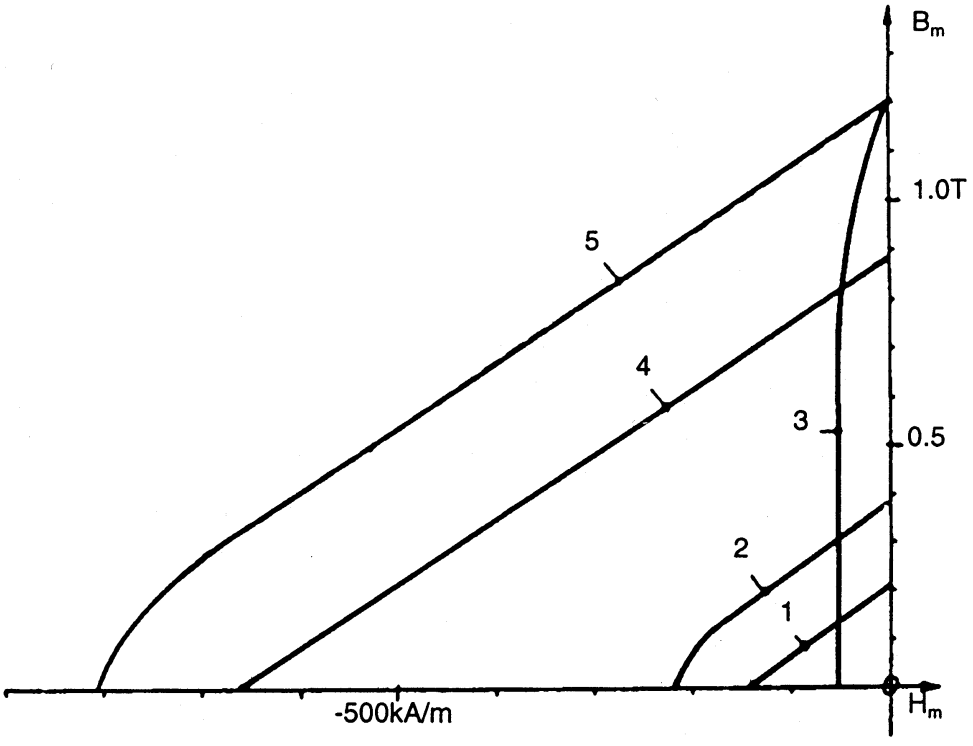

Figure 2.2: Demagnetisation charateristics of (1) isotropic Ferrite, (2) anisotropic Ferrite, (3) Alnico, (4) SmCo and (5) NdFeB magnets.

With only small additional demagnetising field due to armature reaction, the operating point may be forced well down the steep part of the characteristic, and upon removal of that field will recoil within that curve resulting in considerable loss of magnet energy. At peak rated load of the motor, the lowest operating point should be always on the right hand side of the knee in the demagnetisation curve, otherwise the magnet would be fully demagnetised. Thus Alnico magnets are seldom used in motors where the magnets are placed adjacent to the air-gap, as such a location would make them exposed to the armature demagnetising field.

Although Alnico magnets have the lowest resistance to demagnetisation, they have the best resistance to temperature effects of all the magnetic materials available at present. They can be used in environments ranging up to 550°C and hence ideal in applications where stability is needed across wide temperature ranges. Very often Alnico magnets will be magnetised in the assembled motor. If magnetised outside the motor, the load line may be so low that the magnet is even partially demagnetised before assembling. Thus in most cases Alnico motors should not be disassembled. This assembling method results in increased cost of production and the overall end product.

2.2.2. Ferrite magnets

Ferrite magnets, commonly known in the American continent as ceramic magnets, were developed and became commercially available in the mid 1940s. Ceramic magnets led to the development of commercial and industrial PM battery operated motors. Despite its unattractive low remanence feature compared to Alnicos, they managed to dominate the motor market place due to their relatively low cost, making Ferrite motors viable for mass production and they

became widely used in the automotive industry. Unlike Alnico magnets, Ferrites have approximately a linear demagnetisation characteristic and a relatively high coercivity. Thus they can be magnetised prior to assembly and used in motors where the magnet is placed adjacent to the air-gap with no loss of magnet energy. However the flux density derived from Ferrite magnets are quite low. Hence they are frequently designed to operate well above the $(BH)_{max}$ point, closer to the remanence flux density, to get more flux at the expense of additional magnet length. Ferrite magnets are best suited for environments under 250°C. As the temperature coefficient of intrinsic coercivity is positive, there is a risk of permanent demagnetisation in magnet systems with low working points.

2.2.3. Rare-earth magnets

Samarium Cobalt (SmCo) was developed and became commercially available during the late 1960s. SmCo magnets have a much larger energy product than both Alnicos and Ferrites, and they are also thermally very stable. Among the high-energy materials, SmCo offers the best resistance to temperature effects and several grades are suitable for applications up to 350°C. SmCo magnets created a great impact on the design of PM electrical motors due to their high energy density feature. However, as they cost considerably more than Ferrites, SmCo magnets could not penetrate the market of mass-produced low-cost electrical motors. In spite of their superior properties, they only find use in applications requiring precise performance over extended temperature ranges such as in aerospace applications, thus making Ferrite magnets the ideal choice for the majority of motor applications. Apart from being extremely expensive they are also brittle, which makes handling and construction more difficult.

Neodymiun-Iron-Boron magnets (NdFeB) with a higher energy density than SmCo became commercially available in the mid 1980s. These rare-earth magnets are available in the sintered and bonded form. The characteristic illustrated in Figure 2.2 represents represents the sintered NdFeB magnets. NdFeB have a virtually linear demagnetisation curve and yields the high flux levels required for high performance applications. This group of magnetic materials provide the highest available magnetic energies of any material, ranging from 26 to 48 MGOe. Because of their high cost, but cheaper than SmCo, they should be designed to operate near to the $(BH)_{max}$ point to minimise the magnet volume. Also with its high magnetising force, it will need only a very short length compared to that required by other currently available magnets. Although Sintered NdFeB magnets produce the highest magnetic properties, they are brittle and sensitive to heat. These magnets are liable to suffer from both reversible and irreversible losses at high temperatures compared to SmCo. Due to this high temperature dependence coercive field strength feature, electrical motors made from NdFeB magnets should not be used in high operating temperature environments (e.g. applications that exceeds 200°C) especially when safety and reliability are of paramount importance. Also for motors for the application considered here the temperature dependency of NdFeB might cause variations in the remenance thus causing variations in flux and in the torque.

Unlike Ferrites, Alnico and SmCo magnets, NdFeB, due to their high content of iron, are particularly susceptible to corrosion. Thus a layer of coating usually is used. There are a variety of coatings suitable for these magnets, ranging from Nickel and Tin platting to Teflon and epoxy coatings. The choice will depend on the application and environment. In some high-speed applications,

motor manufacturers house the magnets in an external casing, to protect the magnets from corrosion and damage.

The major reason for choosing NdFeB magnets is due to their high flux density and lower cost in comparison to SmCo.

1.12. MOTOR TOPOLOGIES

Selection of the driving motor depends on the conditions under which it has to operate and the type of load it has to handle. Guiding factors for such a selection can be classified into four main categories as follows:

- *Electrical Considerations*: starting and running characteristics, speed control and braking requirements.
- *Mechanical Considerations*: type of enclosure, bearings, cooling, noise level and method of transmission.
- *Size and Ratings*: requirement for continuous, intermittent or variable load cycle and overload capacity.
- *Cost*: capital and running costs.

The mechanical output of the selected motor has to be matched with the load requirement. In practice the complete selection process requires the analysis and synthesis of not only the load and the proposed motor but also the complete drive assembly and the control equipment which would include rectification or frequency changing. For example, if a standard controller is available, the system designer would need to consider only the traction motor and its suitability for the application and how would it match the available controller.

There is a number of drive system topologies that can be considered for low power electric vehicles (LPEV) application, as illustrated in Fig. 2.3. These will now be reviewed.

2.3.1. Conventional dc motors

The conventional dc motor has a stationary magnetic field (stator) and a rotating armature (rotor). The power delivered depends on the air-gap diameter and effective axial length.

As the armature rotates, the brushes switch the currents in the phase coils undergoing commutation so that the total pattern in space, of rotor slot currents, remains stationary. This continuous switching process gives the conventional dc motor the following properties:

1. All, phase coils, other than those being switched, continuously carry full current and are therefore fully utilised.
2. The resultant square spatial waveform, of slot currents around the armature periphery, is optimum for interaction with the square field flux waveform, and these two waves are always held in the correct relative relationship so that overall the greatest possible torque per watt of I^2R loss is achieved.
3. Full four-quadrant operation occurs without any special provision, as operating conditions are varied.
4. Torque ripple with shaft rotation is low and the same form of variation of torque with speed is obtained for all set no-load speeds.
5. All the above requires no special control signals, to initiate switching at the right instant or vary switching strategy with the operating regime.

From the above, it is no surprise that commutator-type dc motors were identified decades ago as ideal for traction applications. The main disadvantage of this type of motor is of course the maintenance requirements due to the commutator and brush gear.

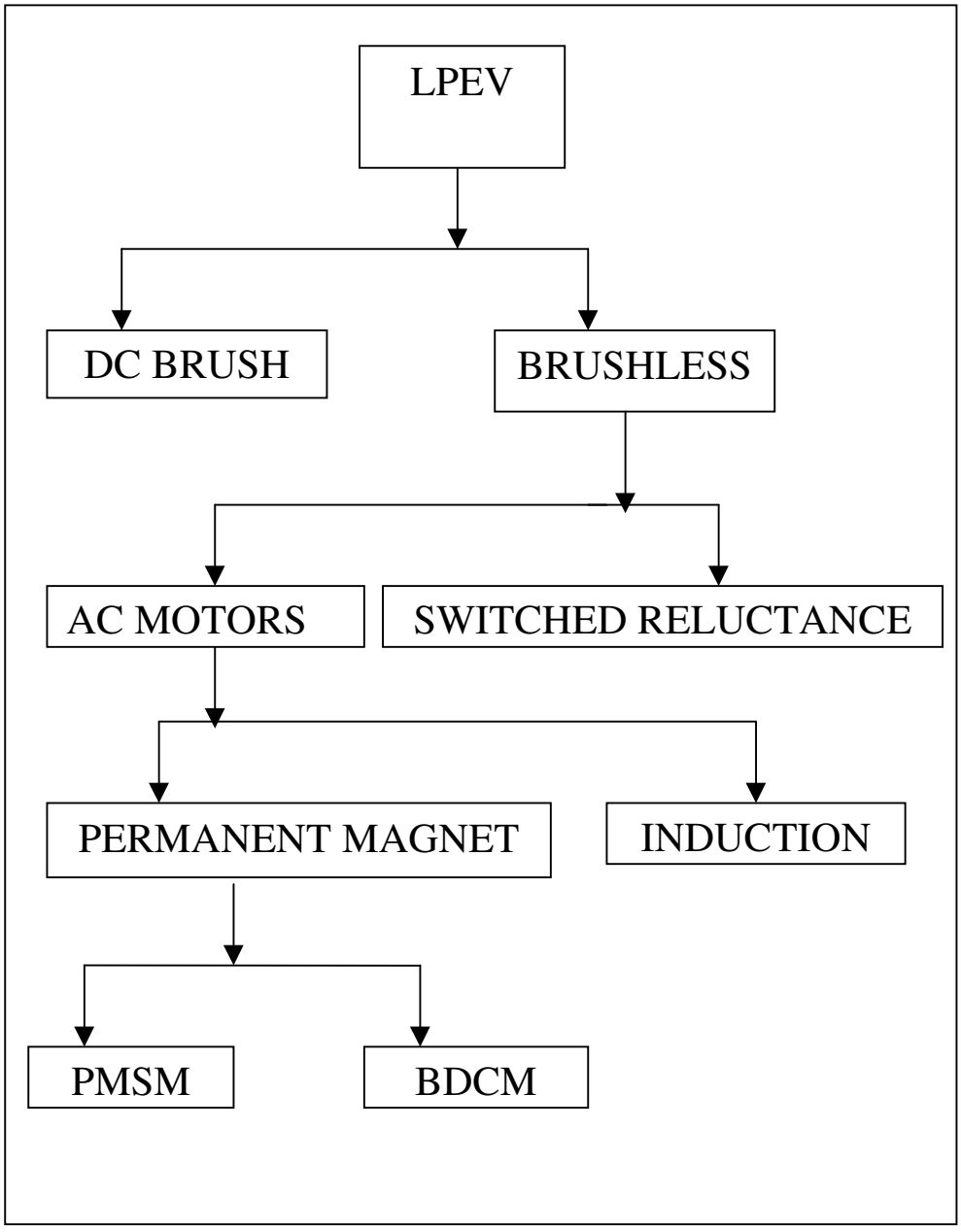

Figure 2.3: Possible drive systems for LPEV.

2.3.2. Switch-reluctance drives [1]

Any motor with a rotating stator field may be operated as a synchronous motor of a variable-reluctance type if the rotor is suitably designed and some other means of starting the motor is provided. The motor construction must result in variation of reluctance with the rotor angle, such that salient poles are created, that is, regions of differing reluctance separated by 90 electrical degrees.

The centres of the low and high reluctance regions are referred to as the *d* (direct) and *q* axis (quadrature), respectively. Under steady-state operation, this will produce an angular displacement between the stator *mmf* and the *d* axis. Such a condition is illustrated in Fig. 2.4. The result is reluctance torque. This torque has a nonzero average value only at synchronous speed. Therefore, a reluctance motor must develop starting torque by some other means.

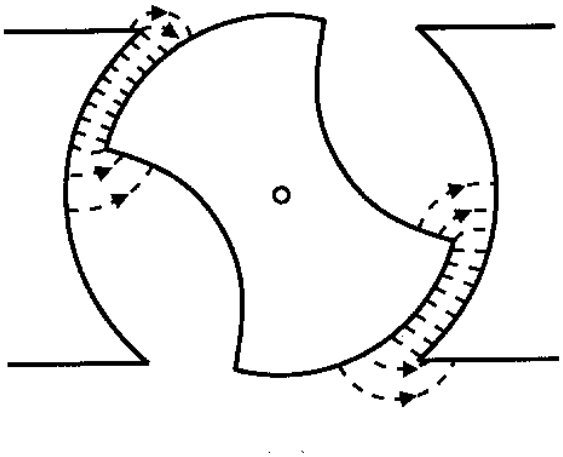

Figure 2.4: The principle of SR motors [1].

Reluctance torque is in fact present in many ac machines. For example, a salient-pole synchronous machine may develop significant reluctance torque. At light loads, it will be sufficient to

maintain synchronism, even with zero field excitation and negligible residual magnetism.

A reluctance motor can therefore be defined as an electric motor in which torque is produced by the tendency of the rotor to move to a position where the inductance of the excited winding is maximum. The winding can consist of a number of electrically separate circuits or can be of the conventional polyphase type. This definition encompasses both the *switched reluctance* motor (SRM) and the *synchronous reluctance* motor (SynRM).

The switched reluctance motor has a wide speed range with good low speed torque. It is inherently a pulsating torque machine. Thus it exhibits high torque ripples at low speeds. It is mainly suitable for high-speed applications. This drive topology is judged as being unsuitable for direct-drive applications since smooth torque over the operating range is required. Furthermore, efficient design of SR motors stipulates a very small air-gap (e.g. 0.2 mm). Apart from the obvious intricate mechanical structure, such a small value of air-gap may be difficult to maintain during operation in certain traction applications.

Of course, as current switching is done electronically, SR drives belong to the brushless drive system family. They are treated separately here as the torque production mechanism is different from the other types discussed below.

2.3.3. Brushless drive systems

This represents a family of drive topologies having the advantages traditionally associated with conventional dc motors but in which the process of commutation (or current switching) is done by

electronic means. Although no form of electronic commutation can fully match the list of virtues outlined above of the conventional brushed dc motor, other significant compensating advantages are offered, as follows:

1. The need for periodic mechanical maintenance and overhaul due to sliding contact is removed with the elimination of brushes and commutator. This gives improved reliability and enhanced life.
2. The arching problem with mechanical commutation limits machine size. Electronic commutation remains possible at the largest size.
3. Centrifugal force limits rated shaft speed with mechanical commutator. Electronic commutation is not restricted in this way. Hence brushless dc motors can be designed for high-speed operation.
4. Brushless motors of the permanent magnet type are inverted. The wound armature becomes the stator. This Inverted structure offers some useful thermal advantages. The stator allows large slot areas, giving lower copper loss, and all the heat is generated in the stator, from where it is more easily dissipated. Magnet heating is reduced, brushgear heating eliminated, and stator winding temperature monitoring made easier.
5. The rotor tends to be lighter and torque/inertia ratio higher.
6. Electromagnetic interference, associated with mechanical commutation, is eliminated, and acoustic noise is reduced.

There are three distinct types of motors whose application, design and performance characteristics are completely different which fall into the brushless motor family. The three types are [13]:

- The ac motor/inverter- consists of an induction or synchronous motor with an inverter to eliminate brushes in a dc system.

This technique is useful in systems requiring good speed regulation when input voltage and shaft load varies.

- Limited rotation- by proper design this motor will provide a constant output torque over a relative large angle of rotor position.
- The electronically commutated motor- It is an ac synchronous motor with permanent magnets on the rotor that create the rotor flux and windings in the stator that are energised to create magnetic poles. The rotor is attracted by the energised stator phase, generating a rotation. By using appropriate sequence to supply the stator phase, a rotating field on the stator is created and maintained. This action of the rotor chasing after the electromagnet poles on the stator is the fundamental action used in synchronous permanent magnet motors. The lead between the rotor and the rotating field must be controlled to produce torque. This synchronization is achieved by mounting rotor position sensors on the rotating shaft.

Figure 2.5 shows the schematic of a typical brushless dc motor drive system. The three essential elements that influence the overall system performance are: the motor itself, current control system and the power electronic drive circuit incorporating solid-state switching circuitry. Three phase motors are the most common since they offer a good compromise between control and the number of power electronic devices required to control the stator currents.

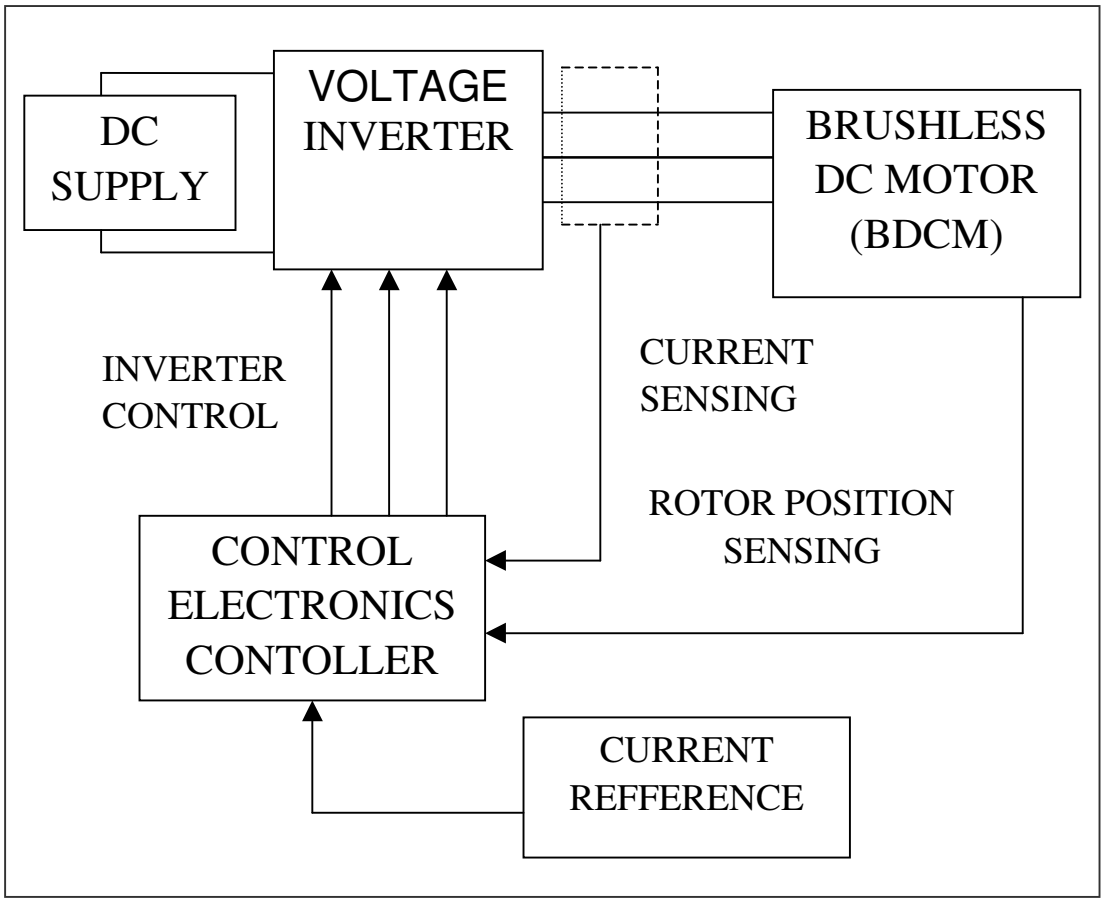

Figure 2.5: Schematic of a typical brushless dc drive system.

Brushless dc and permanent magnet synchronous motors

There are two types of permanent-magnet ac motor drives available. These are the permanent-magnet synchronous motor (PMSM) and the brushless dc motor (BLDC). PMSM is a replica of the wound rotor synchronous motor while BLDC is an inside-out version of the brushed PM dc motor. The PMSM has a sinusoidal back *emf* and requires sinusoidal currents to produce smooth torque while the BLDC has a trapezoidal back *emf* waveform and requires rectangular shaped currents to produce smooth torque. As the speed range of a drive is determined by the peak current ratings, maximum voltage available, motor parameters and the back *emf* waveform,

these two drive systems have somewhat different operating characteristic. The sinusoidal back *emf* waveform and currents makes PMSM more suitable for high-speed application.

There are much similarities in the overall drive scheme of the PMSM and the BDCM, however the sinusoidal and rectangular excitation requirement for producing smooth torque results in both having different control algorithms and circuitry. Both drives require position feedback devices to convert the stator current to phase current references however require different rotor position information. The same motor designed for as a BLDC can be used as a PMSM one, by using an appropriate controller and feedback device.

Due to the sinusoidal current and flux density requirement of the PMSM, the magnets need to be appropriately shaped and the stator is wound to reduce the harmonic content. The PMSM would require a more expensive absolute encoder while only three, less expensive, sensors are required in the BLDC for rotor position information. Since only two phases conduct at any one time in the BLDC, compared to three in the PMSM, the output of the BLDC is approximately 2/3 that of the PMSM.

Rotor magnet configurations

There are many ways of mounting the magnets to the rotor. The three most common ways widely adopted are shown in Figure 2.6. Depending on the configuration adopted, different properties of the motor are obtained.

With projecting magnet designs, the magnets are glued to a cylindrical rotor iron. The low permeability of modern high-energy

magnets makes the effective air-gap length equal to that of the magnet radial thickness. Since air-gap reluctance variation

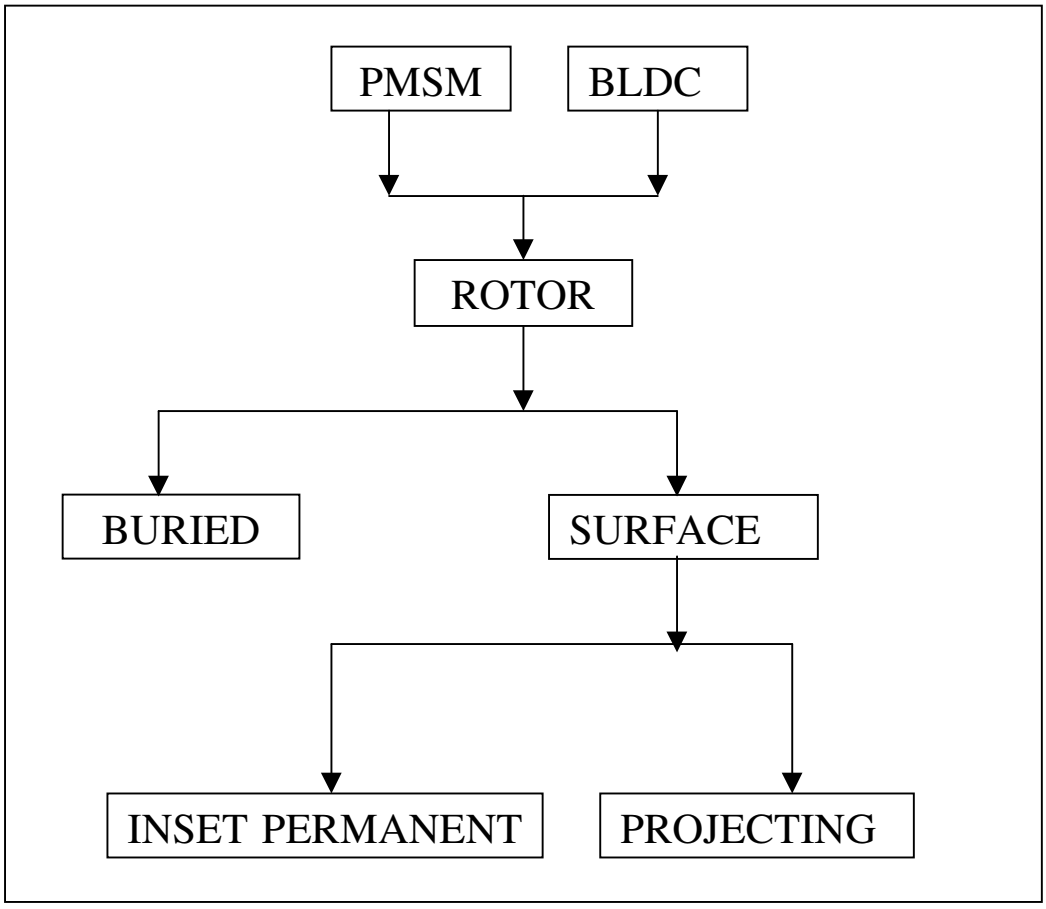

Figure 2.6: Permanent magnet rotor configurations.

with rotor position is small, the stator inductance is low as well as being independent of rotor position. Thus the *q* and *d* axis inductance are approximately equal resulting in negligible reluctance torque. Thus, total motor torque is produced via interaction between the rotor permanent magnet assembly and stator excitation field. This makes the control of the machine much easier.

With buried magnet designs, the magnets are inserted into punched slots in the laminated rotor iron. This protects the magnets from physical damage and high demagnetising currents. Flux

concentration is possible since the magnets can be placed close to the circumference, or in the V-shape slots. Thus low energy magnets can be used and still obtain a high flux density in the air-gap, this is not common though in modern drives. Since the magnets are placed into V-shaped slots the magnets are separated from each other by steel of high permeability. The space occupied by the magnet in the *d*-axis would be occupied by steel in the *q*-axis. This not only makes the effective length of the air-gap to be non-uniform, it also results in large variation in reluctance around the rotor periphery. Hence the *q*-axis inductance can be much larger than the *d*-axis inductance. The difference in L_d and L_q results in the total motor torque of the machine being the sum of the electric torque and the reluctance torque component, which is an added advantage. The greater the difference in the inductance the greater the motor torque will be.

With inset magnet design, the magnets are placed in radial slots or grooves cut at the rotor surface. This of course causes the stator inductance to be position dependent. There is a reduced tendency for armature reaction to demagnetise the magnets at large torque angles compared to the projecting magnet design rotor. Unlike surface mounted magnets, with inset magnets operation above base speed is possible. Therefore, this configuration is widely utilised in application where operation above base speed is frequent. Since the magnets are separated from each other by steel, as is the case of the buried magnet design, the L_d and L_q are not equal. However the reluctance torque component in inset magnet design is smaller than that of buried magnet designs.

The mechanical strength of the projecting machines depends on the strength of the epoxy glue used. This limits the maximum operating speed in both inset and surface magnet designs. Buried magnet

machines are more robust and tend to be used for high-speed applications. The additional reluctance torque component in the buried and inset magnet rotor could result in a machine of higher torque per unit volume. Among the rotor configuration discussed above, it is evident that buried magnet machines produce the highest output torque per unit current. However buried and inset magnet machines are difficult to build and would increase the overall manufacturing cost significantly.

2.3.4. Other types of pm motors

In addition to motors/drive systems described above, there are a number of permanent magnet motors that, although are not seen as obvious candidates for the present drive requirements, are reviewed below for completeness.

Printed Motor (Flat Armature Pancake Motor)

The first dc printed circuit motor was invented in 1958 and it has a single rotor sandwiched between two stators [15,16]. The armature is of a disc shape and the stator field is provided by permanent magnets. The pancake-shaped armature is typically a few millimetres thick, with radial-lying conductors. It contains no soft magnetic material, and the wire-wound armature winding and commutator are encapsulated in a thermosetting resin or plastic. The armature windings are sometimes produced by stamping conductors from a copper sheet, welding them together and placing them on a disc, and then joining them to a commutator at the centre of the disc [17,18]. The power developed, unlike the conventional dc motor, is independent of the axial core length, which is determined by the size of the armature winding and is only dependent on the outside and inner diameter. The ratio of these diameters is one of the most important parameters in the design of this type of machine.

Advantages:

- Motor is shorter and lighter but slightly larger in diameter resulting in a greater power-to-weight and diameter-to-length ratio.
- Elimination of heavy iron not only results in no waste of armature core material associated with formation of the slots but also reduces the rotor inertia and hence mechanical time constant. This enables achieving a very fast response. Since the armature is a coil of comparatively few turns with relatively poor inductive coupling, the absence of significant inductance contributes to a short electrical time constant. This allows the motor to develop torque more rapidly. The large number of commutation periods (high commutation frequency) combined with the low armature resistance and inductance (typically 0.5Ω and 50 μH) gives low electrical noise generation, enhanced reliability due to long brush life and good commutation up to very high speeds.
- The output torque is directly proportional to armature current. With no magnetic material present, core losses that occur in conventional machines are therefore eliminated resulting in a high efficiency motor. The virtual absence of armature reaction results in a motor with good speed regulation [18]. Also the maximum torque achieved (and hence, the maximum pulse current) for a particular design is only limited by the instantaneous power dissipating capability of the conductive elements. By passing forced air over the armature the allowable power dissipation capability may be increased.
- The absence of iron also eliminates cogging torque and with large number of conductors on the armature surface, providing a smooth path for the brushes, ripple torque disturbances

generated by the motor are minimised ensuring smoothness during low speed operation.

- Since there is minimal inductance to cause arching at high speeds and no cogging present to limit the low speed performance, the motor may be used over an effective speed range of practically 0 to several thousand rev/min. The construction results in a substantial saving of copper achieved by the elimination of the excitation windings and conventional commutator.

Apart from the single rotor and two stators configuration described in reference [15] single stator single rotor, single stator sandwiched between two rotors, and variety of multiple rotors/stators configuration also exist. The single rotor and stator configurations are rarely adopted as the stator and rotor experience strong magnetic pulls.

Application of this type of motors includes video recorders, paper feed mechanisms for line printers, disc file magnetic head actuator, programmable stepping servos for precision assembly processes, machine tools applications and automotive-window winder.

Hollow rotor motor ***[19-21]***

In this type of motors, the armature-coil wire is wound to form cylindrical shell, which is then reinforced with glass yarn, coated with epoxy resin and cured. The hollow, or basket, rotor rotates about a stationary iron core.

The resulting design causes the motor armature inertia to be 10 times lower than disc designs and 100 times lower than iron-core designs. This gives the motor an exceptional acceleration and deceleration capability much greater than that of conventional dc

and disc motors. For example, a hollow rotor dc motor can accelerate at 100,000 rad/s^2; a similar conventional iron-core unit speeds up at only 40,000 rad/s^2. Since the motor has low inductance, typically 1000 times lower than that of an iron-core design, rapid built up and decay of rotor current takes place and the motor's torque can follow the variations in applied voltage closely. Apart from having a low inertia and inductance these motors provide uniform cogging-free rotation.

These motors are used in high-performance, low-power and high speed incrementing systems requiring good start-stop dynamic characteristic such as in computer tape transports, high speed printers, low cost real-real cassette/cartridge systems, X-Y positioning, optical scanning and coil winding. Also they are particularly suited for high gain, wide-bandwidth servo systems.

Stepper Motors

Stepper motors are electromechanical incremental actuators, i.e. they rotate discretely in a uniform magnitude rather than continuously as in conventional motors. Stepper motors can rotate clockwise or counterclockwise in discrete steps to a precise position corresponding to the sequence of pulses supplied to one of its stator windings. By varying the pulse rate they can be made to advance from as little as a fraction of a degree to 90 degrees per pulse very slowly or rotate stepwise at high speeds

There are two board categories of stepping motors: PM and variable reluctance motor (VRM). The VRM, which is magnetically similar to the SR motor, consists of a stator wound to form salient multi-poles. It often has four, five, or eight main poles whose phases are often slotted to create a number of teeth. When the windings on the stator is energized in a proper sequence the rotor will tend to move

to equilibrium points of minimum reluctance situated between the stator salient poles and rotor, giving rise to stepped rotation. The rotor consists of toothed cylindrical soft magnetic iron. For a given drive system the number of teeth (or salient poles) on the rotor and stator determines the stepping angle. Steps angle of 18°, 15°, 7.5° and 1.8° are common [22-25].

The PM stepping motors are similar to the VRM except that the rotor has toothed north and south magnet poles. The field created by the PM rotor interacts with the magnetic flux pattern created when the stator windings are energized in a sequence. Due to the presence of permanent magnets, the motor develops a *detent torque* which keeps the rotor in place even when the stator windings are not energized. Unlike other motors, the number of poles in the stator and rotor of a stepper motor can never be equal. This difference in poles must exist to enable stepper motors to step as they do.

The PM stepper motor, compared with the VR motors, are more efficient, and have small stepping angles, detent action when power is off, better damping characteristics, and hence relatively high speed of operation and high power handling capability.

Although stepper motors were available in the late fifties, they become widely used only in the 1970's with the development of solid-state integrated circuit control packages and digital control techniques. Stepper motors offer the advantage of very simple open-loop speed and position control, high reliability, long-life and direct compatibility with digital control. Since the number of revolutions are known to an accuracy of one step this permits the motor to be used when motion and position have to be precisely controlled such as in numerically controlled machine tools, X-Y plotters, typewriters, tapedecks, valve and printers and throttle control in car engines [23]

Slotless Axial flux PM motor ***[26-30]***

Instead of winding copper wires through slots in laminated steel stack, as in the case with conventional brushless motors, slotless motor wires are wound against silicon-steel laminations. Then they are encapsulated in a high-temperature epoxy resin to maintain their orientation with respect to the stator laminations and housing assembly.

Assessment:

- Although some form of laminated return path is necessary to optimise motor performance, the stack of the slotless motor can be designed with low cost industrial washers punched from electrical grade steel. This eliminates the more expensive tooled slotted laminations. This element effectively reduces the design time, raw material costs and lengthy delivery cycles.
- This configuration, which replaces the stator teeth, eliminates cogging and results in quiet operation.
- Damping losses related to eddy currents are reduced as the distance between laminated iron and magnets is greater.
- Low magnetic saturation allows the motor to operate at several times its rated power for shot intervals without perceptible torque roll-off at high power levels.
- Slotless construction significantly reduces inductance, improving current bandwidth for fast response and acceleration.
- Slotless motors have a larger rotor diameter for the same outside diameter and have higher inertia.

- In motors with toothed laminations the cross section area available to place the copper wire is limited. This reduces the maximum effective strength of the electromagnetic field.

Performance comparison between slotted and slotless designs, given the same rotor size, windings, housing, and other parameters, indicates that a slotted motor would be more powerful than a slotless one. This is because the teeth of a slotted motor (around which the windings is wound) place the iron closer to the magnets, so the magnetic circuit is completed more effectively. By reducing the air-gap between iron and magnets, slotted designs have higher torque. Also slotted motors will typically cost less than slotless motors due to the use of these high-energy rare-earth magnets and a more time-intensive manufacturing process.

2.4. MOTOR SELECTION

The main practical objective of this work is to replace the geared dc brushed motor with a direct-drive brushless system due to its well-known advantages. The switched reluctance motor has a wide speed range with good low speed torque but it exhibits high torque ripples at low speeds. It is more suited to high-speed applications than the low speeds encountered in direct drives for applications such as wheelchairs and forklift trucks. Since smooth torque over the operating speed range is required, the switched reluctance motor is omitted and the selection process is narrowed down to PM motors and induction motors.

Of course, induction motors have their place in electric vehicle traction. Indeed, it is believed that the first production line electric vehicles (General Motors EV1) utilised a 3-phase induction motor. The available space for integrated in-wheel motors for LPEV is very limited as normally the motorised wheel would replace a gear-driven

wheel in order to limit the number of new components required. This places a paramount importance in achieving the highest possible force density. After evaluating the comparison performed by Mhango and West [8,9,31-34] it became evident that a permanent-magnet drive is superior to an induction motor drive in this respect and, therefore, is a more suitable choice for LPEV application.

CHAPTER III

FORCE DENSITY LIMITS IN INTEGRAL-SLOT MACHINES

3.1. INTRODUCTION

The outstanding properties offered by modern permanent magnets have made PM motors viable, on the basis of cost and performance, for a variety of demanding applications. They have found use in disk drives, household domestic equipment, generators, and many high performance aerospace applications. One area that have benefited extensively from the innovations of these materials are the battery powered electric vehicles. The main applications include power wheelchairs, electric scooters, forklift trucks, electric golf carts, electric vehicle and electric bicycles.

In low power traction applications, when in-wheel motors are used, they must be designed with very high force densities to fulfil the peak torque requirement within the given space envelope available. Low-speed, directly driven generators (such as those used for wind applications) would also require high force densities in order to achieve optimised designs suitable for mounting and transportation [3,4,35].

The achievable force density in practice will depend, for a given machine, mainly upon four general factors: thermal, inductance,

saturation and cost. The way the thermal limit for the winding and the stator inductance influence the force density of a slotted PM machine was discussed in paper A, Appendix I, using a magnetically-linear model. Depending on the application, the force density predicted from such a model would be greater than that can be achieved in practice since saturation in the stator core can significantly limit the force density.

The primary aim of this chapter is to provide a full investigation of the influence of magnetic saturation on the force density. The maximum force density achievable for slot depths within the range of 10 mm to 1000 mm with different magnitudes of current loading is found for both surface-mounted and inset magnet rotor configurations. Some of the work presented in this chapter is as per paper B, Appendix I.

Of course, not all possible designs are considered here. Instead a number of designs are used to illustrate the saturation limits and to provide better understanding of saturation effects. By applying scaling laws, the results can be used as a guide in tailoring a specific design towards fulfilling demanding technical specifications. The findings in this chapter would be useful to a machine designer that requires a fast estimation on the required slot depth for preliminary calculations. Indeed, the results are already being incorporated into a software package aimed as a design and selection tool of traction motors employed in hybrid electric vehicles [36].

The slot depth limits above which force density degradation would occur for specific applications are identified. It is up to the reader's discretion to interpret the results presented for their application by applying the established scaling laws of machine design [2].

3.2. SCOPE OF THE INVESTIGATION

The investigation is limited to low-speed machines: multi-pole, three-phase, permanent magnet machines with slotted full-pitch and fractional-slot windings. However similar results are expected for a variety of machine types utilising concentrated full pitch windings. It is important to note that the machine variables selected in the present investigations are not targeted to a specific application or one machine size. The assumptions presented apply equally to chapter 4, where fractional-slot designs are considered.

The investigated machines are designed for maximum force density, within the given limits, and they are therefore not optimized for cost, weight or size. Because high pole numbers are considered, the air-gap diameter has been assumed to be large enough for the curvature of the stator to be neglected when analysing only one pole.

The force density of an electric machine can be found from investigating just one pole of the machine, without direct influence of the air-gap diameter, stator length or the speed. This approach is advantageous since it makes the results more generally applicable than otherwise. But there are second order effect may make, for example, the air-gap diameter and length, and speed influence the force density to some extent. The errors introduced by these must be investigated and the credibility of the presented result due to neglecting these errors must be first established. These factors are briefly discussed below.

The air-gap clearance will have a minimum value, due to mechanical reasons, or by the stator current loading, due to the risk of demagnetisation. In machines with high force density, demagnetisation will normally be the most important limit for the choice of the air-gap. Therefore, the influence of stator diameter and

length on the air-gap has not been given detailed consideration in this work.

The axial length of the stator will influence the force density, since the end windings will increase the losses and also the temperature rise in the winding hot spot. However, the end windings contribution to the total loss and temperature rise can be neglected if they are short compared to the active part of the winding. With very high pole numbers the active length of the stator will often be many times that of the end winding and machines designed for very low speeds are typically of this type.

Mainly, winding current and magnetic flux density will determine the force in the machine, while speed will not have a direct influence on the force. Core losses will depend on the speed, and if they increase they will require a reduced current density, in order to be within the temperature limit. However, in machines for very low speed the core losses can usually be neglected, as they are much smaller than the copper losses. For example, in a 32 rev/min 500 kW wind-turbine generator the full load core losses are only about 3 kW while the copper losses are 23 kW [3].

3.3. FORCE DENSITY

There are several ways in which force production can be explained, but a very easy way is to start from the well-known formula for force on a current-carrying conductor situated in a magnetic field:

$$F = B\,I\,l \qquad (1)$$

This equation will work rather well on non-salient machines, although it is actually a simplification of the real force producing

mechanism. The total tangential force on the stator will be the sum of the forces produced on each stator conductor. Since, in a non-salient machine, the magnetic flux produced by the stator itself will not contribute to the net force production, only the flux density produced by the permanent magnets on the rotor is used in the force calculation. Assume that, in the absence of magnetic saturation, both the current loading from the stator and the flux density from the permanent magnets are sinusoidally distributed around the air-gap, with peak values J_p (A/m) and B_p (T) respectively. The displacement between these peaks is defined as the angle α. The force density can then be found by first reformulating equation (1) to be valid for an infinitesimal part of the air-gap circumference. Integrating over one pole pair and dividing by the corresponding air-gap surface area, we obtain the average force density produced as follows:

$$f = 0.5\ B_p\ J_p\ \cos(\alpha) \qquad [N/m^2] \qquad (2)$$

In this equation the space harmonics ability to produce force is neglected since their contribution, compared to the fundamental component, is very small. Equation (2) shows that the force density is at a maximum when the no-load flux density and stator current loading are kept in phase and their product is maximised.

The maximum value of air gap-flux density, B_{max}, is limited by saturation of the stator teeth and is thus mainly a function of the ratio between slot and tooth width, b_s and b_d; respectively:

$$B_{max} = B_{sat}\ k_{Fe}\ \frac{b_d}{b_s + b_d} \qquad (3)$$

where B_{sat} is the flux density at which the stator iron saturates and k_{Fe} is the iron fill factor of the stator core. Normal electric steels

have a saturation flux density of approximately 1.7 T. The fundamental component of the flux density distribution will have a higher peak value than the actual flux density. For a square shaped magnet with 180º pole arc, the ratio will be in the order of approximately 1.2 giving:

$$B_p \approx 1.2\, B_{max} \tag{4}$$

The peak current loading J_p (A/m) is a function of *rms* current density in the conductors, J_s (A/mm^2), slot depth (h_i) and also the ratio between slot and tooth width, therefore:

$$J_p = \sqrt{2}\, J_s\, k_{Cu}\, (h_s - 2\, h_i)\, \frac{b_s - 2\, h_i}{b_s + b_d} \tag{5}$$

where k_{Cu} is the copper fill factor of the coil. However, since the allowed current density will depend primarily on the cooling, it will itself be a function of slot depth, tooth width and slot width.

From the above discussion it is clear that the machine designer can influence the force density mainly by varying the ratio between slot and tooth width and the slot depth. But there is a conflict between increasing flux density and current loading by changing the slot-to-tooth-width ratio. If the tooth width is increased the flux density can be increased, but the current loading will be decreased at the same time. Therefore, the slot-to-tooth-width ratio cannot be used to increase the force density significantly. Instead the designer is left with the slot depth as the main mean to significantly increase the force density.

3.4. SATURATION LIMITS

3.4.1. Models description

The magnetic model shown in Figure 3.1 was developed using a commercially available finite-element package in order to investigate the force density limit in slotted machines. Figures 3.1 (b) and (d) show the magnetic model used for the surface (SMR) and inset magnet rotor (IMR) configuration respectively while Figures 3.1 (c) and (e) show the flux-plots of both rotors.

The investigation was confined to only rectangular open slot machines. These are assumed because the coils with large cross sections, normally used in deep slots, would be otherwise difficult to mount. Closed slots will lead to approximately 10% greater force density than that achieved in open slots. The following describes the magnetic model for the investigation.

The excitation flux is obtained from the permanent magnet assembly mounted on the rotor. Only machines having 1 slot per pole per phase are considered here. This is because efficient designs of in-wheel motors and low speed generators would have a large number of poles (e.g. 28). Integral slot designs with slots per pole per phase of more than unity would, therefore, be impractical. Indeed, in many cases a value of less than unity will be required, leading to fractional-slot windings, which are dealt with in the next chapter.

With reference to Figure 3.1 (a), thin layers of air are assumed to exist between the conductors and the slot walls, to accommodate the slot liners. The thickness of stator yoke and rotor core are taken as 5 times the width of the stator tooth. Tables 3.1 and 3.2 give the dimensions of the stator and magnet used in the model. With the surface mounted magnet rotor (SMR) configuration the magnet pole

arc used throughout the investigation is fixed at 180 electrical degrees since it maximises the achievable force density whereas the pole pitches were varied in the inset magnet (IMR) configuration.

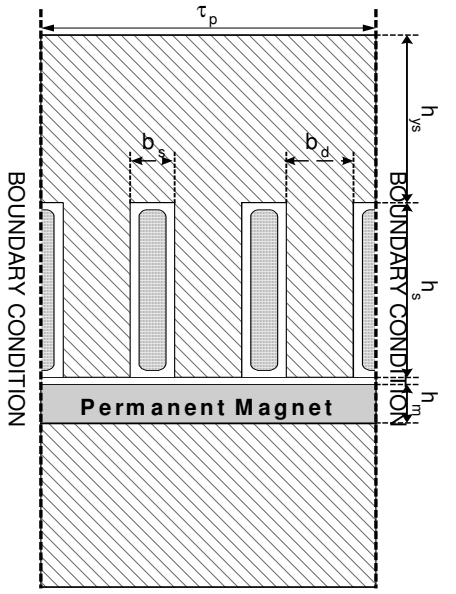

a

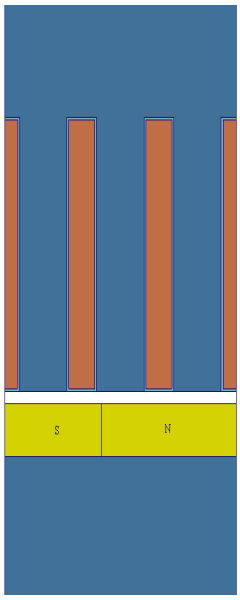

b(180° Pole Arc)

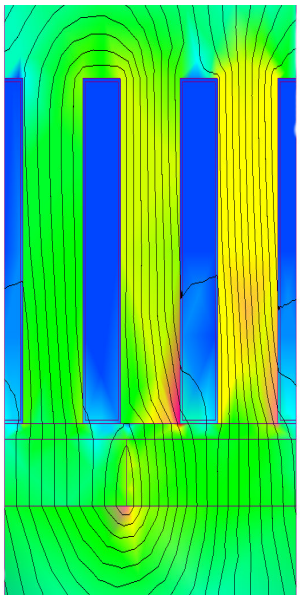

c

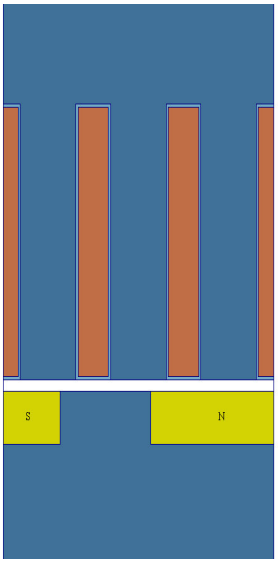

d (120° Pole Arc)

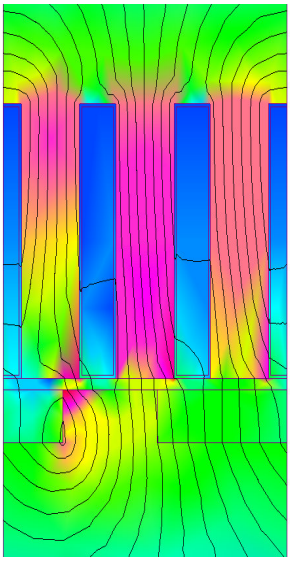

e

Figure 3.1: (a) Magnetic Model Parameters, (b) Surface Magnet Rotor FEM Model, (c) Surface Magnet Rotor Flux Plot (d) Inset Magnet Rotor FEM Model (e) Inset Magnet Rotor FEM Model

Table 3.1: SMR machine variables for different slot depths.

h_S (mm)	b_S (mm)	b_d (mm)	τ_P (mm)	J_S (A/mm^2)	h_m (mm)
10	6,11	7,79	41,7	12,01	6,26
15	6,22	8,42	43,9	10,35	6,59
20	6,52	9,19	47,1	9,17	7,07
30	7,15	10,67	53,5	7,62	8,02
50	8,24	13,14	64,2	5,91	9,62
75	9,29	15,60	74,6	4,77	11,20
100	10,12	17,64	83,3	4,07	12,49
150	11,43	21,04	97,4	3,21	14,61
200	12,47	23,88	109,1	2,69	16,36
300	14,14	28,63	128,3	2,06	19,25
500	16,66	36,14	158,4	1,44	23,76
750	19,10	43,63	188,2	1,05	28,23
1000	21,16	49,99	213,5	0,84	32,02

Table 3.2: IMR machine variables for different slot depths.

h_S (mm)	b_S (mm)	b_d (mm)	τ_P (mm)	J_S (A/mm^2)	h_m (mm)	τ_{120}	τ_{150}	τ_{170}
10	6,11	7,79	41,7	12,01	6,26	6.95	3.47	1.16
15	6,22	8,42	43,9	10,35	6,59	7.32	3.66	1.22
20	6,52	9,19	47,1	9,17	7,07	7.85	3.92	1.38
30	7,15	10,67	53,5	7,62	8,02	8.91	4.45	1.48
50	8,24	13,14	64,2	5,91	9,62	10.69	5.34	1.78
75	9,29	15,60	74,6	4,77	11,20	12.44	6.22	2.07
100	10,12	17,64	83,3	4,07	12,49	13.87	6.93	2.30
150	11,43	21,04	97,4	3,21	14,61	16.23	8.15	2.70
200	12,47	23,88	109,1	2,69	16,36	18.17	9.09	3.02
300	14,14	28,63	128,3	2,06	19,25	21.38	10.69	3.56
500	16,66	36,14	158,4	1,44	23,76	26.39	13.20	4.39
750	19,10	43,63	188,2	1,05	28,23	31.36	15.68	5.22
1000	21,16	49,99	213,5	0,84	32,02	35.57	17.78	5.92

In the IMR machine, computation is performed for magnet arcs of 120, 150 and 170 electrical degrees. The last three columns of Table 3.2 give the width of the rotor steel section either side of the magnet pole-piece, otherwise the same dimensional variation is assumed as in the case of the SMR machine.

The pole pitch (τ_P), tooth width (b_d), slot opening (b_S) and magnet height (h_m), all vary with slot depth (h_S). The allowable current density (J_s) in the conductors is determined according to the thermal limits presented in [5]. The current density values given in Tables 3.1 and 3.2 correspond to continuous operation ratings. During transient operation, higher values are used to satisfy the traction requirements of 100% overload. Since the peak force density achievable is of prime interest, rotor magnets with a remanence of 1.25 T and coercive force of 905 kA/m are assumed. It should be noted that such figures are well within the capability of commercially available materials.

In order to confirm the validity of the model and investigate the severity, or otherwise, of saturation on the force density, the stator steel of the magnetic model was simulated assuming both linear and non-linear demagnetisation characteristics, with both models having the same dimensions and slot current values. This makes the results directly comparable, with only one variant; namely the magnetic saturation effects.

3.4.2. Simulation procedure

To begin with, the force density variation with rotor position for the SMR machines listed in Table 3.1 was determined. For each machine (represented by a row in Table 3.1) the force density values were determined for 40 rotor positions across the full pole pitch. The

current fed into the slots were forced to vary sinusoidally with rotor position. These results are shown in Figure 3.2.
It is seen in Figure 3.2 that the force density is a cyclic function of rotor position, with the period corresponds, approximately, to one slot pitch. One, therefore, concludes that force density computation should not be performed at only one rotor position as such a value would be either higher or lower than the average force density, depending on the position of the rotor assumed. It should be noted that the peak force density does not occur when a north (or a south) pole is centred (0 degree), as shown in Figure 3.1 (a). Contrary, this is the worst rotor position as it corresponds to the minimum force density value.

In Figure 3.3 it is shown, for a number of stator current values, the variation of the force density with rotor position for a SMR machine having a fixed dimension corresponding to a pole pitch of 200 mm. Again, the periodic nature of the variation is observed. Hence to avoid errors in determining the achievable force density, the values obtained at various rotor positions must be averaged. Such an average value is more likely to conform with practical machines as the torque developed at the shaft corresponds to the average value.

While working with average force density values enhances the reliability and practical significance of the data, obtaining only one such a value would involve solving tens numerical field problems. Since various slot depths, pole pitches and current loadings are varied throughout the data collection process, it would be a tedious procedure and will be prone to errors. For maximum flexibility and productivity, a program was coded in visual basic that automates the computation. The machines parameters are set in excel and visual basic, which acts as inter-media, transfers the machine variable as an input to finite-elements package. This approach enables many

simulations to be performed without the presence of the investigator and a database, containing thousands of stator and rotor dimensions, can be compiled.

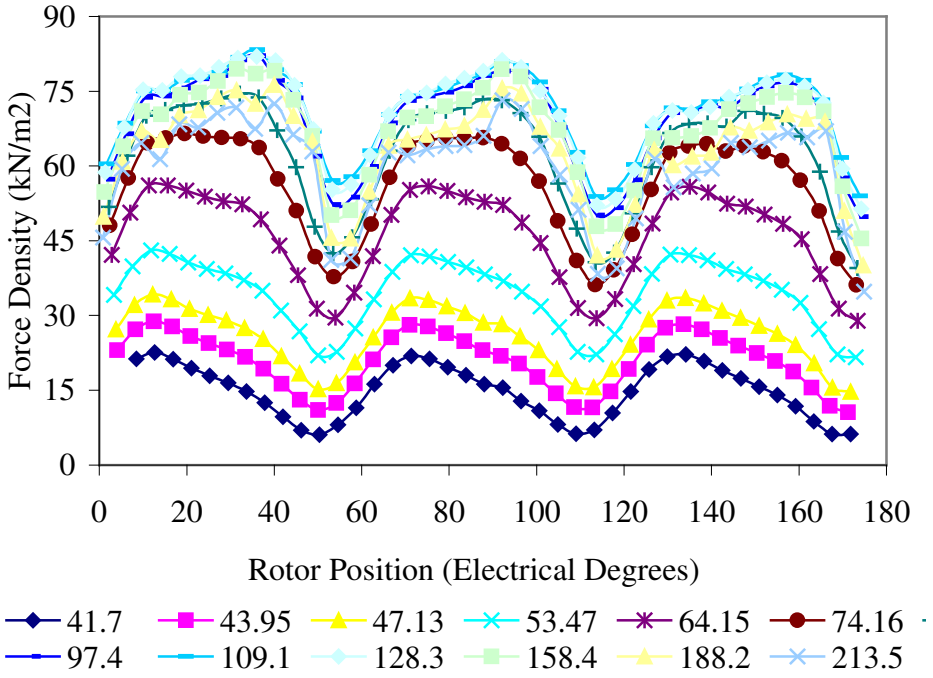

Figure 3.2: Force density versus rotor position for SMR machines.

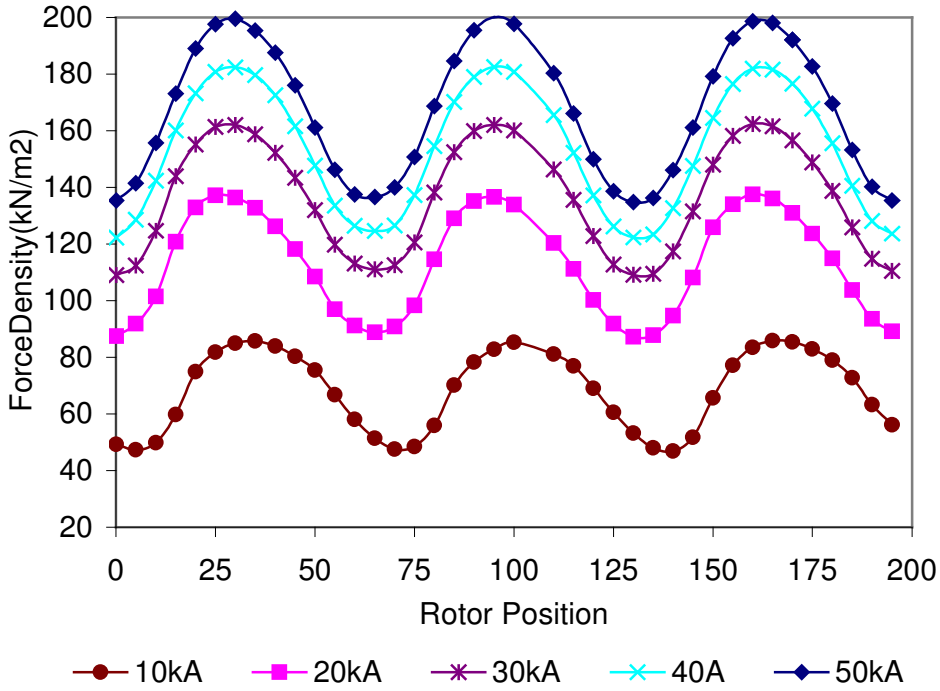

Figure 3.3: Force density versus rotor position for τ_P =200 mm.

3.4.3. Effects of magnetic non-linearity

The objective of this section is to determine how severely does saturation in the core material affect the computed force density values. To this end, the machines whose details are given in Table 3.1 are modelled first when a constant value of the relative permeability of the core material (30,000) is assumed and then solving the same problems after assigning a typical magnetisation characteristic of silicon-iron laminations to the cores. The results are presented in Figure 3.4 where curves A and B represent the non-linear and linear magnetic materials, respectively. Curves A1 and B1 are obtained with the *rated* slot current values of Table 3.1, determined by the thermal limits. Curves A2 and B2 show the force density characteristic during transient condition, when the slot current is twice the rated current. It should be noted that each data point in Figure 3.4 represent the average force density at a given slot depth.

The force density curves increase rapidly to a peak and tend to level off at a much slower rate towards the x-axis. The curves for non-linear iron (A1 and A2) show a marked difference from that of the linear iron (B1 and B2) and permit a comparison between ideal (linear) and non-linear conditions.

With a linear material the force density at thermally rated current predicted from the FEM result (B1) increases with slot depth linearly with current loading. Theoretically, high force density levels are achievable, limited only by the temperature rise. Thus the curves for the linear iron "level off" only due to thermal limitations. As the slots become deeper, the current density has to be reduced to avoid overheating. As a consequence of this, the current loading and force

density does not grow linearly with slot depth. In paper A, Appendix I, this curve is derived and explained in detail.

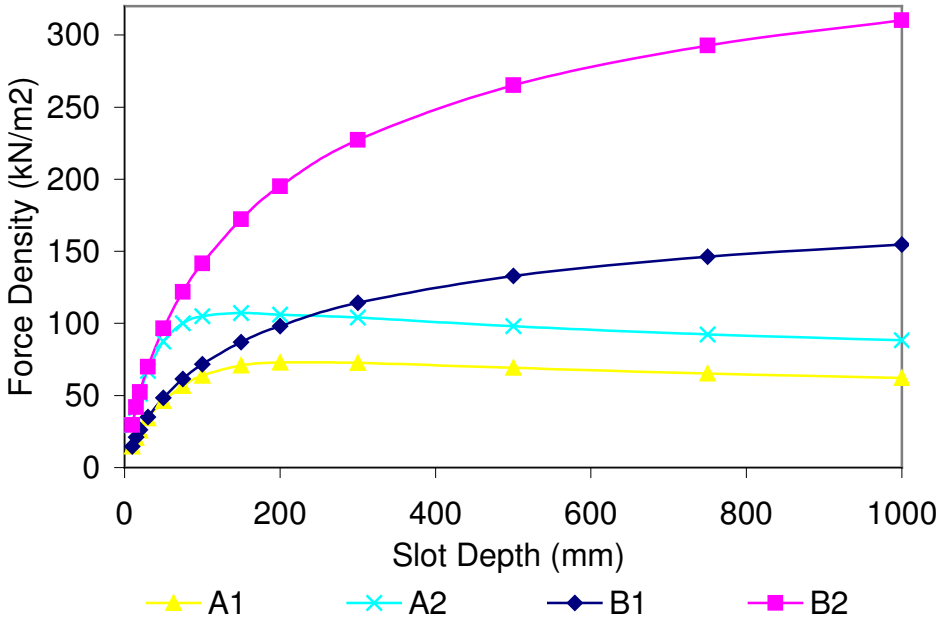

Figure 3.4: Force density versus slot depth with non-linear (curves A1 and A2) and linear materials (curves B1 and B2).

However in practice, where magnetic saturation would normally be present, the force density behaviour (A1) tends to deviate significantly from the above-mentioned ideal characteristic. Saturation of steel is a complex function of applied magnetic field, contributed by the rotor magnet and stator current flux. Close examination of Figure 3.4 indicates that the force density is not directly proportional to current loading because magnetic saturation sets in after the slot depth (and current loading) is increased beyond a certain level. At low slot depths, the linear and non-linear cases lead to almost the same force density but as the slot depth exceeds 50 mm, saturation reduces the force density significantly.

At a slot depth of 200 mm the force density achieved with the non-linear material at rated condition is approximately 75% of that

achieved with a linear material. With 2 times higher armature current this reduces to 55%. At a slot depth of 1000 mm force densities of 88 kN/m^2 and 310 kN/m^2 are obtained from the non-linear and linear model, respectively during transient operations. Thus, these results show that saturation in the stator reduces the force density, under the stated conditions, by a remarkable factor of 3.5.

The force density curve peaks at about 72 kN/m^2 (continuous) and 107 kN/m^2 (transient) corresponding to a 200 mm and 150 mm slot depth respectively. A further increase in slot depth causes a decrease in the force density due to increasing saturation. Curves A1 and A2 indicate that the force density does not change in proportion to armature current levels with large slot depths.

Above 150 mm and 200 mm, for both rated and 100% overload conditions, the increase in current loading with increasing slot depth lead to a reduction in force density due to the armature reaction contribution to the saturation of the magnetic circuit. Thus, most of the flux lines that are supposed to contribute to force production do not link with the whole winding as the leakage flux increases. Although the current is increased with slot depth according to the thermal limit, the high leakage flux is primarily the dominating factor in limiting the achievable force density. Thus from the results presented in this section, it is evident that magnetic saturation has a remarkably significant effect on predicting the achievable force density values.

3.4.4. Achievable force density values

The objective of this section is: (1) to determine the force density versus slot depth envelopes for various current loadings, and (2) to

investigate the behaviour of the optimum slot depth that maximizes the force density at various current loadings. Figures 3.5 to 3.8 show the force density against slot depth curves determined in the same manner as in the preceding section, corresponding to the slot and magnet dimensions of Tables 3.1 and 3.2 for both rotor types (SMR and IMR). To enable comparison of results, the slot current in Tables 3.1 and 3.2 during continuous operating conditions are increased by a fixed factor. The total slot current of curve X2 is twice the magnitude of that of curve X1 while X9 has a total slot current 9 times that of X1. Some of the current levels are probably too high to be used even at transient state, due to thermal limits.

By examination of Figures 3.5-3.8, it is readily apparent that an optimum slot depth, at which the force density is a maximum, exists for each current loading. It is interesting to notice the changes in the gradient of the force density curves. The force density curves initially exhibit positive gradients, reach a maximum and then decrease with a negative gradients. Also evident in the plot is the fact that, the negative gradient of the curves becomes steeper with increasing slot current.

Examination of the curves indicate that, due to saturation effects, the difference in distance between adjacent envelopes decrease; although the slot current is increased gradually up to a factor of 9 (X9), the peak force density only increased by approximately three-fold in the SMR configuration. This factor decreases with the decrease in the pole arc for the IMR configuration.

Figure 3.9 is obtained with the aid of Figure 3.5. It shows the variation of slot depth at which the peak force density occurs, and the peak force density values, with the current multiplication factor. It is interesting to note that at high values of current (higher than 3 times the thermal rating), the peak force density occurs at

approximately the same slot depth of 100 mm. As stated above, at rated condition, (X1), a peak force density of approximately 70 kN/m^2 is achieved with a slot depth of 200 mm. However, with a multiplication factor between 3 and 9, a peak force density of 120 kN/m^2 and 190 kN/m^2 is achieved with approximately the same slot depth of 100 mm.

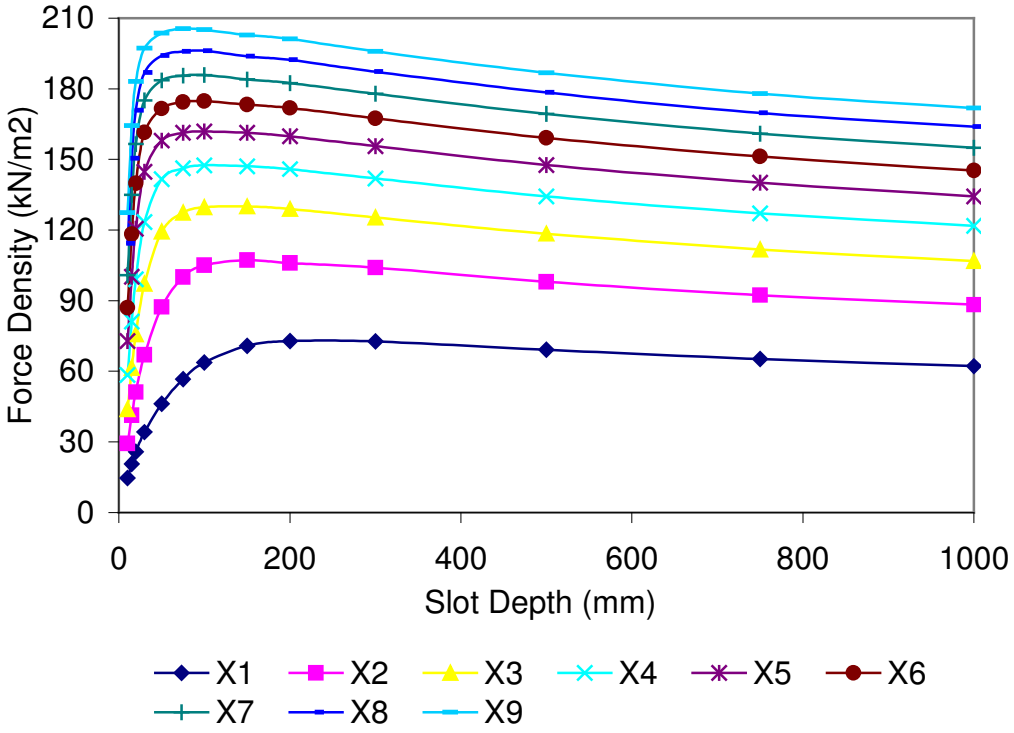

Figure 3.5: Force density versus slot depth for SMR machines.

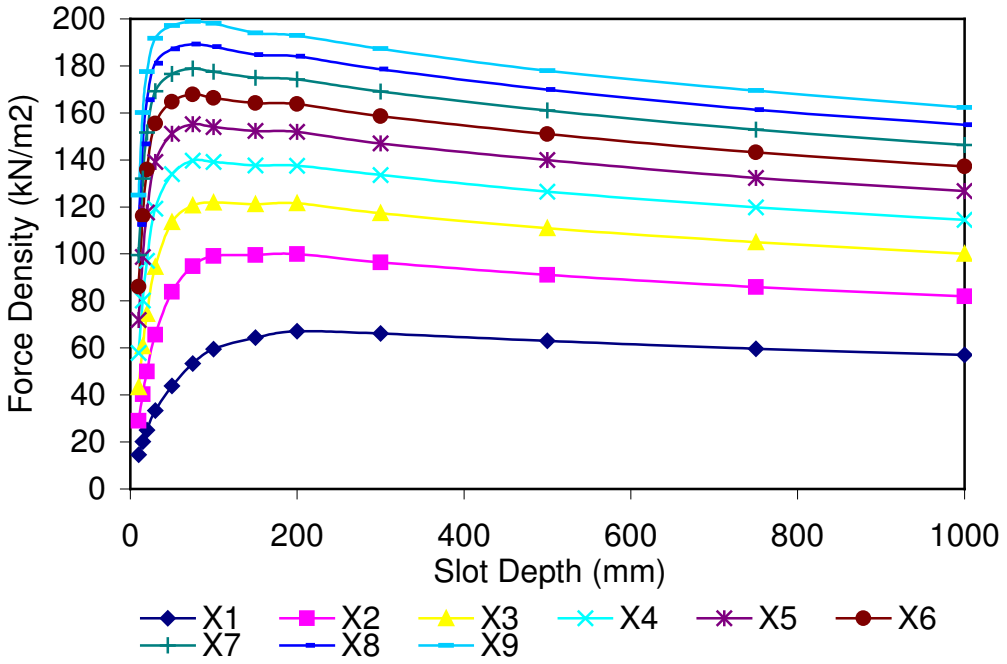

Figure 3.6: Force density versus slot depth for IMR machines ($\tau = 170^{o}$).

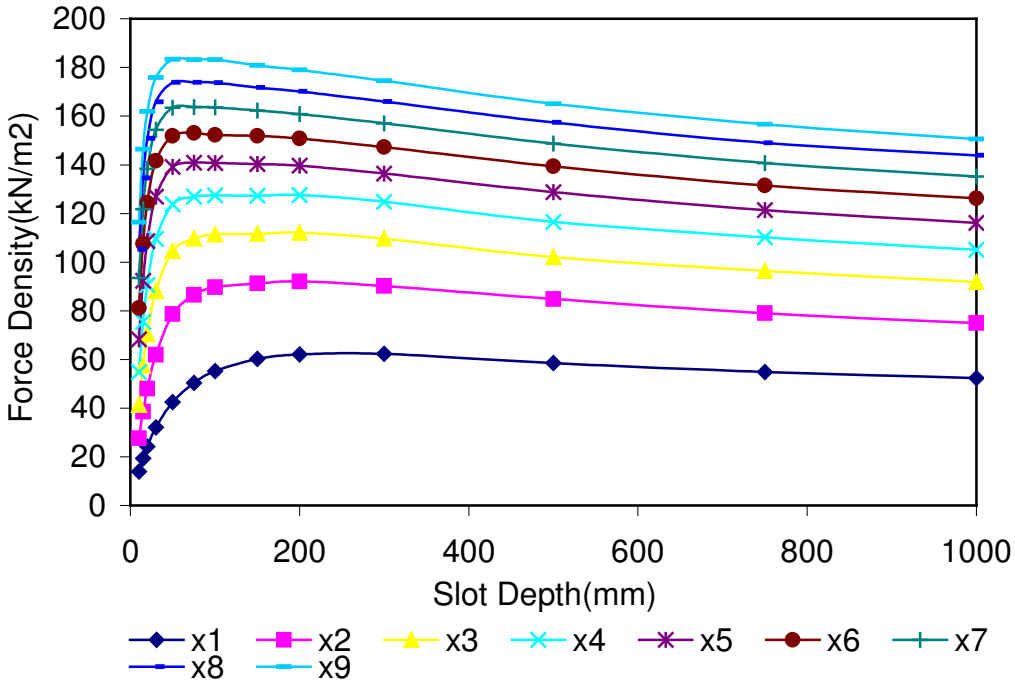

Figure 3.7: Force density versus slot depth for IMR machines ($\tau = 150^{o}$).

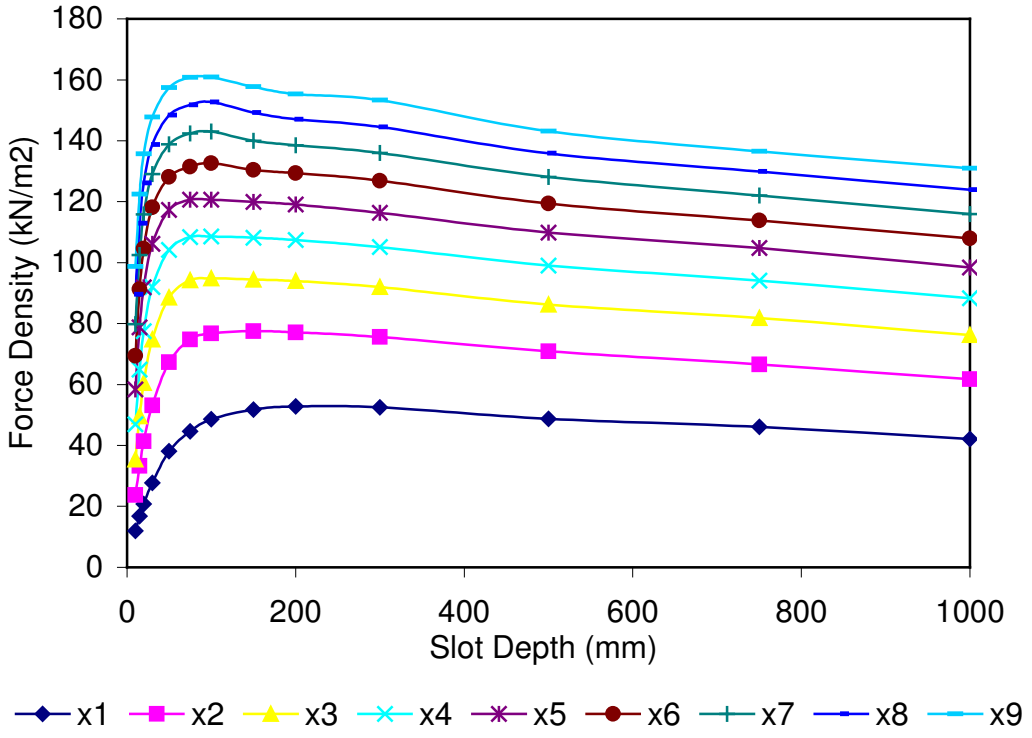

Figure 3.8: Force density versus slot depth for IMR machines ($\tau = 120^{o}$).

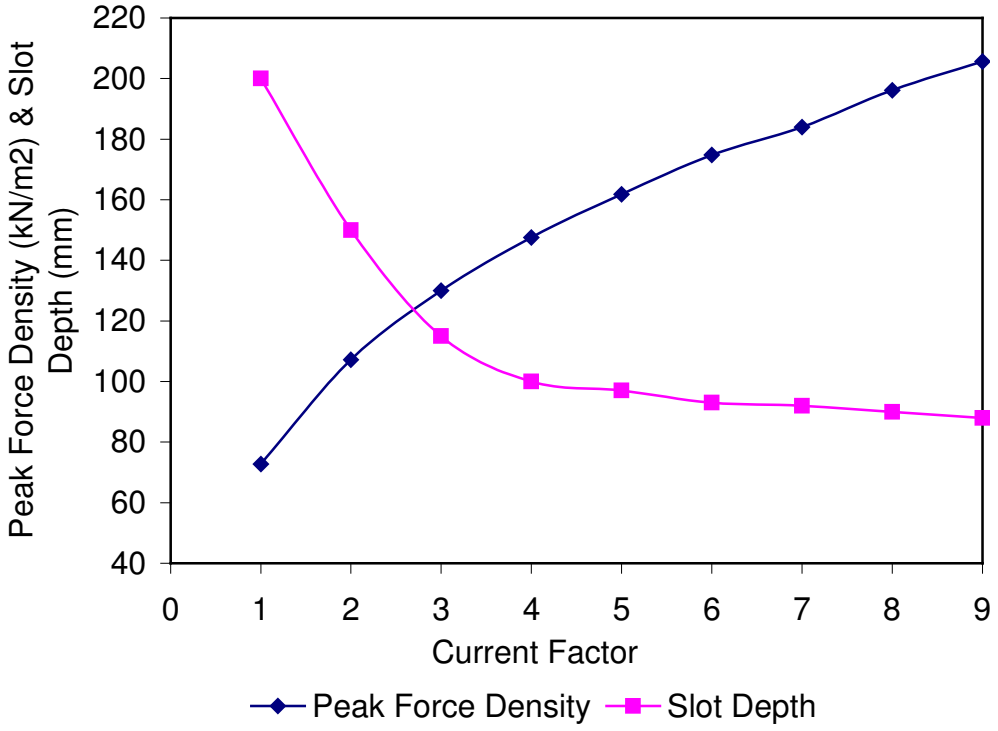

Figure 3.9: Averaged peak force density values and corresponding slot depths versus current multiplication factor.

For continuous load operations, (X1), a force density no grater that 72 kN/m^2 can be achieved. For transient operation, within a one-minute time frame, current factor of 3, no greater than 120 kN/m^2 can be achieved. At extreme transient operations (X9), for say one second, no greater that 205 kN/m^2 can be achieved.

These results stresses the important fact that, in applications involving high slot currents and experience high armature reaction effects, the use of deep slots yields no advantages. A smaller slot depth would enhance the performance at high current levels, but will have the opposite effect at low current levels. From figure 3.9, it is obvious that for any current loading greater or equal to 3 times the rated condition of Table 3.1, a slot depth of approximately 100 mm should not be exceeded.

When a machine is designed, one tends to concentrate on the peak and rated torque. Deep slots up to 200 mm would result in an acceptable peak force density during rated condition. However a 200 mm slot depth would have an adverse effect on the achievable peak force density during transient conditions. Therefore, the slot depth chosen would depend on the relative importance between the transient and continuous torque for a particular application due to the conflict between them.

Table 3.3, summarizes the approximate maximum force density obtained from figure 3.5 to 3.8 with respect to the assumed current loading for SMR and IMR machines.

Table 3.3: Summary of maximum force density values.

Operating Conditions	Current Condition	Peak Force Density (kN/m^2) (SMR)	τ_{120} (IMR)	τ_{150} (IMR)	τ_{170} (IMR)
Continuous	I_{Rated}	70	53	62	67
Peak	$3I_{Rated}$	120	92	92	100
Extreme	$8I_{Rated}$	190	183	183	199

3.5. FORCE DENSITY VARIATION WITH WINDING CURRENT DENSITY

The aims of this section are to investigate the force density behaviour for a range of slot depths with increasing current density (but keeping slot and tooth width constant) and to obtain force density versus slot depth characteristics, for a range of winding current densities, which can be used as a design tool.

In the first part of the investigation, simulations were performed only for a fixed rotor position (the position shown in Figure 3.1) since the behaviour of the force density rather than actual values is of interest. This is sufficient to highlight the way the current loading in each slot influence the force density. Thus as the slot depth increased the stator and rotor dimensions listed in Table 3.4 were held constant with gradual increase in slot current density. The slot depth was varied in steps from 20 to 300 mm. Simulation was only performed for the SMR configuration as the same behaviour pattern would be expected with the IMR designs.

Table 3.4: Machine dimensions (in mm) for different slots depths

τ_p	h_m	b_S	b_d	h_S
200	20	33.33	33.33	Varied

Although some of the current density and slot depth combinations may not be used in practice, due to thermal limits and mechanical constraints, nonetheless, these are considered in the investigation in order to facilitate the understanding of the saturation effects; the effect of saturation on the force density will become more obvious at these extremes.

Figure 3.10 shows the force density against current density for various slot depths for a pole pitch of 200 mm. It is evident that the force density increases with current density. However the gradient of the curves becomes greater with increasing slot depth. Thus for a fixed current density, a deeper slot would yield a higher force density. For current density values greater than 3 A/mm^2 the curves with slot depths of 150, 200 and 300 mm tend to converge to the same characteristic. Above 3 A/mm^2 the force density achieved for all of the 3 slot depths are approximately the same for all current density values. The three curves merge at a current density of 4 A/mm^2 corresponding to a force density of 88 kN/m^2. Thus with a current density of 6 A/mm^2 a force density of 100 kN/m^2 can be achieved by using a slot depth of 100 mm just as well as 150, 200 or 300 mm.

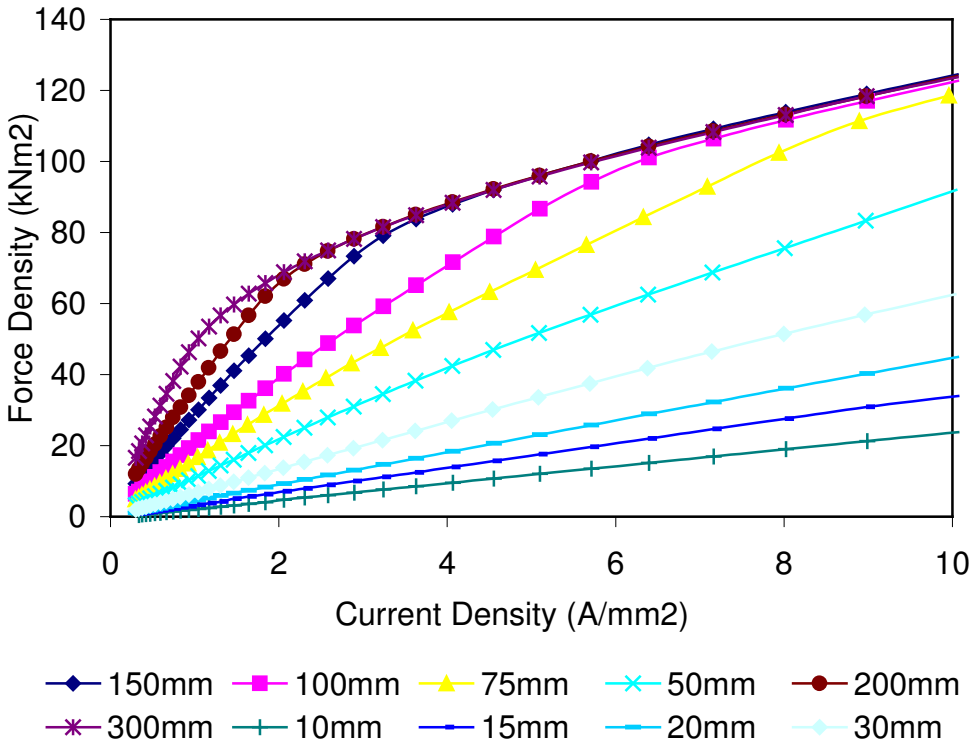

Figure 3.10: Force density versus current density characteristics.

Increasing winding current density by a factor of 2.5 to 10 A/mm^2 in these slots results in an increase in the force density by a factor of only 1.4 achieving 124 kN/m^2. This factor increases approximately to 2.1 for slot depths of 75 mm and 50 mm. At very high current density levels (outside the range shown in Figure 3.10) all curves will eventually merge. The current density level at which this occurs will vary for each slot depths, with the 10 mm slot depth being the highest.

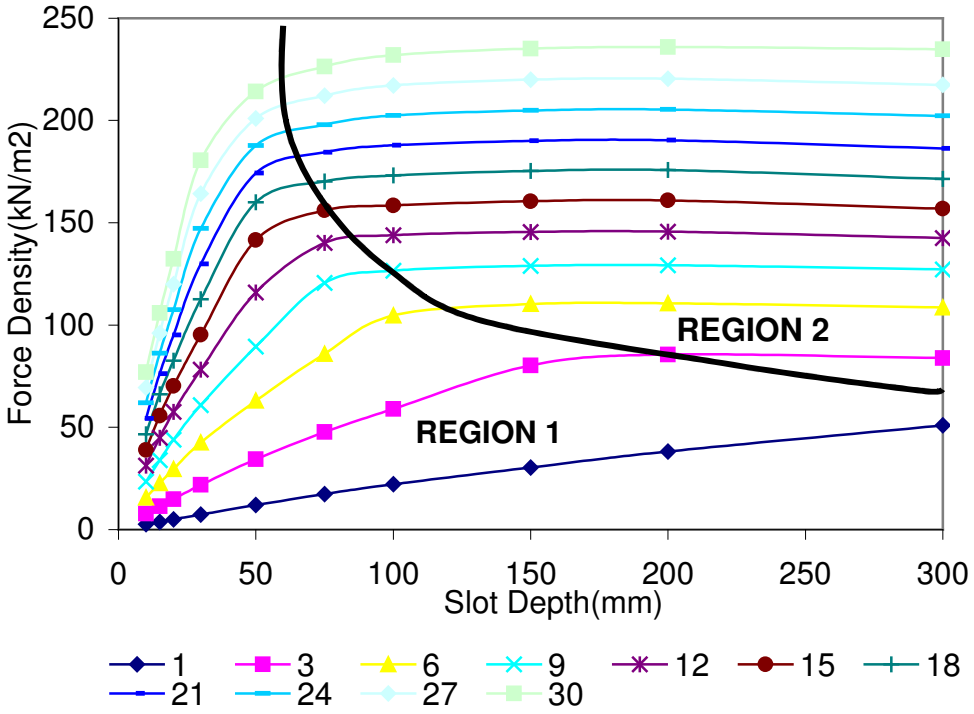

Figure 3.11: Force density versus slot depth curves for various current density values.

From the above discussion, two interesting regions having opposite characteristics can be seen to exist. In order to illustrate these regions, the data of Figure 3.10 are represented in a slightly different format in Figure 3.11. It shows the force density variation with slot depth for current densities up to 30 A/mm^2. *Region 1:* For fixed current densities, a greater force density is achieved with deeper slots. *Region 2:* For fixed current densities, equal force densities are achieved with shallow slots. In the linear region the effect of slot depth is negligible and the force density increases directly with total slot current. In the non-linear region, however, the saturation is due to combination of total slot current and slot depth. It is seen that for current densities of 3, 6 and 12 A/mm^2, the slot depth above which no further increase in force density with increased slot depth (and machine size) is 150, 100 and 75 mm respectively.

Data as those of Figure 3.11 can be used as a guide for the machine designer. From such characteristics the maximum allowable slot depth for a given current density can be determined. However in-order to utilise these curves for design purposes, the resultant average of the force density must be determined. Determining these curves for a range of pole-pitches, will enable one to produce a useful database, that can be used to establish if the specification can be met within the given space. The force density versus slot depth characteristics for different values of winding current density, and for a range of pole-pitches, are given in Appendix II. It can be seen that the allowable slot depth above which no increase in force density is observed increases with the pole pitch. For example, with a $3A/mm^2$ a maximum slot depth of 100 mm is viable with a pole pitch of 41.7 mm. However a greater maximum slot depth of 150 mm is permitted with a pole pitch of 109.05 mm.

3.6. FORCE DENSITY AND FLUX-LINKAGE

Flux-linkage versus current graphs are very useful in modelling the behaviour of an electric machine seen from its terminals. Compared to the equivalent circuit models, they represent a much more general model since saturation effects, space and time harmonics can be included. The model has rotor position and current as inputs and has flux-linkage and torque as its output. The advantages of the flux-linkage analysis may be summarised as follows:

- Allows a unified theory for investigating all different types of electric machines
- Includes all phenomena that influence the machine electrically
- Can be used to calculate the torque (if the losses are dealt with outside the model)
- Allows time transient calculations

- Can be used for control design

The main disadvantages are:

- It is a black-box model that gives less insight into the mechanisms which are the base for the machine function
- More complex to use for analysis than a circuit model
- Is not so useful during machine design. More useful for modelling and designing controller and the power electronic converter for a given machine.

Staton et al [37] used the flux-linkage versus current diagrams to illustrate the difference between the torque production mechanisms in different machine types. It is therefore interesting to see in what way they can explain the maximum force density that can be achieved in low speed PM machines. The flux-linkage versus current diagram is now used to discuss the same phenomena investigated earlier in this chapter, namely, to determine the influence of slot depth variation on the loop area of the flux-linkage versus current diagram.

In order to obtain the data for the flux-linkage analysis the machine whose dimensional details are given in Table 3.4 is selected. The slot current is varied from –50kA to +50kA in steps of 1kA, for 11 different rotor position from 0 to 180 electrical degrees. The same evaluation is performed for three different slot depths and the corresponding flux-linkage versus current characteristics are obtained, as shown in Figure 3.12 and 3.13. The diagrams represent all possible combinations of current and rotor position with one flux-linkage curve for each rotor position. Here it is assumed that the phases are fed symmetrically. Without this assumption, three electrical terminals and three different flux linkage values for all combinations of slot currents would be needed for each slot depth. It should be noted that, for motor operation, only some of the

combinations of flux-linkage and current are relevant. This is because the current has to vary as a function of rotor position in a manner that produces torque in an efficient way.

The electric energy fed into the machine during one electric cycle can be expressed in terms of the internal voltage, U, and current, I, as follows:

$$W_{el} = \int U I \, dt \tag{6}$$

This can be recast in terms of the flux-linkage (ψ) as:

$$W_{el} = \int I . d\Psi \tag{7}$$

The RHS of Equation (7) represents the area enclosed by the trajectory of the machine's flux-linkage and current. If we neglect the mechanical losses then the mechanical energy produced must equal the electrical energy. For one electrical cycle we have:

$$2\tau p . F_{average} = W_{el} \tag{8}$$

from which the average force over one cycle can be obtained as follows:

$$F_{average} = \frac{W_{el}}{2.\tau_p} = \frac{1}{2.\tau_p} . \int I d\Psi \tag{9}$$

The average force during continuous operation can be obtained from Figures 3.12 and 3.13 noting that (from Table 3.1) for slot depths of 30, 50, 100 and 200 mm the peak current has to be limited to about 5, 7, 10 and 12 kA, respectively, for thermal reasons. Thus the maximum torque that can be produced during continuous operation will correspond to the areas A, B and C in Figures 3.12 and 3.13.

These areas correspond to approximately 2800, 3500, 4000 and 5500-Watt.sec/cycle, respectively. Thus the continuous torque does not increase linearly with slot depth.

If we assume that the machine, for a short time, can withstand twice the value of the rated current, we can see that the transient torque will correspond to areas D, E and F.

It is seen that the machine with 200 mm deep slots would not produce higher transient torque than the one with 100 mm slots. With 50 mm slot depth, the force will however be lower than with 100 mm.

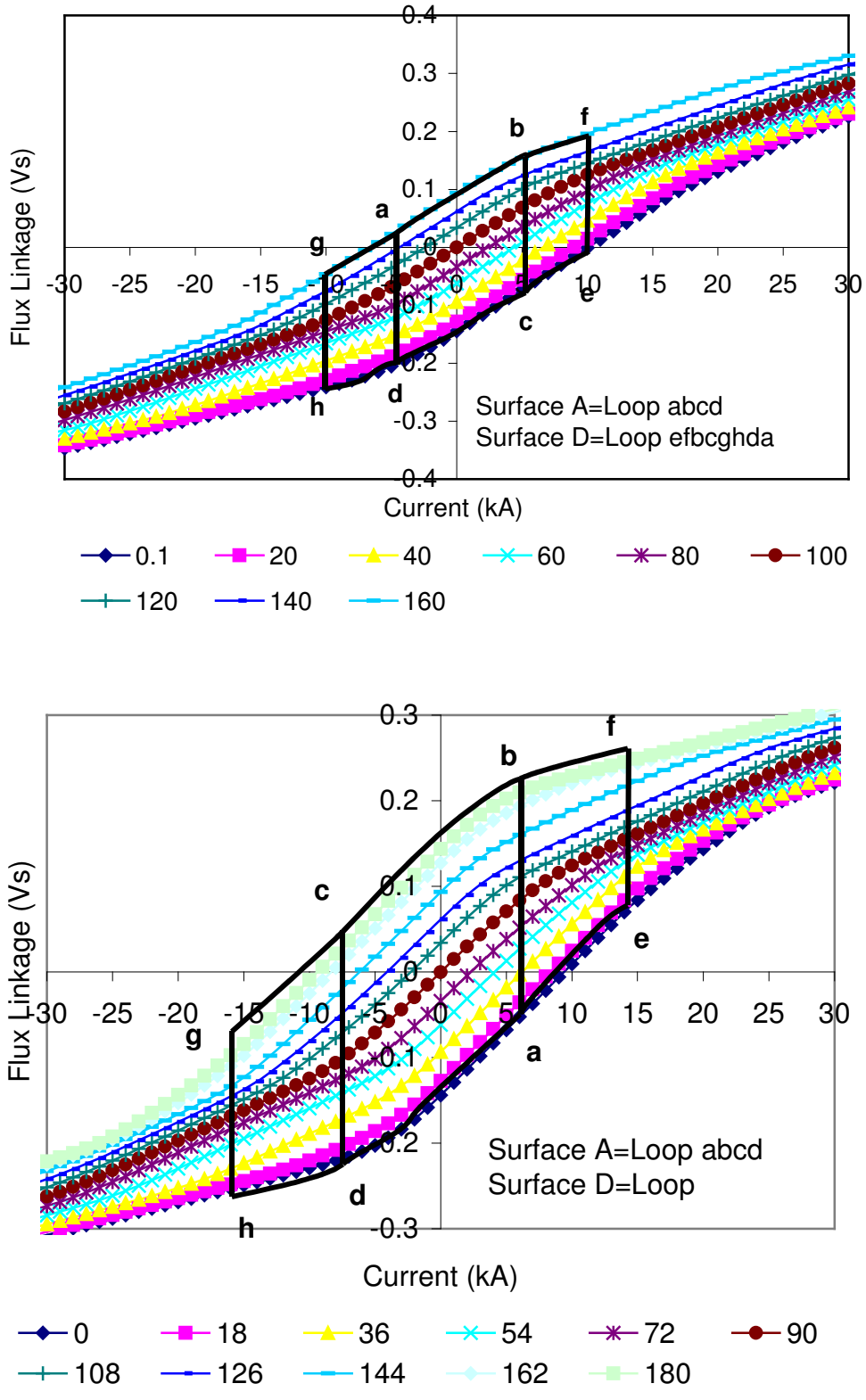

Figure 3.12: Flux Linkage versus slot current at different rotor positions – Top: 30mm slot depth, bottom: 50 mm.

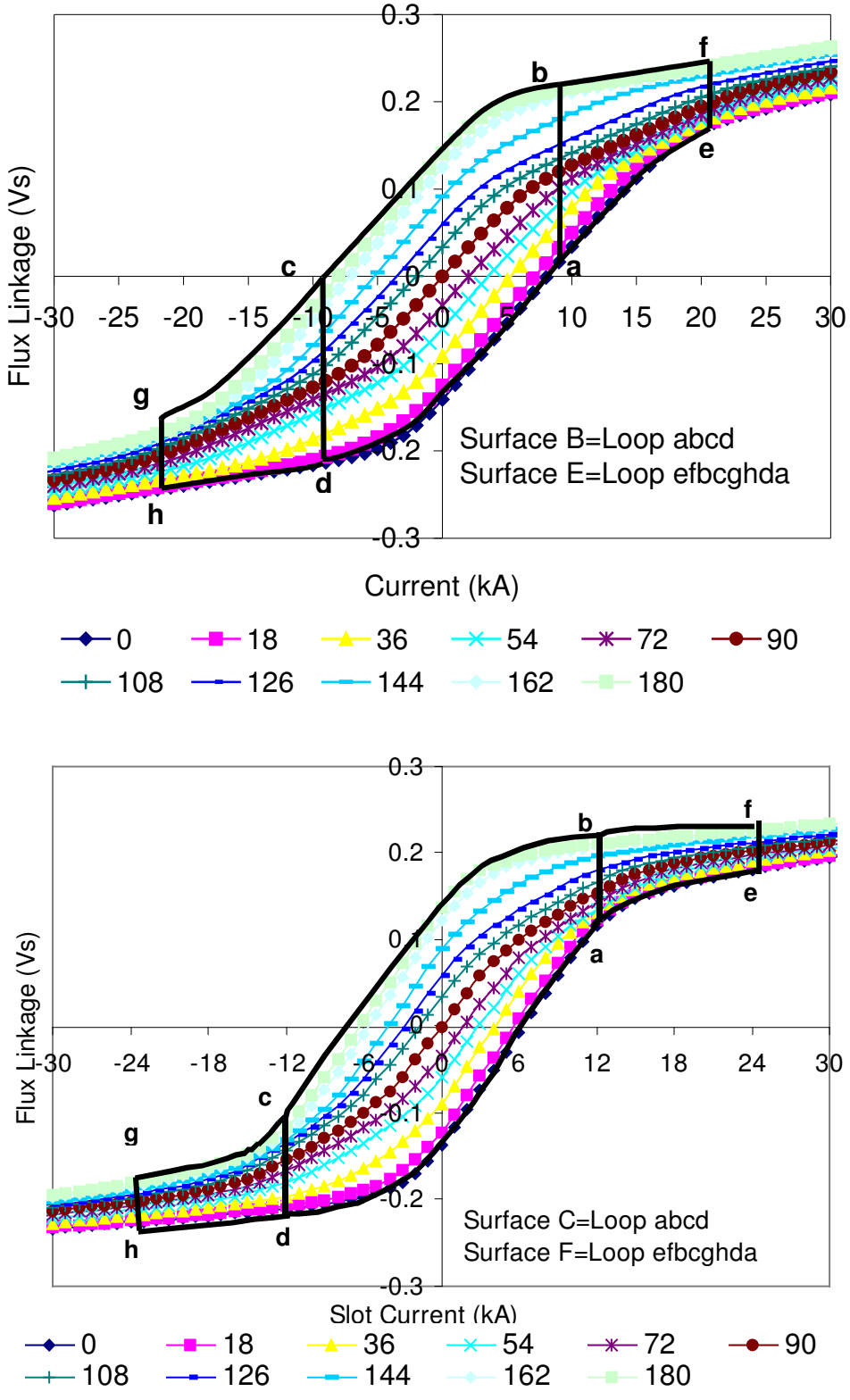

Figure 3.13: Flux Linkage versus slot current at different rotor positions – Top: 100mm slot depth, bottom: 200 mm.

The force density increases with the stator current amplitude. Thus the loop area of ψ-I characteristic is directly related to the force density and it varies greatly with slot depth. From the plots of Figures 3.12 and 3.13, it is obvious that a 200-mm slot depth yields a relatively thin loop with smaller enclosed area compared to that of a 50-mm slot depth. While the force density and rated torque increase with current magnitude, the deeper the slot the lower will the peak torque capability be. It decreases both because saturation makes loop area smaller and also because the peak flux linkage is reduced with slot depth due to increased leakage. Obviously, for a given application and stator cooling arrangements, there is a slot depth at which the force density is a maximum, as indeed was illustrated in the previous sections following a totally different treatment.

It may be noted the Ψ-I graphs presented here are very different than that presented in [37]. This is due to the deep slots and high currents assumed here which lead to higher flux-linkage values. The Ψ-I graphs in [37] are more applicable to *normal* low force density machines.

Figure 3.14 and 3.15 show the flux-linkage versus current density for slot depths of 30, 50, 100 and 200 mm. If we assume that at continuous and transient condition a slot current density of 10 A/mm^2 and 20 A/mm^2 is accepted, it is evident from the plots that the smaller slot depth of 30 mm would be more suitable to produce a higher force density.

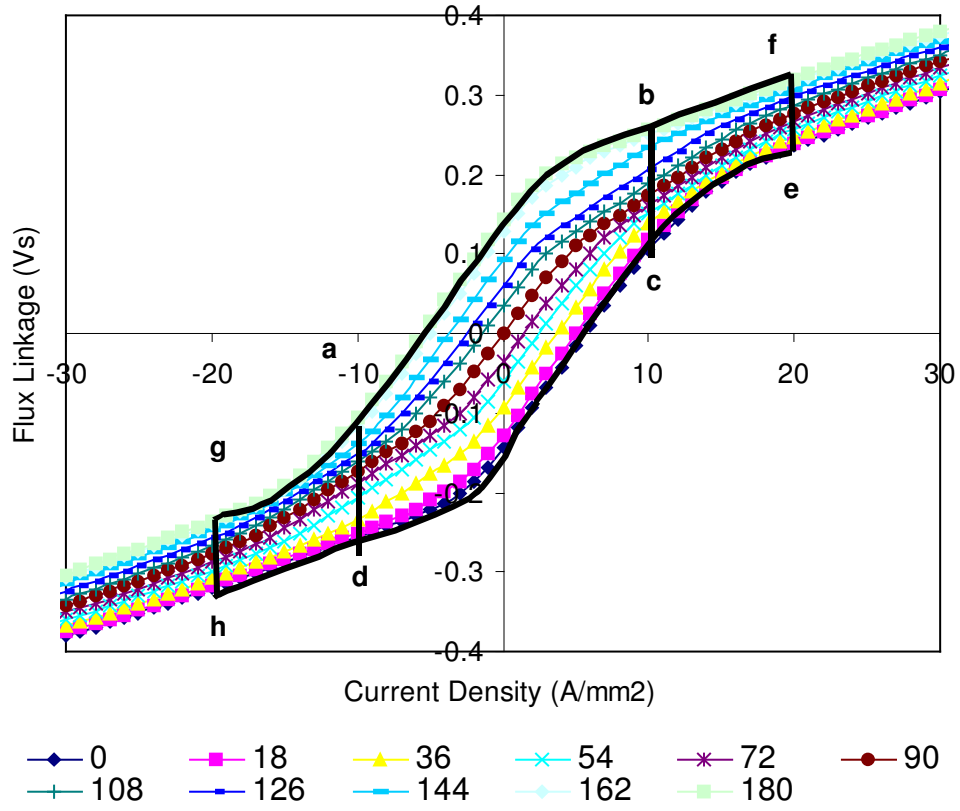

Figure 3.14: Flux Linkage versus current density at different rotor positions. Slot depth: 30 mm (top) 50 mm (bottom).

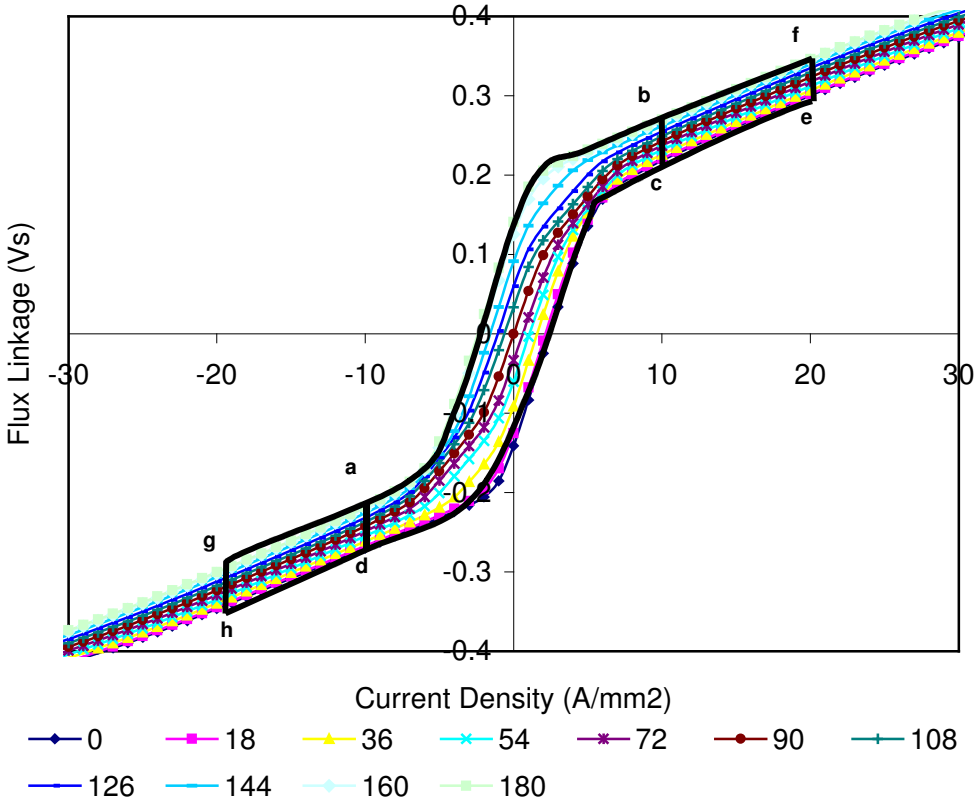

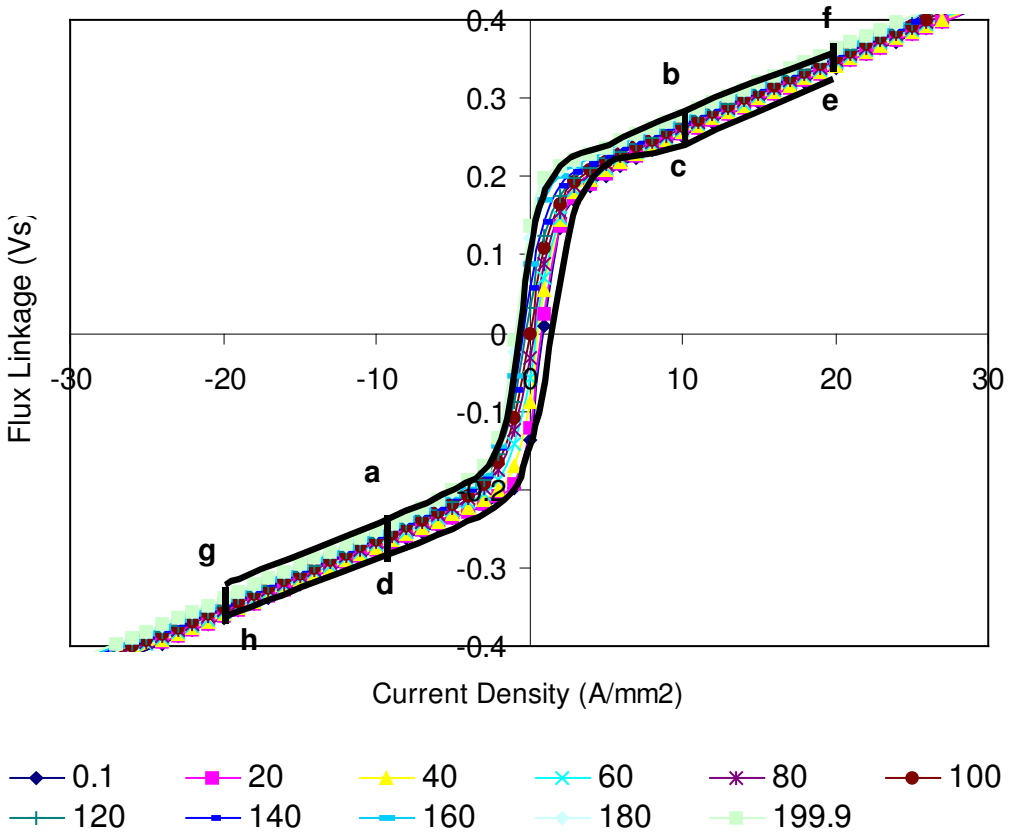

Figure 3.15: Flux Linkage versus current density at different rotor positions. Slot depth: 100 mm (top) 200 mm (bottom).

3.7. APPLICATIONS

Although the objective of the work presented in this chapter is primary to determine the approximate peak force density limits and the way they generally vary with slot depth and current density, the approximate force density values for four direct-drive applications are presented here in order to demonstrate the practical significance of this research work.

The choice of slot depth depends on the relative importance of meeting continuous and transient operating conditions. In applications where high force densities and electric loading are required due to limited space and the short-term peak torque requirements is of high importance, such as direct-drive in-wheel

traction motors, slot depths of no greater than 100 mm should be used to fulfil the peak torque requirement. On the other hand, in applications where continuous operation is more important than transient operation, such as wind generators, slot depth up to 200 mm can be used. A slot depth greater than this value would not result in an increase in the achievable peak force density as this would only lead to an increase in the converter kVA requirement due to the greater inductance [5].

Table 3.5 categorises example applications according to the relative importance of peak and rated condition and summarises the maximum slot depth that can be used by the designer. The slot depths ranges of the first three applications, in Table 3.5, are determined with respect to the typical hub size of the wheels. The traction in-wheel motors for wheelchair, golf carts and forklift trucks, are mainly designed to meet the peak torque requirement instead of the rated torque. The minimum peak force density required in a wheelchair, golf cart and forklift truck motors would be approximately 20 kN/m^2, 18 kN/m^2, 50 kN/m^2, respectively. This would enable the motor to be fitted into the hub of the wheels within the available space.

In wind generators, however, the continuous rated conditions are of greater importance. The force density would typically be 70 kN/m^2 with a 150 mm slot depth (Figure 3.4 and 3.5). For a 1.5 MW wind generator having a rated speed of 18 rev/min, transportation and mechanical considerations limit the diameter and active length to about 4.2 and 1.5 m, respectively. With a rated torque of approximately 800 kNm, one would require a force density of, approximately, 50 kN/m^2.

The peak force density required in each of the applications will increase as the active axial stack length is reduced. The percentage

in which this reduction is permitted will be set by the thermal limits, as a greater electric loading will be essential in fulfilling the peak torque requirement.

Table 3.5: Force density values and slot depth range for four directly-driven machines

Application	Operating Condition	Slot Depth Range (mm)	Required Force Density (kN/m^2)	Possible Force Density (kN/m^2)
Wheelchair	Transient	<35	20	30
Golf-cart	Transient	<45	18	32
Forklift Truck	Transient	<70	50	70
Wind Generators	Continuous	<200	50	70

CHAPTER IV

FORCE DENSITY LIMITS IN FRACTIONAL-SLOT MACHINES

4.1. INTRODUCTION

The previous chapter considered the achievable force density in machines of integral-slot designs. More specifically, a machine having one slot per pole per phase (q) was assumed. This is of course fully justified in view of the large number of poles required in the low-speed in-wheel motors considered in this thesis. Machines with a small whole number of slots per pole per phase, however, have appreciable high-order harmonic *emfs* induced in the armature winding. This is because the corresponding winding elements of each phase under different poles occupy similar positions with respect to the pole flux; the *emf* harmonics of all groups of the winding phase therefore add algebraically and their full magnitude contributes to the resultant *emf* of the entire armature. If the winding is wound with a fractional number of slots per pole per phase (q), and has a sufficiently well selected fractional coefficient, the separate elements of the winding belonging to a given phase would be under different poles, in different positions relative to the magnetic field. The displacement of these elements relative to the

pole axis may be chosen so that the fundamental *emf* will be only slightly reduced but the higher-order harmonics will diminish.

In this chapter the force density limits are investigated for machines utilising fractional-slot windings. This type of windings although have been used in some specialised applications, such as electric clocks, for many years, it is uncommon in industrial applications. A brief review of ac machine winding design, with some focus on fractional slot arrangements, is therefore presented first.

4.1.1. ARMATURE WINDING FOR AC MACHINES [1,2]

In a rotating electric machine, coils are so arranged that when one coil-side is under the influence of a north pole, the other coil-side, of the same coil, is under the influence of a south pole, i.e. the coil span is approximately one pole-pitch. The reason is obvious since in this way, although the *emf* is outwards in one coil-side and inwards in the other, the back-to-back connection causes the *emfs* to be additive round the coil circuit. There are some advantages, as will be explained later, in having chorded coils in which the coil-sides are not exactly one pole-pitch apart. The coils are laid in succession round the armature periphery and are normally embedded in slots which, in general, may be open, semi-closed or closed. New adhesives have permitted direct bonding of the coils onto a smooth iron core, leading to a slotless design.

The coils may be interconnected in a variety of ways and it is really in this that windings differ. There are two basic physical types of arranging the coils, namely single-layer and double-layer windings. Figure 4.1 illustrates a single-layer arrangement in which the whole of the slot is occupied by the side of one coil. Such a single layer

would either contains a number of turns insulated from each other or have a copper section subdivided to reduce eddy-current losses. To limit the number of awkward bends in the end connections, single-layer coils are placed concentrically in small groups, which are interlinked in such a way as to minimise both the space taken up outside the slot in the end connections, and the number of different coil shapes. Single-layer coils lend themselves to the use of semi-closed or closed slots, the coils being preformed at one end, pushed through the slots and connected up at the free end during the winding process.

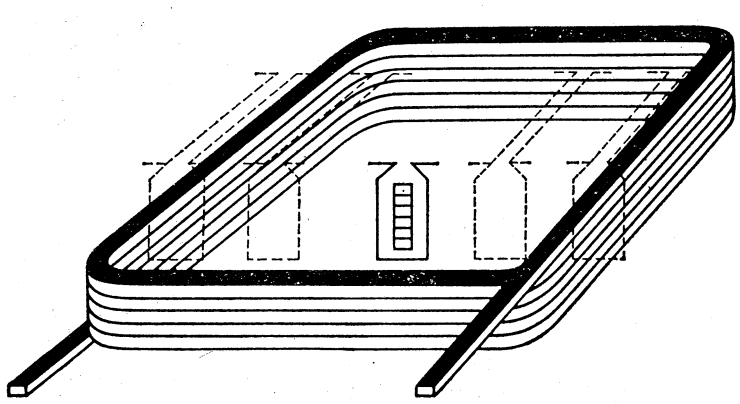

Figure 4.1: Single-layer concentric coil.

In the double-layer winding one coil-side lies in the top half of the slot and the other side in the bottom half of another slot approximately one pole-pitch away, as shown in Figure 4.2. The double-layer winding gives greater flexibility in design because of the ease with which the coil pitch can be chosen. Open slots are frequently used and the coils are laid in them one after the other round the periphery. There are two ways of bending the front-end connections of each coil; inwards yielding a *lap* winding, or outwards to form a *wave* winding.

In a poly-phase ac winding, the ends of each phase are normally brought out to the terminal box and any desired interconnections can

be made externally. In a three-phase winding, the conductors are arranged in three balanced sections. These must be identical in every way except for the physical displacement which gives rise to the mutual time-phase displacement of 120 electrical degrees in the generated phase *emfs*.

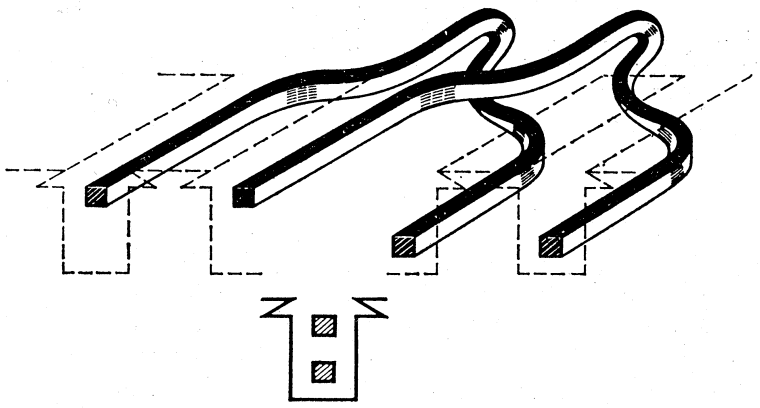

Figure 4.2: Illustration of a double-layer winding.

WINDING FACTOR

A winding circuit consists of a large number of conductors in series, for which the *emfs*, in general, are not all in phase. This phase displacement occurs for two reasons: (i) distribution of the winding in several slots and (ii) coil pitch may not be equal to pole-pitch. Since the vector sum of these conductor *emfs* must be obtained, both of these effects reduce the machine's induced voltage, but this is not an overall disadvantage.

The time variation of *emf* for a single conductor corresponds to the spatial variation of air-gap flux density. This is not purely sinusoidal, being often particularly rich in lower-order harmonics. By suitable winding design, the percentage reduction of the harmonics can be made much greater than that of the fundamental.

Consequently, the waveform of the circuit voltage approaches more nearly to a pure sine wave.
The winding factors express mathematically the per unit reduction of the fundamental and each harmonic which takes place as a result of distribution and chording. In practice the fundamental is rarely reduced by as much as 10% whereas the harmonics are often reduced to negligible proportions. The same winding factors apply to the space distribution of *mmf* and so reduce the *mmf* space harmonics.

Distribution factor k_d

Figure 4.3 shows the components and the resultant of the *emfs* due to a phase group for a machine having 3 slots per pole per phase (q = 3). Each component phasor is proportional to the *rms* value of the fundamental voltage for a slot conductor. It is displaced from the conductor voltage of a neighbouring slot by the slot angle, α, expressed in electrical degrees. The distribution factor is the ratio of the phasor sum to the arithmetic sum of the component *emfs*. From the geometry of Figure 4.3 we get:

$$k_d = \frac{2R\sin(q\alpha/2)}{q\times 2R\sin\alpha/2} = \frac{\sin(q\alpha/2)}{q\sin\alpha/2} \qquad (4.1)$$

Equation (4.1) gives the distribution factor for the fundamental *emf*. In case of harmonics, the distribution factor can be readily obtained by noting that the pole-pitch of the n^{th} harmonic is 1/n times that of the fundamental. Therefore, electrical angles based on the n^{th} harmonic would be n times those of the fundamental. Thus, the distribution factor of the n^{th} harmonic becomes:

$$k_{dn} = \frac{\sin(q\,n\alpha/2)}{q\sin(n\alpha/2)} \qquad (4.2)$$

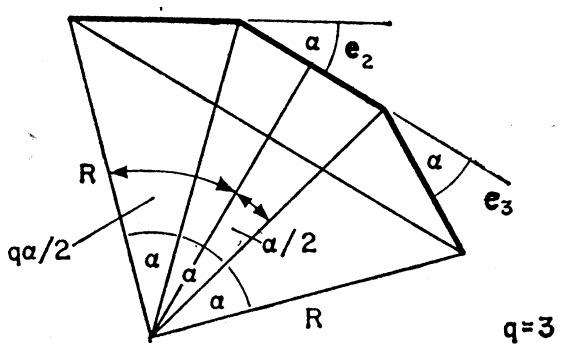

Figure 4.3: Distribution factor k_d.

Coil pitch factor k_c

If a coil is chorded, i.e. coil-pitch is not exactly equal to the pole-pitch, the *emfs* of two coil-sides will not be in phase and must be added vectorially. The coils are usually short-pitched, i.e. the pitch is $x\pi$ electrical radians, being less than the full pitch by the chording angle β, taken as 30^o in Figure 4.4, while x is the per unit pitch.

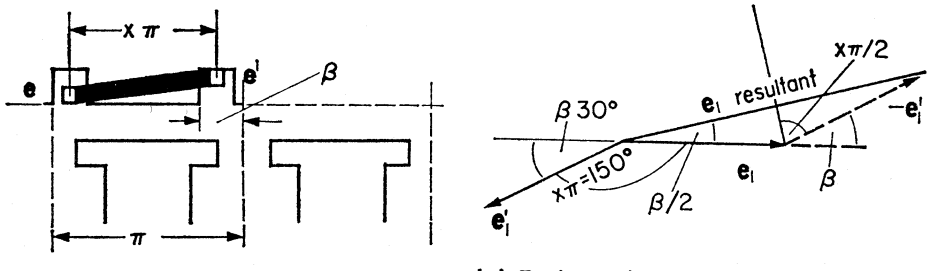

Figure 4.4: Chording factor k_p.

The coil pitch factor is defined as the ratio of the phasor sum of coil-sides *emfs* to their arithmetic sum. Therefore:

$$k_p = \frac{2e \sin(x\pi / 2)}{2e} = \sin\frac{x\pi}{2} \qquad (4.3)$$

Whether the coil is under- or over-pitched by the electrical angle β, the pitch factor is still given by the sine of half the pitch angle. The general expression for the nth harmonic is:

$$k_{pn} = \sin\frac{nx\pi}{2} \qquad (4.4)$$

4.1.3. Fractional-Slot Windings

These are an advanced form of winding in which the number of slots per pole per phase, q, is not an integer. If, for example we have $q = 5/2$ (say, 30 slots, 3 phase and 4 poles), in practice, this would mean that in one pole-pair the phase group (or coil-pitch) would be alternately 3 and 2 giving 5 slots per pole-pair per phase. In this case the winding pattern will be repeated every two poles. If there had been 27 slots instead of 30, q would have been equal to $9/4$ and the pattern would have required four poles to complete. The denominator gives the number of poles required for a complete pattern and the numerator determines the number of slots that each phase takes up in this distance.

This type of winding permits the use of a standard lamination range for a wide variety of pole numbers. It is of course necessary for a three-phase balanced winding that the total number of slots is divisible by 3, but it is no longer necessary that it should be divisible by the number of poles as well. Another advantage is that the angle between the various conductor *emfs* is reduced. As it is shown above, this in turn reduces the harmonic content of both *emf* and *mmf* waveforms.

End-turns do not contribute to the motor performance. Hence it is often important to have their length minimised. Not only does this save on space; but also minimising end turn length will minimise wire usage thus reducing motor cost. The winding configuration affects the end turns length. The end turns are short when the coil-pitch is one or 2 slots. Anything above 2 requires considerable overlapping of end connections. Table 4.1 shows the coil span or pitch for different slot and pole combination, the benefits of fractional-slot winding are clearly demonstrated. It should be noted that a coil span of one slot, although it requires $q<1$, it offers a distinct advantage as far as manufacturing cost is concerned.

This chapter deals with fractional-slot machines with q = 0.375, 0.5 0.75. The winding pattern spans 8, 2 and 4 poles, respectively, and this is the minimum pole numbers that can be used in these cases. The acceptable number of poles must be an integer number of these values. With q values of 0.375 and 0.5 the end windings cross from one slot to the preceding slot over one tooth only while with q values of 0.75 the windings spans 2 slots. These combinations can be automatically wound easily and are economical to make.

Table 4.1 Coil span for different slot/pole/phase values

Slot/pole/phase (q)	Coil span in slot-pitches	Winding Type
0.25	1	Fractional
0.375	1	Fractional
0.5	1	Fractional
0.75	2	Fractional
1	3	Integral
1.25	3	Fractional
1.5	4	Fractional

1.75	5	Fractional
2	6	Integral

4.1. MODEL DESCRIPTION

The investigation presented in here follow pretty much the same steps adopted in the previous chapter where integral-slot windings are considered. As before, the investigation is limited to low-speed machines where large number of poles will be required. However, here only the surface magnet rotor configuration is investigated. The magnetic model shown in Figure 4.5 was developed in order to investigate the force density in fractional-slot machines. It is shown the geometrical arrangement and typical field plots. Again, the model assumes rectangular open slots and non-linear magnetisation characteristics are assumed for the core material.

4.2. CONTINUOUS AND TRANSIENT FORCE DENSITY

The pole pitch (τ_P), tooth width (b_d), slot opening (b_S) and magnet height (h_m), all vary with slot depth (h_S). Model dimensions are given in Tables 4.2-4.4 for slot per pole per phase values of 0.375, 0.5 and 0.75, respectively. In all cases, rotor magnets with a remanence of 1.25 T and coercive force of 90.5 kA/m are assumed. The winding current density values are, again, used as determined by the thermal limitations [5], but allowing for the unique winding configuration in each case.

The slot currents are increased in steps by multiplying the continuous rated current by a factor varying between 1 and 9.

Figures 4.6-4.8 show the force density variation with slot depth for different current multiplication factors.

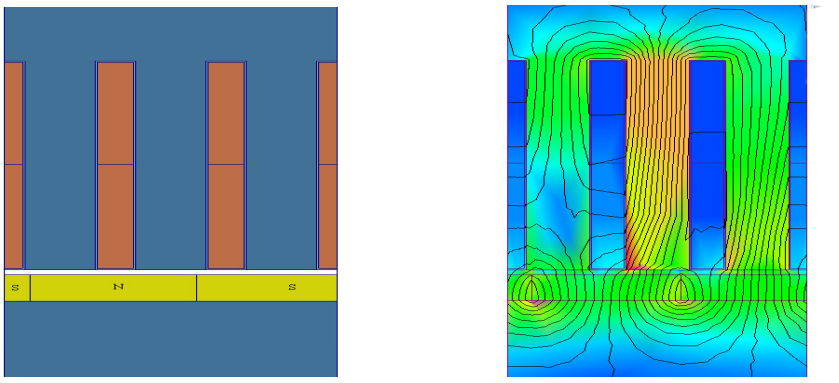

a

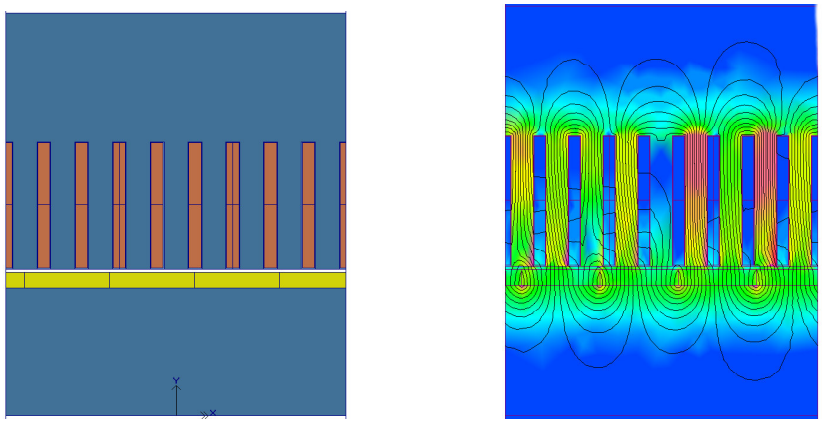

b

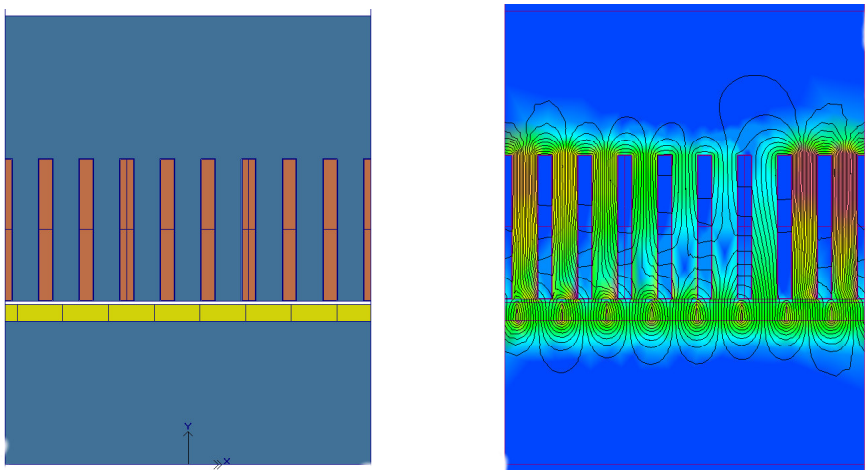

c

Figure 4.5: Model of a fractional-slot machine,

(a) q = 0.5 (b) q = 0.75 (c) q=0.375

Table 4.2: Machine variables for different slot depths, $q = 0.375$.

h_S, mm	b_S, mm	b_d, mm	τ_P, mm	h_m, mm
10	6,11	7,79	15.64	6,26
15	6,22	8,42	16.46	6,59
20	6,52	9,19	17.66	7,07
30	7,15	10,67	20.06	8,02
50	8,24	13,14	24.08	9,62
75	9,29	15,60	27.98	11,20
100	10,12	17,64	31.24	12,49
150	11,43	21,04	36.53	14,61
200	12,47	23,88	40.91	16,36
300	14,14	28,63	48.11	19,25
500	16,66	36,14	59.40	23,76
750	19,10	43,63	70.58	28,23
1000	21,16	49,99	80.06	32,02

Table 4.3: Machine variables for different slot depths, $q = 0.5$.

h_S, mm	b_S, mm	b_d, mm	τ_P, mm	h_m, mm
10	6,11	7,79	20.85	6,26
15	6,22	8,42	21.95	6,59
20	6,52	9,19	23.55	7,07
30	7,15	10,67	26.75	8,02
50	8,24	13,14	32.1	9,62
75	9,29	15,60	37.3	11,20
100	10,12	17,64	41.65	12,49
150	11,43	21,04	48.7	14,61
200	12,47	23,88	54.55	16,36
300	14,14	28,63	64.15	19,25
500	16,66	36,14	79.2	23,76
750	19,10	43,63	94.1	28,23
1000	21,16	49,99	106.75	32,02

Table 4.4: Machine variables for different slot depths, $q = 0.75$.

h_S, mm	b_S, mm	b_d, mm	τ_P, mm	h_m, mm
10	6,11	7,79	31.28	6,26
15	6,22	8,42	32.93	6,59
20	6,52	9,19	35.33	7,07
30	7,15	10,67	40.13	8,02
50	8,24	13,14	48.15	9,62
75	9,29	15,60	55.95	11,20
100	10,12	17,64	62.48	12,49
150	11,43	21,04	73.05	14,61
200	12,47	23,88	81.83	16,36
300	14,14	28,63	96.23	19,25
500	16,66	36,14	118.80	23,76
750	19,10	43,63	141.15	28,23
1000	21,16	49,99	160.13	32,02

As was observed with the integral-slot windings, it is seen that for each current loading value there is an optimum slot depth at which the force density is a maximum. Again, the effect of saturation is demonstrated here with the distance between successive characteristics decreasing as the current multiplication coefficient is increased.

To enable comparison between fractional- and integral-slot windings, Figure 3.5, which gives the force density for various current multiplication factor for $q = 1$, is reproduced here, for convenience, as Figure 4.9.

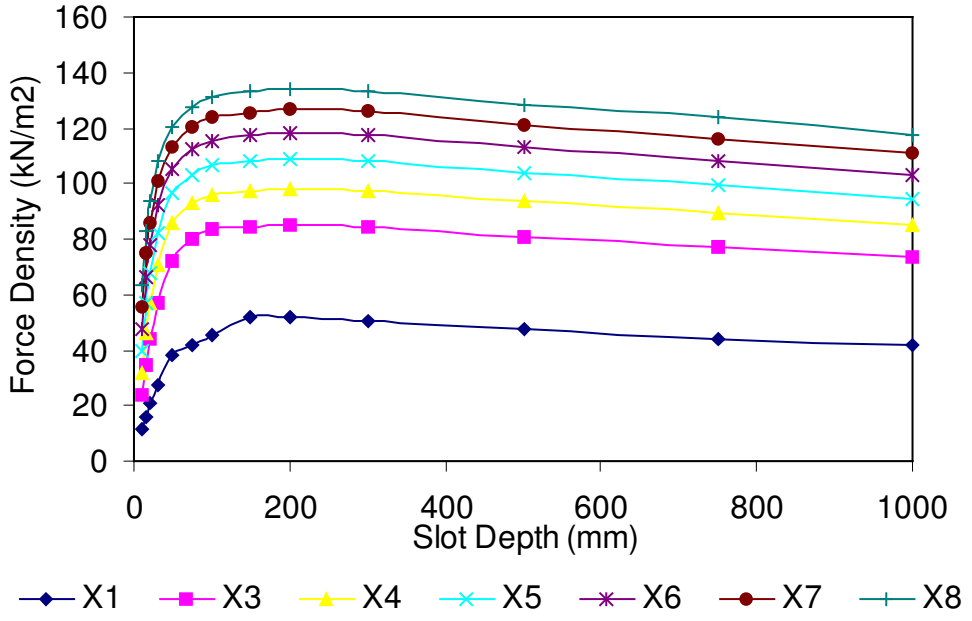

Figure 4.6: Force density versus slot depth, $q = 0.375$.

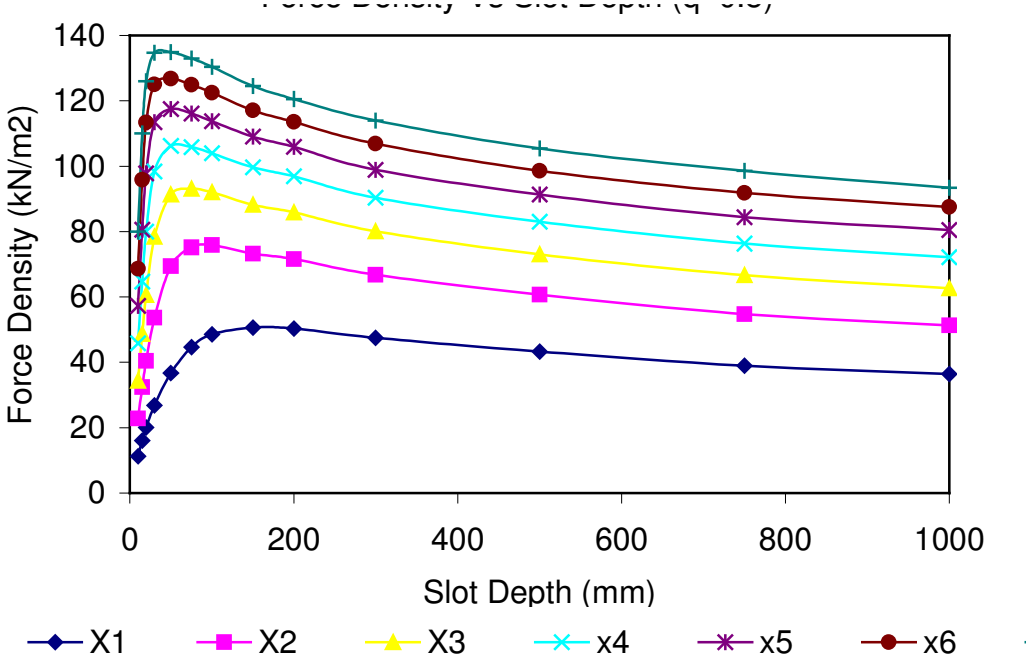

Figure 4.7: Force density versus slot depth, $q = 0.5$.

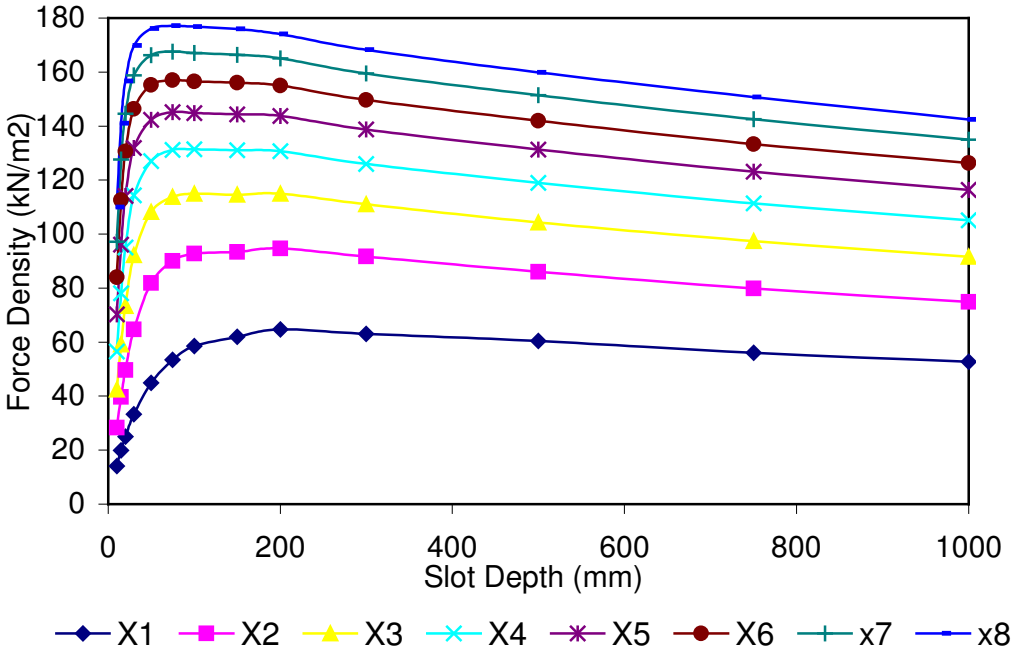

Figure 4.8: Force density versus slot depth, $q = 0.75$.

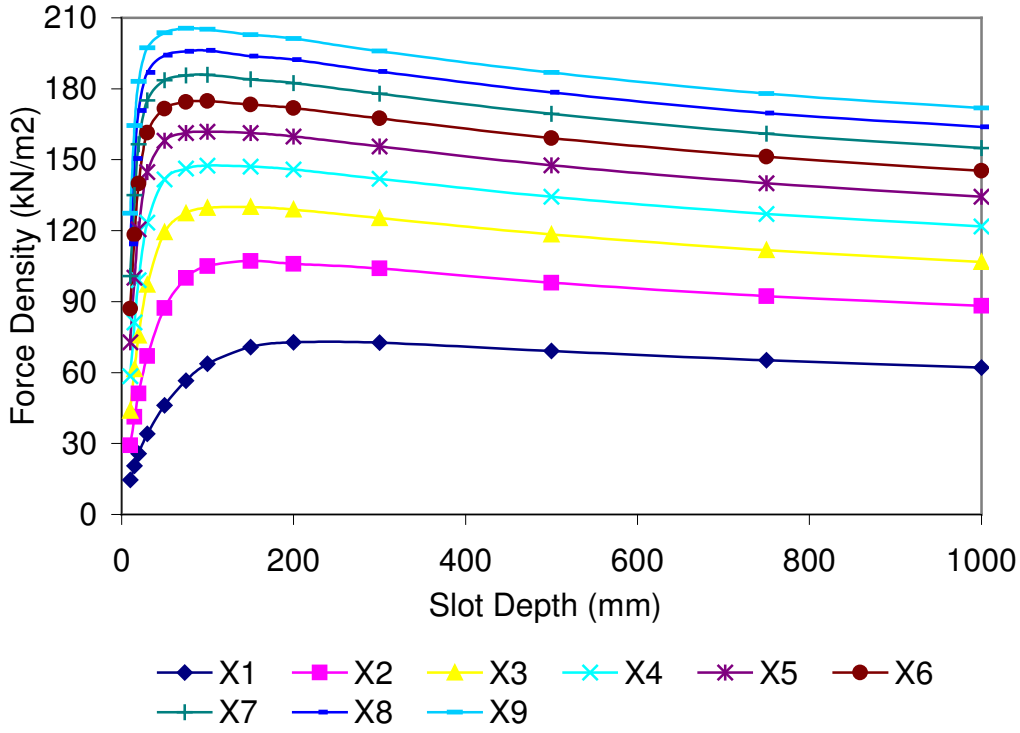

Figure 4.9: Force density versus slot depth, $q = 1$.

Figures 4.6-4.9 demonstrate that the force density values for a fractional-slot winding are less than those of the integral-slot winding. This is expected and is, of course, due to the reduction of the *emf* induced in the stator windings caused by lower values of the winding factor. It is seen that the reduction in force density values is almost independent of the current multiplication factor.

The winding factor for $q = 0.5$ is about 0.866 and it is seen that the force density values for this case, Figure 4.7, are reduced, compared with Figure 4.9, by about the same factor (taking, for example, a slot depth of 200 mm and current multiplication factor of unity, Figures 4.9 and 4.7 give force density of about 65 kN/m^2 compared with 55 kN/m^2, respectively). It should be noted that the winding factor of a full pitch winding having one slot per pole per phase is nearly unity and if an integer value of q greater than one were to be used, the percentage reduction will be less. Of course, for a given air-gap diameter, a longer stack will be needed to obtain the same torque value but the advantages offered by the simple winding construction with $q = 0.5$ would still make such a choice viable in some applications.

Comparison of Figures 4.6 and 4.9 ($q = 0.375$ and 1, respectively) shows that significant reduction in the force density values occur in such a fractional-slot winding (in the order of 25%). At the same time, a value of q less than 0.5 offers only a marginal simplification to the manufacturing process, namely smaller skew angle would be required. Use of slot per pole per phase of less than 0.5 would lead to a substantially longer lamination stack to obtain the required torque and force values and this more than offsets any advantages to be gained.

With q = 0.75, it is seen (Figures 4.8 and 4.9) that the reduction of the force density values are about 7%. Such a fractional-slot winding, although having coils spanning 2 slot pitches, still offers the advantages of ease of winding and harmonic reduction. However, the winding is not as simple as that of a machine having q = 0.5 and the end connections are also longer.

It is the main conclusion of this section that slot per pole per phase values less than 0.5 should only be used when the application requirement warrants this and can tolerate the increased stack length. In the development of the in-wheel motor for wheelchair application, which is described in the following chapter, q = 0.5 is used.

4.3. FORCE DENSITY VARIATION WITH WINDING CURRENT DENSITY

The aim of this section is obtain force density versus slot depth characteristics, for a range of winding current densities, which can be used as a design tool. In-order to be able to utilise these curves for design purposes, they must be produced in terms of the average force density values. Determining these curves for a range of pole-pitches, will enable one to produce a useful database, that can be used to determine if the specification can be meet within the given space. The force density versus slot depth characteristics for different values of winding current density, and for a range of pole-pitches, are given in Appendix III for fractional-slot windings having slot per pole per phase values of 0.375, 0.5 and 0.75. It should be noted these curves are produced for the SMR configuration. Similar treatment can be followed to produce force density characteristics for other rotor designs.

CHAPTER V

DESIGN AND EXPERIMENTAL EVALUATION

5.1. DESIGN SPECIFICATIONS

In this chapter three LPEV applications (a wheelchair, a golf cart and a forklift truck) are considered and brushless solutions are thought. The work concerning the wheelchair was carried out in collaboration with an industrial partner in the UK who provided the technical specifications and stipulated the practical design and manufacturing constraints. It was the requirement of the industrial partner that a geared, brushless, solution be identified, to enable comparison with the in-wheel one, for their commercial decision making purposes. Such a solution was indeed identified. It is not described in this thesis as it lies outside its main theme. The author would be prepared to provide commercially unclassified information regarding the geared solution to interested parties. The design targets for both the in-wheel and geared motors for wheelchair applications are given in Table 5.1.

The specification and design targets for the forklift truck are obtained from a Swedish manufacturer. The specifications used in the work presented below are believed to represent development ideas rather than an existing, geared, product. The industrial

specifications assumed a dc link voltage value of 24V. These specifications are given in Table 5.2. However, the investigation considered the case of doubling the assumed dc link voltage, to 48 V, in order to demonstrate the advantages of increasing system voltage.

Table 5.1: Design specifications for a wheelchair drive.

	Direct-Drive	Geared
DC supply voltage, V	24	24
Controller peak current limit, A	65	35
Short term torque rating (1-min, 1/2 speed)	65 Nm	1.82 Nm
(a) Short term rated output power, W	510	285
Continuous rated speed, rev/min	150	3000
Continuous rated power, W	285	150
Ambient temperature range, °C	-25 to 50	-25 to 50
Insulation class	Class F	Class F

Table 5.2: Design specifications for a forklift truck.

	Direct-Drive	
DC supply voltage, V	24	48
Controller peak current limit, A	300	300
Short term torque rating	445 Nm	445 Nm
Short term rated output power, kW	3.2	3.2
Continuous rated speed, rev/min	258	258
Continuous rated power, W	595	595
Ambient temperature range, °C	-25 to 50	-25 to 50
Insulation class	Class F	Class F

Table 5.3: Design specifications for a golf cart.

	Direct-Drive	Geared
DC supply voltage, V	48	48
Controller peak current limit, A	65	35
Short term torque rating (1-min, 1/2 speed)	65 Nm	1.82 Nm
Short term rated output power, W	1000	571
Continuous rated speed, rev/min	300	6000
Continuous rated power, W	570	300
Ambient temperature range, °C	-25 to 50	-25 to 50
Insulation class	Class F	Class F

The golf cart specifications, as per Table 5.3, are derived by the author utilising catalogue information of a number of manufacturers. The system voltage of the majority of normal duty golf carts is 48 V.

For the wheelchair in-wheel motor, a large constant torque is required at low speeds, from zero to 75 rev/min. From 75 rev/min up to the maximum speed, a constant power control is required. The peak torque in the constant range is 65 Nm and the maximum speed is approximately 250 rev/min. The motor must be designed to fit within the hub of an existing wheel having an outside diameter of 12 inches (305 mm); as was stipulated by industry. The wheel speed must be limited to 250 rev/min. For the geared motor, a constant torque of 1.82 Nm is required from zero to 1500 rev/min. From 1500 rev/min to 3000 rev/min, a constant power control is required. The wheelchair and the golf cart have similar peak torque requirements with the later requiring a larger speed range. This can be achieved with a system voltage of 48 V.

The hub of the wheel of the forklift truck was fixed, by industry, at 280 mm. This size is comparable to an in-wheel motor of a power electric wheelchair having a peak torque requirement of only 65

Nm. However, the peak torque requirement in the forklift truck, at 445 Nm, is approximately comparable with the requirements of an electric passengers vehicle having an outer diameter of, say, 340 mm. The losses in a motor producing such a high peak torque are very large (compared to the wheelchair motor) and additional cooling features would be required. Thus the forklift truck motors are designed with respect to their peak torque requirement instead of their thermal capacity, as limited information on the drive cycle is available. If the drive cycle was available, the intermittence could be known and a comparison between the thermal time constant and drive cycle could be made for each motor designed. Hence the motors could be sized according to their thermal demands instead of their peak torque tailoring the optimisation process towards a final design of reduced volume. Much of the design work presented below is directed at achieving a high efficiency motor with low torque ripple, keeping in mind the cost factor, size constraints and demands made on the motor.

5.2. DESIGN CONSIDERATIONS

Lamination and winding design are the main factors that influence the ability to automatically and economically assemble a stator. They must be considered at the design stage in order to minimise the stator assembly cost. The wire size, number of turns, winding configuration and pole-slot combination all affect the ease, or otherwise, of building the stator. The lamination itself cannot be altered without paying large penalty in modification to tooling. Unlike, the lamination design, winding specification can be changed without major penalty. The following describes some design features that has to be considered to enable realisation of an optimised and economically manufactureable design.

5.2.1. STATOR LAMINATION

Since the laminations are cut from stripped material the diameter of the lamination will be important from the material savings standpoint. This must be considered when direct drive machines are used due to the greater machine size.

It is always desirable to have large slot opening for simplicity of manufacture. However a larger slot opening will result in low motor performance and increase in audible noise. Usually the slot opening selected should be a compromise between the design requirements and manufacturing process. The slot opening should be set no less than 2 mm. Also it was recommended, by industry, that the slot opening should be set to 0.5 to 0.7 mm greater than the wire thickness which will, obviously, vary depending on the motor size. The tang angle should be kept as small as possible. A maximum limit of 30 degrees was set. This is important as the tooth dimensions directly affects the injection blade design.

5.2.2. SLOT SHAPE

It is usually desirable to have deep, narrow slots. This ratio of slot depth to width would be typically about 4. In applications where space is limited this factor must be optimised to obtain the highest possible force density, as was illustrated in the previous two chapters.

Generally there are 2 types of slot configuration, the round and square bottom. The round bottom slots are the preferred shape as during insertion process the wire has the tendency to fill the back of the slot and roll into the corners; thereby yielding a good fill factor.

The probability of this occurring in the square bottom slot is low, as the winding tend to stay at the back of the slot.

5.2.3. STATOR WINDING

Winding specifications, such as wire size, turns and number of strands are important for automatic stator processing. Unlike lamination, wire sizes and the number of turns can be varied to a certain level without affecting drastically the machine performance. Generally there are two basic types of winding configuration: concentric and lap windings. The concentric type winding is usually preferred, as lap windings cannot be automatically inserted into the slots.

5.2.4. ROTOR DESIGN

The choice of pole numbers depends on many factors such as inertia, torque, cogging torque and speed. With high pole numbers it becomes possible to use a one coil per group, short-pitched, winding which can eliminate the overlap of the end turns. The greater the pole number the smaller becomes the size of the machine.

The effect of increased flux by using magnet overhang can be quite significant on a short-stack motor.

5.3. THE WHEELCHAIR MOTOR

In order for the electric motor to be suitable for use in a direct-drive system, it must have a relatively low mass, high torque to mass ratio, low cost and operate at a reasonably high efficiency in order to maximise vehicle range. A drop in motor efficiency increases the current drawn from the battery and decreases its life and efficiency. The motor should have physical dimensions that are amenable to

location in the drive wheel. Slotted stators in brushless motor cause cogging which adversely affects motor performance especially when the motor is directly coupled to the load. Cogging contributes to efficiency loss, motor and load vibration, and noise. Cogging also is a component of torque ripple, which prevents smooth motor operation especially at low speeds. Thus cogging torque should be reduced to an acceptable level for smooth operation.

Another requirement of the design described here is that the phase inductance must be kept as low as possible to allow the use of an existing brushless motor controller forming part of the industrial partner's range of system modules. The controller is optimised for trapezoidal back *emf* windings and it may be programmed to operate with wide range of 3-phase BLDC motors and wheelchair configuration.

In deciding whether to opt for a sinusoidal or a trapezoidal type motor, compatibility with the existing controller was a prime factor. This is designed for constant current (squarewave) operation and the BLDC design was hence adopted.

The approach followed in arriving at designs that meet the specifications is to utilise established design rules to obtain a preliminary design, utilise a circuit based CAD, time-stepping simulation program (which has in-built databases for typical and user-defined magnet and steel materials) to examine and improve the design, including parameters of the power-electronic converter and control, and then employ the finite element method to fine-tune the magnetic circuit. Such CAD and FE packages are of course calculating, rather than design, tools. Hence they improve the productivity of the design engineer enabling evaluation of

alternative designs efficiently, but can make no judgement and this is still the designer's task!

5.3.1. NUMBER OF POLES

In the initial stage of the design process, the pole numbers were varied keeping the outside diameter and air-gap diameter constant at 200 mm and 184 mm, respectively, as this is determined by the wheel size, and choosing sintered NdFeB as the magnet material. Design calculations assumed an operating temperature of 100^{o}C.

Table 5.4 summaries some of the designs studied. It shows that there is a small improvement in overall performance as the pole number is reduced from 36 to 28 due to the reduction in stator iron losses, but any further reduction yields inferior performance manifested in a reduction in peak torque. This is due to the increasing size of the end windings and flux return paths.

Table 5.4: Effect of number of poles on motor performance.

Design number	D1	D2	D3	D4	D5
Number of poles	36	32	30	28	26
Slots	42	48	45	42	39
Coil span	1	1	1	1	1
Packing factor	0.273	0.236	0.239	0.256	0.257
Pole arc	180	180	180	180	180
Stack length, mm	57	62	70	80	80
Slot depth, mm	25	20	25	20	23
Tooth width, mm	4.5	5	5	5	5.8
Turns/coil	4	4	4	4	4
Wire diameter, mm	1.5	1.12	1.3	1.3	1.4
Strands	2	3	3	3	3
Back iron depth, mm	4	5	4	5	5
Copper weight, kg	0.894	0.724	1.018	1.075	1.174
Iron weight, kg	6.23	7.36	9.44	9.29	9.08
Efficiency, %	83.4	82.6	83.4	84.5	86
Peak torque, Nm	76.5	73.7	75.61	77.92	75

5.3.2. PROTOTYPE DESIGN

Having established that 28 poles yield the most balanced design, design D4, Table 5.4, was subjected to further modifications. It was necessary, for mechanical reasons, to redesign assuming an outside diameter of 190 mm, compared to 200 mm in design D4. A finite element field plot, shown in Figure 5.1, confirms that is achievable while the flux density values everywhere in the magnetic circuit remaining below saturation levels. Furthermore, a smaller wire diameter was chosen, for manufacturing reasons, and an appropriate increase in the number of turns per coil was made. Table 5.5 gives the details of the experimental in-wheel motor.

Table 5.5: Design details of a wheelchair in-wheel motor.

Number of pole	28
Number of slots	42
Stack length, mm	56
Magnet axial length, mm	60
Outside diameter of rotor back iron, mm	190
Inside diameter of rotor back iron, mm	184
Rotor air-gap diameter, mm	178
Stator air-gap diameter, mm	177
Stator bore diameter, mm	144
Magnet layout	Radial configuration, 180^{o} pole arc.
Magnet material	Sintered NdFeB, Br=1.29T
Stator stack	1 slot pitch skew
Winding	3 phase, 0.5 slot/pole/phase, double layer, 5 turns per coil, 14 coils per phase.
Turns in series per phase	70
Bare wire diameter, mm	1.2
Drive	Squarewave
Steel material	M19-24 gage

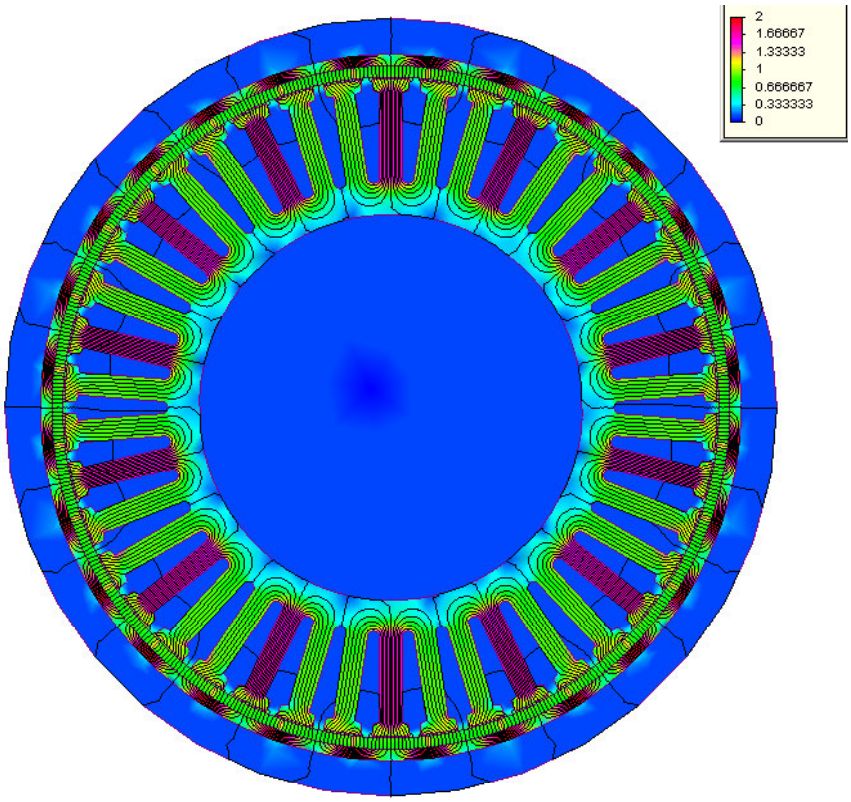

Figure 5.1: Field plot and flux density values (top right) – wheelchair motor.

The motor's main components are the stator and rotor assemblies and the position sensing arrangements. These are now described in details.

Stator Assembly

The 42 equally spaced, slotted stator in which the 3-phase windings that generates the electromagnetic field are lodged, is constructed using high quality silicon-iron steel lamination sheets to reduce the core losses that increases rapidly at high flux densities. The stator laminations were spark eroded from the material M19-24, 0.56 mm. Each individual lamination is covered with an insulating varnish and laminations were arranged into a vertical stack, pressed and then fused to form the solid uniform 56 mm core shown in Figure 5.2.

Figure 5.2: Stator core and bearing.

The 42 stator teeth have a circumference tooth width of 6 mm, a tooth height from the root to the tip of 28 mm and a 3-mm thick tooth tip. The circumference slot opening between adjacent teeth is 3 mm with each tooth having a tang angle of 30°. The stator yoke thickness is 18.5 mm and the available shaft space is 84 mm diameter to enable sufficient space to mount the stator-mounting boss.

To ensure the performance of the motor at high torque, the tooth width and back iron depth were made sufficiently large to ensure that the quasient flux density was somewhat below saturation level to allow armature reaction flux to flow without distortion of the back *emf* waveform and risking excessive reductions in torque per ampere.

A stator-mounting boss, shown in Figure 5.3, was milled from an aluminium block and is used to clamp the steel lamination sheets in place. With reference to Figure 5.3, when the screws in the stator-mounting boss are tightened the steel lamination sheets will be tightly clamped. When screws are released the stator lamination stack can be skewed to any angle desired. This arrangement enabled changing of the skew angle during development. Of course, the mounting boss was not used in the pre-production prototype where skewed laminations were fused together. The wheelchair shaft is 25 mm in diameter. Two keys are machined into the shaft. An axial groove keyway is machined into the inner surface of both stator-mounting bosses. During assembly both keys on the shaft lodge into the keyway creating a rigid lock.

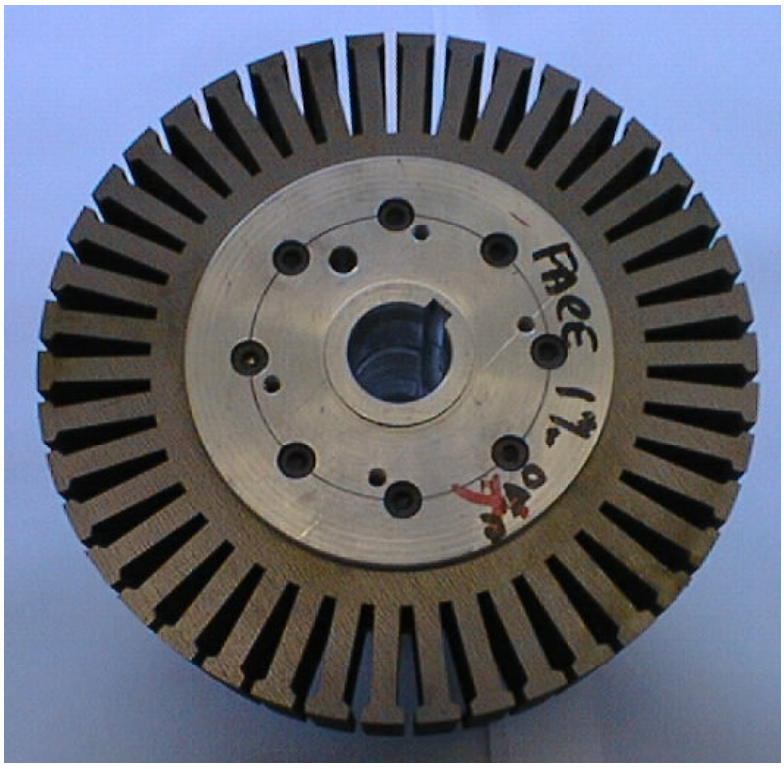

Figure 5.3: Mounting boss.

The winding was arranged so that each slot carries 10 conductors, 1.2 mm thick in diameter insulated to class F. There are 3 strands per conductor and 5 turns per coil, 14 coils per phase, (i.e. 28 coil-sides per phase), and 70 turns in series per phase. Each coil has a mean turn length of 141 mm. The winding arrangement is of the double-layer, fractional slot, concentric, bobbin type. The motor has 1.5 slot/pole i.e. 0.5 slot per pole per phase. Hence the bobbin winding used has a span of 1 slot-pitch or 120 electrical degrees. This results in a compact design with no bulky end windings caused by overlapping. The assembly process is simplified and the winding insertion in the slot is less tedious. The total area occupied by the windings in the slot is 32.8 mm^2. The slot area for the final design was 120 mm^2. Thus the fill factor was approximately 35%. Although a larger fill factor could be obtained, during the design stage a fill factor of 35% was a realistic figure. A greater fill factor is possible and a machine of higher efficiency can be obtained for the same current. The winding factor is 0.716. A slot linear of 0.20 mm thickness was used to insulate the windings from the slot walls.

Rotor Construction

The outer rotor is provided with 28 magnet segments. The magnets were delivered machined to their final shape. Each pole segment is 3 mm in radial thickness and is made up of 2 blocks of 30 mm arranged axially resulting in an overall axial length of 60 mm, taking into account the 2 mm magnet overhang at each end of the rotor. Due to the large outer diameter the magnets were approximately square shaped. The magnet segments are epoxyed to the inner surface of a 190 mm diameter, mild steel rotor tube of 70 mm overall axial length, to keep the rotor poles in place. The steel tube that acts as a rotor yoke (return path completing the magnetic circuit) has a radial thickness of 3 mm. Figure 5.4 shows the rotor casting and end cover.

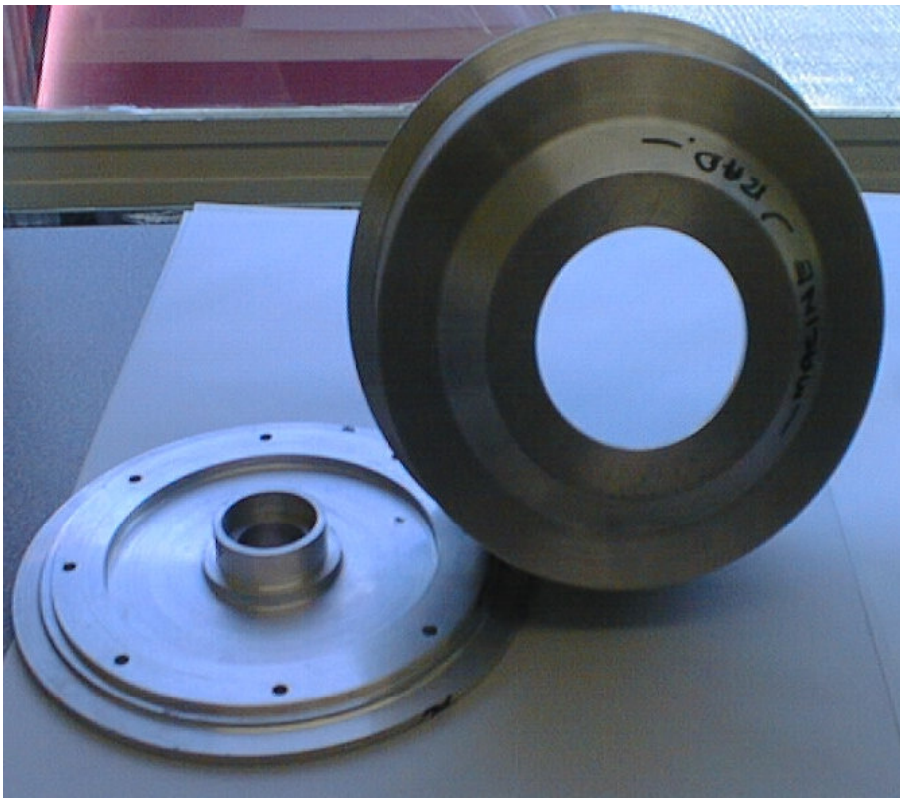

Figure 5.4: Rotor casting (right) and end cover (left).

Eight holes were drilled on the end cover and surface of the stator casting. These holes where the screws are lodged in, and the end cover retaining ring serves the purpose of locking the end cover and the stator casting together making these components to act as a single unit, as shown in Figure 5.5.

The permanent magnet blocks are magnetised to have an approximately trapezium-shaped magnetic field distribution over the circumference. The magnet material used (NdFeB) is characterised by linear demagnetisation, good thermal stability, high coercivity and high energy density. The B_r and H_c of the magnet material chosen are 1.29 T and 940 kA/m respectively. The high energy density results in a smaller motor, and the high coercivity allows higher peak-to-continuous torque ratios without risk of demagnetisation.

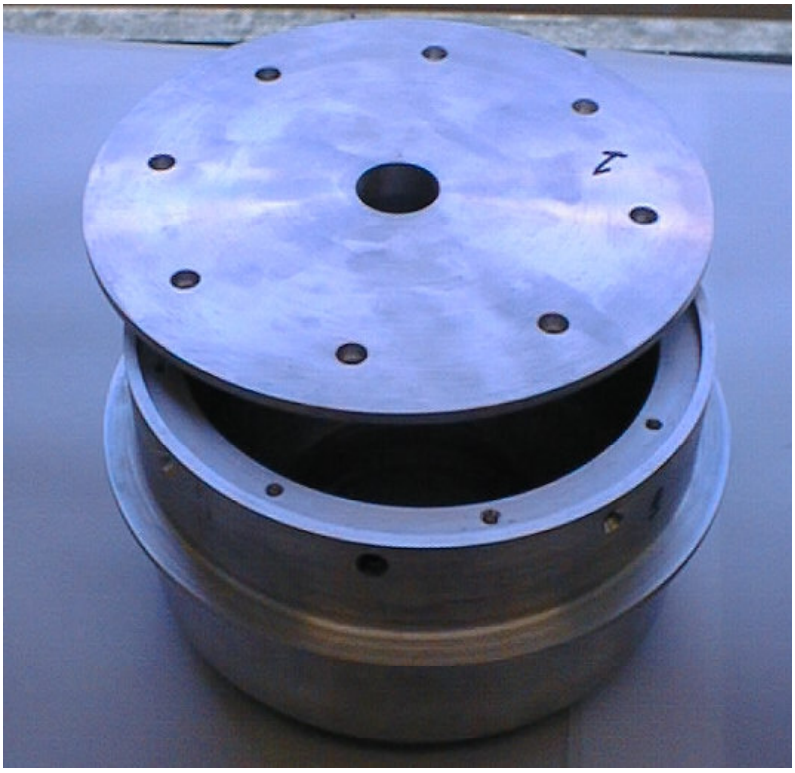

Figure 5.5: End cover retaining ring.

With NdFeB the higher flux density allows a smaller electric loading (hence less copper) in the motor while the high resistance to demagnetisation allows radially thin magnets (3 mm) to be used. Since the motor will be operating at high peak currents as the rotor rotates, stator *mmfs* cause large disturbances to the flux density distribution in the air-gap and magnets. It is therefore expected that sections of the magnet will experience stator *mmfs* which tend to weaken the rotor magnetic field. Hence it was ensured that the magnet operating point does not move too far down the demagnetisation characteristic. This is to avoid the operating point moving beyond the region of linear demagnetisation, hence avoiding problems of irreversible loss of magnetisation. Low permeability material such as NdFeB have the advantage over steel alloy permanent magnet materials that a given stator *mmf* causes less disturbance to the flux density distribution in the air-gap. Both the experimental and prototype motor, like most rare-earth magnet motors feature a relatively high specific torque output.

Position sensing

Initially the sensing system was based on a 28-pole magnet disc and 3 hall sensors. During preliminary tests it was observed that the motor's trapezoidal back *emf* waveform could not be brought into simultaneous alignment with the sensor signals. This resulted in significant mismatches between the controller output signals and the motor current requirements. It was discovered that the problem was caused by the sizes of successive poles on the 28-pole magnet disc being distinctly non-uniform. After due consideration it was decided to replace the sensor system by a one based on a specially developed toothed aluminium disc and 3 optical sensors. This proved to be satisfactory. The sensors are placed 8.57° (mechanical) or 120° (electrical) apart, as shown in Figure 5.6. A 14 equally spaced slotted aluminium disc mounted on the rotating shaft is used to break the light beam. The sensors are operated at a reduced voltage of 5V to provide long life capability.

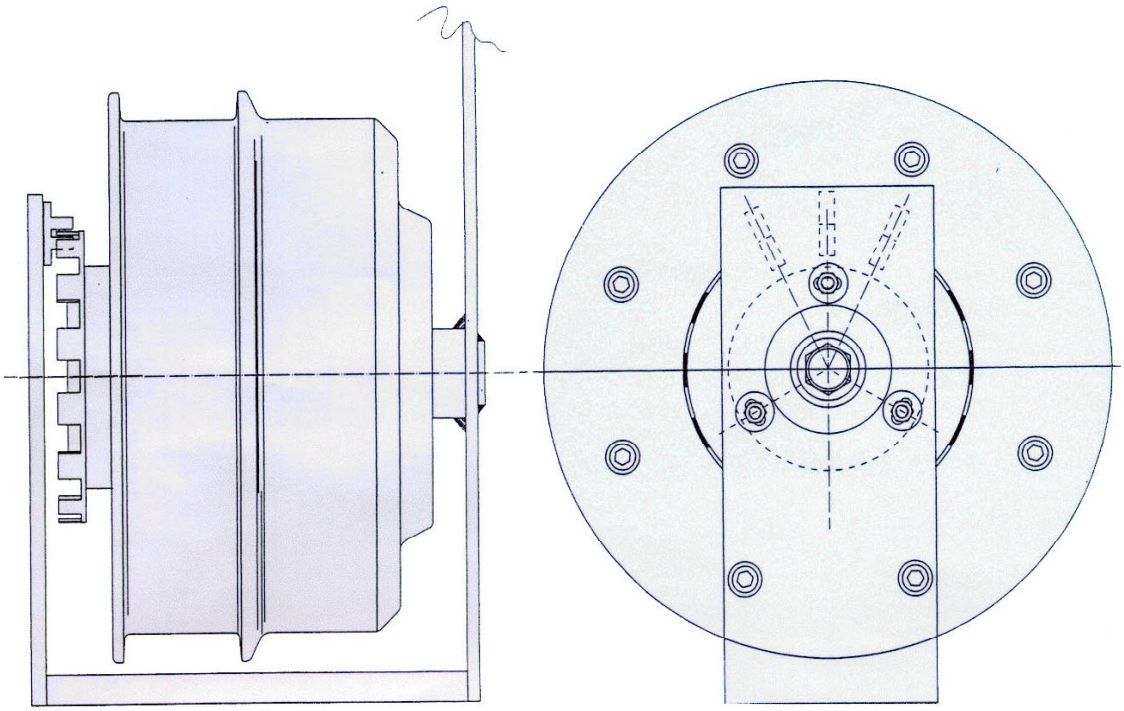

Figure 5.6: Rotor position sensing arrangement.

Effect of Skewing

Cogging torques are produced by the circumferential component of attractive forces between the magnet and the stator teeth (alignment between successive stator teeth and individual magnets). Cogging torque, even when non-integral values of slots per pole per phase are employed, can be high and is practically unacceptable in direct-drive low-speed motors where smoothness is important. It is independent of the phase current and so can become dominant at low torques values. It can be minimised through choice of slot number, tooth width, pole number, and pole width combination that minimises the number of stator-rotor edges that can simultaneously align as the rotor revolves. Skewing also helps here and, as with conventional machines, a typical skew is one stator slot-pitch. Either the stator or the rotor can be skewed. If the stator is skewed, the insertion of the winding will then be a little more difficult. The alternative is to skew the rotor magnet excitation system but this is difficult and was not justified at the development stage, so stator skew was used.

A disadvantage of low number of slots/pole/phase employed is that one slot stator pitch corresponds to a large electrical angle of 120 degrees, giving a winding factor of 0.716. The resulting reduction in *emf* per speed and torque per ampere caused by the skew is therefore significant, so the impact on the cogging torque of differing levels of skew was investigated during construction prior to winding. Figure 5.7 shows the predicted cogging torque versus rotor position for various skew angles. The lowest cogging torque is achieved with a skew angle of 1 slot and this was used in the experimental motor. However, if we assume that 3% cogging torque is acceptable a skew angle of half a slot-pitch would be sufficient. This will enhance the machine's capability and a shorter axial stack length will be required to produce the same output torque. Indeed, the pre-production prototype employed a stator skewed by only half a slot-pitch.

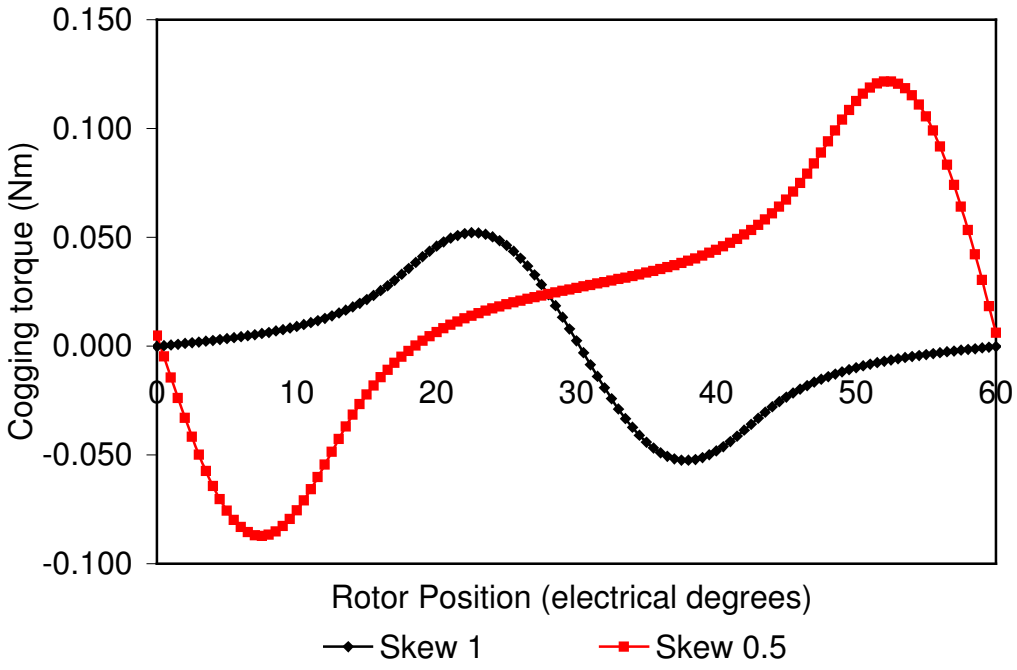

Figure 5.7: Cogging torque characteristics.

5.3.3. TESTING

The experimental machine described above was built and subjected to a series of laboratory and field test. Figure 5.8 shows the in-wheel motor fitted to a wheelchair. The laboratory tests were limited to cogging torque measurement and performance evaluation.

The cogging torque characteristic was determined experimentally by displacing the stator and measuring the induced torque. The stator was rotated, via a flexible coupling and a torque sensor, by a rotary table mounted so that its axis was collinear with the stator. Of course, stator excitation was absent throughout this test. The rotary table was driven by a stepper motor via a worm-wheel gearbox. The resolution of the stepper motor was 200 steps per revolution and the gearbox had a speed ratio of 90:1. The estimated backlash in the gearbox was less than 0.1 degrees.

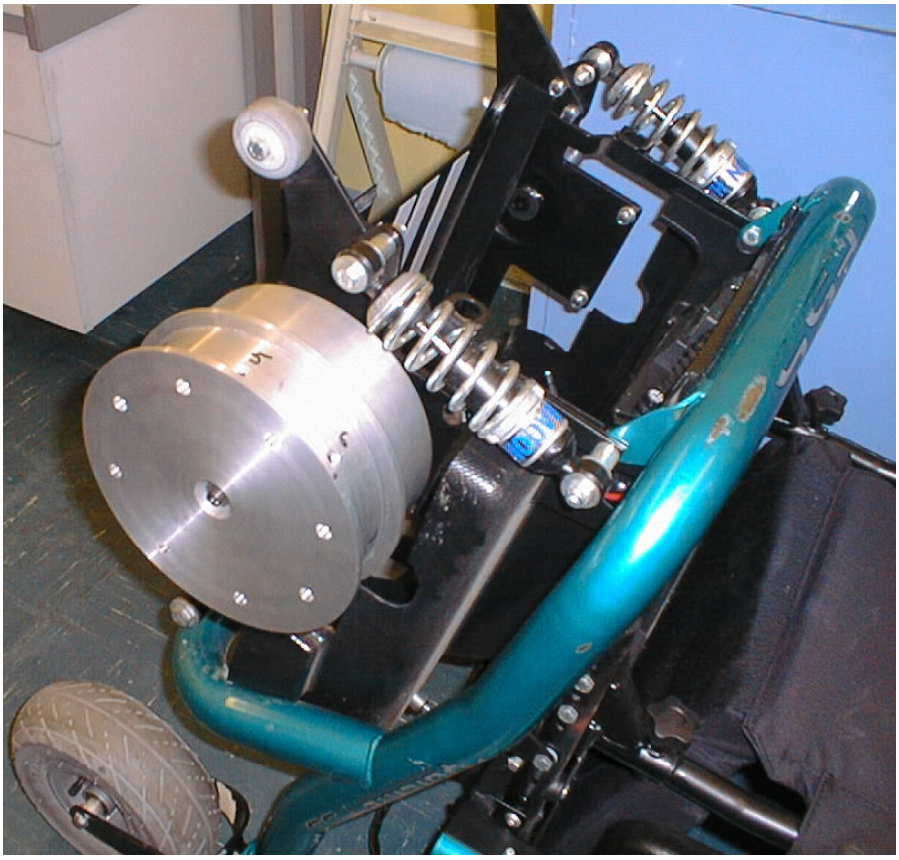

Figure 5.8: Prototype motor fitted into existing power wheelchair.

The torque was measured using a lord six-component sensor. A PC-based data acquisition system capable of recording and processing up to 1000 measurements per second was used. The resolution of the system was 1.4 mNm. To measure torque- displacement curves, stator was rotated in increments of 0.8 degrees and after allowing the readings to settle, the torque about the shaft axis was recorded. The effect of friction was eliminated by incrementing the shaft in one direction a total of 25.7 mechanical degrees (representing 2 pole pitches) and then reversing direction. Torque readings were taken in both directions and the results were averaged.

The measured cogging torque characteristics showed an excellent agreement with those predicted, giving a peak value of 0.105 Nm compared with 0.125 Nm computed.

The experimental motor was tested initially with the current limit set so high that the maximum capability of the experimental motor could be determined. Of course, in normal operation the current limit will be set at such a value that no damage can occur to both motor and controller. Thus Figure 5.9 shows the maximum capability of the motor.

During testing, the motor was fed from a square-wave controller and mechanical load was applied to the outer rotor via a friction mechanism attached to a pre-calibrated spring balance which recorded the braking force. The speed was recorded via an optical tachometer. Since both voltage and current are non-sinusoidal, the input power to the motor was obtained with the aid of a power analyser.

It is seen, Figure 5.9, that at a rated speed of 150 rev/min the shaft power is approximately 600 W, and the corresponding torque is about 42 Nm. Of course, for the wheelchair only requires 285 W (17.8 Nm) at rated speed. However if the machine was set to its required operating conditions we would get power to weigh ratio of 41W/kg. Power-to-weight figures for low speed machines motors are inherently low. At the half speed point of 75 rev/min, the machine is capable of delivering approximately 68 Nm with an efficiency of 55%.

It should be noted that two identical experimental machines were fitted to the back wheels of a wheelchair and tested according to some random duty cycle. The industrial partners were completely satisfied with the performance and work started immediately afterwards on pre-production prototypes. The author was not granted permission to include details of field testing of experimental motors or prototype testing in this thesis.

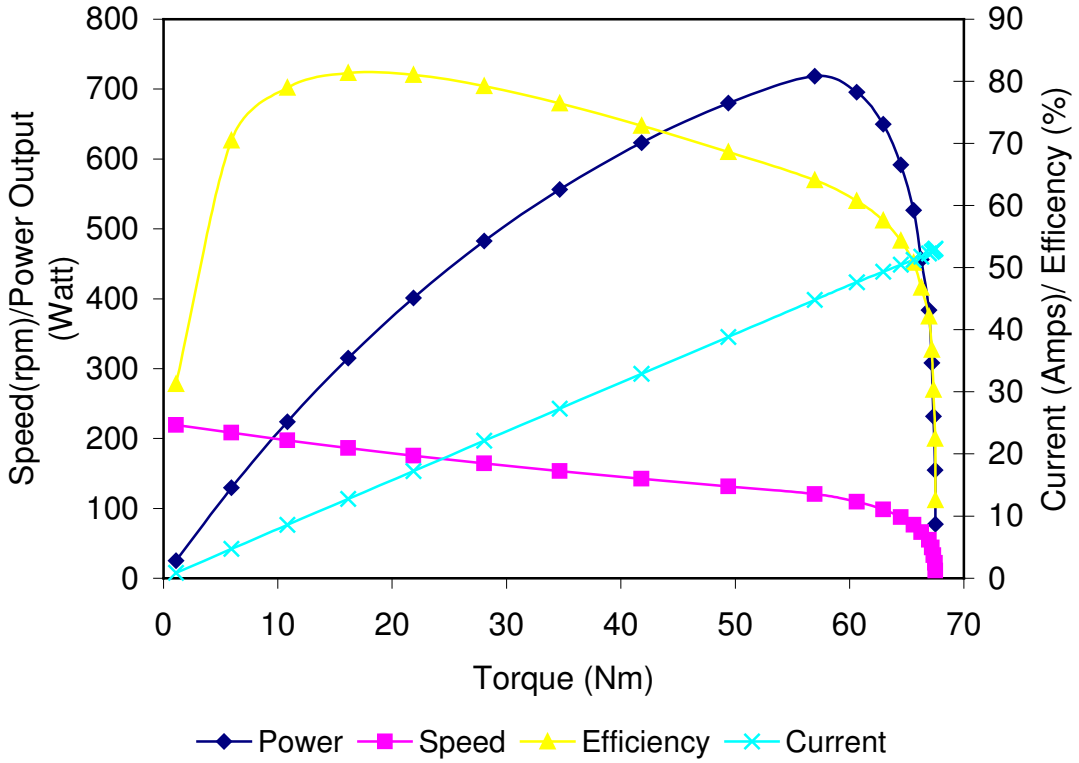

Figure 5.9: Performance characteristics of experimental wheelchair motor.

5.4. FORKLIFT TRUCK MOTORS

The speed-torque requirement as with provided by a Swedish forklift manufacturer are given in Table 5.6. The system voltage was specified at 24 V dc.

Table 5.6: Drive requirements of a 24 V forklift truck.

	Speed (Rev/min)	Torque (Nm)
Peak Acceleration	68	445
At max gradient	80	290
At max weight	237	62
Maximum speed	258	22

Again, in deriving a solution, established design roles are used to obtain preliminary dimensions and winding details, a circuit based simulation program enables examination and improvement of

preliminary electromagnetic design and the power-electronic converter and control strategy, and finally the finite element method is employed to fine-tune the magnetic circuit. After a number of iterations an electromagnetic design whose details are given in Table 5.7 was identified.

Table 5.7: Data of forklift truck motor, Design D1.

(b) Rotor outside diameter, mm	280
Rotor Yoke, mm	8
Magnet radial thickness, mm	5
Pole arc of magnet, elec. deg.	140
Poles	16
Air-gap radius, mm	127
Air-gap radial length, mm	1
Tooth tip radius, mm	126
Slots	24
Tooth width, mm	13.5
Slot depth, mm	60
Stator yoke thickness, mm	16
Stator bore radius, mm	50
Axial stack length, mm	200
Total coils	24
Turns per Coil	4
Number of Strands	14
Bare wire diameter, mm	1.5
Total conductors	192
Turns in series per phase	32
Layers	2
Mean turn length, mm	470
Conductor area, mm^2	24.74
Slot area, mm^2	637
Slot fill factor	0.31

The design assumes a fractional-slot, double-layer, star-connected winding design with 0.5 slot per pole per phase. Such a winding layout will result in a short stator end winding with no crossovers and is much easier to wind using existing induction motor winders. The reduction in end-winding length will reduce the copper loss during peak torque operation considerably and thus limit the temperature rise of the winding and magnets. The stator has 24 coils consisting of 4 turns each. A bare wire of 1.5 mm in diameter is used as any greater would be much harder to wind.

The external rotor utilises 16 magnet blocks radially magnetized and the windings are placed in the 24 parallel stator slots. It can be seen that, as the rotor rotates only 1.5 poles align with the tooth edges at every instant. This will reduce the cogging torque compared with an integral-slot design. After various design tradeoffs the peak current in the motor windings was set at 300 A. Such a high current necessitates the use of 14 strands. The conductor area thus is approximately 25 mm^2. The minimum *rms* current density achieved was 8.5 mm^2.

Figure 5.10 shows the flux density plot corresponding to maximum current operation. It is seen that the motor is designed very close to saturation with a peak tooth flux density of 1.9 T. The dc flux density in the rotor yoke was limited to approximately 2.0 T. Figure 5.11 gives the air-gap flux density waveform obtained at its centre.

Examination of the torque-speed characteristics predicted for this design, Figure 5.12, reveals that the constant torque range, in the absence of controller phase advance angle, is very limited indeed. The characteristic exhibits approximately constant torque of 520 Nm from 0 to 68 rev/min. It is seen that above the base speed 68 rev/min the torque decreases rapidly. Therefore, the torque requirements at 80, 237 and 258 rev/min, shown in Table 5.6 could not be fulfilled.

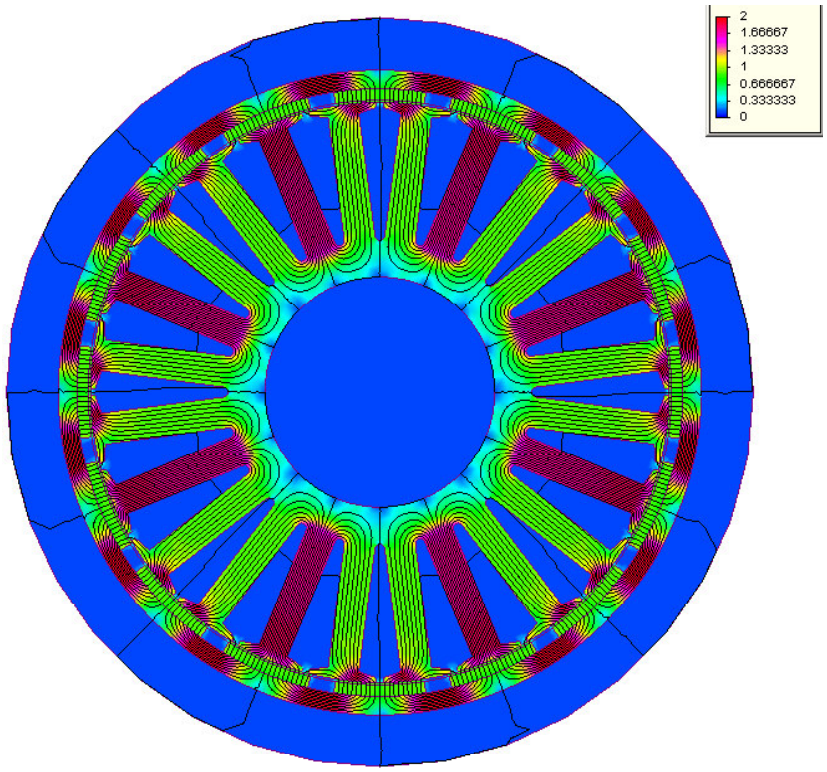

Figure 5.10: Forklift truck motor flux plot.

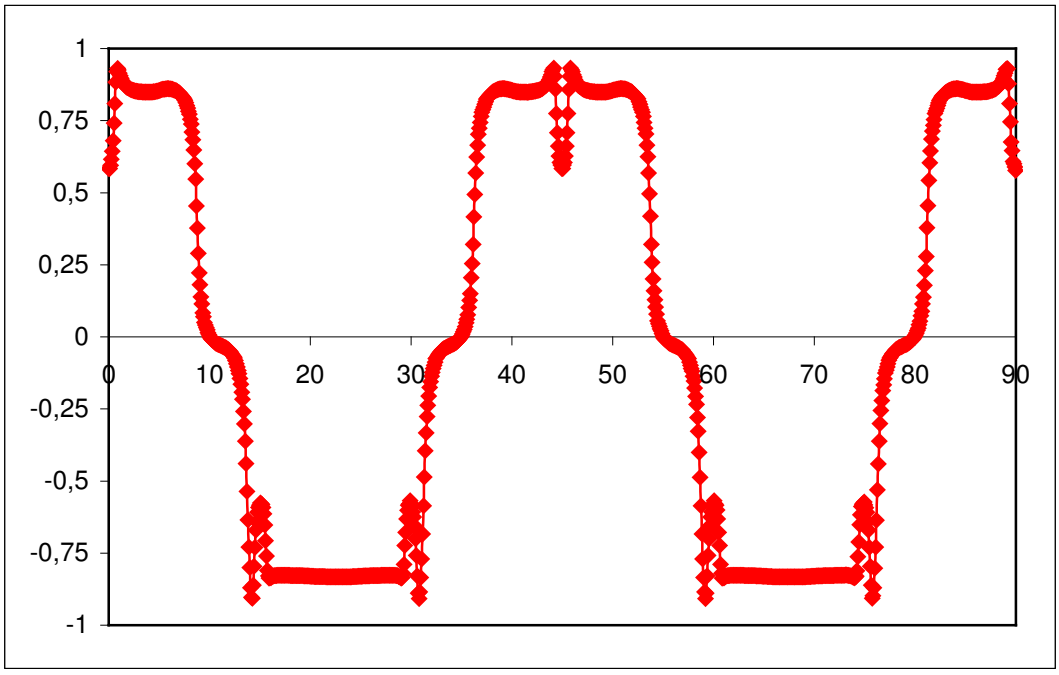

Figure 5.11: Air-gap flux density waveform.

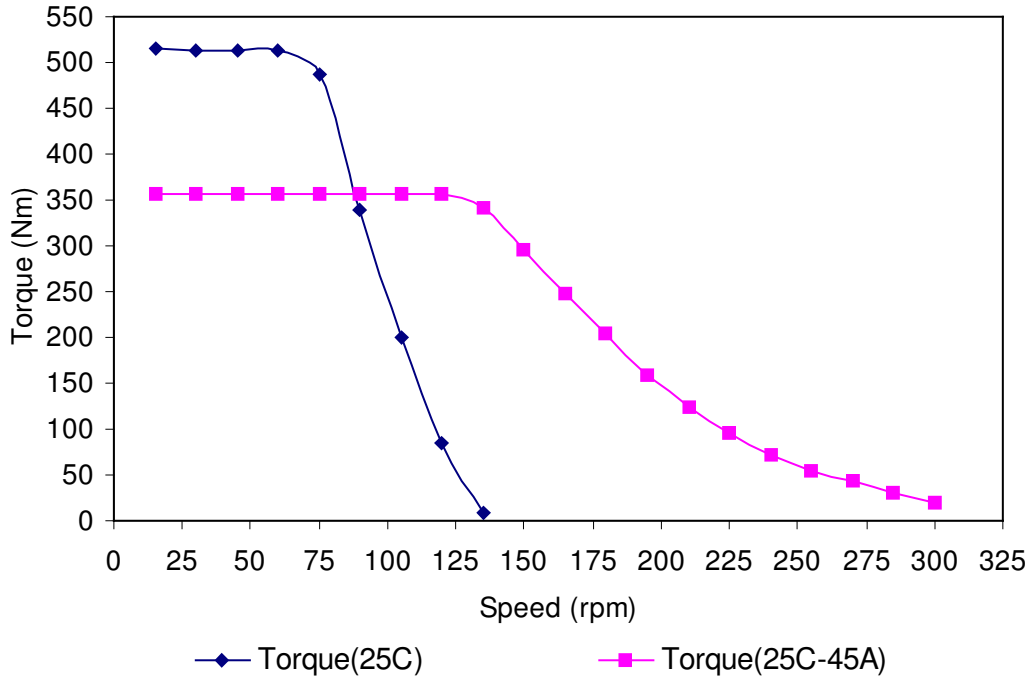

Figure 5.12: Torque-speed characteristics with 0 and 45^{o} advance angle, Design D1.

Hence to extend the torque-speed envelope, various phase-advance switching angles were examined. It was found that a phase advance angle of 45 degrees was sufficient to meet the requirements over the full speed range specified. Indeed, with such a phase advance angle design D1 exceeds the requirements and, therefore, can be further improved.

In an attempt to improve the first design (D1), the maximum winding current density was reduced to 7.5 mm^2. This was affected by setting the peak current limit to 260A leading to the second design (D2). Such an assumption enables meeting both the peak and maximum gradient torque requirements of 445 Nm, Table 5.6. A phase advance angle of 45^{o} yields 60 and 30 Nm at speeds of 237 and 258, respectively. Therefore, the torque requirement, over the specified speed range, was still met with this current limit.

5.4.1. EFFECT OF SKEWING

It was noticed that with no skewing, the cogging torque was considerably high although a fractional-slot design was used. Various values of skew were assumed and, while keeping the stack length constant, the effect of skew level on both cogging and electromagnetic torque was investigated. Figure 5.13 shows the predicted torque values at 68 rev/min. It is seen that minimum cogging is achievable with a skew angle of both 1 and 0.5 slot-pitch. However, a skew of 1 slot-pitch reduces the torque per ampere considerably resulting in an electromagnetic torque of approximately 465 Nm which also fulfils the requirement. As the skew angle is increased the winding factor, k_w, deviates from that of a sinusoidally wound machine of 0.995. A skew of 0.5 and 1.0 slot-pitch reduce k_w to 0.827 and 0.716 respectively. A skew angle of 0.5 is recommended, as an electromagnetic torque of 528 Nm will be available with an acceptable peak cogging torque.

Keeping the skew constant at 0.5 slot-pitch constant, the effect of changing the stack length, L_{stk}, on the torque values is investigated, as shown in Figure 5.14. It can be seen that the maximum electromagnetic torque is obtainable with a stack of 210 mm. A stack of 200 mm was chosen, in design D1, as any greater than this will result in a much larger machine.

Design D1 gives a peak torque which is higher than the application requirement (approximately 520 Nm compared with 445 Nm). Figure 5.14 indicates that the minimum stack length required to just meet the drive specification is 180 mm. Design D1 was therefore modified to the reduced value of active length, and this yielded design D3. The torque-speed curve of design D3 is shown in Figure 5.15.

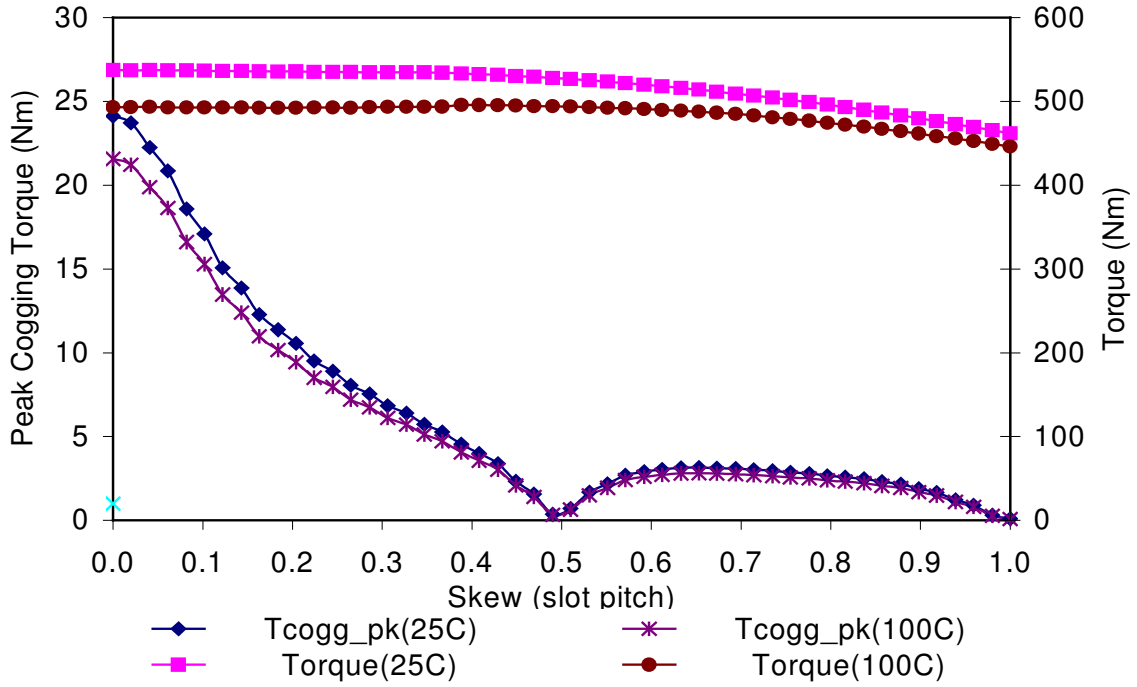

Figure 5.13: Peak cogging torque and electromagnetic torque versus skew angles.

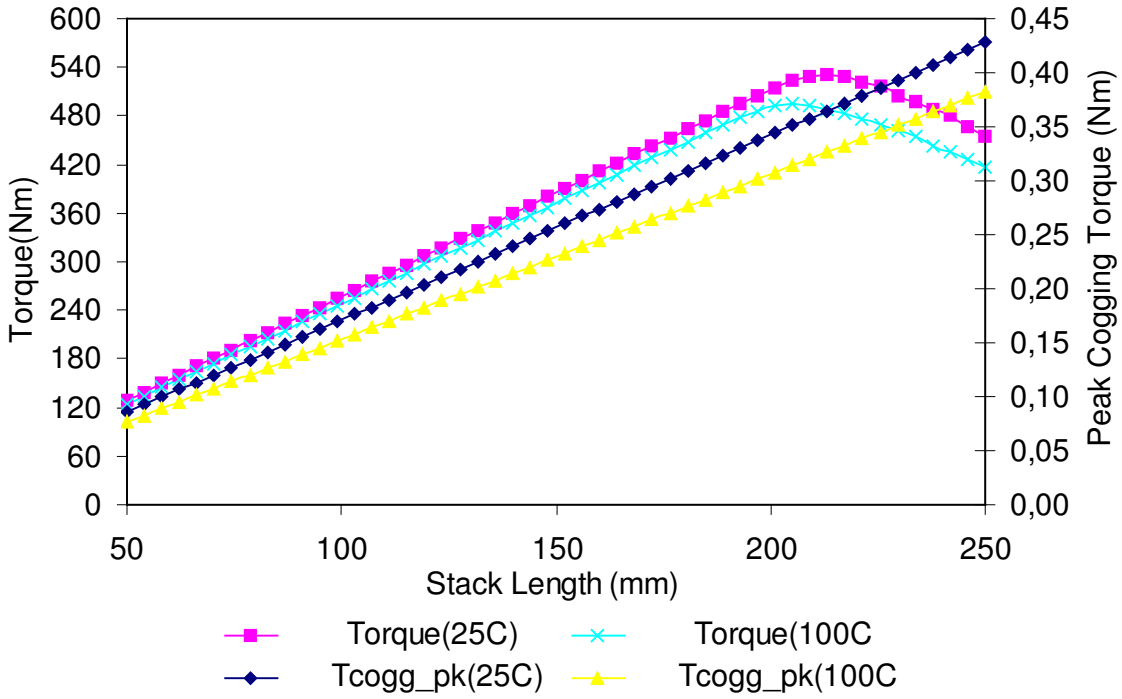

Figure 5.14: Cogging and electromagnetic torque versus stack length.

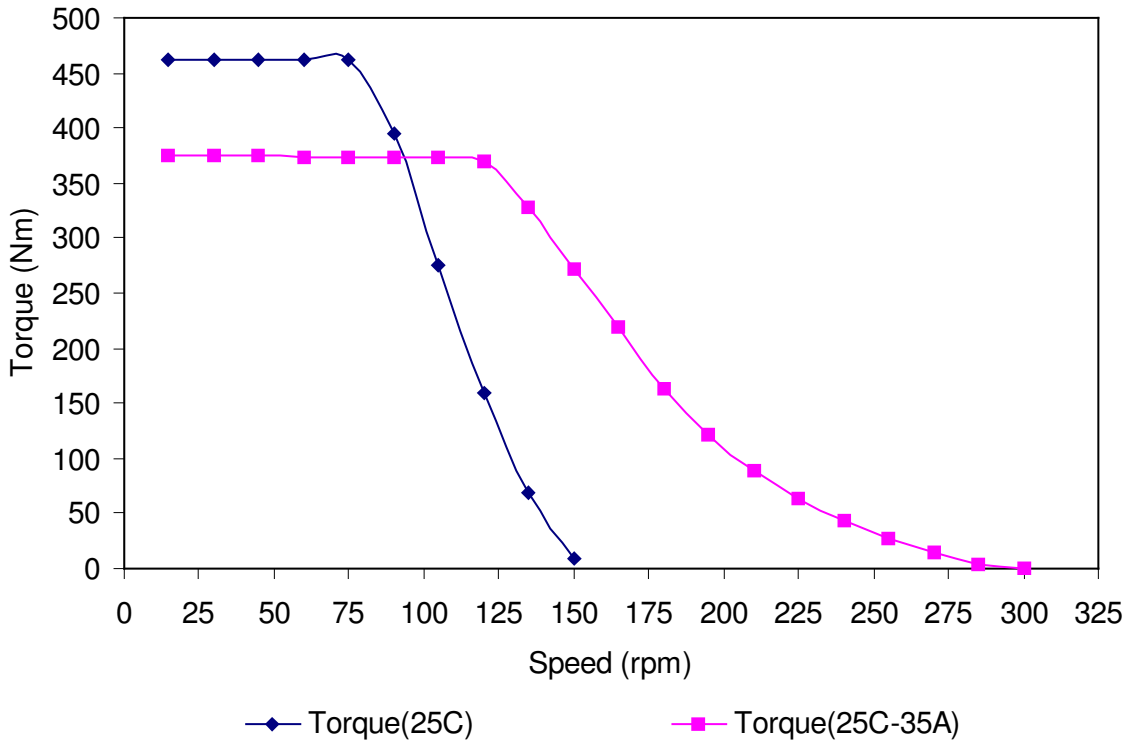

Figure 5.15: Torque against speed with 0 and 35 degrees phase advance angle

This design (D3) gives a constant torque of 460 Nm over the speed range 0 to 80 rev/min. Due to the reduced active stack length, design D3 has a wider speed range compared to design D1. However like D1, the torque requirements at 80, 237 and 258 rev/min could not be met without phase advance angle. After investigating a range of advance angles, it was found that the drive requirement over the full operating speed range can be met with a phase advance angle of 35°, as shown in Figure 5.15. Due to a 20-mm reduction in stack length, the maximum active weight of design D3 was reduced to approximately 59 kg compared with 74 kg in design D1.

5.4.2. SUMMARY OF PROPOSED DESIGNS

The performance expected from the three designs described above are summarised in Table 5.8. It is seen that the three solutions all meet the drive specifications in different ways. Designs D1 and D3 while they are identical as far as the drive motor is concerned, their controllers are quite different. This is because of the phase advance

requirement of design D2 that yields a more complex power conditioner but reduces the thermal stresses on the motor's insulation system.

In design D3, a shorter stack length (180 mm) was used and this of course results in savings in copper, iron and magnet weight. Table 5.9 gives comparison of weight and losses for the proposed designs.

Table 5.8: Comparison between three forklift motors, boldface figures represent required phase advance angle.

Speed (Rev/min)	Torque, Nm		
	D1	D2	D3
68	527	445	463
80	475	445	450
237	70 (**45**°)	60 (**45**°)	68 (**35**°)
258	60 (**45**°)	30 (**45**°)	23 (**35**°)

Table 5.9: Losses and components' weight

	D1 & D2	
Copper loss (25°C), kW	1.4	1.24
Core loss (25°C), W	25	20.3
Copper loss 100°C, kW	1.7	1.6
Total weight, kg	73.69	50.49
Copper weight, kg	9.905	8.723
Iron weight, kg	58.912	45.56
Magnet Weight, kg	4.870	4.215

5.4.3. SYSTEM VOLTAGE

In order to illustrate the effect of increasing the system voltage on the drive system performance, a brief design study was carried out with the aim of meeting the specifications given in Table 5.1

assuming a dc link voltage of 48 V. Figure 5.16 shows the torque-speed characteristics of one such a design. This design assumes the same dimensions as for design D1 described above, but the current limit was set at 270 A; just enough to give the required short-term torque of 445 Nm.

It is seen that with increased system voltage, the required shaft torque values are obtainable over the whole speed range without any sacrifice in efficiency due to the absence of phase advance angle.

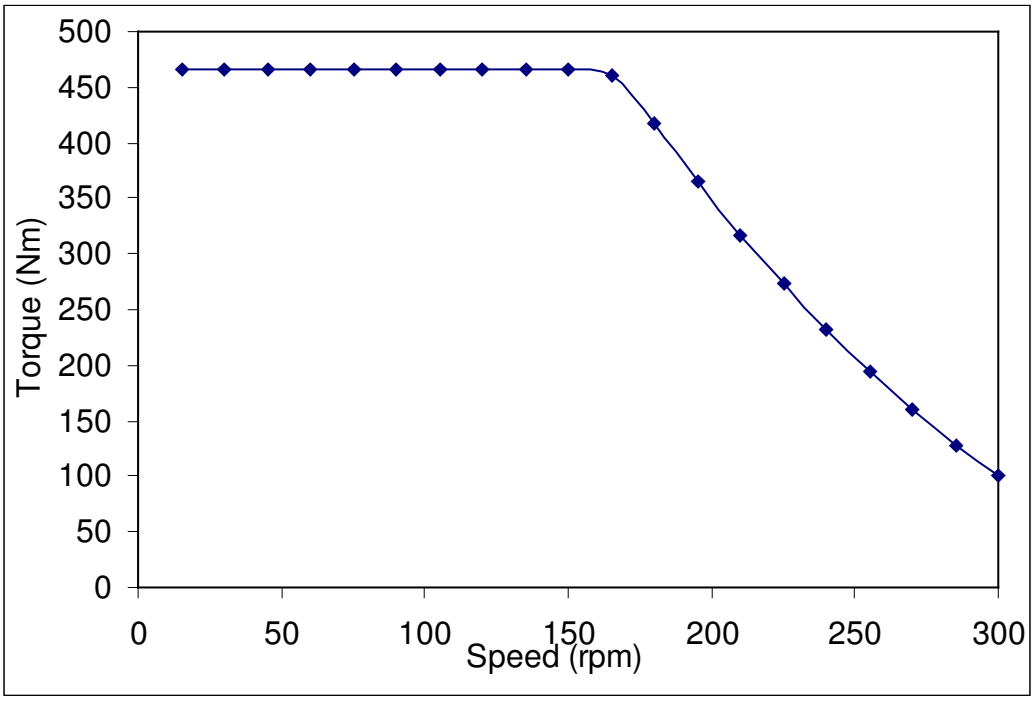

Figure 5.16: Drive system characteristics obtainable with 48 V.

CHAPTER VI

CONCLUSIONS AND FUTURE WORK

6.1. CONCLUSIONS

The force density limits, imposed by thermal conditions and magnetic saturation, are investigated for a class of low-speed permanent/magnet machines. Such a machine can be found in direct-drive traction applications, such as those employed in wheelchair, golf carts and forklift trucks, and low-speed directly-driven generators, such as those employed in wind and low-power hydro applications.

The investigation focused on in-wheel motors for LPEV and its first conclusion is that magnetic saturation plays an important role in limiting the force density values achievable. Force density values from models in which magnetic non-linearity is ignored will be considerably overestimated.

The work then arrived at the conclusion that an optimum slot depth, at which the force density is a maximum, exists for each current loading and that the optimum slot depth value decreases with increase in slot current. The dependence of the optimum slot depth value on the winding current presents the designer with an

interesting compromise to make between fulfilling the continuous and short-term rating requirements. For short-term current loading greater than three times the rated value the work presented in this thesis concludes that degradation in force density values occurs for slot depth values greater than 100 mm. A smaller slot depth would enhance the performance at high current levels, but will have the opposite effects at low current levels. Therefore, the slot depth chosen for a particular application would depend on the relative importance between transient and continuous torque due to the small conflict between them. It is given in Table 6.1 recommended slot depths range for a number of low-speed applications, together with their approximate force density requirements.

Table 6.1: Recommended force density values for direct-drive machines.

Application	Design condition	Slot depth range, mm	Required force density, kN/m^2
Wheelchair	Transient	<35	20
Golf cart	Transient	<45	18
Forklift Truck	Transient	<70	50
Wind generators	Continuous	<200	50

As they lend themselves to simpler and automated manufacturing techniques, fractional-slot windings were evaluated. The work demonstrates that the force density values for a fractional-slot winding are less than those of the integral-slot winding. This is expected and is, of course, due to the reduction of the *emf* induced in the stator windings caused by lower values of the winding factor. Compared with a winding having slots per pole per phase (q) of unity, the force density values obtained from fractional-slot windings having q of 0.375, 0.5, and 0.75 would be reduced by about 25%, 14% and 7%, respectively. This will require a longer stack to meet the drive requirements. It is concluded that slot per

pole per phase values less than 0.5 should only be used when the application requirement warrants this and can tolerate the increased stack length.

The design work presented in the previous chapter indicates not only that wheelchair drive requirements can be met with commercially viable in-wheel permanent-magnet motors, but also that such a motor can be easily adopted to meet the drive requirements of golf carts. An experimental motor was built and tested yielding good performance that warranted development of a pre-production prototype by the sponsoring company. The designs presented for the forklift truck motor demonstrate how demanding such an application is as far as force density is concerned. The work concludes that the specified forklift drive requirements can only be met by employing switching phase advance angle or by doubling the system voltage.

The force density versus slot depth characteristics for different values of winding current density, and for a range of pole-pitches, are given in Appendices II and III for integral- and fractional-slot windings. These are intended as a design tool to help the designer to establish whether or not specific requirements can be achieved, at least theoretically.

6.2. RECOMMENDED FUTURE WORK

The investigation throughout this thesis was limited to only slotted, radial flux, permanent-magnet machines. If the force density values achievable with other machine topologies can be determined, following a similar general treatment, comparisons would become possible. This will enable designers to determine the most appropriate topology to fulfil a demanding specification.

These curves given in Appendices I and II can be incorporated into a CAD procedure. The input parameter to the package would only be the peak torque, accepted winding current density and the available space envelope. The package would evaluate all slot and pole combinations that can meet the specification, calculate the machine dimensions and, through a link to a FEM software, optimise the magnetic circuit and winding design. This work has already started by the author and other members at Chalmers' Machines and Drive Systems Group.

Sensorless control can simplify the drive system design of the LPEV. However, applications such as those considered in this thesis would require sophisticated algorithms specially developed to meet their respective specific requirements.

References

1. Hamdi, E.S. “Permanent magnet and variable reluctance drive systems”, ETI Press,Gothenburg, Sweden, 2003.
2. Essam S. Hamdi. “Design Of Small Electrical Machines”, John Wiley & Sons Ltd.
3. A Grauers, "Design of Direct-driven Permanent-magnet Generators for Wind Turbines", Ph.D. dissertation, Dept. Electric Power Eng., Chalmers Univ. of Technology, Göteborg, Sweden, 1996.
4. P. Kasinathan, A Grauers and E Hamdi "Force Density in Low-speed PM Machines: Saturation limits”, Proc. 2002 IEEE Power Engineering Society, Submitted.
5. A.Grauers, P.Kasinathan, “Force Density in Low-speed PM: “Temperature and Inductance limits”, Proc. 2002 IEEE Power Engineering Society, Submitted.
6. Murugesen, S: “An overview of electric motors for space applications”, IEEE Transcations On Industrial, Electronics And Control Instrumentation, Vol. IECI-28, No. 4, November 1981, pp261-265
7. S. K. Pal, "Direct drive high energy permanent magnet brush and brushless DC motors for robotic applications, ” in Robot Actuators, IEE Colloquium on, 1991, pp. 12/1-12/4.
8. L. M. C. Mhango, “Brushless DC machines with rare-earth magnets for high speed aerospace drives, ” presented at,6-7 Nov. 1990, Birmingham, UK, 1990.
9. L. M. C. Mhango and R. Perryman, “An assessment of high power density brushless DC motor technology with neodymium-iron-boron excitation”, presented at 1994 Universities Power Engineering Conference (UPEC),14-16 Sept. 1994, Galway, Ireland, 1994.
10. L. M. C. Mhango, “Design ideas for low-inertia high-speed electronically commutated PM motors for special

applications", in Variable Speed Drives and Motion Control, IEE Colloquium on, 1992, pp. 9/1-9/5.

11. S. K. Pal, "Comparative study of the design and development of direct drive brushed and brushless DC motors with samarium cobalt, neodymium-iron-boron and ceramic magnets", in Permanent Magnet Machines and Drives, IEE Colloquium on, 1993, pp. 7/1-7/7.
12. S. K. Pal, "Comparative study of the design and manufacturing processes of electrical motors with low and high energy permanent magnets", in Electrical Machines and Drives, 1993. Sixth International Conference on (Conf. Publ. No. 376), 1993, pp. 339-346.
13. Fink, R.A.: "The brushless motor-types and sources", Control Engineering, August 1970, pp.42-45.
14. Knights, D E: "Prospects for the printed motor", Design Engineering, March 1975, pp.199-202.
15. Hans Waagen: "Motors with printed circuit armatures", Design Engineering, January 1970, pp.52-55.
16. Casanova D: " The permanent magnet dish motor an assessment of the quality of mechanical commutation", Motorcon Proceedings, September 1982, pp.446-450.
17. Werninck, E.H: "The methodology of motor selection", Second International Conference on Small and Special Electrical Machines, IEE Conference Publication No. 202, 22-24 September 1981, pp1-5.

    Carl M. Fink and Dennis F. Brown: "The permanent magnet dc pancake motor-An assesment of the quality of mechanical commutation", Motorcon, March 1982, pp693-699.
18. Mazurkiewcz, J.: "Consider hollow-rotor motors", Electronic Design 11, May 24, 1975, pp.76-79.
19. Mazurkiewcz, J.: "The drive motor of a servo", Electronic Design 15, July 19, 1976, pp.110-113.

20. Theodore Wildi.: “Electrical machines, drives and power systems” pp.417-436.
21. Wang Zong-pei, Cheng Shu-Kang.: “Bipolar drive three phase variable reluctance step motor”, Second International Conference on Small and Special Electrical Machines, IEE Conference Publication No. 202, 22-24 September 1981, pp50-54.
22. A Huges, D.J.MacLoed.: “Hybrid and variable reluctance small-angle stepping motors”, Second International Conference on Small and Special Electrical Machines, IEE Conference Publication No. 202, 22-24 September 1981, pp50-54.
23. Acarnley, P.P.: “Stepping motor control techniques”, Conference on Drives/Motors/Controls, 24-26 October 1984, Brighton,United Kingdom, pp106-112.
24. Bimbra, P.S.: “Generlized theory of electrical machines”, Fifth Edition, Khanna Publishes,pp1034-1036.
25. Caricchi F., Crescimbini F., Honorati O., Di Napoli A., Santini E., “Compact Wheel Direct Drive for Evs”, Industry Applications Magazine, IEEE, 1996
26. Spooner E., Chalmers B.J., “TORUS: A Slotless, Toroidal-Stator, Permanent Magnet Generator”, Proceedings-B, IEE, Nov. 1992, Vol. 139, No.6
27. Caricchi F., Crescimbini F., Mezzeti F., Santini E., “Multistage Axial-Flux PM Machine for Wheel Direct Drive”, Transaction on Industry Applications, IEEE, 1996, Vol. 32, No.4
28. Caricchi F., Crescimbini F., Honorati O.,“Modular Axial-Flux Permanent Magnet Motor for Ship Propulsion Drives”, Transaction on Energy Conservation, IEEE, 1999, Vol. 14, No.3

29. Caricchi F., Crescimbini F., Fedeli E., Noia G., “Design and Construction of a Wheel-Directly-Coupled Axial-Flux PM Motor Prototype for EVs”
30. J. G. W. West, “PM DC motors with series field characteristics”, in Permanent Magnet Machines, IEE Colloquium on, 1988, pp. 5/1-5/5.
31. J. G. W. West, “DC, induction, reluctance and PM motors for electric vehicles", in Power Engineering Journal, vol. 8, 1994, pp. 77-88.
32. J. G. W. West, “The present status of electrical machines in vehicles", Machines for Automotive Applications (Digest No. 1996/166), IEE Colloquium on, 1996, pp. 1/1-121.
33. J. G. W. West, “Propulsion systems for hybrid electric vehicles", Electrical Machine Design for All-Electric and Hybrid-Electric Vehicles (Ref. No. 1999/196), IEE Colloquium on, 1999, pp. 1/1-1/9.
35. J Hystad, "Transverse Flux Generators in Direct-driven Wind Energy Converters", Ph.D. dissertation, Dept. Electrical Power Eng., NTNU, Trondheim, Norway, 2000.
36 Hasan El Hinaoui, “Green Car, Traction Motors” PhD project.
37 D.A.Staton, R.P.Deodhar, W.L.Soong and T.J.E.Miller., “Torque Prediction Using the Flux-Mmf Diagram in AC, DC, and Reluctance Motors.”, Transactions on Industry Application, IEEE, vol.32, no 1, Jan/Feb 1996
38 SGM Magnets Limited Catalogue, Sussex, United Kingdom
39 Magnet Application Catalogue, United Kingdom

APPENDIX I

Paper A

A.Grauers, P.Kasinathan, "Force Density in Low-speed PM: Temperature and Inductance limits", Proc. 2003 IEEE Power Engineering Society, Submitted.

Anders Grauers and Prakashraj Kasinathan

Force Density Limits in Low-speed PM Machines Due to Temperature and Reactance

Abstract-- **This paper discusses two of the mechanisms that limit the attainable force density in slotted low-speed permanent-magnet electric machines. Most of the interest is focused on the force density limits imposed by heating of the windings and by stator reactance. The study is based on analytical models for the force and reactance calculations and a lumped parameter thermal model. It is found that, in a machine with indirectly cooled stator, it is difficult to achieve a force density greater than 100 kN/m^2 due to temperature limits. A high force density is achieved by using deep slots, which lead to high reactance. The high reactance severely increases the converter kVA requirement and total system cost. In machines with one slot per pole and phase, the reactance limited the useful slot depth to approximately 200 mm. However, in machines having greater number of slots per pole and phase the reactance becomes no longer an important limiting factor for the slot depth and force density.**

Index Terms-- **Electric machines, Force density, High Torque, Inductance, Low speed, Permanent magnet, Reactance, Thermal limits.**

I. Introduction

Due to the development of high energy permanent magnet materials, permanent magnet machines are being considered for many new applications. One important trend is that electric machines are designed specifically for the required speed, primarily to eliminate the gearbox. Since the rated torque, rather than the rated power, determines the cost and size of a machine, low-speed machines will be big and expensive. As a consequence, low-speed machines will generally be designed for very high force densities. One typical application where high force density is vital, in achieving a size suitable for transportation and mounting, is low-speed direct-drive generator for wind turbines.

The main aim of this paper is to discuss the influence of winding temperature limit and stator reactance on the achievable force density in slotted PM machines. The results presented will help a design engineer in achieving good solutions and compromises in the design of low-speed machines. However, the values presented should only be considered as rough estimates of the force density that can be achieved in the investigated type of machine. The exact values will depend very much on the application and also on other limiting factors like saturation and cost.

The investigation covers a large range of slot depths and current densities, far beyond what will be found in normal machines. Nonetheless, these extreme machines are also included in the investigation, as they will help illustrate the discussed phenomena better.

II. ASSUMPTIONS AND LIMITATIONS

This investigation is limited to synchronous machines designed for continuos operation with

- high pole number,
- low-speed,
- slotted, three-phase integral-slot windings,
- surface mounted permanent-magnet rotor configuration.

The investigated machines are designed for maximum force density, within the given limits, and they are therefore not optimized for cost, weight or size. Because high pole numbers are considered the air gap diameter has been assumed to be large enough for the curvature of the stator to be neglected when analyzing only one pole. The cross section of one pole is shown in Figure 1.
An electric machine is basically a force-producing device. The force density can be found from investigating just one pole of the machine, without direct influence of the air gap diameter, stator length or the speed of the machine. This simplicity is an advantage since it makes the results more generally applicable than otherwise. But there are second order effects that make the diameter, length and speed influence the force density to some extent. The errors introduced by these must be investigated and the credibility of the presented result due to neglecting

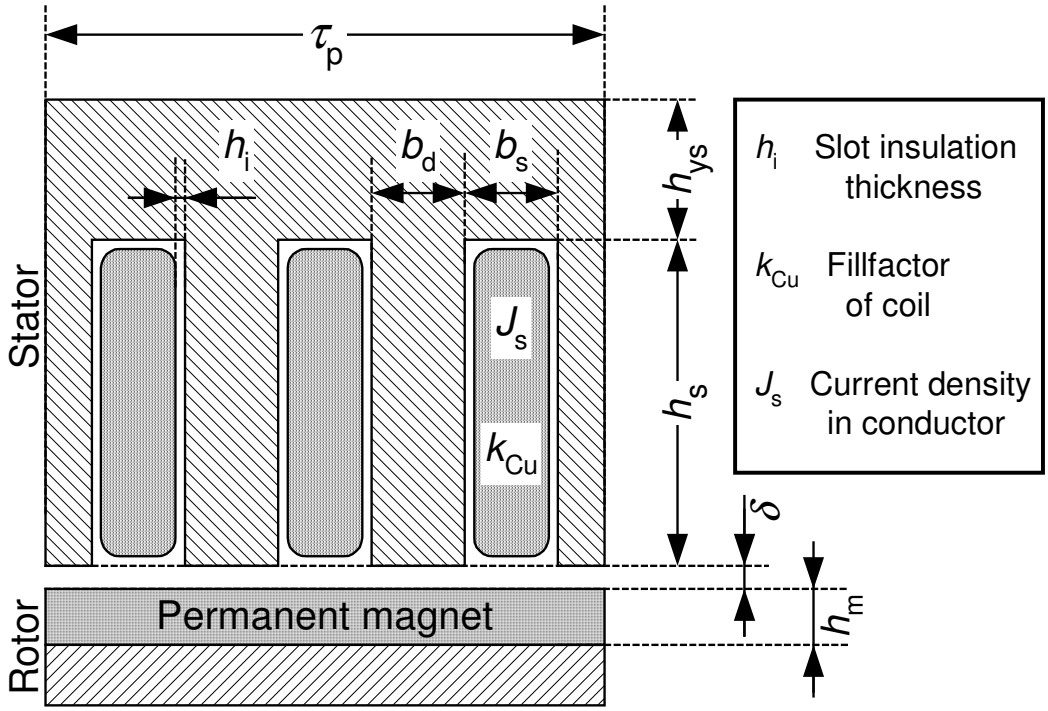

Figure 1 One pole of the investigated type of machine

these errors must be first established. Each of them will be discussed shortly below.

The air gap clearance will have a minimum value, either determined by stator diameter and length, due to mechanical reasons, or by the stator current loading, due to the risk of demagnetization. In machines with high force density, demagnetization will normally be the most important limit for the airgap. Therefore, the influence of stator diameter and length on the air gap has not been given detailed consideration in this paper.

The axial length of the stator will influence the force density, since the end windings will increase the losses and also the temperature rise in the winding hot spot. However, the end windings contribution to the total loss and temperature rise can be neglected if they are short compared to the active part of the winding. With very high pole numbers the active length of the stator will often be many times the end winding length and machines designed for very low speeds are typically of this type.

Mainly current and magnetic flux density will determine the force in the machine, while speed will not have a direct influence on the force. Core losses will depend on the speed, and if they increase they will require a reduced current density, in order to be within the temperature limit. However, in machines for very low speed the core losses can usually be neglected, as they are much smaller than the copper losses. For example, in a 32-rpm 500-kW wind-turbine generator the full load core losses are only about 3 kW while the copper losses are 23 kW [2].

III. FORCE DENSITY

To determine and discuss the achievable force it is necessary to start from the basic mechanism of force production in electric machines. There are several ways in which force production can be explained, but a very easy way is to start from the well-known formula for force on a current carrying conductor situated in a magnetic field.

$$F = B\ I\ l \tag{1}$$

This equation will work rather well on non-salient machines, although it is actually a simplification of the real force producing mechanism. The total tangential force on the stator will be the sum of the forces produced on each stator conductor. Since, in a non-salient machine, the magnetic flux produced by the stator itself will not contribute to the net force production, only the flux density produced by the permanent magnets on the rotor is used in the force calculation. Assume that both the linear current loading from the stator and the flux density from the permanent magnets are sinusoidally distributed around the stator, with peak values J_p (A/m) and B_p (T) respectively. The displacement between these peaks is defined as the angle. The force density can then be found by first reformulating equation 1 to be valid for an infinitesimal part of the air gap circumference. Integrating over one pole pair and dividing by the air-gap surface of one pole pair results in the average force density produced

$$f = 0.5\ B_p\ J_p\ \cos(\alpha) \qquad [\mathrm{N/m^2}] \tag{2}$$

In this equation the space harmonics ability to produce force is neglected since their contribution compared to the fundamental component is very small. Equation 2 shows that the force density maximizes when the no-load flux density and stator current loading are kept in phase and their product is maximized.

The maximum value of air gap flux density, B_{max}, is limited by saturation of the stator teeth and is thus mainly a function of the ratio between slot and tooth width

$$B_{max} = B_{sat}\ k_{Fe}\ \frac{b_d}{b_s + b_d} \tag{3}$$

where B_{sat} is the flux density at which the stator iron saturates and k_{Fe} is the iron fill factor of the stator core. Normal electric steels have a saturation flux density of approximately 1.7 T. The fundamental component of the flux density distribution will have a higher peak value than the actual flux density. For a square shaped magnet with 180º pole arc the ratio will be in the order of approximately 1.2 times giving

$$B_p \approx 1.2\, B_{max} \tag{4}$$

The peak current loading J_p (A/m) is a function of rms current density in the conductors, J_s (A/mm^2), slot depth and also the ratio between slot and tooth width.

$$J_p = \sqrt{2}\, J_s\, k_{Cu}\, (h_s - 2h_i)\, \frac{b_s - 2h_i}{b_s + b_d} \tag{5}$$

where k_{Cu} is the copper fill factor of the coil. However, since the allowed current density will depend primarily on the cooling, it will in itself be a function of slot depth, tooth width and slot width.

From the above discussion it is clear that the machine designer can influence the force density mainly by varying the ratio between slot and tooth width and the slot depth. But there is a conflict between increasing flux density and current loading by changing the slot-to-tooth-width ratio. If the tooth width is increased the flux density can be increased, but the current loading will be decreased at the same time. Therefore, the slot-to-tooth-width ratio cannot be used to increase the force density significantly. Instead the designer is left with the slot depth as the only means to significantly increase the force density.

IV. THERMAL LIMITS

Since the primary aim is to maximize the force density of the machine, the maximum allowable current must be initially determined. In this section the maximum allowable current is found by calculating the current density that leads to the maximum allowable winding temperature.

With class F insulation materials the allowable maximum winding temperature would be 155ºC. However an average temperature of 130ºC is used to allow margins for local hotspots. The winding is assumed to be cooled indirectly, by cooling air at the outer surface of the stator. More sophisticated cooling methods, like direct water cooling of the winding has not been considered, as the cost of manufacturing these machine must be kept low for the investigated low-speed applications. Since the low-speed electric machine will be one of the most expensive parts of the electric drive system the machine simply has to be of a low cost type, in order to compete with existing geared drives. Of course there exists special application where cost is not an issue, but they are not considered here.

A. Thermal model

The thermal model, which is used to calculate the highest allowable current, only includes one slot pitch of the stator and does not include the rotor. This is acceptable since the losses in a low-speed permanent-magnet rotor are small and can be neglected. Also the core losses are neglected, because of the low speed.
The thermal model is based on dividing the stator iron into 6 and the winding into 4 rectangular cells. The thermal lumped parameter circuit used to model each cell is shown in figure 2. The circuit includes two negative thermal resistances between the loss source and the thermal resistances for the heat flow through the cell. These negative thermal resistances takes into account that the real losses are distributed evenly over the cell, while the losses in the model are fed into only the node in the center of the cell. The way this thermal model is built up is presented in [2].

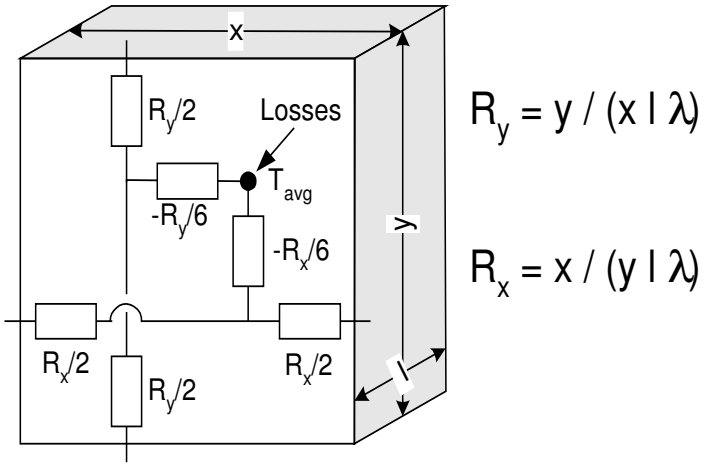

Figure 2: The thermal lumped-parameter model for a rectangular cell of homogenous material and with evenly distributed losses.

The thermal model is shown in Figure 3. The winding and the tooth are divided into 4 cells, to facilitate the study of the internal temperature distribution in these parts. The remaining two cells represents the stator yoke. The model is cyclic so the boundary nodes I to V are connected to the other side of the model. All thermal resistances used are calculated from the geometry of the slot and tooth together with the material properties. Thus, the main variables for the thermal model are slot depth, slot width, tooth width and yoke thickness. All of these will influence the thermal resistances and the allowed slot current. The yoke thickness, however, has not been used as a free variable. Instead it is set to 1.5 times the tooth width, which is a reasonable value for a three-phase machine

with one slot per pole and phase. The heat transfer coefficient between

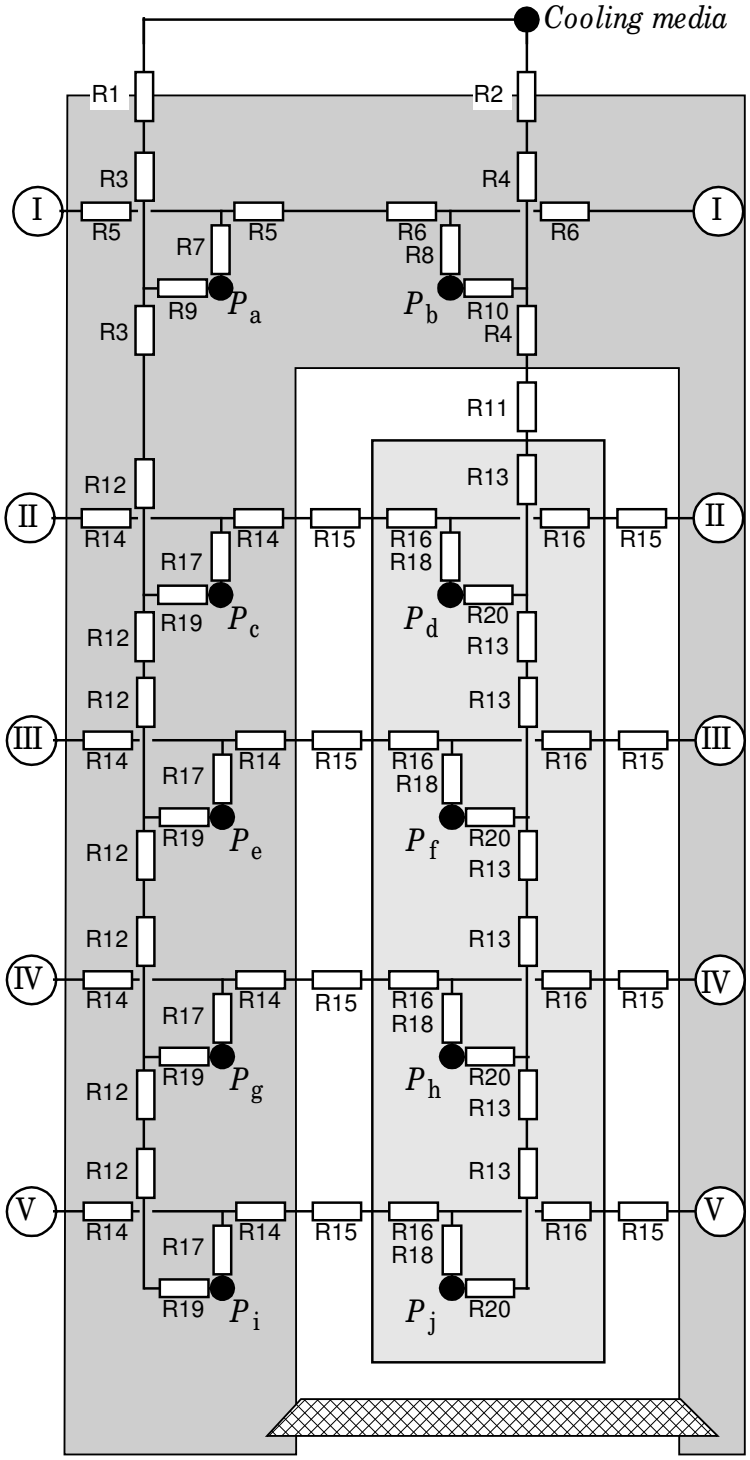

Figure 3: The thermal model for one slot pitch.

stator yoke and cooling air is assumed to be 60 W/(K m^2) while the surface for heat dissipation is assumed to increase by a factor of 2.5 since cooling fins are present.

B. Thermally determined current density

The main way to increase the force density of a machine is to make the slots deeper, in order to increase the cross section of the conductors. However, having a deeper slot with the same current density will increase the temperature rise for two reasons. First, the total copper losses will increase linearly with the copper cross section. Therefore, the loss per machine outer surface will increase, leading to a higher temperature rise between stator yoke and cooling air. Secondly, the heat from the winding will have a much longer path to flow, due to the longer teeth, leading to a greater temperature rise. For these reasons the current density must be decreased with increasing slot depth, to keep the winding temperature below its maximum value.

The main variable investigated with the thermal model is the maximum current density possible, as a function of slot depth. Since the slot and tooth widths influence the temperature rise they must be carefully selected when determining the maximum current density. Thus, for every value of slot depth, the slot and tooth widths are both varied to find the values that maximize the force density. These slot and tooth widths are plotted in Figure 4. The air gap and magnet height is also varied to keep the flux density in the tooth at the saturation limit and to avoid demagnetization of the rotor permanent magnets. Table 1 lists all the variables that will be used later in this paper, covering slot depth ranging from 10 to 1000 mm. However, it is important to realize that in many machines there may be many other requirements that will require changes in one or more of these variables. The penalty of such requirements will be a reduced force density.

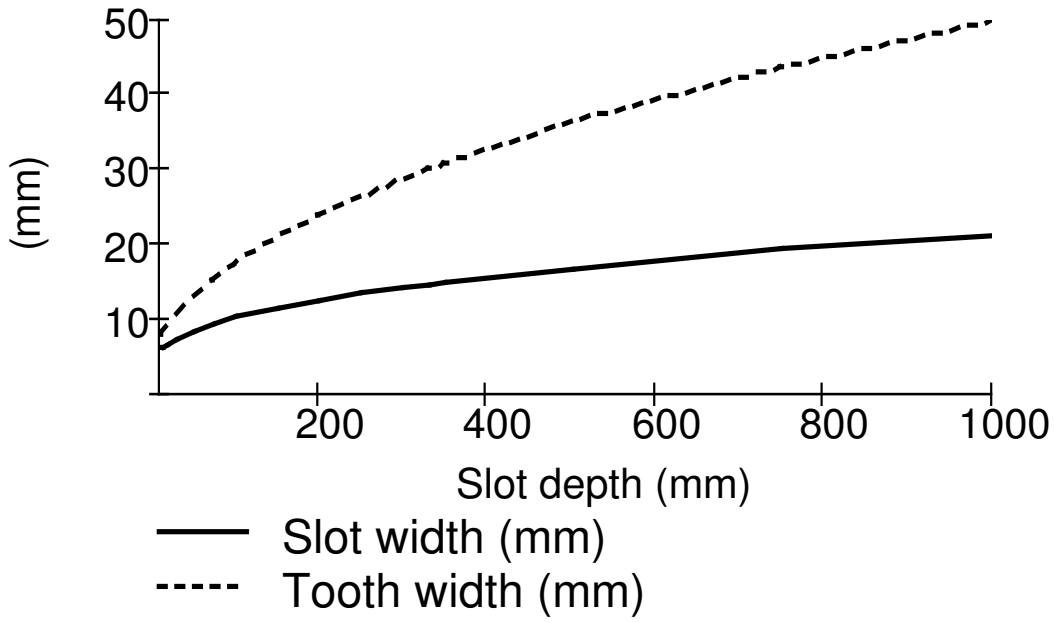

Figure 4: The slot- and tooth-width that maximize the force density.

h_S (mm)	b_S (mm)	b_d (mm)	τ_P (mm)	J_S (A/mm²)	h_m (mm)
10	6,11	7,79	41,7	12,01	6,26
15	6,22	8,42	43,9	10,35	6,59
20	6,52	9,19	47,1	9,17	7,07
30	7,15	10,67	53,5	7,62	8,02
50	8,24	13,14	64,2	5,91	9,62
75	9,29	15,60	74,6	4,77	11,20
100	10,12	17,64	83,3	4,07	12,49
150	11,43	21,04	97,4	3,21	14,61
200	12,47	23,88	109,1	2,69	16,36
300	14,14	28,63	128,3	2,06	19,25
500	16,66	36,14	158,4	1,44	23,76
750	19,10	43,63	188,2	1,05	28,23
1000	21,16	49,99	213,5	0,84	32,02

Table 1:The machine geometry for different slot depths.

In Figure 4 the optimum tooth-to-slot-ratio can be observed to grow as the slot becomes deeper. The optimum ratio is about 1 for shallow slots but the required tooth width is twice the slot width with 200-mm slot depth. This difference can be explained by looking at the temperature distribution in the stator as the slot depth changes, as shown in Figure 5. For small slot depths, 10 mm, the largest part of the temperature rise is

50º and it occurs between tooth top and winding top. The next largest temperature rise is 40º and occurs between the stator yoke and the cooling air. Only a very small temperature difference is found between the top and bottom part of the tooth. However, as the slot depth increases the temperature distribution changes drastically. For very deep slots almost half the temperature rise is concentrated in the tooth. The temperature rise between cooling air and stator yoke has been reduced. The reason for this is that the increased temperature rise in the tooth must be compensated for by such a large reduction in current density that the total losses of the stator are reduced, even though the volume of copper has been significantly increased. To limit the temperature rise in the tooth a wider tooth is required when deep slots are used.

C. Maximum current loading and force density

The maximum current density allowed by the thermal model, as a function of slot depth, is shown in figure 6. It can be seen that the maximum current density is much reduced with increasing slot depth. Note that with small slot depths very high current densities, greater than 6 A/mm^2, are thermally possible. However, they are normally not used due to the resulting poor efficiency. Figure 7 shows the force density and peak current loading as a function of slot depth. The current loading increase while the current density decreases with increasing slot depth. For small slot depths, increasing the slot depth is an efficient way to increase current loading, but as the slots becomes greater than 200 mm only small increase in current loading can be achieved, due to cooling problems. The force density features the same behavior. With 50-mm deep slots a force density of approximately 50 kN/m^2 is achieved while with 200-mm deep slots only 100 kN/m^2 is achieved, due to the lower current density.

To reach higher force density levels, very deep slots are required. This is mechanically difficult and, therefore, machines that have to be cheap and easy to manufacture are not likely to reach more than 100 kN/m^2 due to thermal limits. The deep slots will of course be difficult to use on

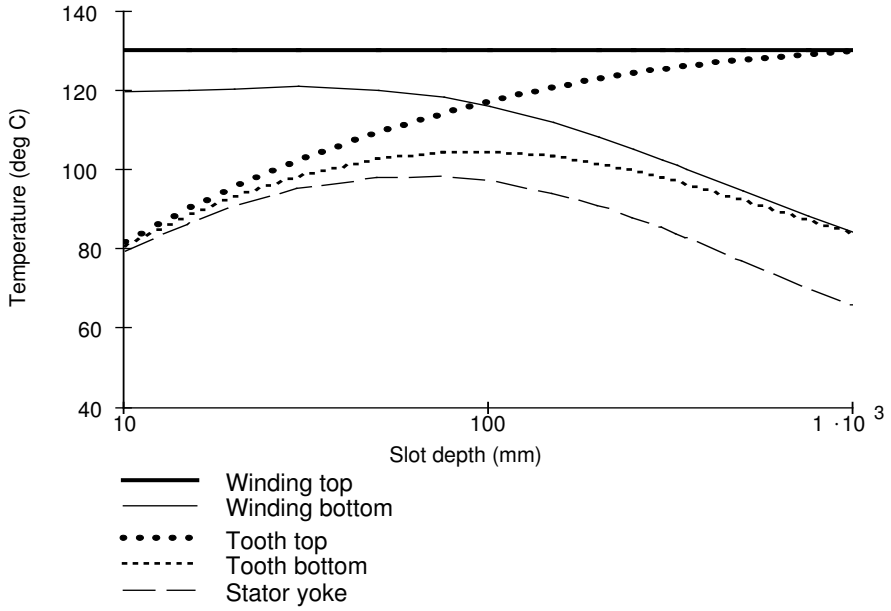

Figure 5: The temperature in the stator at 40ºC ambient temperature.

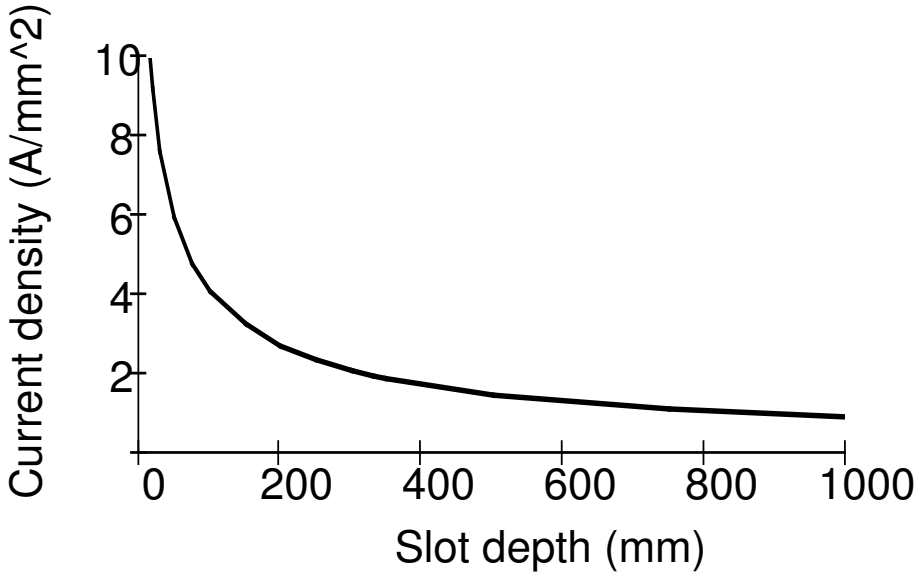

Figure 6: Maximum current density as function of slot depth.

machines with a small diameter, due to space restrictions. In these machines the achievable force density will be smaller.

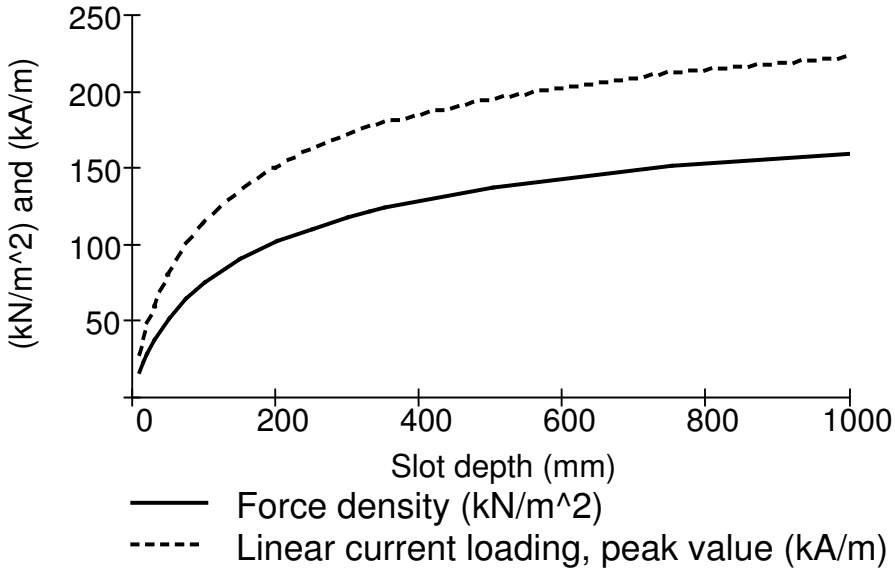

Figure 7: Linear current loading and force density as function of slot depth.

VI. REACTANCE LIMITS

The force density, derived in the earlier section, is based on a situation were it is assumed to always be possible to feed the machine with a current of the desired amplitude and phase angle. However, the possibility to do this depends on the stator impedance together with the voltage that can be fed to the stator winding. Permanent magnet ac-machines are normally fed from power electronic converters. The required stator voltage and rated current of the machine will therefore be very important, since they determine the required converter rating.

At standstill the machine converter is only required to produce DC-current and the winding resistance is the only impedance to overcome. Thus, at standstill the force densities predicted can be easily achieved. However, if the rotor is rotating the machine will need alternating currents. Then the stator reactance will also play an important role in the achievable current amplitude and angle. As noted earlier, high force density is achieved by means of deep slots. The deep slots lead to large leakage flux and therefore large leakage inductance. Hence, machines designed for high force densities can be expected to have higher stator inductance than normal industrial machines. If the inductance becomes very high it will significantly increase the cost for the machine converter and therefore make the machine unrealistic.

To enable one to compare machines of different design with each other the per unit values of current, voltage and reactance are used in the following discussion. The per unit base for voltages is the no-load voltage generated by the permanent magnets and the per-unit base current is the rated current, determined from the thermal model. The base value for the frequency is the value at rated speed.

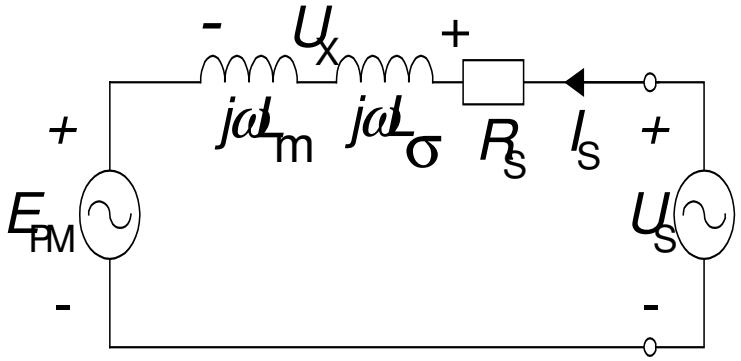

Figure 8: An equivalent single-phase circuit of a PM machine.

D. Why is reactance a problem?

The required voltage to supply the correct current to the machine is highly dependent on the induced emf, the impedance and the required phase angle of the current in the machine. In Figure 8 a single-phase circuit model of the machine is presented. The voltage source E_{PM} represents the voltage induced in the stator winding by the permanent magnets and the inductance's represent the leakage flux ($L_{\square}$) and air-gap flux (L_m) created by the stator currents. From this model the required terminal voltage U_S can be calculated. The stator resistance is neglected, because it will in most machines have to be relatively small for efficiency reasons. The two inductance's represent two different phenomena's in the machine, but are usually lumped together to one total stator inductance when determining the terminal voltage.

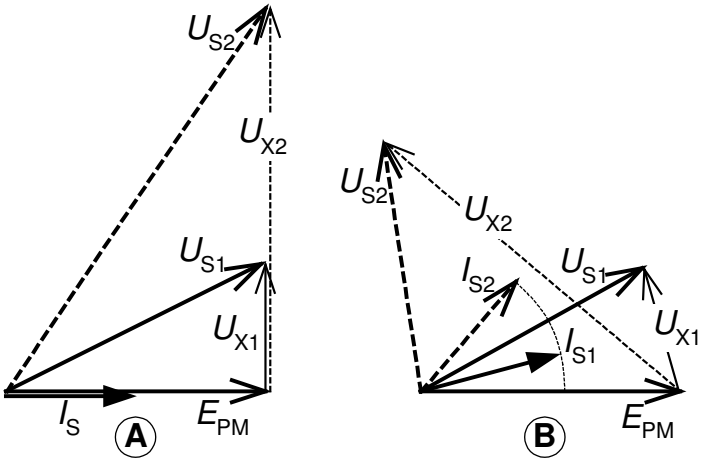

Figure 9: Phasor-diagrams for the PM machine. Index 1 for 0.5 pu reactance and 2 for 1.5 pu.

The terminal voltage required for the machine can be calculated from a phasor diagram. In Figure 9 phasor-diagrams are plotted for the machine, with two different control methods as well as two different stator reactance values. With current control method-A the motor torque per ampere is maximized, by feeding the machine with a current in phase with the internal emf. This correspond to a case in which in equation 2 is zero. With a stator reactance X_1 of 0.5 pu the terminal voltage U_{S1} is only 1.1 times higher than the emf E_{PM}, while at a reactance X_2=1.5 pu the terminal voltage U_{S2} is 1.8 times higher than the emf. Note that the phase-angle between terminal voltage and current increases with stator reactance. Therefore, a high reactance will significantly reduce the frequency converter power factor, which can also be seen in Figure 10. For control *A* the power factor is close to 1 for low reactance's, but starts to drop quickly as the reactance increases. So a machine can be made small by designing it with deep slots, but since the frequency converter rating grows as the inverse of the power factor the consequence of this will be a low power factor and therefore a large and expensive converter. Since the converter cost often is in the same order as the machine cost, a very low power factor will lead to an expensive system.

However, there are various possibilities to influence the power factor of the converter. By using a current that is leading the emf, the terminal voltage can be reduced. This is shown in phasor-diagram B of Figure 9. As can be seen, the required terminal voltage is now equal to the emf, which is much lower than for the earlier method. But since the emf and stator current are no longer in phase with each other the active power produced by the electric machine is reduced and must be compensated for by a greater machine size. This method works well at a reactance of 0.5 pu for which both the converter power factor and the active power can be

kept high. However, the method fails as the reactance grows to 1.5 pu, or higher, since the active power of the machine and the converter power factor both goes towards zero.There are also other possible controls of the stator current, but they will all lead to more or less the same problem. In [3] Jan Hystad presents a third method, here called *C*. It works better than the other methods for reactance's above 1.4 pu. Nonetheless, in this method the power factor also reduces as the reactance grows. Hence is can be seen from the power factor curves, in Figure 10, that there will be a big drawback in designing a machine with a reactance that is much higher than 1 pu.

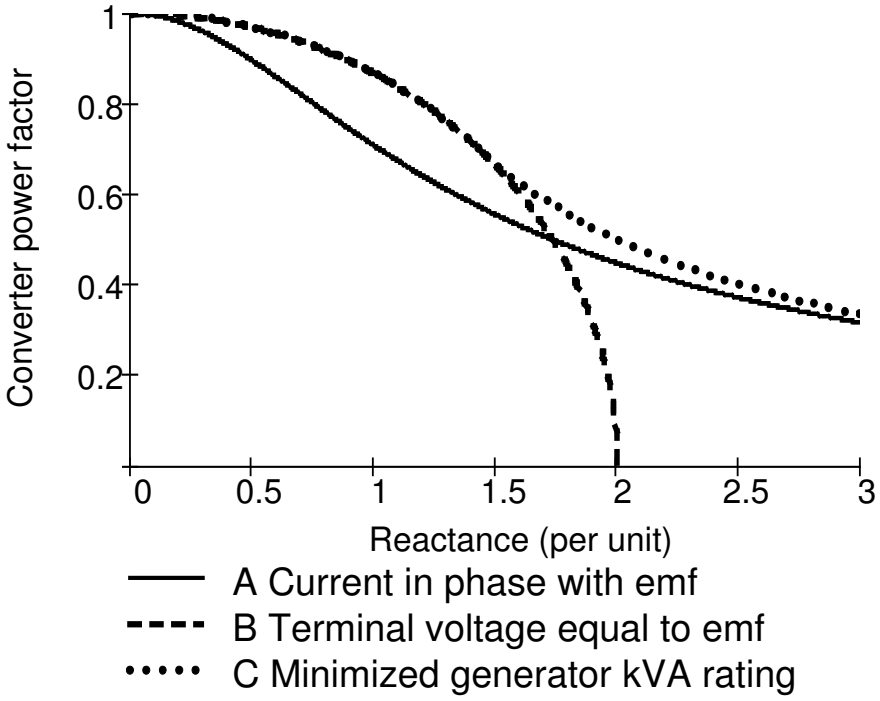

Figure 10. The converter power factor as function of machine reactance.

E. Reactance as function of slot depth

In the last section it was concluded that a large reactance will lead to low power factor values. Therefore, this section investigates the reactance in the machines with different slot depths. When calculating inductance the stator winding is assumed to have only one turn per slot. This would almost never be used in reality, but since the reactance values are presented as per unit values, the number of turns are irrelevant for the results. The inductance is calculated with analytical methods, assuming ideal iron core properties [2].

In Figure 11 the inductance of the machine is plotted as a function of slot depth. It can be seen that the leakage inductance increases much with slot

depth, the increase being slightly less than linear. However, the magnetizing inductance changes very little with increasing slot depth.
The inductance and the rated current are only dependent on the machine geometry and are not functions of the speed. On the other hand the emf, which is the per unit base voltage, will be proportional to the speed. Still it turns out that the speed will not influence the per-unit reactance values since the frequency also grows in the same rate as the emf and the reactance is proportional to the frequency. However, the per unit resistance value will depend on the speed and it will increase as the speed decreases, but since the resistance is neglected, speed does not have to be included in this investigation.
It can be seen that the leakage inductance becomes greater than the magnetizing inductance for slot depths of only 20 mm, for the investigated machine type. The leakage inductance grows almost linearly with slot depth while the magnetizing inductance only increase slowly. The inductance in Figure 11 is recalculated into per unit reactance and presented in Figure 12. The curves of course look like in Figure 11, but they are somewhat different. Note for instance that the magnetizing reactance increase more with slot depth than the magnetizing inductance. This is due to an increase in rated current, as the slot depth increase. Since the rated current is also the per unit base current, the per-unit reactance will increase. For the investigated machine 1 per unit reactance corresponds to approximately 150 mm slot depth. Note that the investigated machines have open slots and the end winding leakage has been neglected. So for real machines even higher reactance's should be expected.

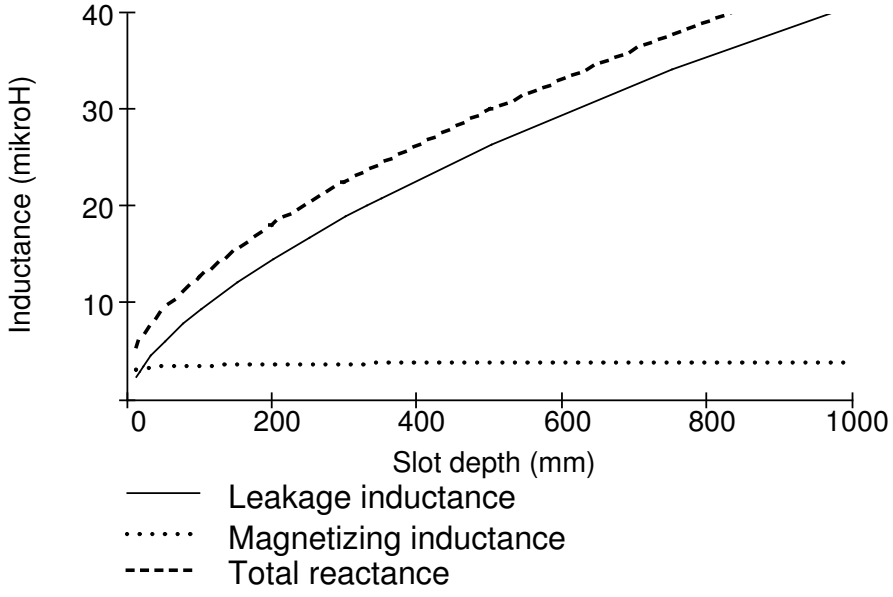

Figure 11. The inductance of the stator.

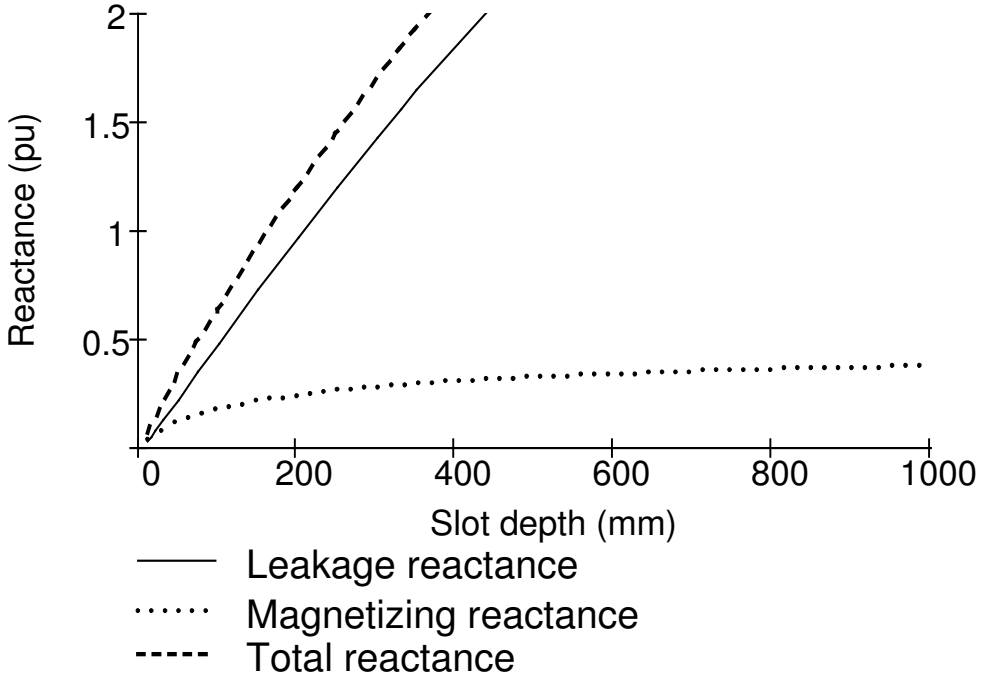

Figure 12. The reactance of the stator.

F. Force density limit due to reactance

The appropriate slot depth and current control method used is an optimization problem and will depend mainly on the cost of the machine and its power electronic converter. The rating of the frequency converter in per unit will be

$$S_{Nconv} = I_S U_S \tag{6}$$

The machine stator will be designed for the highest of the emf and terminal voltage. The stator rating will be

$$S_{Nmachine} = I_S \cdot \max(U_S, E_{PM}) \tag{7}$$

If the specific cost per kVA is similar for both machine and frequency converter, the relative cost of the system will be proportional to the sum of machine and converter kVA-ratings divided by the produced active power. In Figure 13 this relation is plotted for the three control methods. At low reactance's control method B is the best, but for reactance's higher than 1.4 per unit control method C dominates. The presented cost figure is of course a very rough estimation of the system cost and cannot be used for detailed conclusions. However, it does show very clearly that the system cost will increase much with the machine reactance. This will make machines with a high reactance non-economical. The reason is that in the optimization of a machine there is a choice between different ways to achieve the specified rated torque. The specified torque can be reached through increasing the force density, via using deep slots, or the machine

can be made larger by using a longer machine stator or a larger diameter. The cost for increasing the stator length or diameter will for many machines be approximately linear with the increase in torque. The cost for achieving higher force density by making the slots deeper is shown in Figure 14. Here the same curves of Figure 13 are plotted, but with the x-axis now representing the force density. As long as the cost of the converter and machine grows less than linearly with the force density it will be cheaper to increase the slot depth than having a larger machine. To find the cheapest system a curve that increases linearly with force density has been added. Where it reaches the lowest of the three cost curves the cheapest system is found (very roughly). From this it can be concluded that the machine with current control method B, a reactance of about 1.2 pu and a force density of 100 kN/m^2 is the cheapest solution. This suggests that for reactance reasons the slot depth should not be greater than 200 mm.

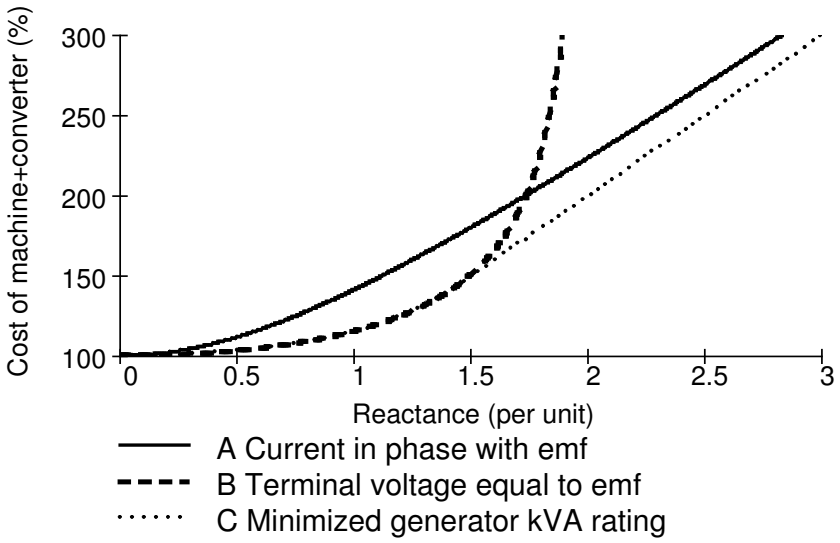

Figure 13. Approximate machine and converter cost as function of machine reactance. (Normalized)

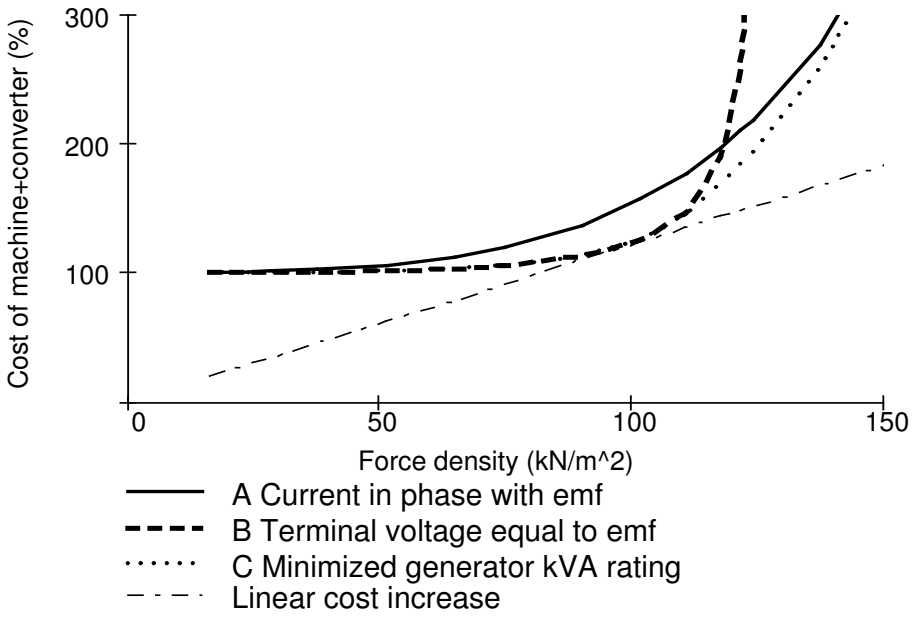

Figure 14. Approximate machine and converter cost as function of force density. (Normalized)

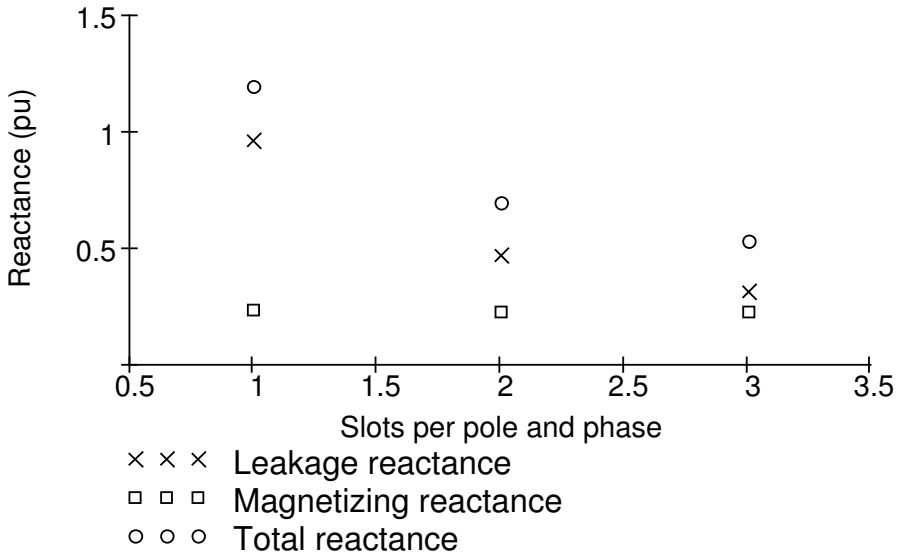

Figure 15. The reactance as function of number of slots per pole and phase.

G. Reduced reactance

It was found that the reactance of the investigated machines is close to becoming a limiting factor for the force density, although thermal limits

seem to be more important. It is, therefore, important to know if the reactance of the machine can be reduced, in order to reduce the machine and converter cost. The main cause for the high reactance is the leakage flux in the slots. This cannot be reduced without reducing the force density. But even if the inductance is fixed the reactance can be influenced, by changing the frequency.

The frequency rating can be reduced by changing the number of poles, which is the same as changing the pole pitch. To change the number of poles, without changing the slot dimensions, the number of slots per pole and phase can be changed. The earlier part of the paper only deals with one slot per pole and phase while now two and three slots per pole and phase are examined. The shape of the slots is kept exactly the same for these three alternatives. This will lead to a pole pitch proportional to the number of slots per pole and phase. In Figure 15 the reactance for the different number of slots per pole and phase are presented. The machines investigated here have the dimensions according to Table 1 and the row for 200-mm deep slots, but the air gap and magnet thickness has been increased proportionally with the pole pitch in order to avoid demagnetization. It can be seen that the leakage reactance decreases with increasing number of slots per pole and phase, while the magnetizing reactance is almost constant. Normally magnetizing reactance grows with pole pitch, but due to the increased air gap and magnet height it remains almost constant. These results shows that it will be good to use larger pole pitch and lower frequency. However, the cost of the permanent magnets will increase much with increased pole pitch and also the end windings length and stator yoke thickness will be greater.

The pole pitch at which reactance becomes a problem will of course depend strongly on the slot depth used. For small slot depths the leakage inductance is much smaller and smaller pole pitch can be used without causing problems.

V. EFFECT OF NON-LINEAR CORE MATERIAL

The assumption that the magnetic circuit is linear is, of course, more or less wrong for machines with deep slots. The no-load flux density was selected to be on the saturation limit. If the terminal voltage is higher than the no-load voltage it must correspond to higher flux density levels than at no-load, at least in some parts of the machine. Thus it can be expected that a machine designed in this way to be clearly saturated. So when assuming linear iron, one very important factor for force density limits was left out. The reason for this was to separate the different phenomena's in order not to confuse the discussion of the two investigated factors.

When designing a machine with high force density the limits presented will be further reduced, due to saturation, in the order of 30 % during continuous operation. In ref [1] the effect of saturation is investigated both for continuous and transient operation.

VI. CONCLUSIONS

The main way to achieve high force densities is by making deep slots. In an indirectly cooled machine a large temperature rise between the top part of the tooth and the stator yoke makes it difficult to achieve a high current loading level, even if very deep slots are used. At a slot depth of 200 mm 150 kA/m can be achieved. For that machine the achievable force density will be in the order of 100 kN/m^2. Above 200-mm slot depth only small increase in force density can be reached. Note that in machines with limited diameter, 200 mm deep slots are not possible and thus lower force density will be achieved. Due to other limits, like saturation or mechanical constraints lower force density limits are expected for most machines.

The high reactance caused by deep slots increase the cost for the frequency converter and, therefore, machines with a total stator reactance much larger than 1 per unit are not likely to be used. For the investigated machine type, with one slot per pole and phase, 200 mm is found to be the approximate slot depth limit also for reactance reasons. By increasing the number of slots per pole and phase the per-unit reactance can be reduced.

VII. REFERENCES

1. P. Kasinathan, A Grauers and E Hamdi "Force Density in Low-speed PM Machines: Saturation limits." *Proc. 2003 IEEE Power Engineering Society, Submitted*.
2. A Grauers, "Design of Direct-driven Permanent-magnet Generators for Wind Turbines", Ph.D. dissertation, Dept. Electric Power Eng., Chalmers Univ. of Technology, Göteborg, Sweden, 1996.
3. J Hystad, "Transverse Flux Generators in Direct-driven Wind Energy Converters", Ph.D. dissertation, Dept. Electrical Power Eng., NTNU, Trondheim, Norway, 2000.

APPENDIX I

Paper B

P. Kasinathan, A Grauers and E Hamdi "Force Density in Low-speed PM Machines: Saturation limits." *Proc. 2003 IEEE Power Engineering Society, Submitted*.

Force Density Limits in Low-Speed Permanent-Magnet Machines Due to Saturation

Prakashraj Kasinathan, Anders Grauers and Essam Hamdi

Abstract--**This paper discusses the practical limits, imposed by magnetic saturation, for the force density in low-speed permanent-magnet electric machines. The force density dependence on current density and slot depth is investigated with the aid of Finite Element Modelling. For saturation reasons, shallow slots are more favourable for achieving high force densities. However for thermal reasons deeper slots become favourable. An optimum slot depth that maximizes the force density for each current density level therefore exists. The maximum allowable slot depth range for four low-speed applications have been identified for a given maximum motor diameter.**

Index Terms—**Electric machines, Force density, Saturation, Low speed, Flux linkage, Rectangular slot**

VIII. INTRODUCTION

The continuous development of new high energy PM materials have given PM machines a promising future. The remarkable properties achieved by using permanent magnets as the excitation source have made PM motors viable candidates for variety of demanding applications. They have found use in disk drives, household domestic equipment, generators, and many high performance aerospace applications. One area that have benefited extensively from the innovations of these materials are the battery powered electric vehicle industry. The main application includes power wheelchairs, electric scooters, forklift trucks, electric golf carts, electric vehicle and electric bicycles. It has been shown, on the basis of dimensional arguments, that traction in-wheel motors for these applications, require very high force densities to fulfil their peak torque requirement. The high force densities achievable using sintered and bonded NdFeB magnets have made direct-drive in-wheel motors, for the above mentioned applications, promising for the future. This was not possible during the time ferrite magnets were in domination. The high force densities minimizes, the required active material used with significant savings in manufacturing cost. This has been the catalyst for the drastic increase in motor manufacturers around the globe investing into research and development for suitable PM topologies for specific

applications. Low-speed direct-drive generators is another main area which would require high force densities in achieving an optimized design suitable for mounting and transportation [1,2,3].
Examination of the peak torque requirement for in-wheel traction motors, for applications such as electric vehicles, forklift trucks, electric golf carts and electric wheelchairs, with the available space and cost as the constraint, shows that the design engineer is working at the technical limit with the present technology. Thus, if the peak force density achievable without exceeding the thermal limits can be determined for various slot dimensions, one could instantly determine if the chosen topology is viable for a specific application. The achievable force density in practice will depend, for a given machine, mainly upon four general factors: thermal, inductance, saturation and cost. The way the thermal limit for the winding and the stator inductance influence the force density of a slotted PM machine was discussed in [1] using a linear magnetic model. Depending on the application, the force density predicted from a linear thermal model would be greater than that achieved in practice since saturation in the stator core will significantly limit the force density.
The primary aim of this paper is to investigate the influence of magnetic saturation on the force density. The maximum force density achievable for slot depths within the range of 10 mm to 1000 mm with different magnitudes of current loading is found. Of course, not all possible designs have been investigated, instead a few designs have been used to illustrate the interesting results caused by saturation effects. By applying scaling laws the results can be used as a guide in tailoring ones design towards fulfilling demanding technical specifications. The findings in this paper would be useful to a machine designer that requires a fast estimation on the required slot depth for preliminary calculations.
The investigation is limited to low-speed machines: multi-pole, three-phase, permanent-magnet machines with slotted full-pitch windings.

However similar results are expected for a variety of machine types utilizing concentrated full pitch windings. It is important to note that, the machine variables selected in the investigations are not targeted to a specific application or one machine size. Thus where appropriate the slot depth limit above which force density degradation would occur for specific applications will be stated. It is up to the reader's discretion to interpret the results presented in this paper for their application by applying the well known scaling laws of machine design [4].

IX. SATURATION LIMITS

A. Magnetic model

The magnetic model shown in figure 1 was developed using a commercially available finite-element package in order to investigate the force density limit in slotted machines.

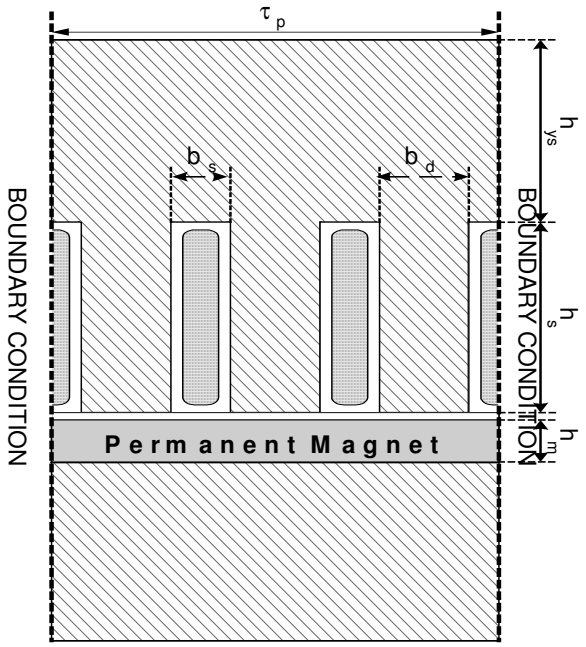

Figure1: Magnetic Model

The investigation is confined to only rectangular open slot machines. Rectangular open slot design was adopted as the very large coils used in deep slots are otherwise difficult to mount. Closed slots will lead to approximately 10% greater force density than that achieved with open slots. The excitation flux is obtained from permanent magnets mounted on the surface of the rotor. Since the aim of the paper is in determining the attainable peak force density, only machines of integral slot design with 1 slot per pole per phase are considered here. With reference to Figure 1, the conductors and the slot walls are separated by a thin layer of air to accommodate the slot liner. The stator and rotor yoke are taken 5 times thicker than the width of the stator tooth. Table 1 gives the dimensions of the stator and magnet used in the model. The pole pitch (τ_P), tooth width (b_d), slot opening (b_S) and magnet height (h_m), all vary with slot depth (h_S). The allowable current density (J_s) in the conductors is determined from a thermal model presented in [1,2].

Table 1:The values of the machine variables for different slot depths.

h_S (mm)	b_S (mm)	b_d (mm)	τ_P (mm)	J_S (A/mm^2)	h_m (mm)
10	6,11	7,79	41,7	12,01	6,26
15	6,22	8,42	43,9	10,35	6,59
20	6,52	9,19	47,1	9,17	7,07
30	7,15	10,67	53,5	7,62	8,02
50	8,24	13,14	64,2	5,91	9,62
75	9,29	15,60	74,6	4,77	11,20
100	10,12	17,64	83,3	4,07	12,49
150	11,43	21,04	97,4	3,21	14,61
200	12,47	23,88	109,1	2,69	16,36
300	14,14	28,63	128,3	2,06	19,25
500	16,66	36,14	158,4	1,44	23,76
750	19,10	43,63	188,2	1,05	28,23
1000	21,16	49,99	213,5	0,84	32,02

The current density values given in Table 1 correspond to continuous operation ratings. During transient operation, higher values are used. The rotor magnets are assumed to be uniformly magnetised. Since the peakforce density achievable is of prime interest, rotor magnets with a remanence of 1.25 T and coercive force of 90.5 kA/m are assumed. It should be noted that such figures are well within the capability of commercially available materials. The magnet pole arc used throughout the investigation is fixed at 180 electrical degrees since it maximises the achievable force density.

In order to confirm the validity of the model and investigate the severity of saturation on the force density, the stator steel of the magnetic model was simulated assuming both linear and non-linear demagnetisation characteristics with each model having the same dimensions and slot current values. This makes the results directly comparable, with only one variant; namely the magnetic saturation effects.

B. Effect of saturation

The force density values should not be obtained at only one rotor position. In a machine, the force developed at the rotor corresponds to the average force. Thus for each row of stator and rotor dimensions in Table 1, the force density was determined for 40 rotor position spanning the full pole pitch. The current fed into the slots were forced to vary sinusoidally with rotor position. Figure 2 shows force density variation with rotor position. If the force density was calculated at only one rotor position, such a value could have been either higher or lower than the average force density, depending on the position of the rotor assumed.

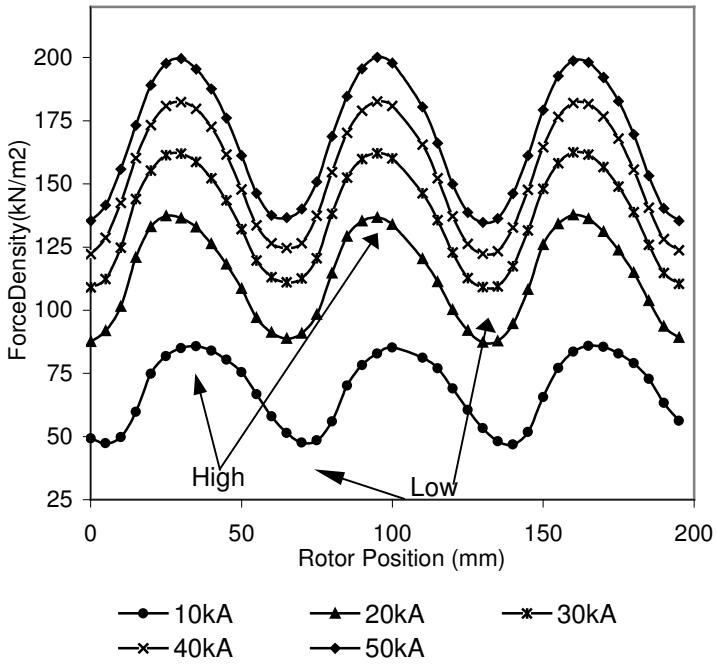

Figure 2: Force density versus rotor position for different peak current levels in the slot. Pole pitch (τ_P=200 mm)

The peak force density does not occur when a north or south pole is positioned under tooth as shown in figure 1. Contrary, this is the worst rotor position leading to minimum force density. Hence to avoid errors in determining the achievable peak force density, the resultant average was determined.

The objective of this section is to determine how severely does saturation in the core material affect the attainable force density in practice. Figure 3 shows the force density characteristic of the machines listed in Table 1; curve A1 and B1 shows the force density as a function of slot depth during rated condition, when the slot current is at the thermal limit; curve A2 and B2 shows the force density characteristic during transient condition, when the slot current is twice the rated current. The magnetic model of curves A1 and A2 uses a non-linear stator magnetic material while that of curves B1 and B2 utilizes a linear magnetic material. The force density curves increase rapidly to a peak and tend to level off at a much slower rate towards the x-axis. The curves for non-linear iron show a marked difference from that of the linear iron and permit a comparison between an ideal and real machine.

With a linear material the force density predicted from the FEM result (B1) shows to increase with slot depth linearly with current loading. High force density levels are achievable, limited only by the temperature rise. Thus the curves for the linear iron "level off" only due to thermal

limitations. As the slots become deeper, the current density has to be reduced to avoid overheating. As a consequence of this, the current loading and force density does not grow linearly with slot depth. In [1] this curve is derived and explained in detail.
However in real machines, in which the stator material exhibits non-linear characteristics, the force density behaviour (A1) tends to deviate significantly from the above-mentioned ideal characteristic. Saturation of steel is a complex function of applied magnetic field, contributed by the rotor magnet and stator current flux. Close examination of Figure 3 indicates that the force density is not directly proportional to current loading because magnetic saturation sets in after the slot depth (and current loading) is increased beyond a certain level. At low slot depths, the linear and non-linear iron lead to almost the same force density but as the slot depth exceeds 50 mm, saturation reduces the force density in real machines significantly.

At a slot depth of 200 mm the force density achieved with the non-linear material at rated condition is approximately 75% of that achieved with a linear material. With 2 times higher armature current this reduces to 55%. At a slot depth of 1000 mm a force density of 88 kN/m^2 and 310 kN/m^2 is obtained from the non-linear and linear model, respectively during transient operations. Thus, these results show that saturation in the stator has significantly reduced the attainable force density by a remarkable factor of 3.5. The force density curve peaks at about 70 kN/m^2 (continuous) and 100 kN/m^2 (transient) corresponding to a 200 mm and 150 mm slot depth respectively. A further increase in slot depth causes a decrease in the force density due to increasing saturation. Curve A1 and A2 indicate that the force density did not change appreciably for the different armature current levels with large slot depths. Above 150 mm and 200 mm (both conditions), the increase in current loading with increasing slot depth lead to a reduction in force density due to the armature reaction contribution to the saturation of the magnetic circuit. Thus, most of the flux lines that are supposed to contribute to force production do not link with the whole winding however appear as leakage flux. Although the current is increased with slot depth according to the thermal limit, the high leakage flux is primarily the dominating factor in limiting the achievable force density. This explains the slow decrease in force density above 150 mm and 200 mm slot depth, as shown in Figure 3.

Thus from the results presented in this section, it is evident that magnetic saturation has a remarkably significant effect on predicting the achievable force density.

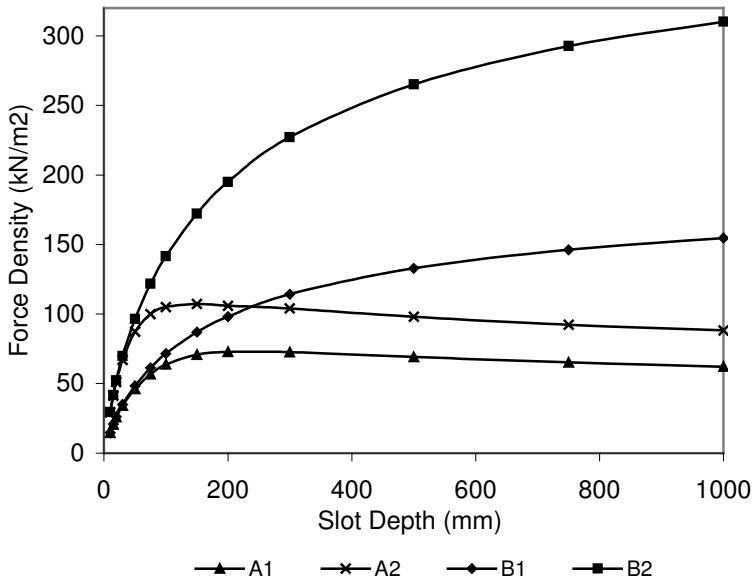

Figure 3: Force density (kN/m^2) versus slot depth(mm) with non-linear material (A) and linear material (B) at rated current (1)and transient load of 200% of rated current(2).

C. Achievable continuous and transient force density

The objective of this section is: (1) to determine the force density versus slot depth envelopes for various current loading (2) to investigate the behaviour of the optimum slot depth that maximizes the force density at various current loading.

Figure 4 shows the force density against slot depth curves determined in the same manner as in section B above, corresponding to the slot and magnet dimensions of Table 1. To enable comparison of results, the slot current in of Table 1 during continuous operating conditions are increased by a fixed factor. The total slot current of curve X2 is twice the magnitude of curve X1 while X9 has a total slot current of 9 times that of X1. Some of the current levels are probably too high to be used even at transient state, due to thermal limits.

By examination of Figure 4, it is readily apparent that an optimum slot depth, at which the force density is a maximum, exists for each current loading. It is interesting to notice the changes in the gradient of the force density curves. The force density curves initially exhibits a positive gradient, reaches a maximum point and then decreases with a negative gradient. Also evident in the plot is the fact that, the negative gradient of the curves becomes steeper with increasing slot current. Examination of the curves indicate that, due to saturation effects, the difference in distance between adjacent envelopes decrease although the slot current is

increased gradually up to a factor of 9 (X9), the peak force density only increased by approximately three fold.

Figure 5 shows, the slot depth at which the peak force density occurs in each of the curves of figure 4, with respect to the current multiplication factor. It is interesting to note that at high values of current, the peak force density occurs at approximately the same slot depth of 100 mm. As stated previously, at rated condition (X1) a peak force density of 70 kN/m^2 is achieved with a slot depth of 200 mm. However, with a current factor of 3 and 9, a peak force density of 120 kN/m^2 and 205 kN/m^2 is achieved with approximately the same slot depth of 100 mm.

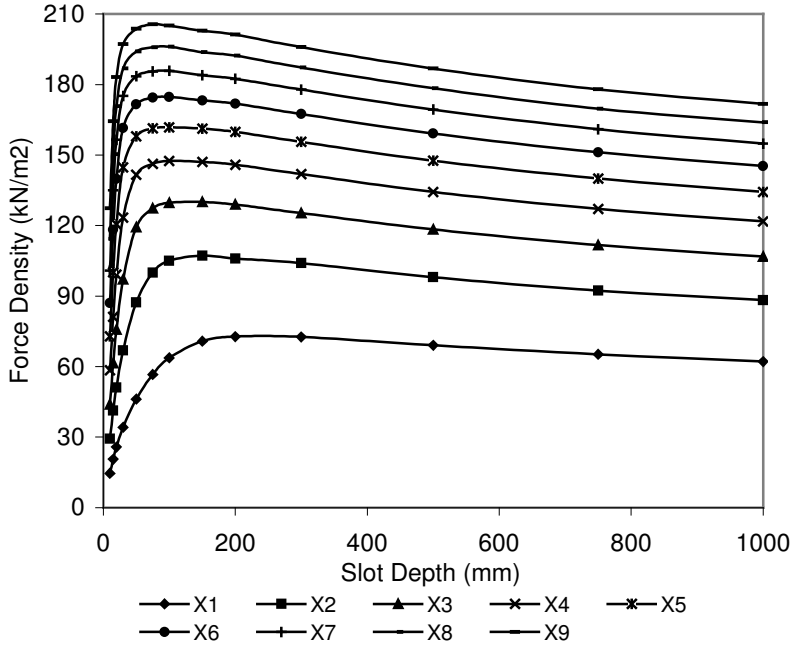

Figure 4:Force density versus slot depth (mm) for multiple slot currents

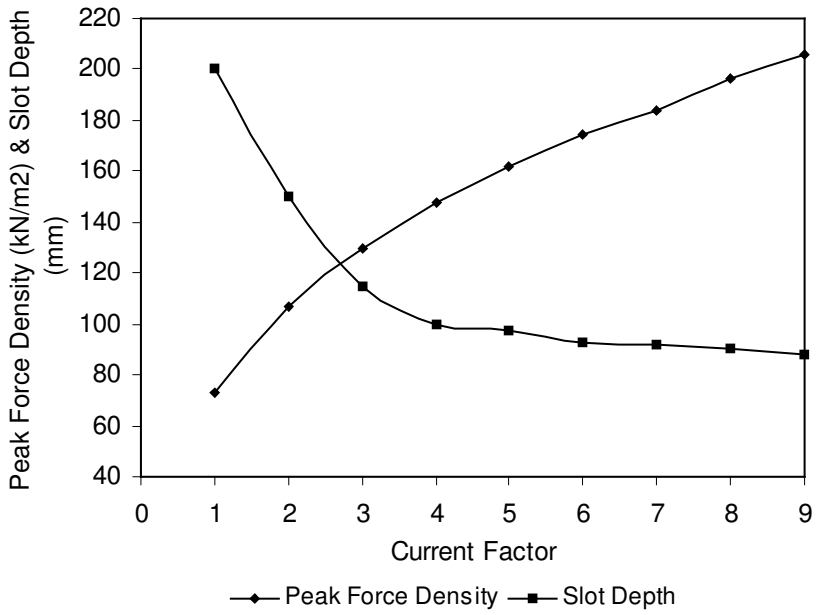

Figure 5: Peak force density (kN/m^2) and slot depth (mm) for which maximum force density occurs is obtained versus current factor.

For continuous load operations a force density no grater that 70 kN/m^2 can be achieved. For transients operation within a one-minute time frame no greater than 120 kN/m^2 can be achieved. At extreme transient operations (X8), for say one second, no greater that 190 kN/m^2 can be achieved.

This result stresses the important fact that, in applications involving high slot currents and experience high armature reaction effects, deep slots should not be used. A smaller slot depth would enhance the performance at high current levels, but will have the opposite effect at low current levels. From figure 5, it is obvious that for any current loading greater or equal to 3 times the rated condition of table 1, the maximum slot depth of approximately 100 mm should not be exceeded.

When a machine is designed, one tends to concentrate on the peak and rated torque. Deep slots up to 200 mm would result in an acceptable peak force density during rated condition. However a 200 mm slot depth would have an adverse effect on the attainable peak force density during transient conditions. Therefore, the slot depth chosen would depend on the relative importance between the transient and continuous torque for a particular application due to the small conflict between achieving the highest possible force density at rated and transient load.

X. MAXIMUM SLOT DEPTH AS A FUNCTION OF CURRENT DENSITY

In section B and C most of the results were concerned with machines in which their variables shown in Table 1 were changed with slot depth in order to have a thermally optimized design. The primary aim of this section is to investigate, the force density behaviour for a range of slot depths with increasing current density but keeping slot and tooth width constant. The simulations were performed only for a fixed rotor position since the actual force density was not of interest. This will be sufficient to highlight the way the current loading in each slot influences the force density values. Thus as the slot depth increased, the stator and rotor dimensions listed in Table 2 were held constant with gradual increase in slot current density. The slot depths considered were limited to 300 mm.

Table2: The values of machine variables for different slots depths

τp	h_m	b_S	b_d	h_S	
(mm)	(mm)	(mm)	(mm)	(mm)	
200	20	33.33	33.33	Varied	
109.1	16.36	12.47	23.88	Varied	Reproduced
41.7	6.26	6.11	7.79	Varied	from table 1

Although some of the combinations, of current density and slot depth may not be used in practice due to thermal limits and mechanical constraints, nonetheless, it was considered in the investigation as it would greatly facilitate the understanding of the saturation effect. Also the effect of saturation on the force density will become more prominent at such extreme slot depths. Figure 6 shows the force density against current density for various slot depths for a pole pitch of 200 mm (Table 2). It is evident that the force density increases with current density. However the gradient of the curves becomes greater with increasing slot depth. Thus for a fixed current density a deeper slot would yield a higher force density. For current density values greater than 3 A/mm^2 the curves with slot depths of 150, 200 and 300 mm tend to superimpose on one another. Above 3 A/mm^2 the force density achieved for all of the 3 slot depths are approximately the same for all current density values. The three curves merge at a current density of 4 A/mm^2 corresponding to a force density of 88 kN/m^2. Thus with a current density of 6 A/mm^2 a force density of 100 kN/ m^2 can be achieved by using a slot depth of 100 mm just as well as 150, 200 or 300 mm. Increasing current density by a factor of 2.5 to 10 A/mm^2 in these slots results in an increase in the force density by a

factor of only 1.4, achieving 124 kN/m^2. This factor increases approximately to 2.1 for slot depths of 75 and 50 mm respectively.

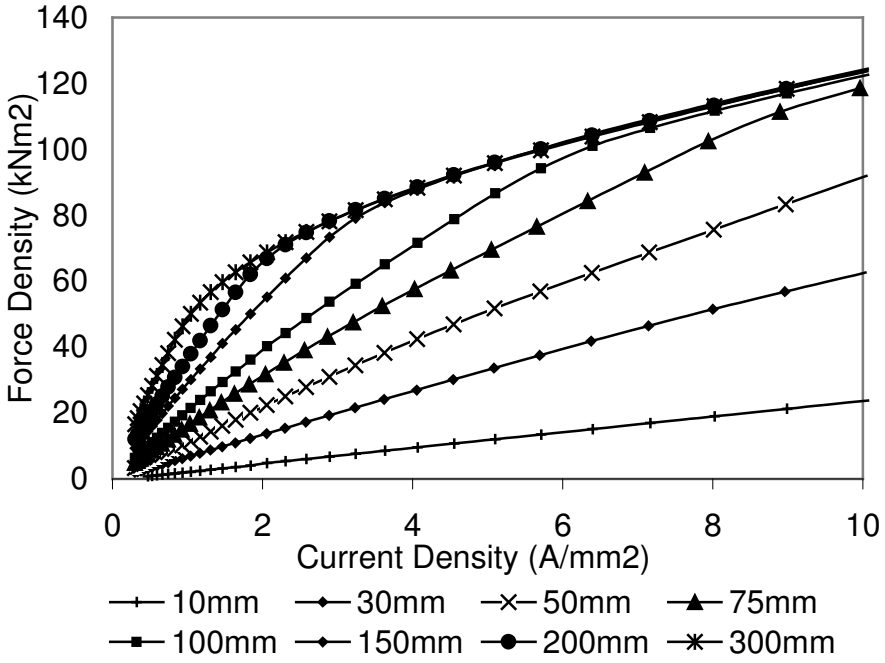

Figure 6: Force density versus current density (τ_P = 200mm , Table 2)

From the above discussion, two regions, having opposite characteristics, can be identified and these are now explained with the aid of Figure 7 which shows the force density variation with slot depth for current densities up to 30 A/mm^2. Although, extremely high, such a value of current density facilitates the investigation of the two important regions. *Region 1:* For fixed current densities, a greater force density is achieved with deeper slots. *Region 2:* For fixed current densities, equal force densities are achieved with a number of different slot depths. In region 1 the effect of slot depth is negligible and the force density increases directly with total slot current. In the non-linear region, however, the saturation is due to combination of total slot current and slot depth. To design a machine to operate in region 2 would be a waste of material since the same performance is achievable with smaller slot depth. Figure 7 can be used as a guide for the machine designer. From this figure the maximum allowable slot depth with a specific current density corresponding to the slot variables of Table 2 can be determined. From the curves, for current densities of 3, 6 and 12 A/mm^2, the slot depth above which will not result in any increase in force density with increasing current is 150, 100 and 75 mm respectively. Figures 8 and 9 show the corresponding curves for two machines with differing pole pitches. Figures 7,8 and 9 were obtained for one rotor position only as

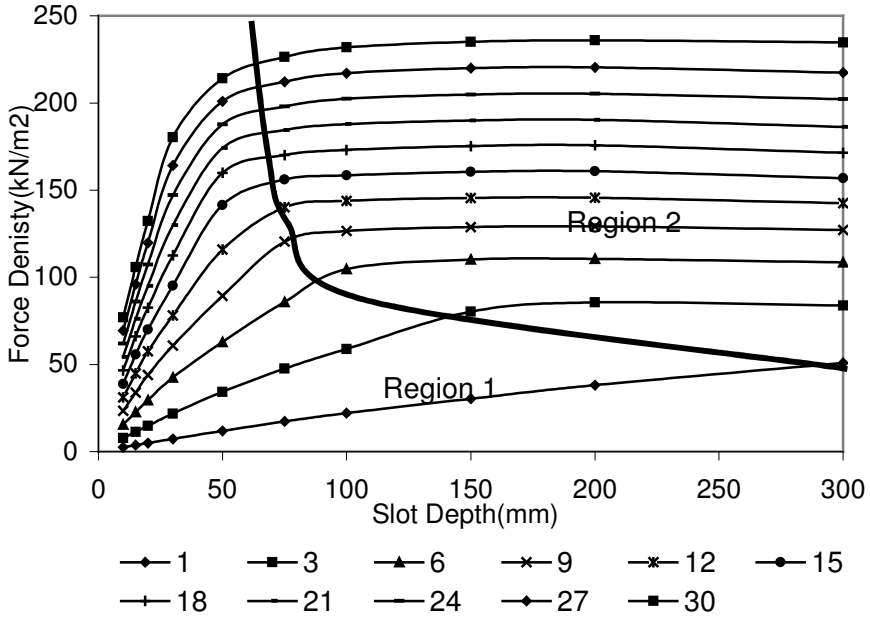

Figure 7: Force density versus slot depth curve for varying current density levels (A/mm^2) corresponding to machine variables of Table 2.

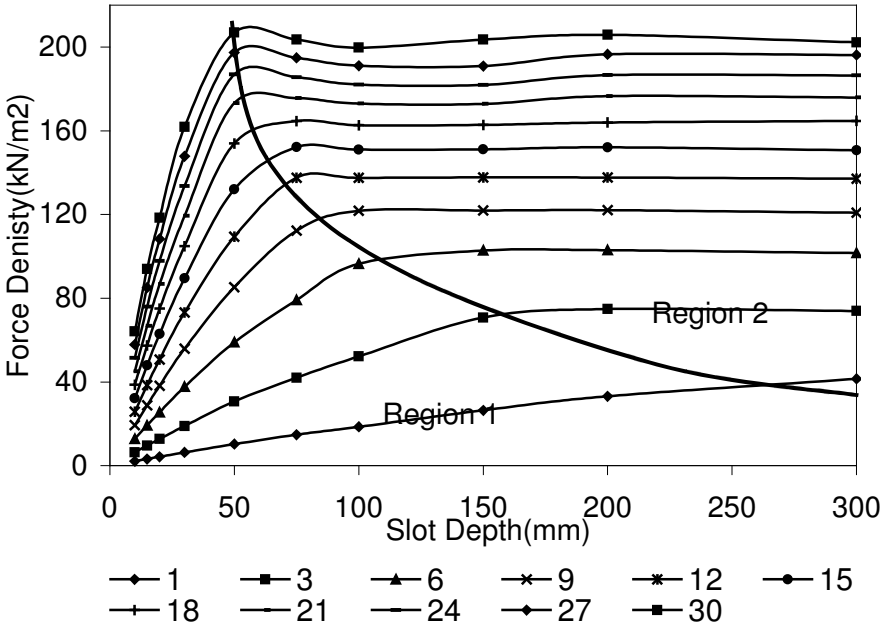

Figure 8: Force density versus slot depth curve for varying current density levels (A/mm^2) corresponding to a τ_P of 41.7 mm (Table 2)

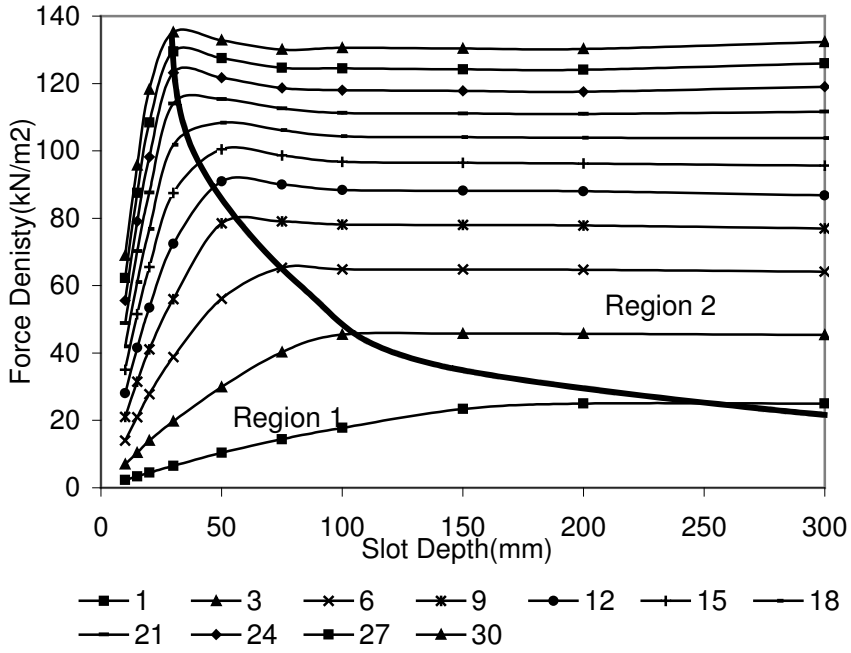

Figure 9: Force density versus slot depth curve for varying current density levels (A/mm^2) corresponding to a τ_P of 109.1 mm (Table 2)

this is sufficient for the aim of this section. However in-order to utilize these curves for design purposes, the resultant average of the force density must be determined as performed insection B and C. Determining these curves for a range of pole pitches, will enable one to produce a useful database, that can be used in determining if the specification can be met within the given space.

XI. FORCE DENSITY SEEN FORM A FLUX LINKAGE POINT OF VIEW

A. Introduction to Flux Linkage-Current Models

Flux Linkage versus current graphs are a very useful way of modelling the behaviour of an electric machine seen from its terminals. Compared to the equivalent circuit models, they represent a much more general model since saturation effects, space and time harmonics can be easily included. The model has rotor positions and current as inputs and has flux-linkage and torque as its output. Table 3 lists pros and cons of the flux linkage-current models.

Table 3: Pros and cons of the flux linkage-current models.

Advantages of flux linkage-current analysis
+Allows a unified theory for investigating all different types of electric machines
+Include all phenomena's that influence the machine electrically
+Can be used to calculate the torque (if the losses are dealt with outside of the flux linkage-current model)
+Allow time transient calculations
+Can be used to simulate the electric machine for circuit simulations
+Can be used for control design
Disadvantages of flux linkage-current analysis
-It is a black-box model: It Gives less insight into the mechanisms which is the base for the machine function
-More complex to use for analysis than a circuit model
-Is not so useful during machine design. More useful once a fixed machine shall be modelled for the design of a controller and design of the power electronic converter

B Flux linkage-Current Analysis

Staton et al [5] extensively used the flux linkage-current diagrams to illustrate the difference between torque production mechanisms in different machine types. It is therefore interesting to see in what way they can explain the maximum force density that can be achieved in low-speed PM machines. The objective of this section is primarily to determine the influence of slot depth variation on the loop area of the flux-linkage versus current diagram. The flux linkage-current diagram is used to discuss the same phenomena's investigated earlier. Although the mechanism involved is not obvious, it is clearly seen from the flux linkage-current diagram that deeper slot lead to higher continuous torque and lower transient torque.

In order to obtain the data for the flux linkage-current model the machine corresponding to one row in Table 2 is selected. The peak slot current was varied from –30 kA to +30 kA in steps of 1 kA for 11 different rotor position from 0 to 180 electrical degrees. The same evaluation was performed for 3 different slot depths and their Flux linkage-Current diagram are shown in Figure 10. The diagram represents different combinations of current and rotor position with one flux-linkage curve for each rotor position. Here it is assumed that the phases are fed symmetrically. Without this assumption, three electrical terminals and three different flux linkage values for all combinations of slot currents would be needed for each machine. For motor operation, only some of the combinations of flux-linkage and current are used. The currents have to vary as a function of rotor position in a manner that the machine produces torque in an efficient way. The electric energy fed into the machine during one electric cycle can be expressed as

$$\mathrm{Wel} = \int \mathrm{u}\,\mathrm{i}\,\mathrm{dt} \qquad (1)$$

This can mathematically be transformed into

$$Wel = \int i\,d\psi \qquad (2)$$

which can be interpreted as the area enclosed by the trajectory of the machine flux-linkage and current. If the determination of the losses is not within the black-box model, the mechanical energy produced must equal the electrical energy. For one electrical cycle that gives

$$2\tau p\,Faverage = W_{el} \qquad (3)$$

from which the average force over one cycle can be derives

$$Faverage = \frac{Wel}{2\tau p} = \frac{1}{2\tau p}\int i\,d\psi \qquad (4)$$

The average force during continuous operation can then be obtained from figure 10: With 50,100 and 200 mm deep slots the peak current has to be limited to about 7, 10 and 12 kA for continuous operation respectively, for thermal reasons. Thus the maximum force that can be produced during continuous operation will correspond to the area of surface A B and C in the diagrams. The area of surface A, B and C corresponds to approximately 3500, 4000 and 5500 Ws/cycle respectively. Thus the continuous force grows less than linearly with increasing slot depth.

If we assume that the machine for short time can use 200% of the rated current, we can see that the transient torque will correspond to surfaces D, E and F. Due to saturation the machine with 200 mm deep slots will not produce higher transient torque than the one with 100 mm slots. With 50 mm slots the force will however be lower than with 100 mm. For 50 mm slot depth the force density can further be increased by 200% of the continuous current. For 100 & 200 mm slot depth only marginal force increase can be achieved by using more that 200% rated current. The area inside this trajectory equals to the force density. From the plots, it is obvious that a 200 mm slot depth have a relatively thin flux linkage-current loop with smaller enclosed area compared to that of a 50 mm slot depth. The deeper the slots the lower will be the peak force capability, as the largest possible surface that can be enclosed decrease with slot depth. It decreases both because saturation makes it smaller in the current

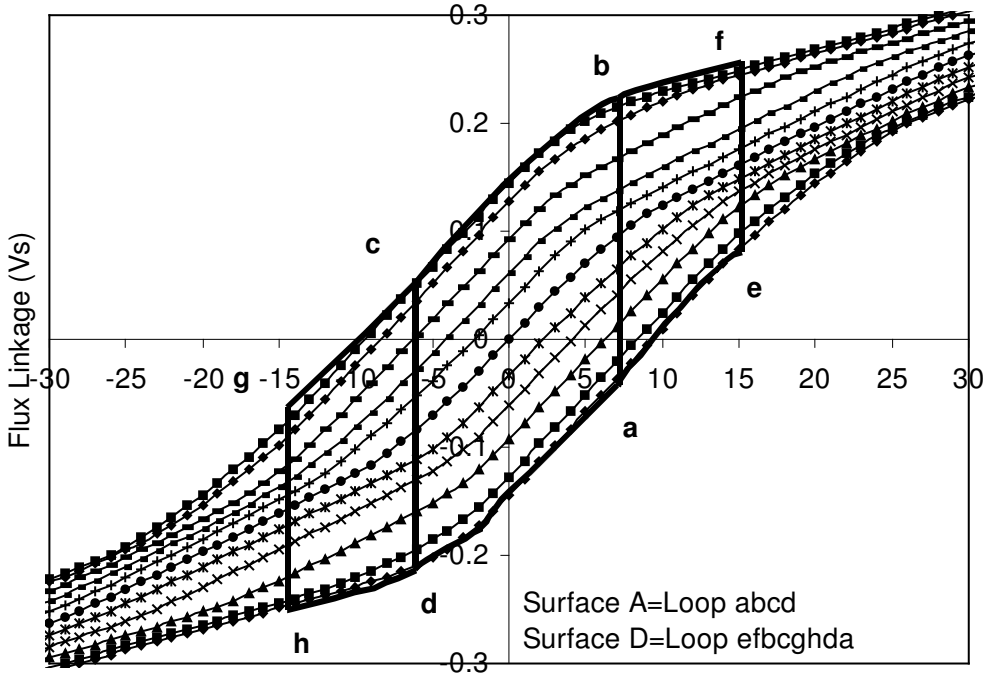

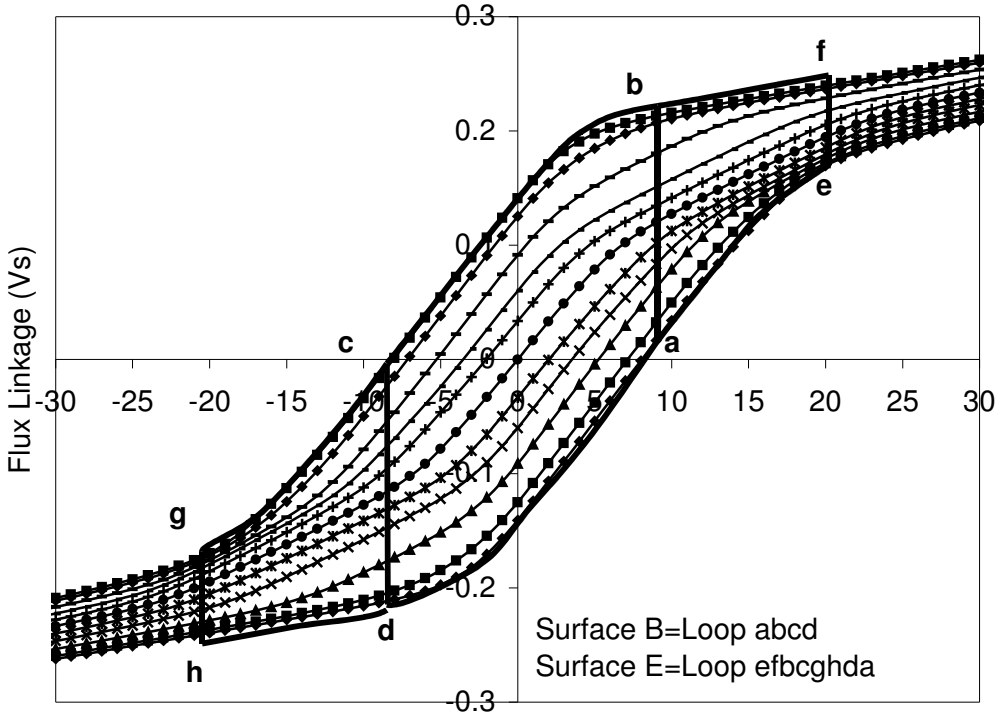

Figure 10 : Flux Linkage versus slot current at different rotor positions (electrical degrees). Top-50-mm, Center-100-mm, Bottom-200-mm slot depth

direction but also because the peak flux linkage is reduced with slot depth due to increased leakage. It is readily apparent from the presented plots that deep slots, which would experience high saturation, will result in low force densities being achieved. For a specific stator and rotor dimension, the decrease in force density with increasing saturation indicates that the force density will be maximised at a specific slot depth. This value of slot depth was determined in sections B and C above. Therefore, it may be implied that the desirability for achieving high force densities can be achieved with smaller slot depths instead. In Figure 10 the rate at which the area of the loop decreases with increasing slot depth in practice, is not only very sensitive to saturation in the core material, but to the thermal properties of the slot.

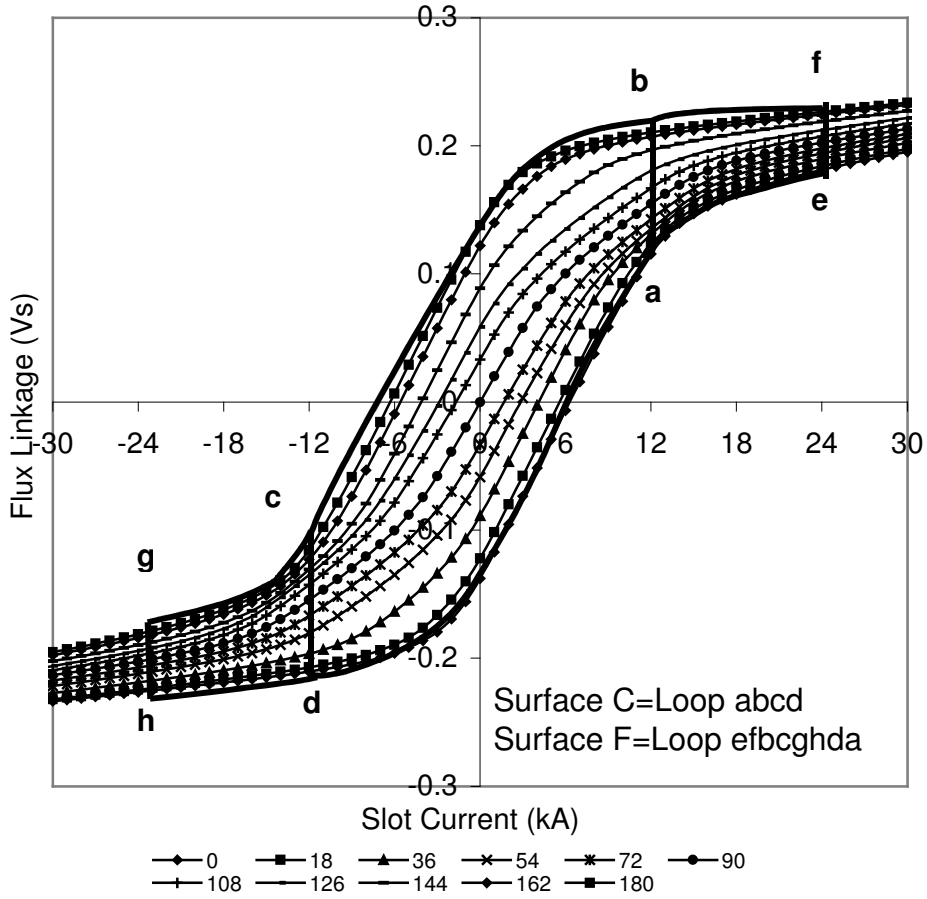

The flux-linkage versus current graphs presented here are very different than those presented in [5]. This is due to the deep slots and high current which lead to the stator current producing a higher flux linkage that the PM's. The graphs in [5] are for more normal low force density machines.

APPLICATIONS

Although the objective of this paper is primary to determine the approximate peak force density limit and the way it generally varies with slot depth and current density, the approximate force density for 4 directly-driven applications are presented here. The choice of slot depth depends on whether a high force density is needed for continuous or transient condition.

In applications where high force densities (and electric loadings) are required due to limited space and the short-term peak torque requirements is of high importance, such as direct-drive in-wheel traction motors for forklift trucks, electric vehicle, wheelchairs and golf-carts, slot depth no greater than 100 mm (see Figure 5) should be used to fulfil the peak torque requirement. On the other hand, in applications where continuous

operation is more important than transient operation, such as direct-driven PM wind generators, slot depth up to 200 mm can be used. A slot depth greater than this value would not result in an increase in the achievable peak force density however would only increase the converter kVA requirement due to the increased inductance [1].

Table categorises the applications according to the importance of peak and rated condition and summarizes the maximum slot depth that can be used by the design engineer. The slot depth range of the first 3 applications in Table 4, are determined with respect to the hub size of the wheels currently used. The in-wheel motors for wheelchairs, golf-carts and forklift trucks, are mainly designed to meet the peak torque requirement instead of the rated torque. The minimum peak force density required in such an application would be approximately 20 kN/m^2, 18 kN/m^2, 50 kN/m^2, for a wheelchair, golf-cart and forklift truck motors, respectively. This will enable the motor to be fitted elegantly into the hub of existing wheels within the available space. However, in wind generators, the continuous torque is of greater importance. The maximum force density for continuous operation would be typically 70 kN/m^2 with a 200 mm slot depth (Figure 3). For a 1.5 MW wind generator having a rated speed of 18 rpm, transportation and mechanical considerations limit the outer diameter and total length to approximately 4.2 and 1.5 m respectively. With a rated torque of approximately 850 kNm, one would require approximately 50 kN/m^2.

The peak force density required in each of the application will increase as the active axial stack length is reduced. The percentage in which this reduction is permitted will be indefinitely set by the thermal limit as a greater electric loading will be essential in fulfilling the peak torque requirement.

Table 4: Direct-Drive Machines

Application	Condition	Slot Depth Range (mm)	Necessary Force Density (kN/m^2)	Possible Force Density (kN/m^2)
Wheelchair	Transient	<35	20	30
Golf-cart	Transient	<45	18	32
Forklift Truck	Transient	<70	50	70
Wind Generators	Continuous	<200	50	70

CONCLUSIONS

In this paper the peak force density limits imposed by saturation, in slotted machines of integral slot design with 1 slot per pole and phase, is presented for various stator and rotor physical dimensions. For all the four investigated applications the investigated machine type can be used with some difficulty as the required force density is close to the practical found limits. Table 5, summarizes the approximate maximum force density obtained from Figure 4 with respect to the assumed current loading for each respective conditions.

Table 5:Maximum Force Density Achievable at Different Current Conditions

Conditions	Current Condition	Peak Force Density (kN/m^2)
Continuous	I_{Rated}	70
Short term	$3I_{Rated}$	120
Extreme	$8I_{Rated}$	190

An optimum slot depth, which maximises the force density for each current density, exists. As the current density in the slots increase, a greater force density is obtainable with a smaller slot depth. The useful slot depth depends on the current density used. At high current densities, only small slot depths are useful. For current loading greater than 3 times the rated condition, the optimal slot depth that maximises the force density for current loadings used in this paper was found to be approximately 100 mm. Open slots are assumed, but the results are expected not to vary greater than 10% for closed slot machines.

The loop area of the flux-linkage against slot current plot, which corresponds to the force density in the machine, is inversely proportional to the slot depth, and is limited by saturation in the stator core. It is obvious from the presented results that saturation has a very important influence on the achievable force density.

REFERENCE

[1] A.Grauers, P.Kasinathan, "Force Density in Low-speed PM:Temperature and Inductance limits", *Proc. 2002 IEEE Power Engineering Society, Submitted*.

[2] A.Grauers., "Design of Direct Driven PM Generators for Wind Turbines", PhD Thesis, 1996 Chalmers University Technology, Gothenburg, Sweden.

[3] B.J.Chalmers, W Wu and E.Spooner., "An Axial-Flux PM Generators For Gearless Wind Energy System", Transactions on Energy Conversion, IEEE, vol.14, no 2, June 1999

[4] Essam S. Hamdi. "Design Of Small Electrical Machines", John Wiley & Sons Ltd.

[5] D.A.Staton, R.P.Deodhar, W.L.Soong and T.J.E.Miller., "Torque Prediction Using the Flux-Mmf Diagram in AC, DC, and Reluctance Motors.", Transactions on Industry Application, IEEE, vol.32, no 1, Jan/Feb 1996

Appendix II

Integral-Slot Machines

Averaged force density in integral-slot machines for various slot depth and current density levels for machines having pole pitches listed in Table 3.1

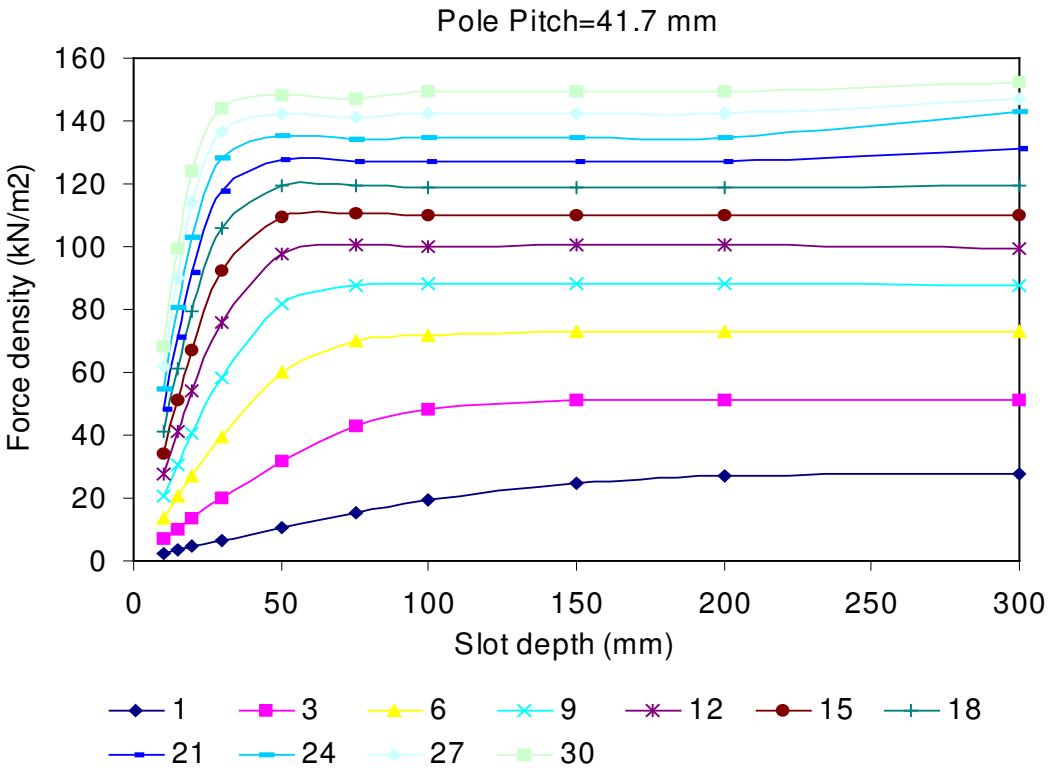
Pole Pitch=41.7 mm
Force density (kN/m2)
160
140
120
100
80
60
40
20
0
0
50
100
150
200
250
300
Slot depth (mm)
1
3
6
9
12
15
18
21
24
27
30

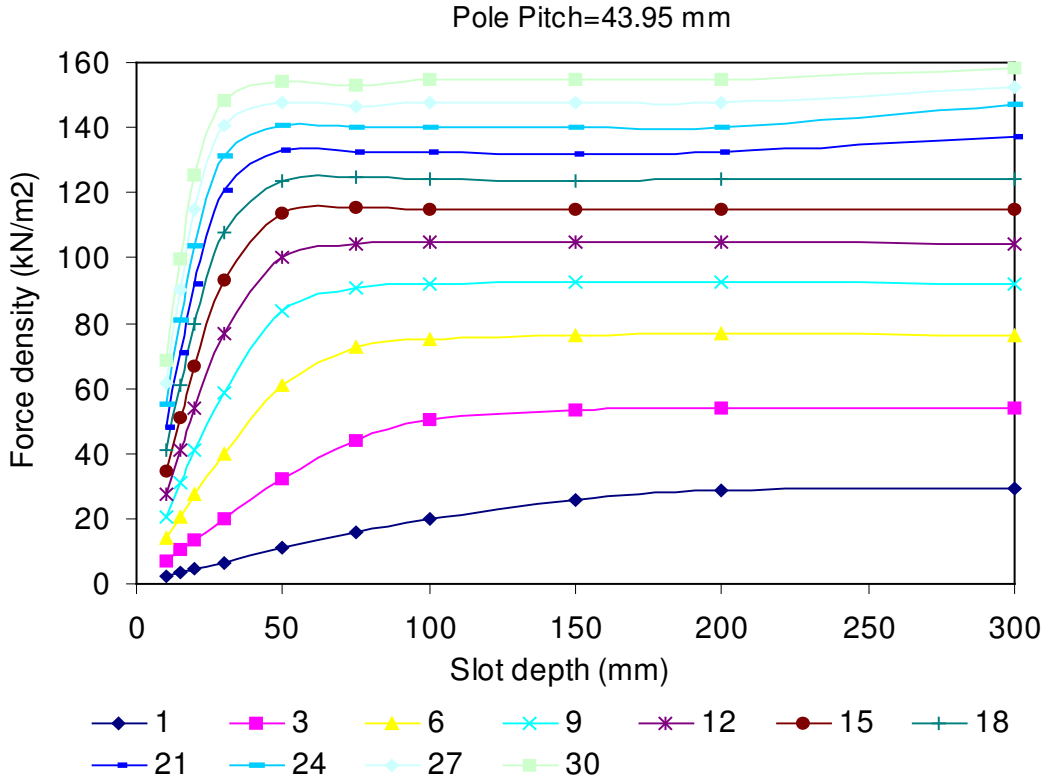
Pole Pitch=43.95 mm
Force density (kN/m2)
160
140
120
100
80
60
40
20
0
0
50
100
150
200
250
300
Slot depth (mm)
1
3
6
9
12
15
18
21
24
27
30

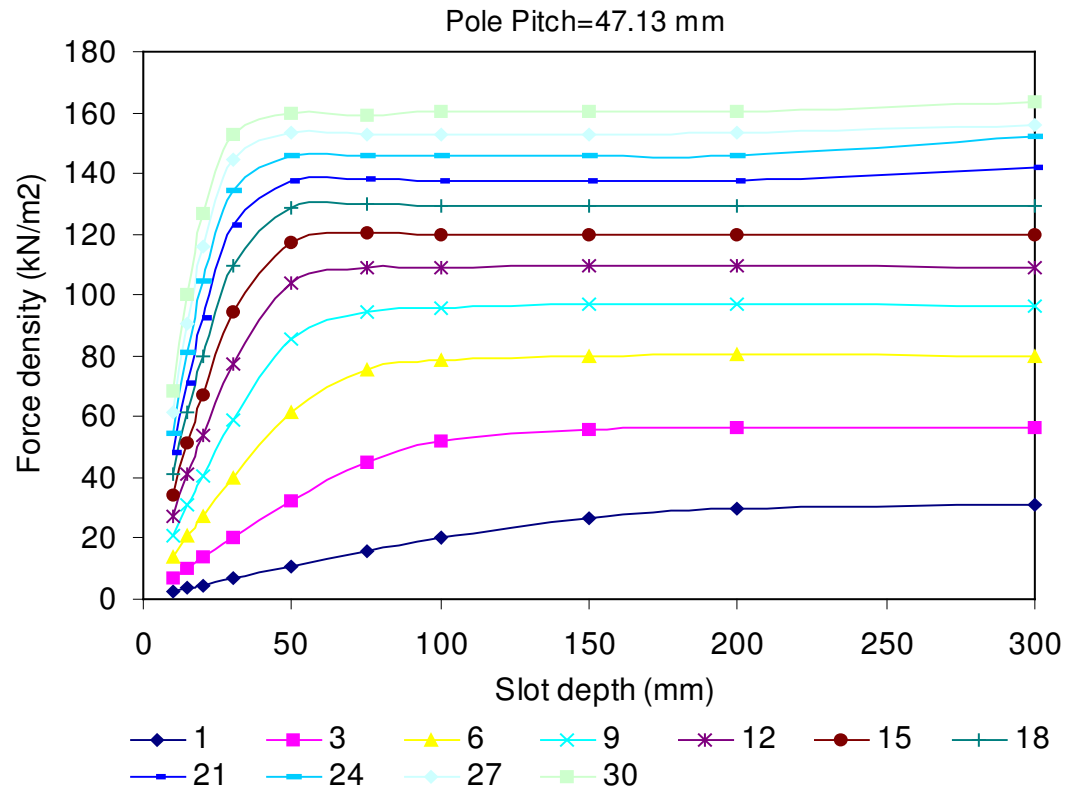
Pole Pitch=47.13 mm
Force density (kN/m2)
Slot depth (mm)
0
20
40
60
80
100
120
140
160
180
0
50
100
150
200
250
300
1
3
6
9
12
15
18
21
24
27
30

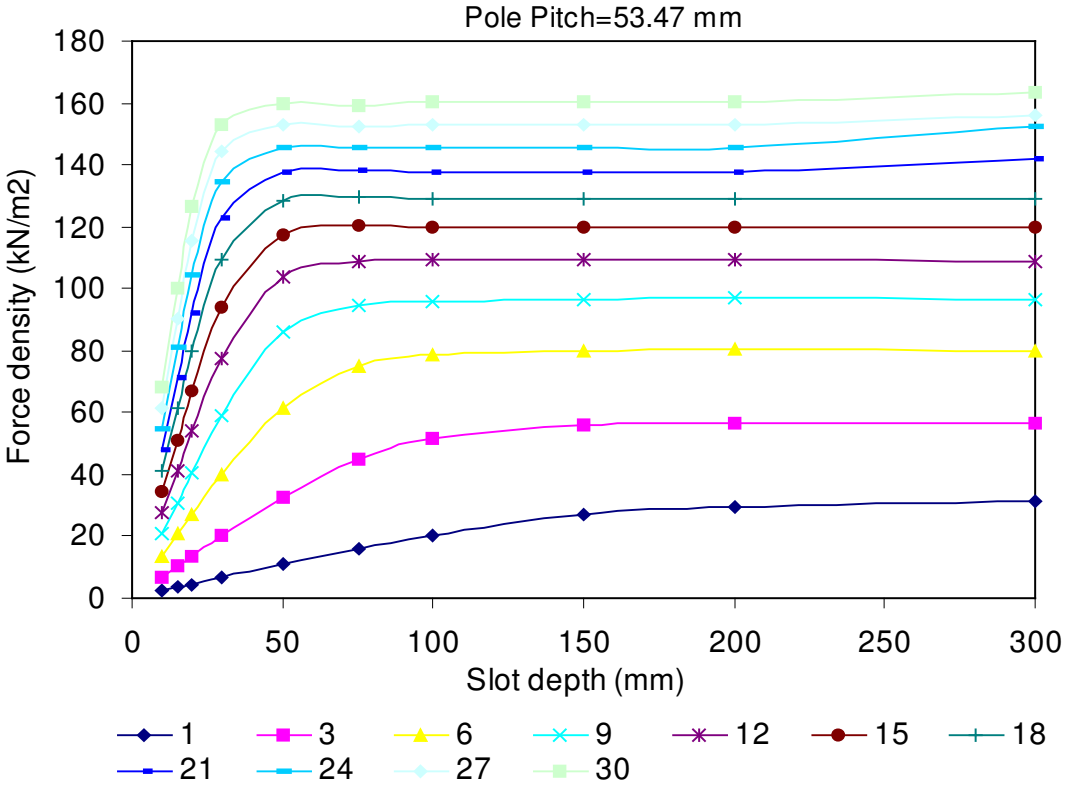
Pole Pitch=53.47 mm
Force density (kN/m2)
Slot depth (mm)
0
20
40
60
80
100
120
140
160
180
0
50
100
150
200
250
300
1
3
6
9
12
15
18
21
24
27
30

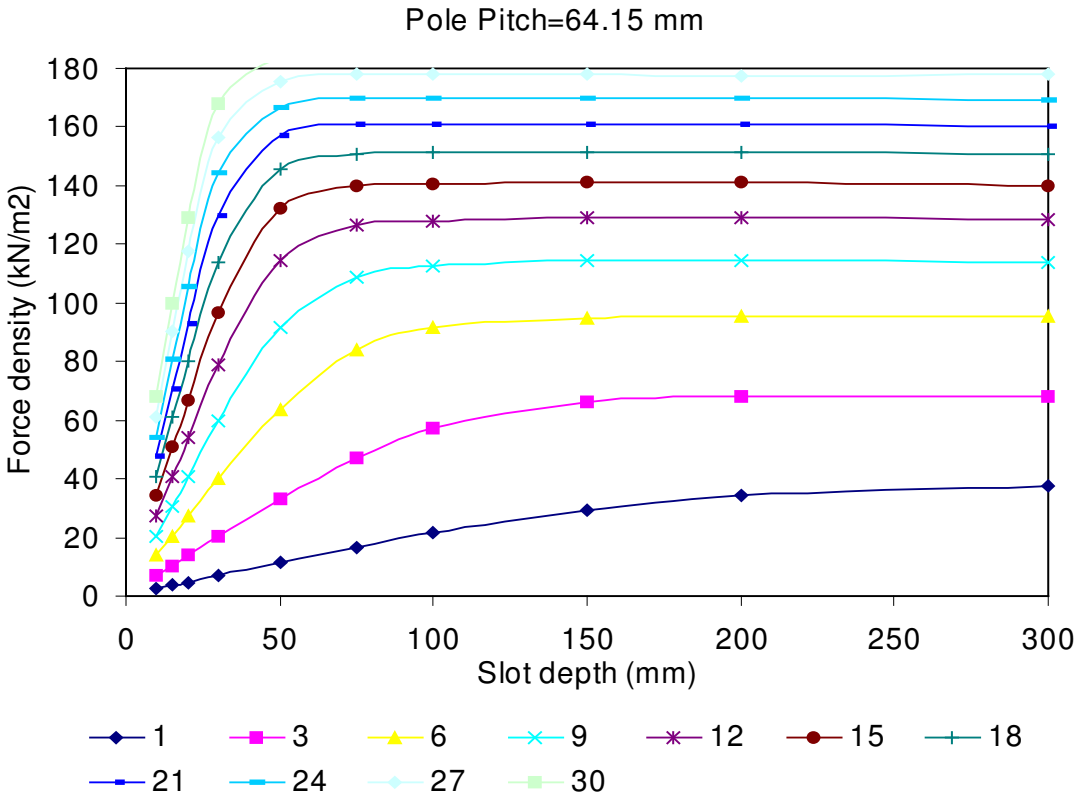
Pole Pitch=64.15 mm
Force density (kN/m2)
Slot depth (mm)
0
20
40
60
80
100
120
140
160
180
0
50
100
150
200
250
300
1
3
6
9
12
15
18
21
24
27
30

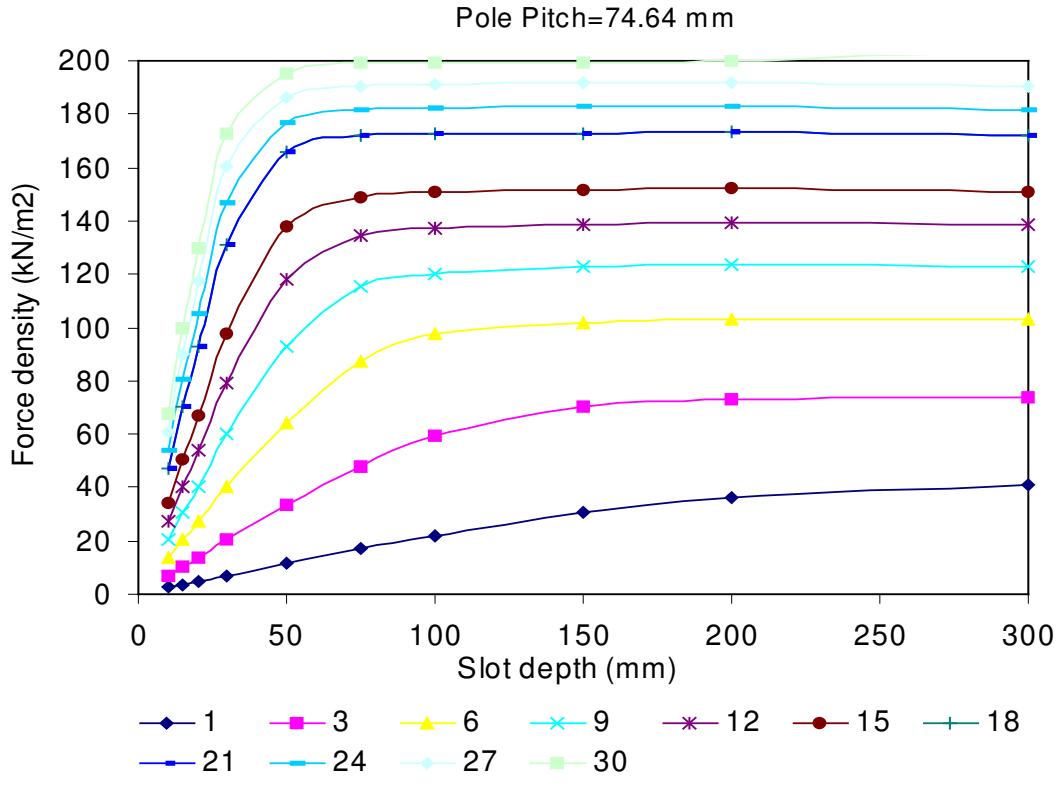
Pole Pitch=74.64 mm
Force density (kN/m2)
Slot depth (mm)
0
20
40
60
80
100
120
140
160
180
200
0
50
100
150
200
250
300
1
3
6
9
12
15
18
21
24
27
30

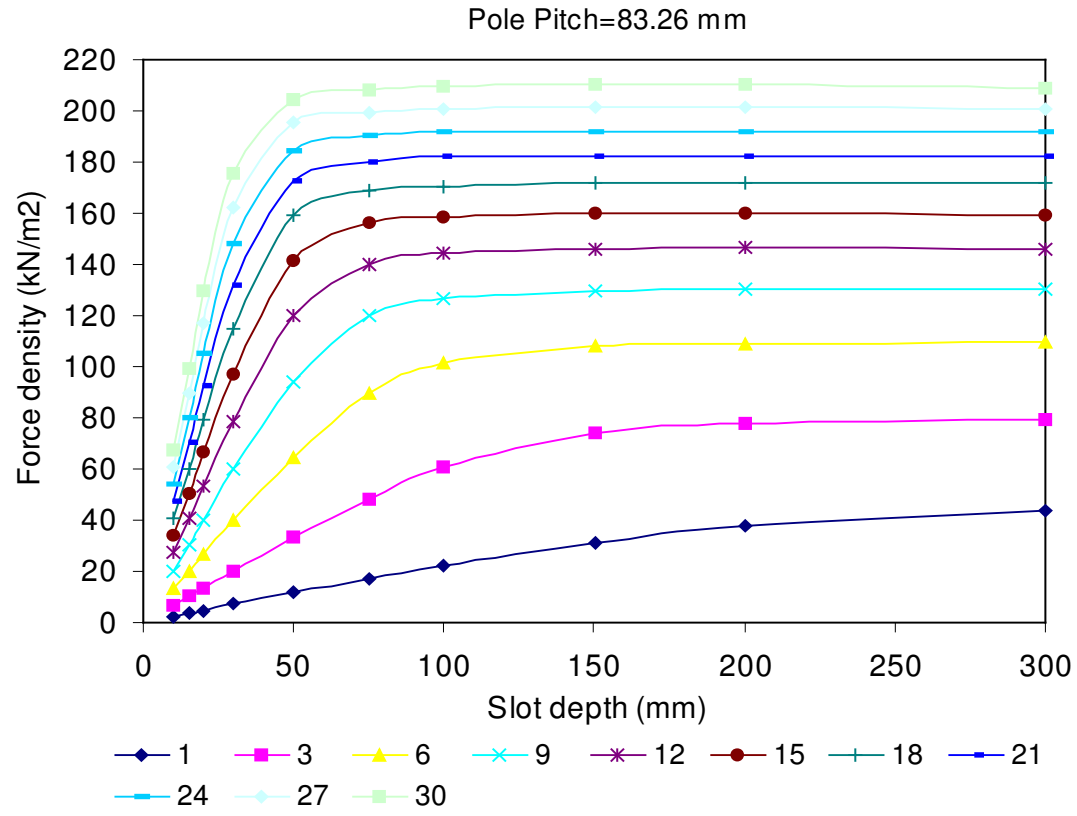
Pole Pitch=83.26 mm
Force density (kN/m2)
220
200
180
160
140
120
100
80
60
40
20
0
0
50
100
150
200
250
300
Slot depth (mm)
1
3
6
9
12
15
18
21
24
27
30

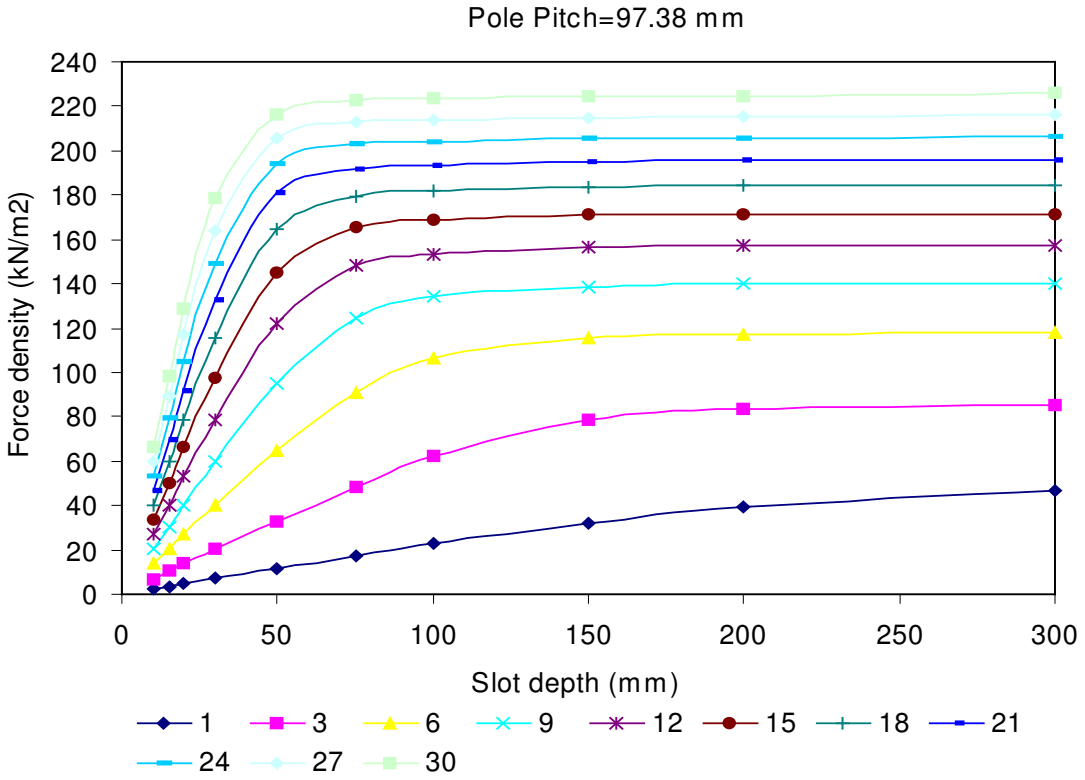
Pole Pitch=97.38 mm
Force density (kN/m2)
240
220
200
180
160
140
120
100
80
60
40
20
0
0
50
100
150
200
250
300
Slot depth (mm)
1
3
6
9
12
15
18
21
24
27
30

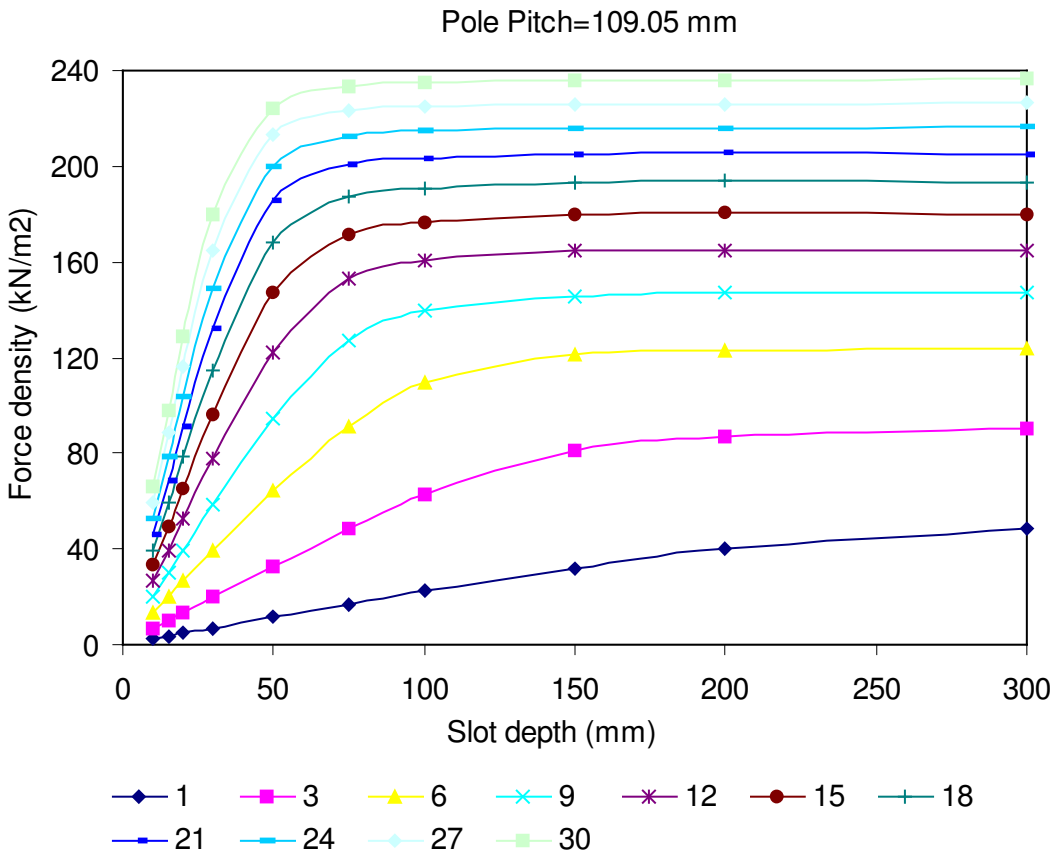
Pole Pitch=109.05 mm
Force density (kN/m2)
240
200
160
120
80
40
0
0
50
100
150
200
250
300
Slot depth (mm)
1
3
6
9
12
15
18
21
24
27
30

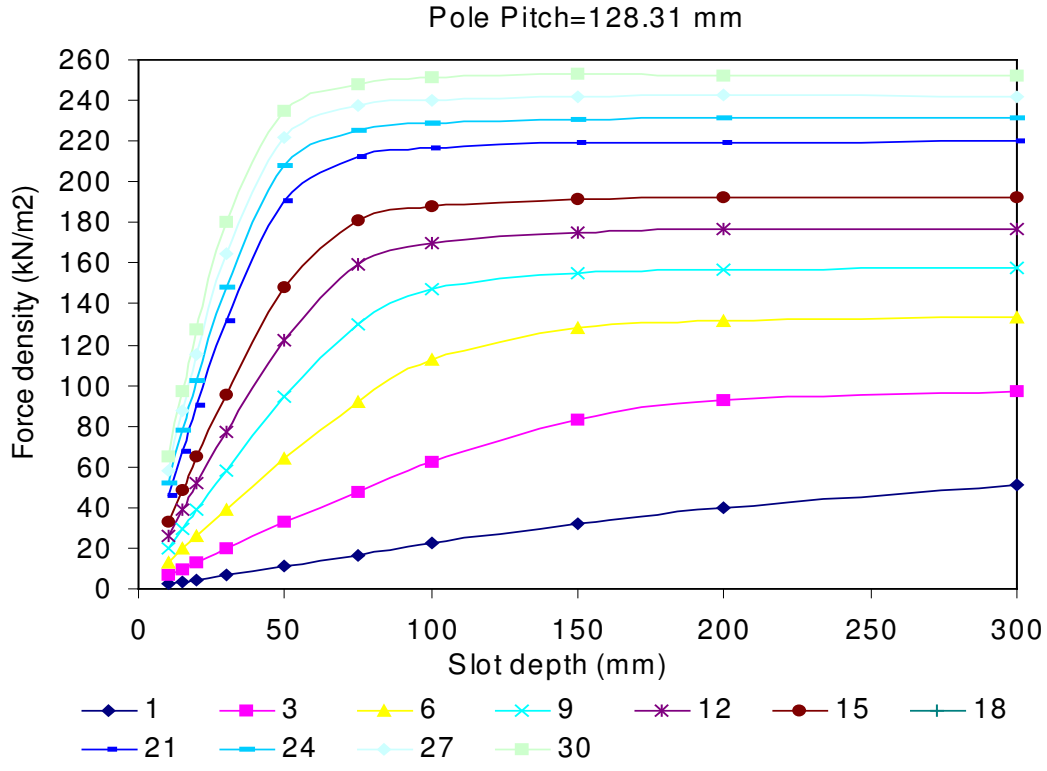
Pole Pitch=128.31 mm
Force density (kN/m2)
260
240
220
200
180
160
140
120
100
80
60
40
20
0
0
50
100
150
200
250
300
Slot depth (mm)
1
3
6
9
12
15
18
21
24
27
30

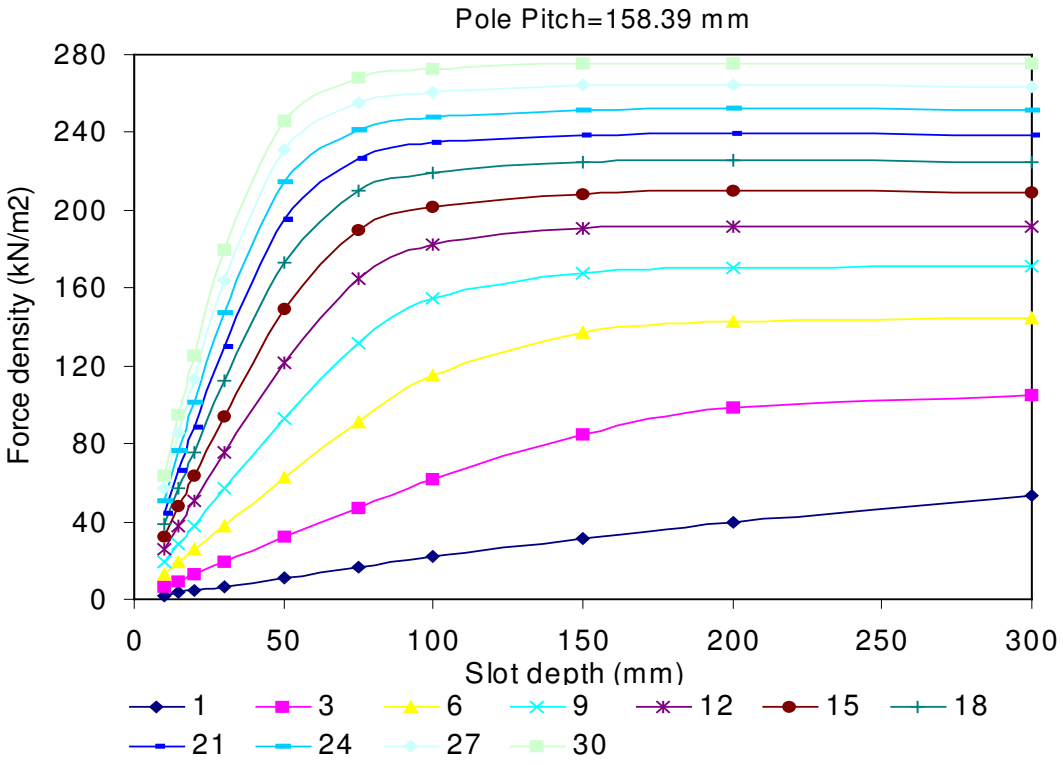
Pole Pitch=158.39 mm
Force density (kN/m2)
0
40
80
120
160
200
240
280
0
50
100
150
200
250
300
Slot depth (mm)
1
3
6
9
12
15
18
21
24
27
30

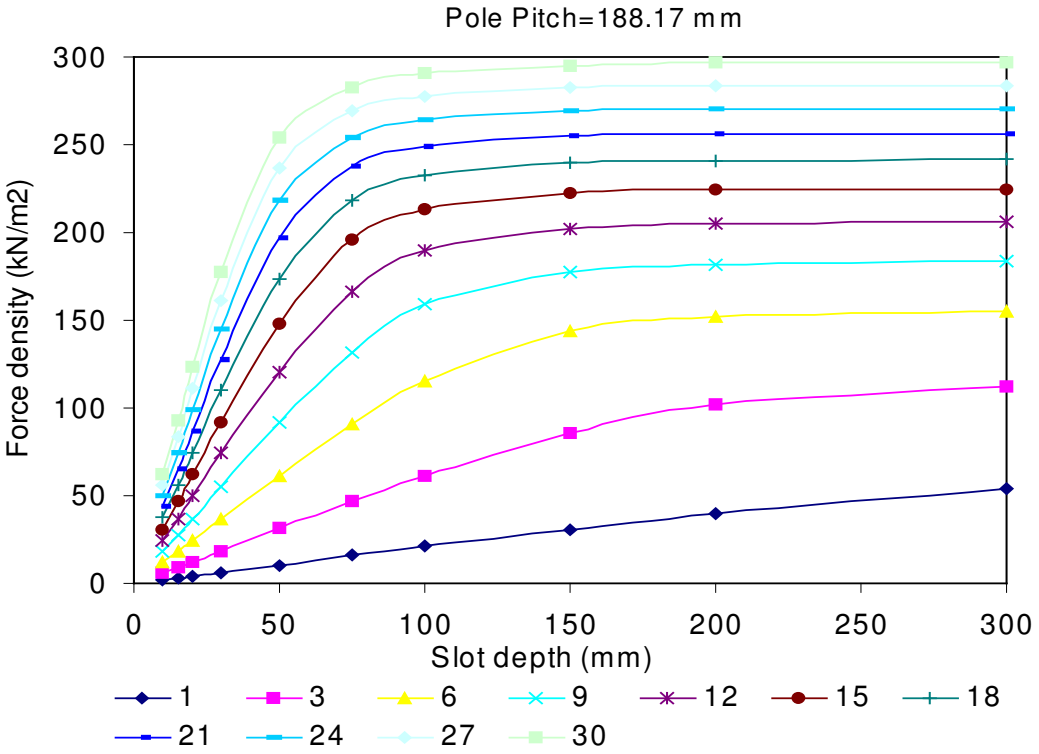
Pole Pitch=188.17 mm
Force density (kN/m2)
0
50
100
150
200
250
300
0
50
100
150
200
250
300
Slot depth (mm)
1
3
6
9
12
15
18
21
24
27
30

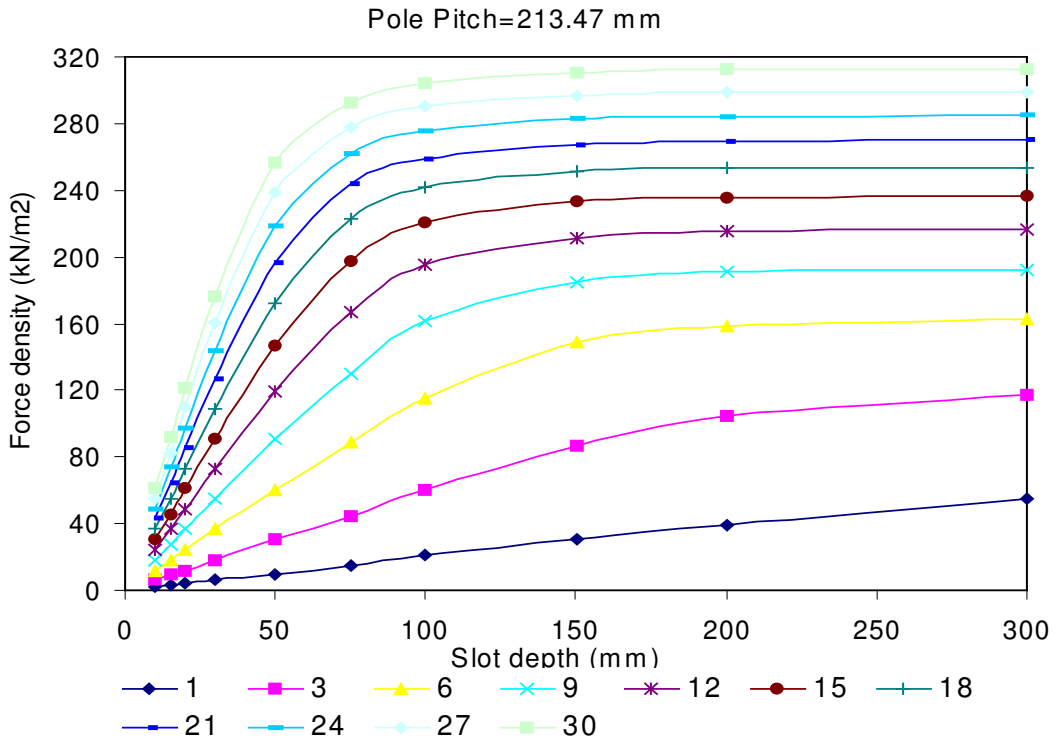
Pole Pitch=213.47 mm
Force density (kN/m2)
320
280
240
200
160
120
80
40
0
0
50
100
150
200
250
300
Slot depth (mm)
1
3
6
9
12
15
18
21
24
27
30

APPENDIX III

Fractional-Slot Machines

Averaged force density in fractional-slot machines for various slot depth, current levels and density slot per pole per phase for machines having pole pitches listed in Tables 4.2, 4.4 and 4.4.

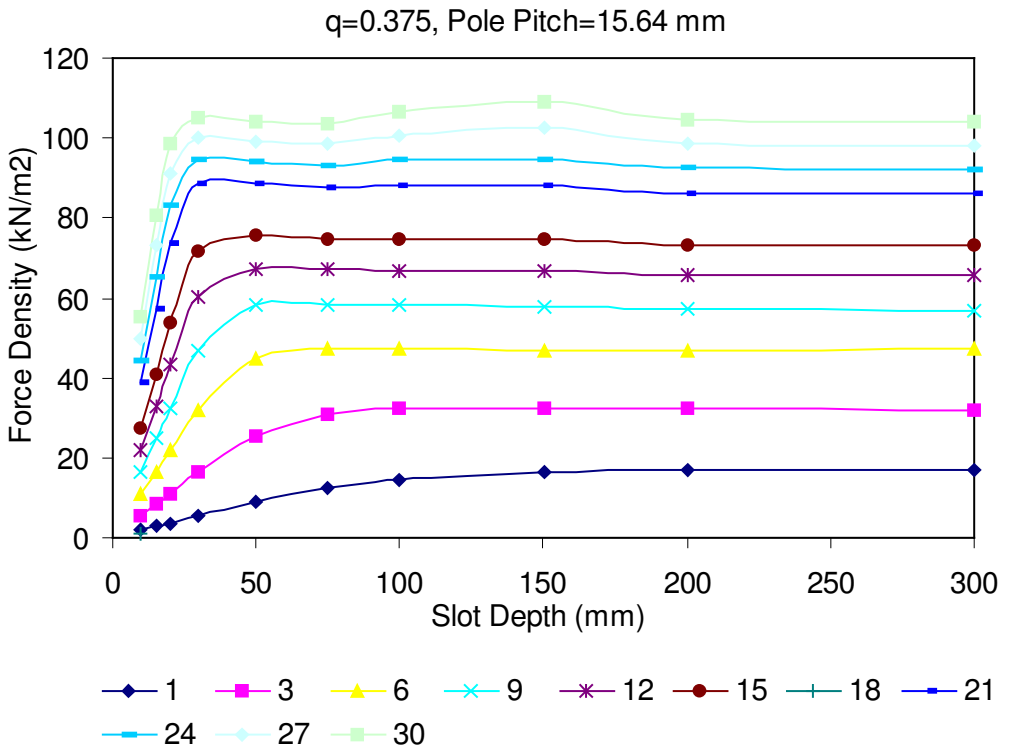
q=0.375, Pole Pitch=15.64 mm
Force Density (kN/m2)
Slot Depth (mm)
0
20
40
60
80
100
120
0
50
100
150
200
250
300
1
3
6
9
12
15
18
21
24
27
30

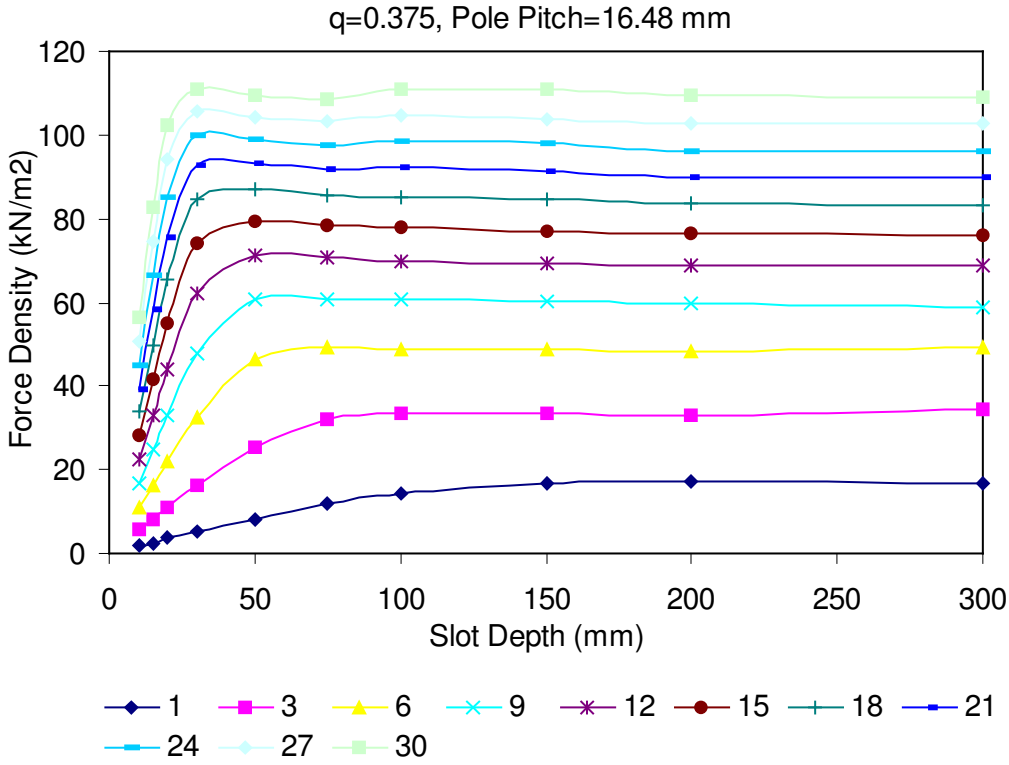
q=0.375, Pole Pitch=16.48 mm
Force Density (kN/m2)
Slot Depth (mm)
0
20
40
60
80
100
120
0
50
100
150
200
250
300
1
3
6
9
12
15
18
21
24
27
30

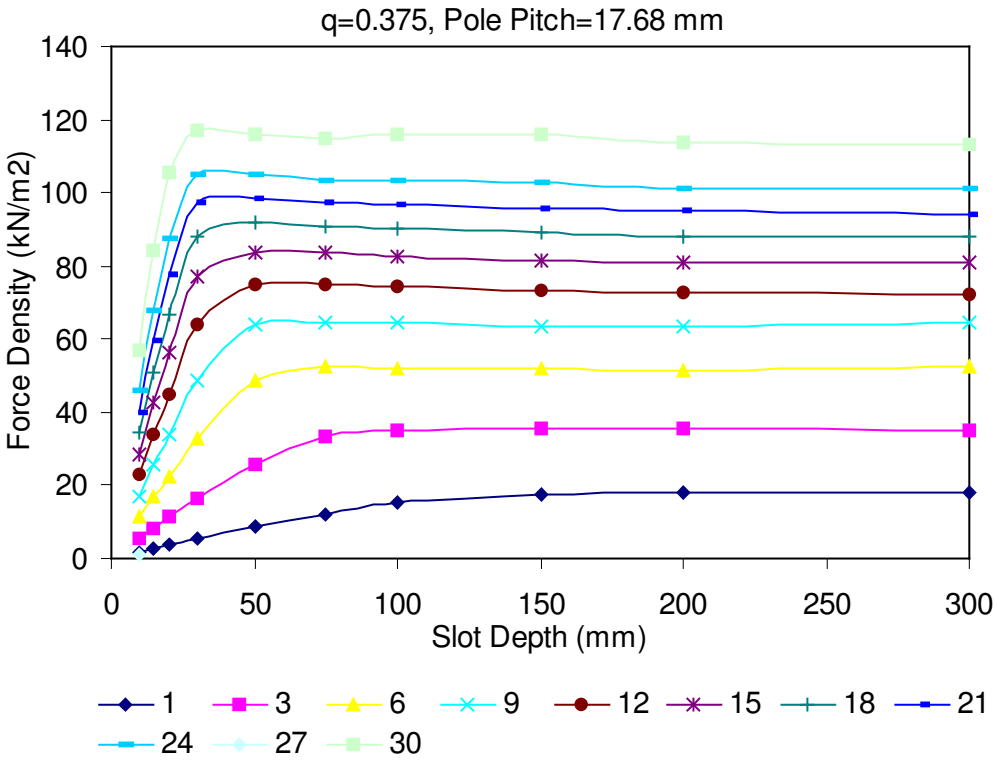
q=0.375, Pole Pitch=17.68 mm
Force Density (kN/m2)
Slot Depth (mm)
0
20
40
60
80
100
120
140
0
50
100
150
200
250
300
1
3
6
9
12
15
18
21
24
27
30

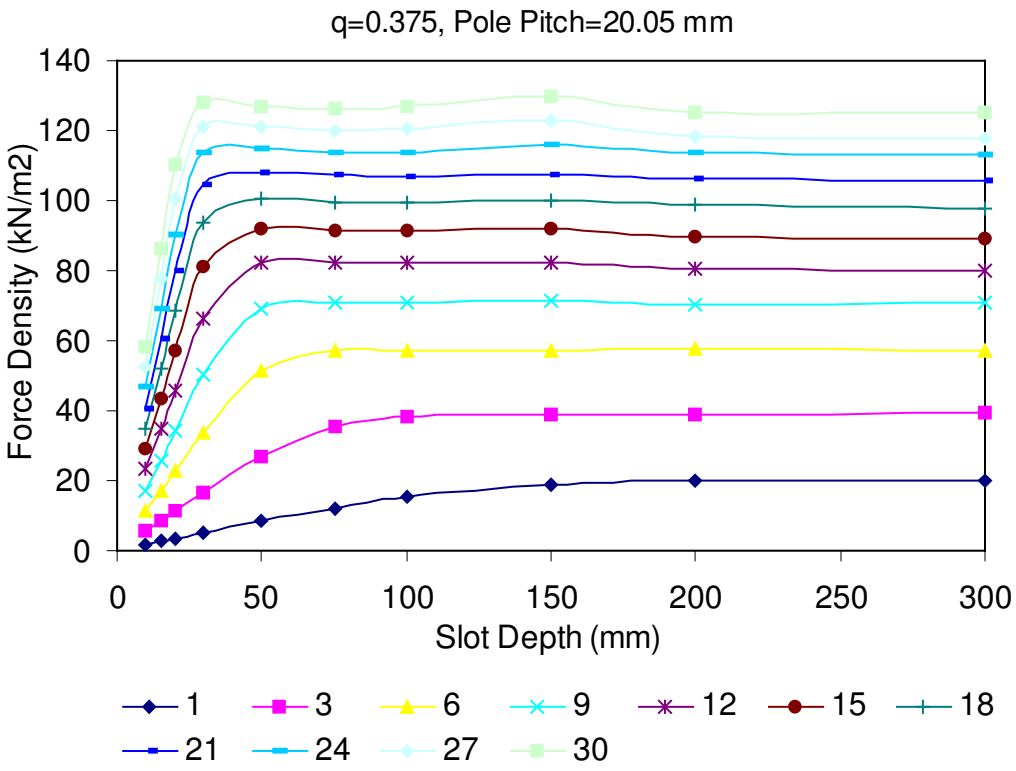
q=0.375, Pole Pitch=20.05 mm
Force Density (kN/m2)
Slot Depth (mm)
0
20
40
60
80
100
120
140
0
50
100
150
200
250
300
1
3
6
9
12
15
18
21
24
27
30

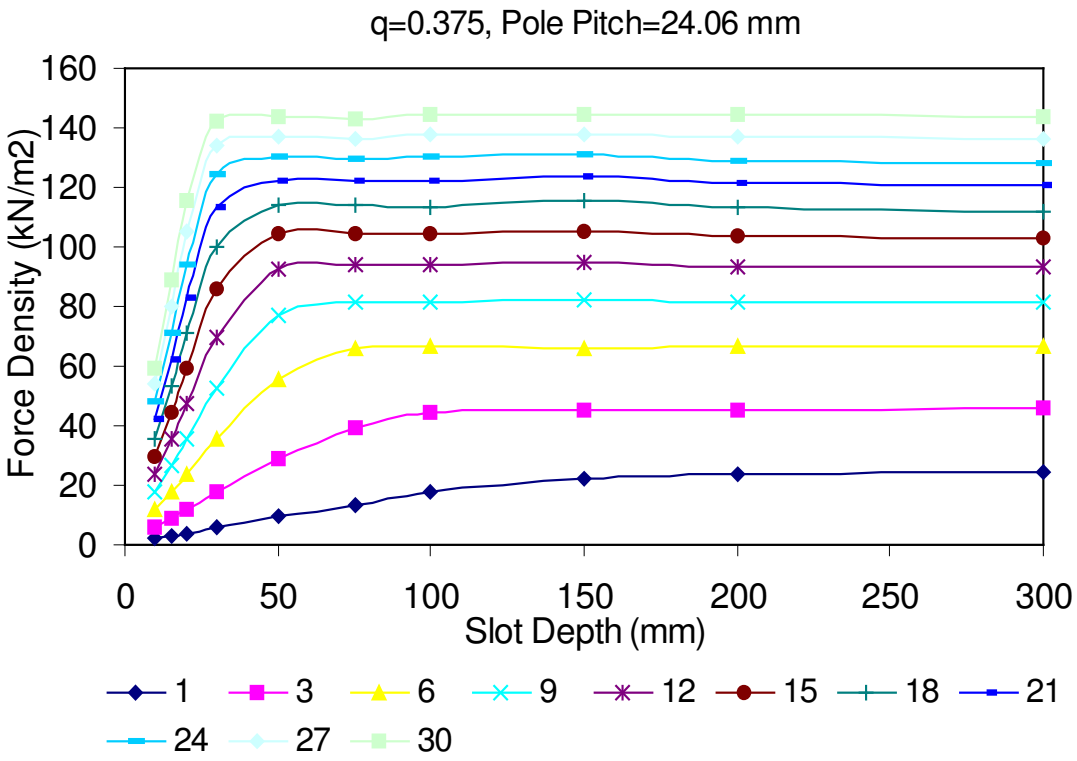
q=0.375, Pole Pitch=24.06 mm
Force Density (kN/m2)
160
140
120
100
80
60
40
20
0
0
50
100
150
200
250
300
Slot Depth (mm)
1
3
6
9
12
15
18
21
24
27
30

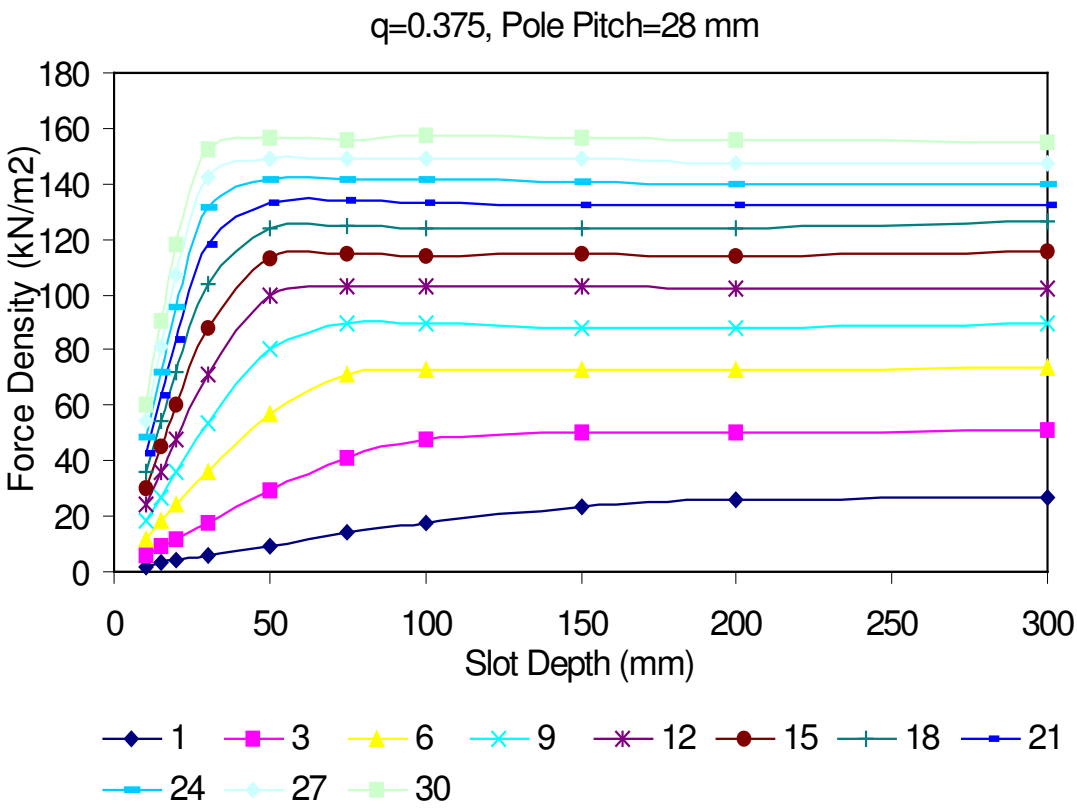
q=0.375, Pole Pitch=28 mm
Force Density (kN/m2)
180
160
140
120
100
80
60
40
20
0
0
50
100
150
200
250
300
Slot Depth (mm)
1
3
6
9
12
15
18
21
24
27
30

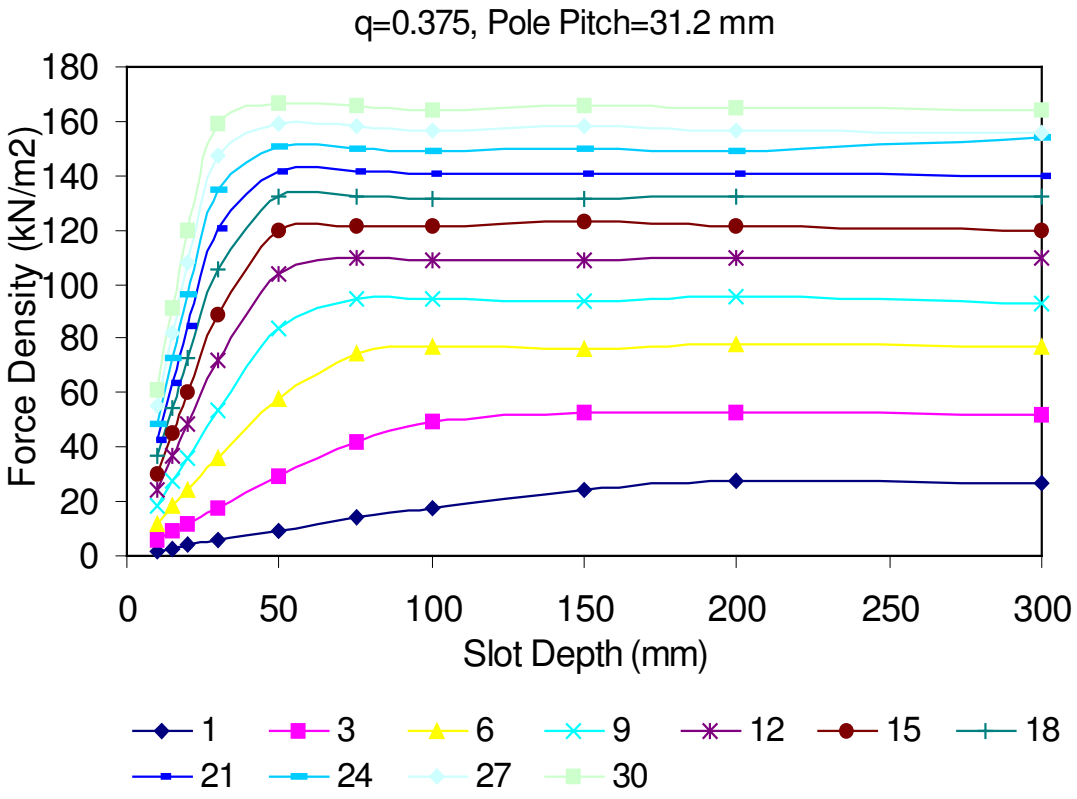
q=0.375, Pole Pitch=31.2 mm
Force Density (kN/m2)
180
160
140
120
100
80
60
40
20
0
0
50
100
150
200
250
300
Slot Depth (mm)
1
3
6
9
12
15
18
21
24
27
30

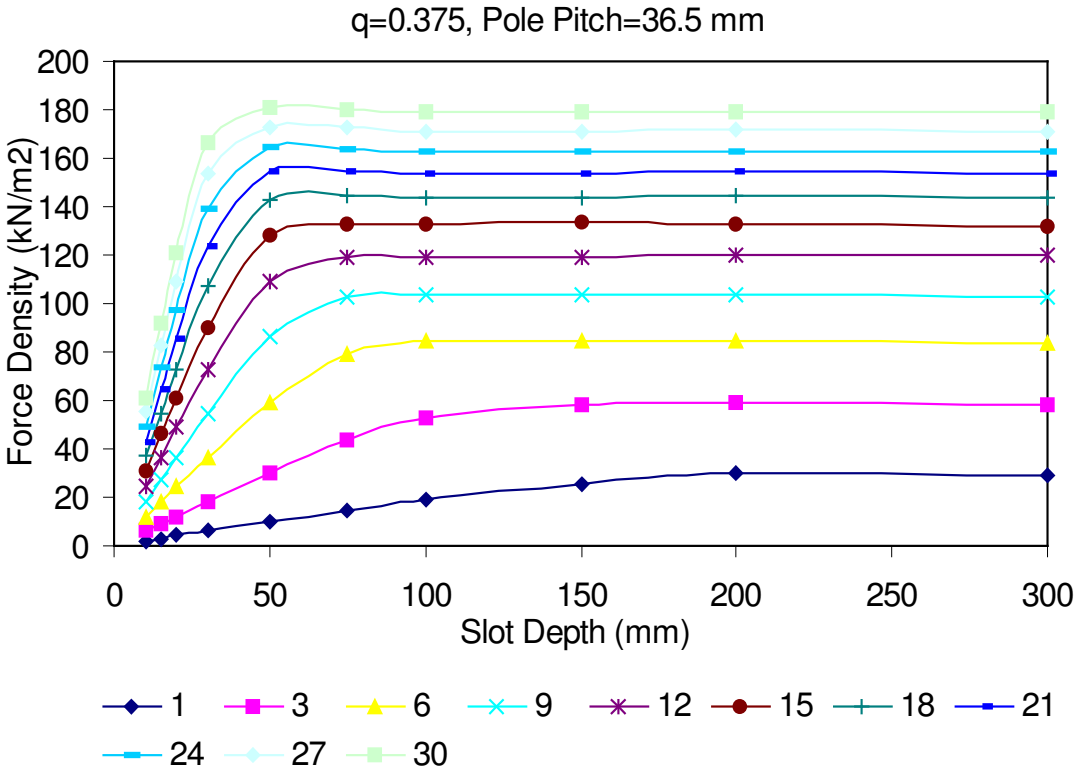
q=0.375, Pole Pitch=36.5 mm
Force Density (kN/m2)
200
180
160
140
120
100
80
60
40
20
0
0
50
100
150
200
250
300
Slot Depth (mm)
1
3
6
9
12
15
18
21
24
27
30

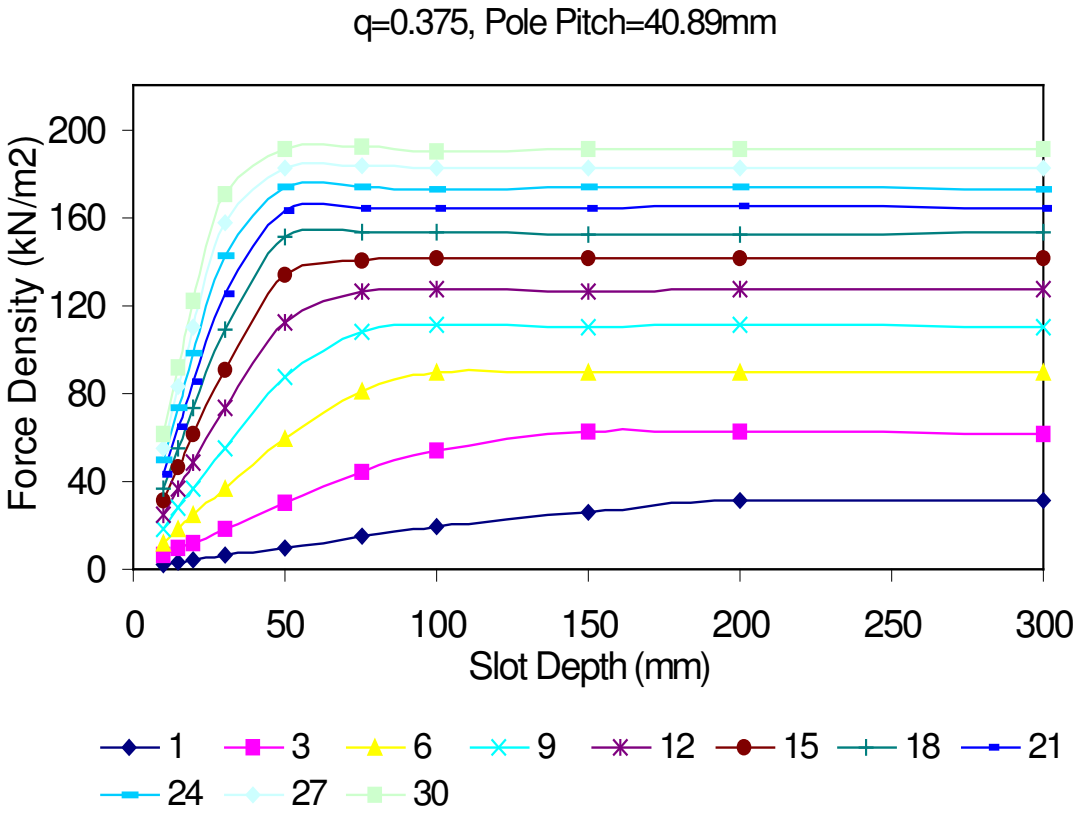
q=0.375, Pole Pitch=40.89mm
Force Density (kN/m2)
200
160
120
80
40
0
0
50
100
150
200
250
300
Slot Depth (mm)
1
3
6
9
12
15
18
21
24
27
30

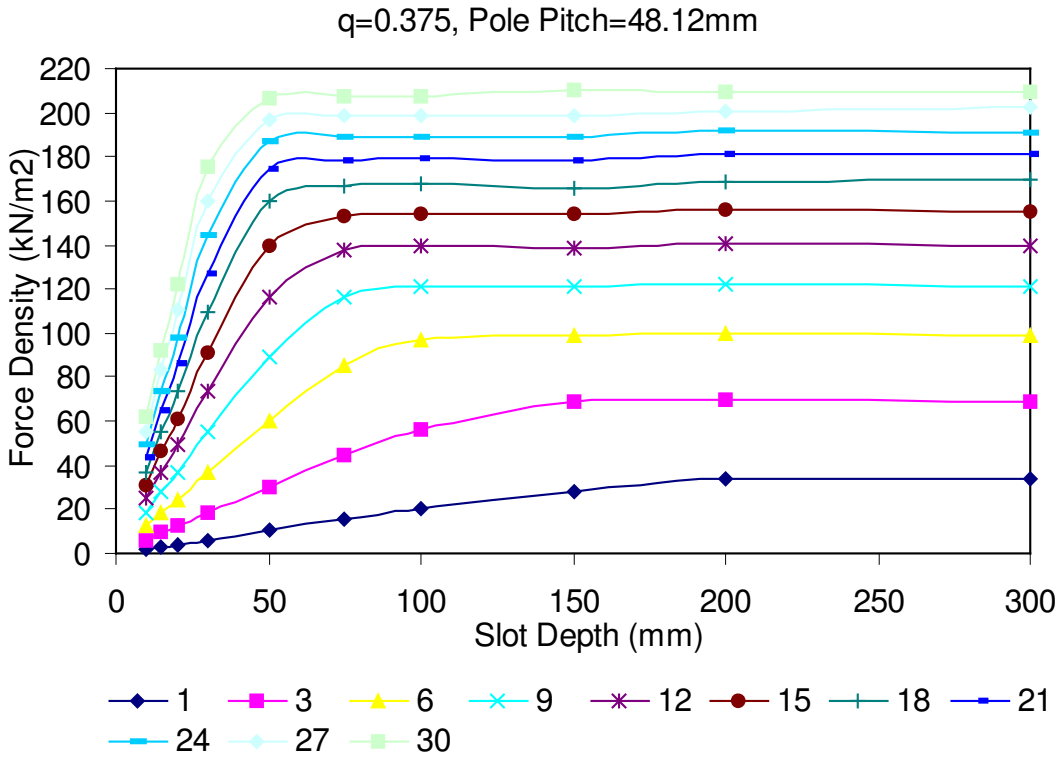
q=0.375, Pole Pitch=48.12mm
Force Density (kN/m2)
220
200
180
160
140
120
100
80
60
40
20
0
0
50
100
150
200
250
300
Slot Depth (mm)
1
3
6
9
12
15
18
21
24
27
30

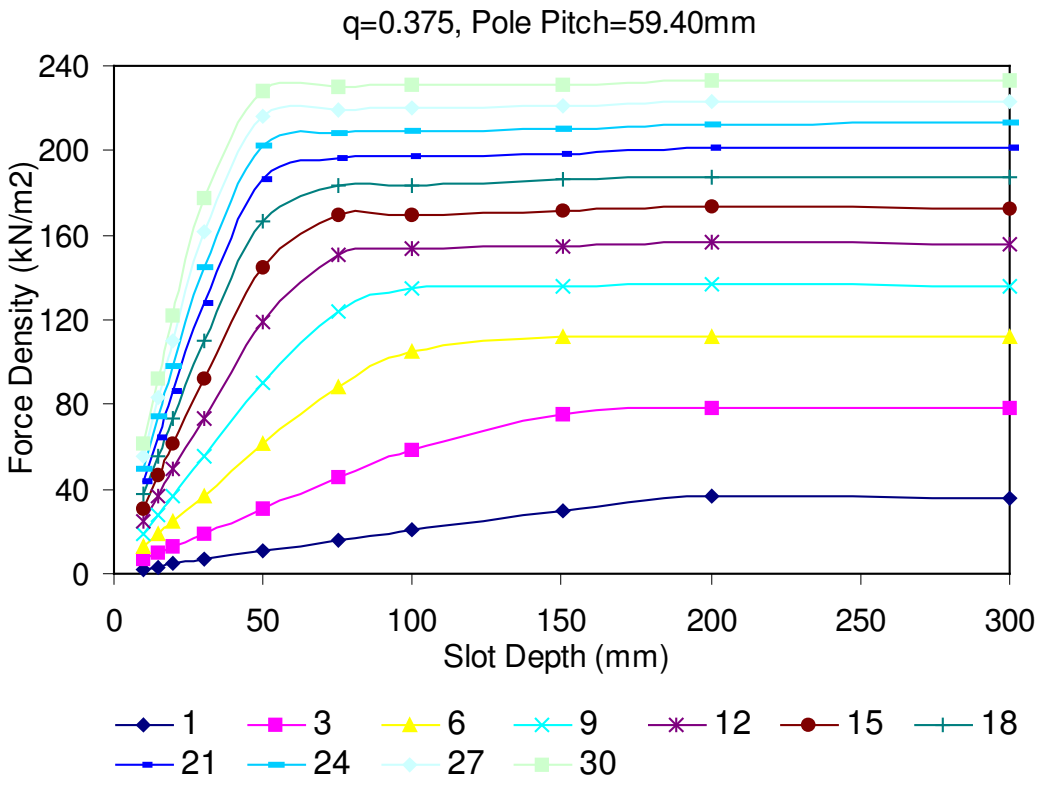
q=0.375, Pole Pitch=59.40mm
Force Density (kN/m2)
240
200
160
120
80
40
0
0
50
100
150
200
250
300
Slot Depth (mm)
1
3
6
9
12
15
18
21
24
27
30

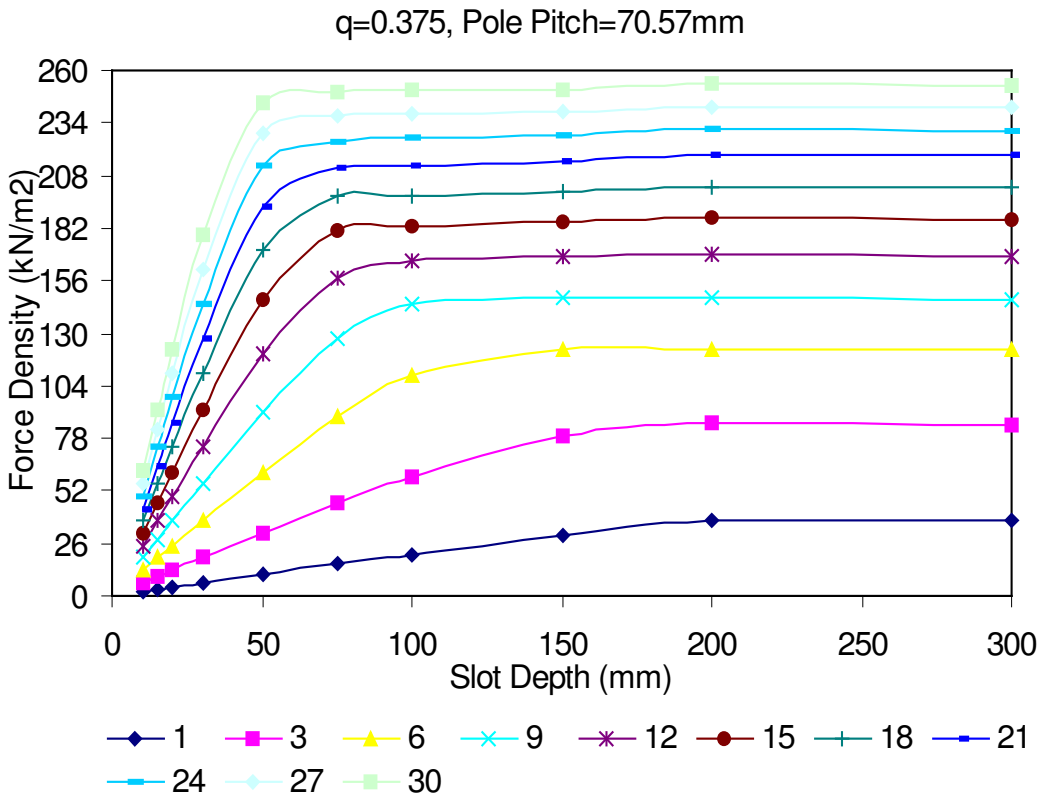
q=0.375, Pole Pitch=70.57mm
Force Density (kN/m2)
260
234
208
182
156
130
104
78
52
26
0
0
50
100
150
200
250
300
Slot Depth (mm)
1
3
6
9
12
15
18
21
24
27
30

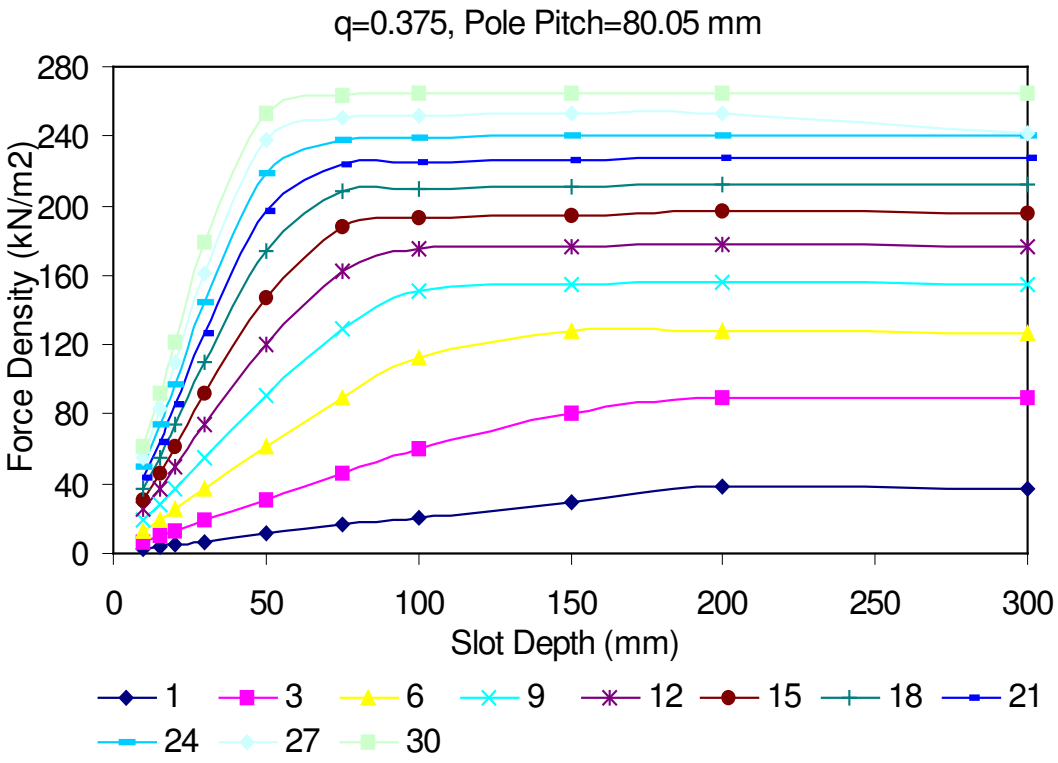
q=0.375, Pole Pitch=80.05 mm
Force Density (kN/m2)
280
240
200
160
120
80
40
0
0
50
100
150
200
250
300
Slot Depth (mm)
1
3
6
9
12
15
18
21
24
27
30

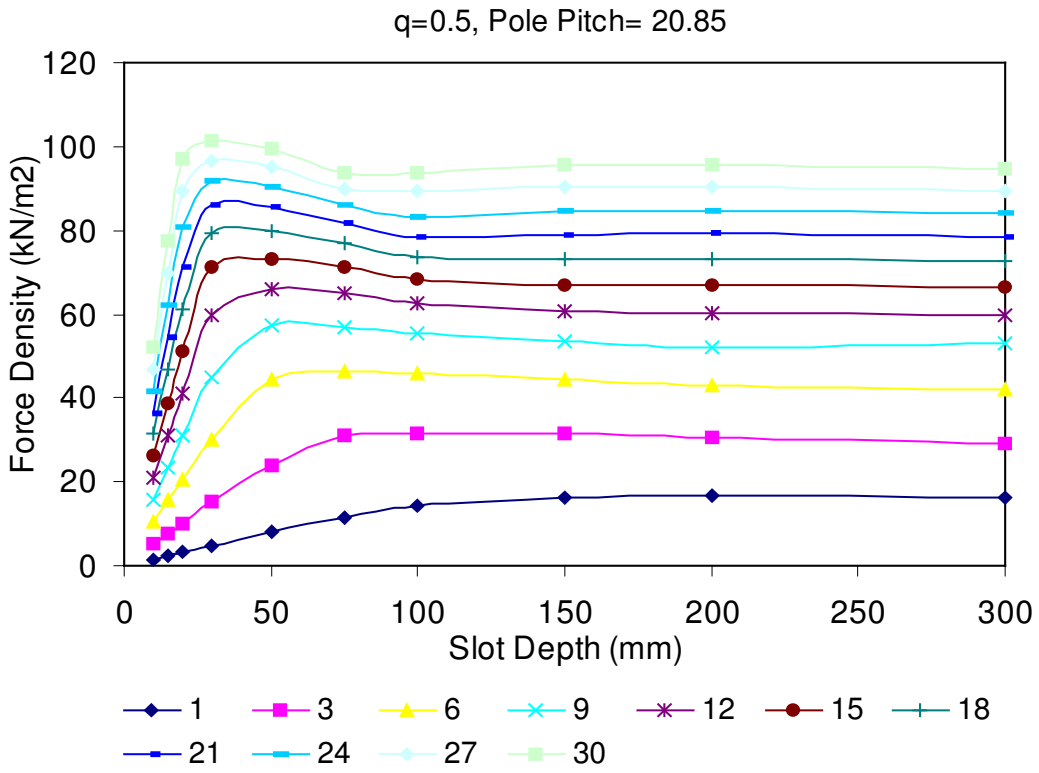
q=0.5, Pole Pitch= 20.85
Force Density (kN/m2)
120
100
80
60
40
20
0
0
50
100
150
200
250
300
Slot Depth (mm)
1
3
6
9
12
15
18
21
24
27
30

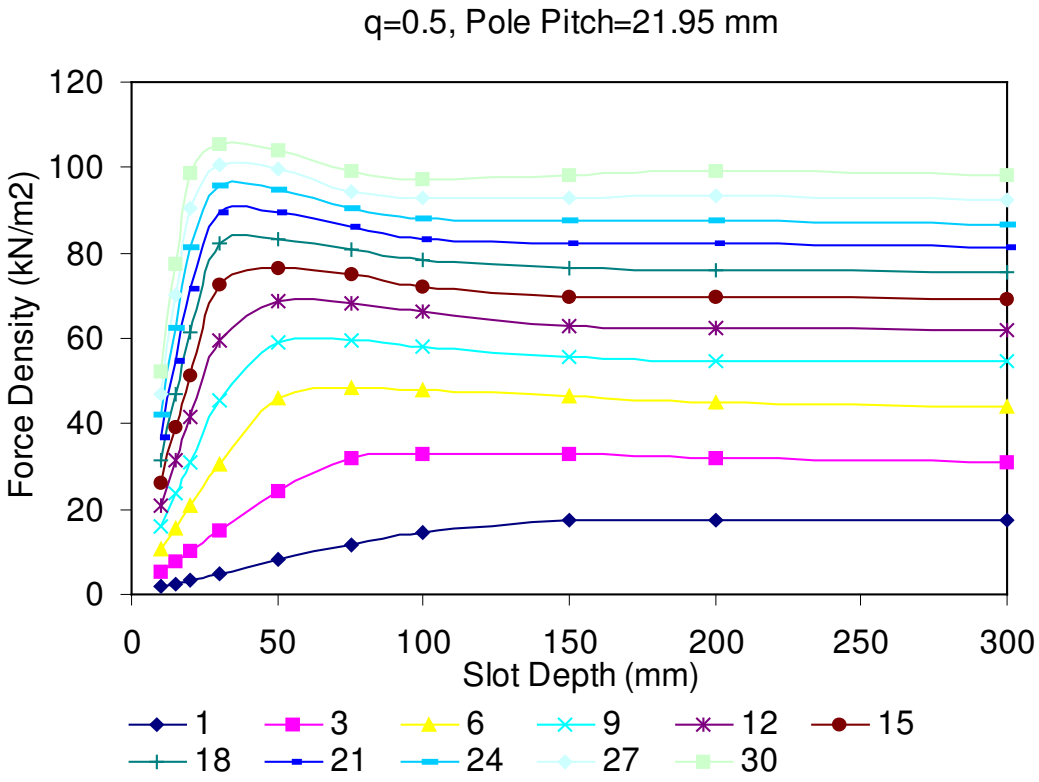
q=0.5, Pole Pitch=21.95 mm
Force Density (kN/m2)
120
100
80
60
40
20
0
0
50
100
150
200
250
300
Slot Depth (mm)
1
3
6
9
12
15
18
21
24
27
30

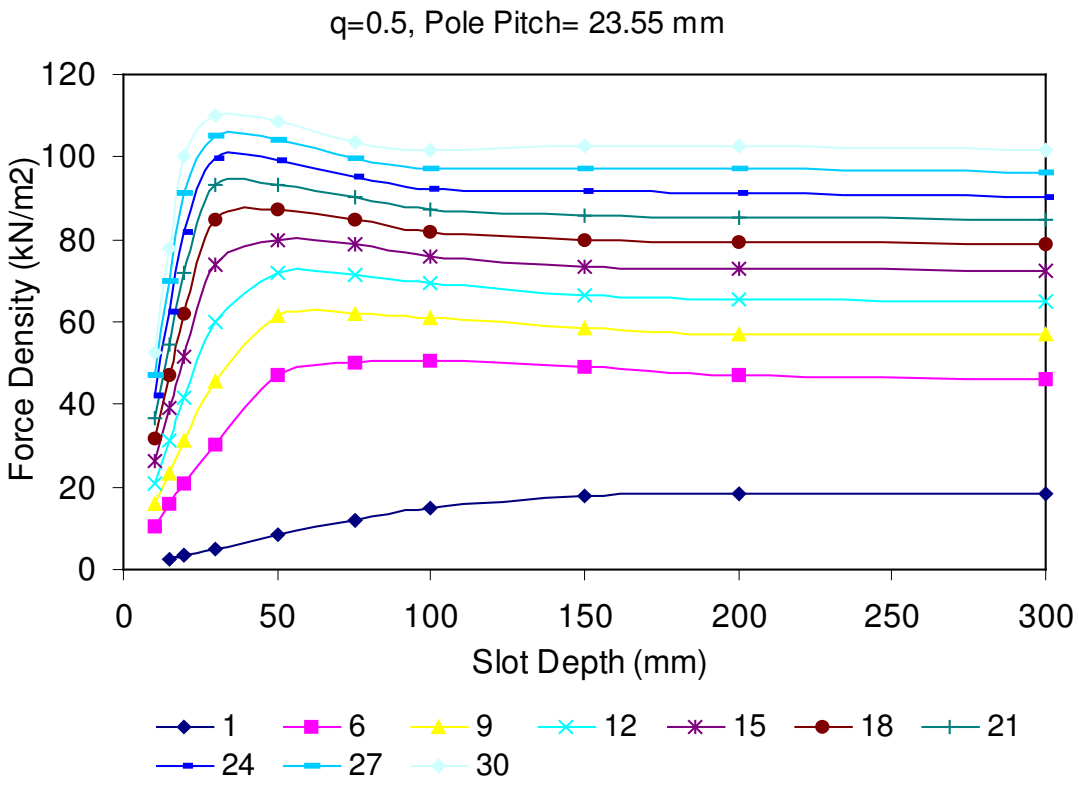
q=0.5, Pole Pitch= 23.55 mm
Force Density (kN/m2)
120
100
80
60
40
20
0
0
50
100
150
200
250
300
Slot Depth (mm)
1
6
9
12
15
18
21
24
27
30

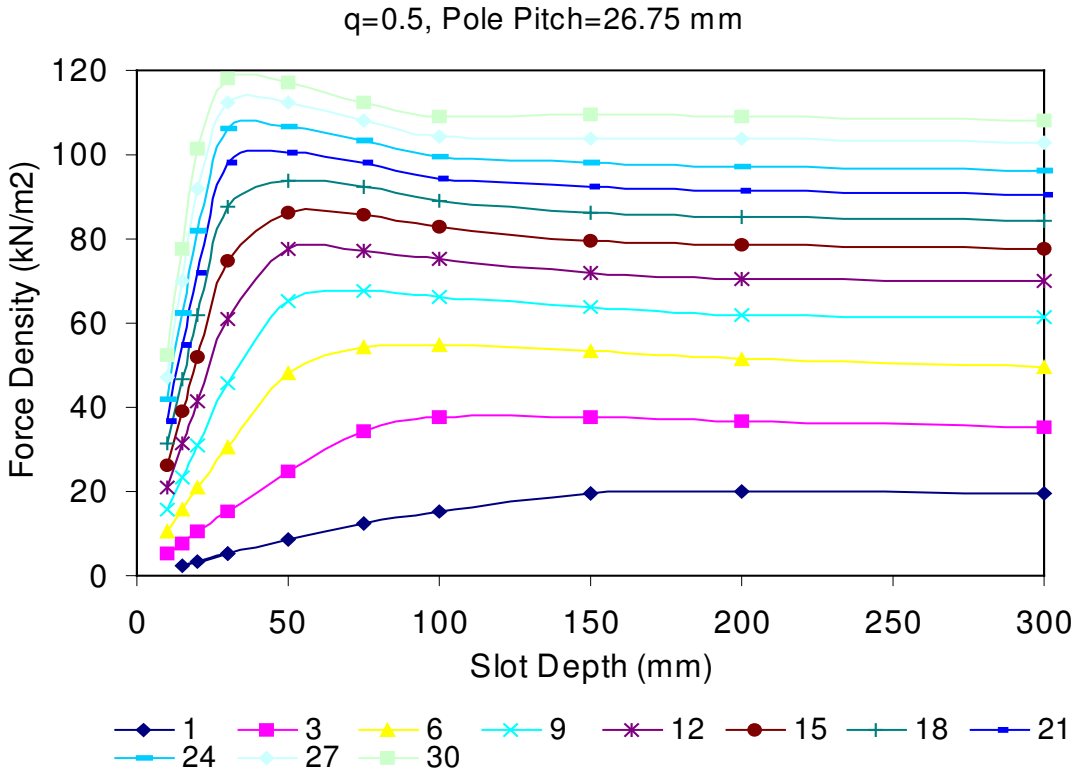
q=0.5, Pole Pitch=26.75 mm
Force Density (kN/m2)
120
100
80
60
40
20
0
0
50
100
150
200
250
300
Slot Depth (mm)
1
3
6
9
12
15
18
21
24
27
30

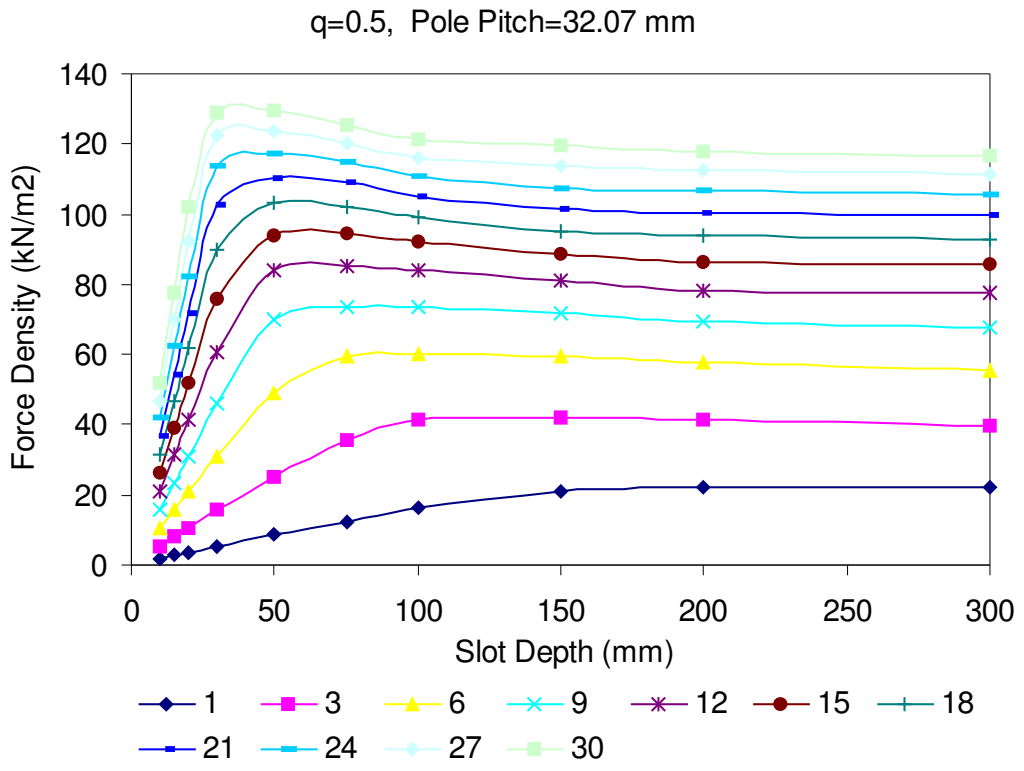
q=0.5, Pole Pitch=32.07 mm
Force Density (kN/m2)
140
120
100
80
60
40
20
0
0
50
100
150
200
250
300
Slot Depth (mm)
1
3
6
9
12
15
18
21
24
27
30

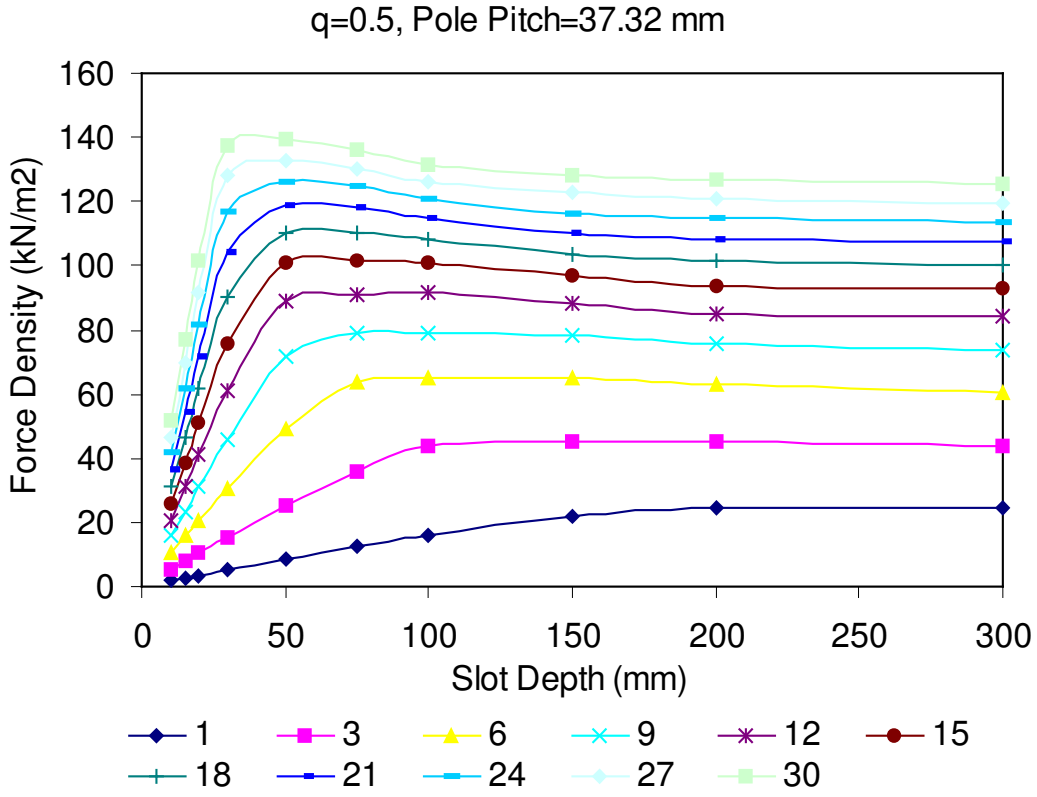
q=0.5, Pole Pitch=37.32 mm
Force Density (kN/m2)
160
140
120
100
80
60
40
20
0
0
50
100
150
200
250
300
Slot Depth (mm)
1
3
6
9
12
15
18
21
24
27
30

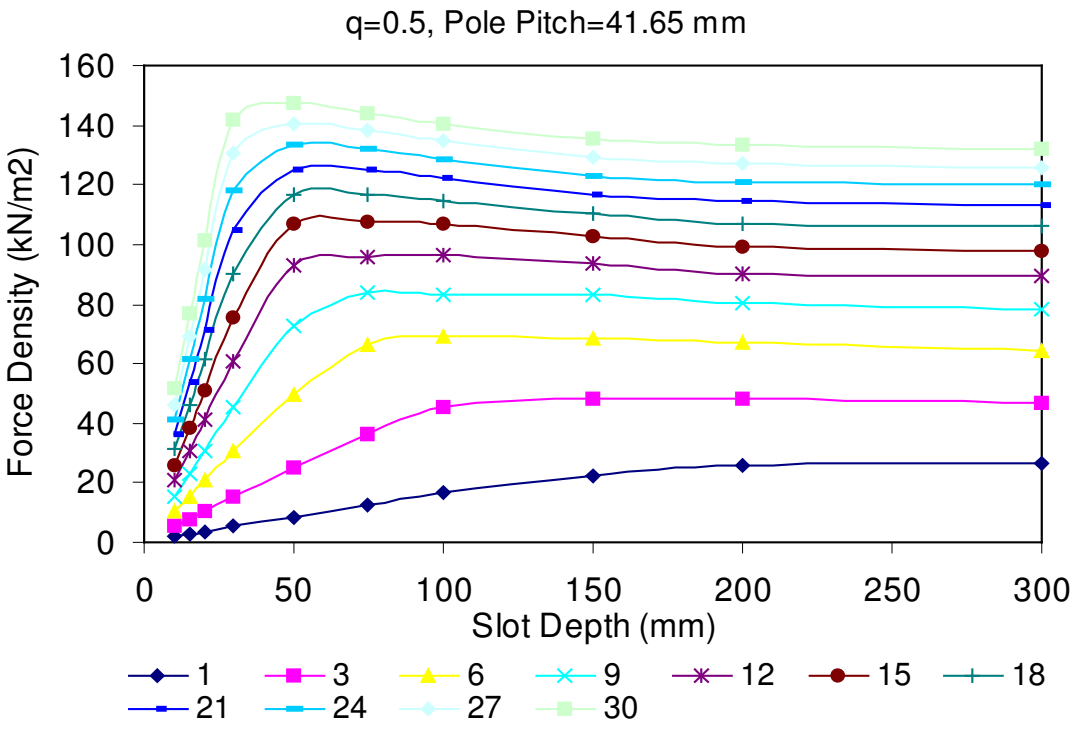
q=0.5, Pole Pitch=41.65 mm
Force Density (kN/m2)
160
140
120
100
80
60
40
20
0
0
50
100
150
200
250
300
Slot Depth (mm)
1
3
6
9
12
15
18
21
24
27
30

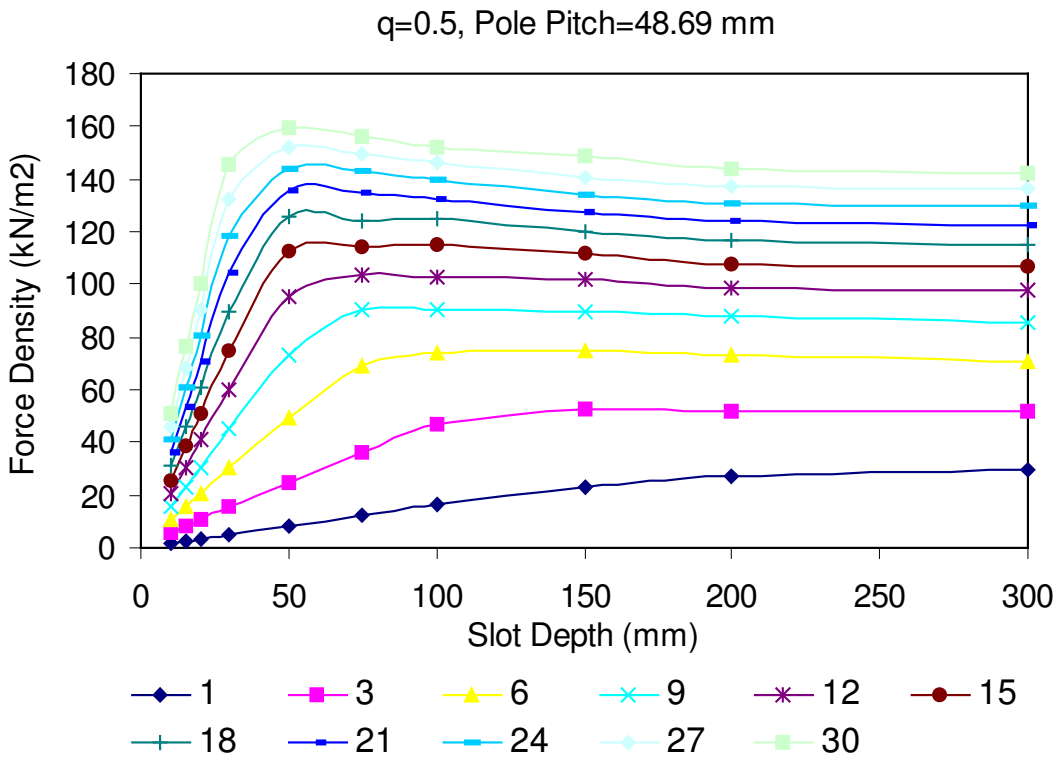
q=0.5, Pole Pitch=48.69 mm
Force Density (kN/m2)
180
160
140
120
100
80
60
40
20
0
0
50
100
150
200
250
300
Slot Depth (mm)
1
3
6
9
12
15
18
21
24
27
30

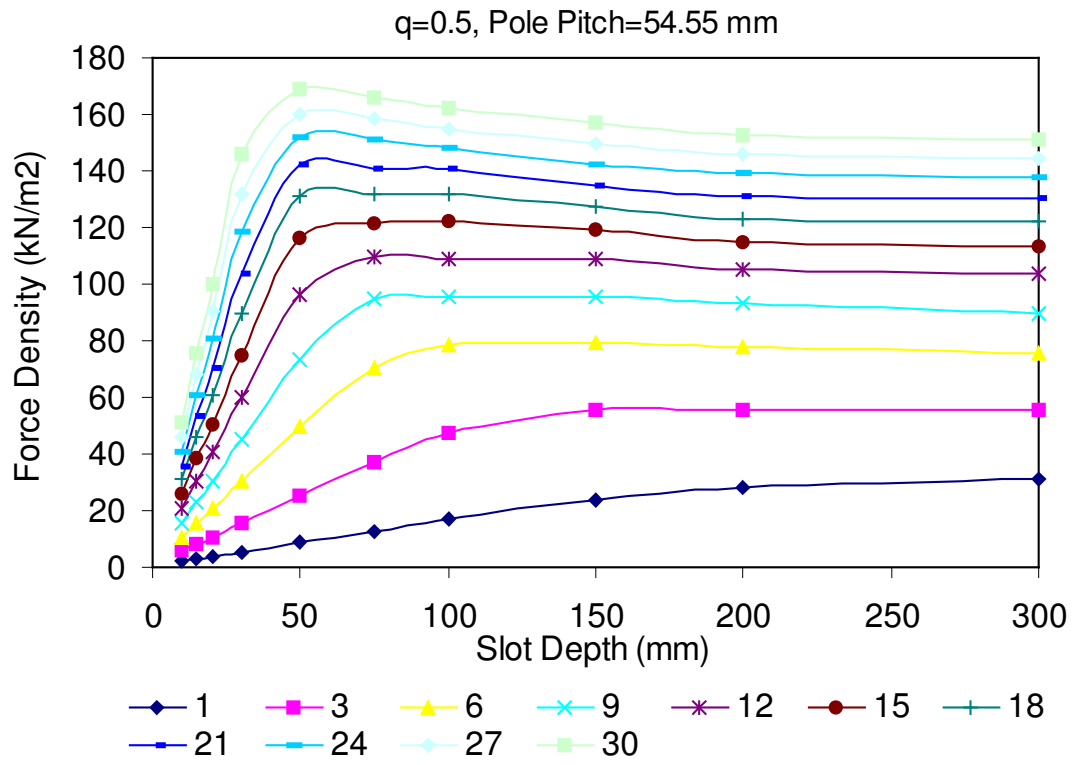
q=0.5, Pole Pitch=54.55 mm
Force Density (kN/m2)
Slot Depth (mm)
0
20
40
60
80
100
120
140
160
180
0
50
100
150
200
250
300
1
3
6
9
12
15
18
21
24
27
30

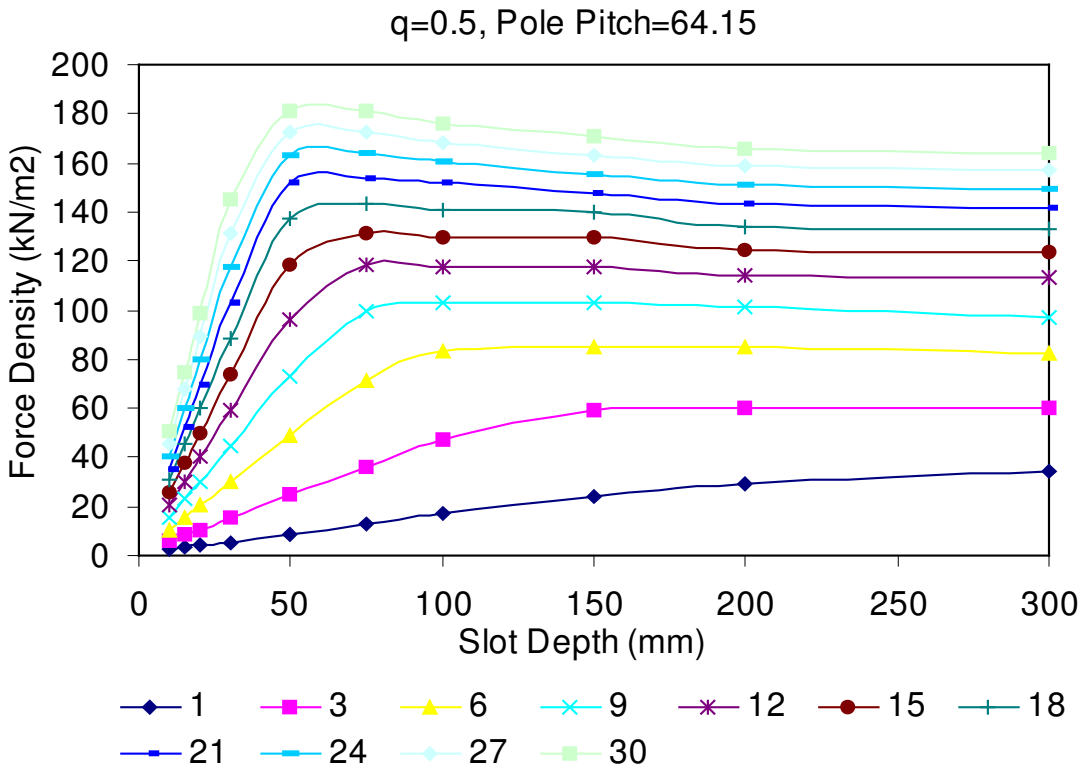
q=0.5, Pole Pitch=64.15
Force Density (kN/m2)
Slot Depth (mm)
0
20
40
60
80
100
120
140
160
180
200
0
50
100
150
200
250
300
1
3
6
9
12
15
18
21
24
27
30

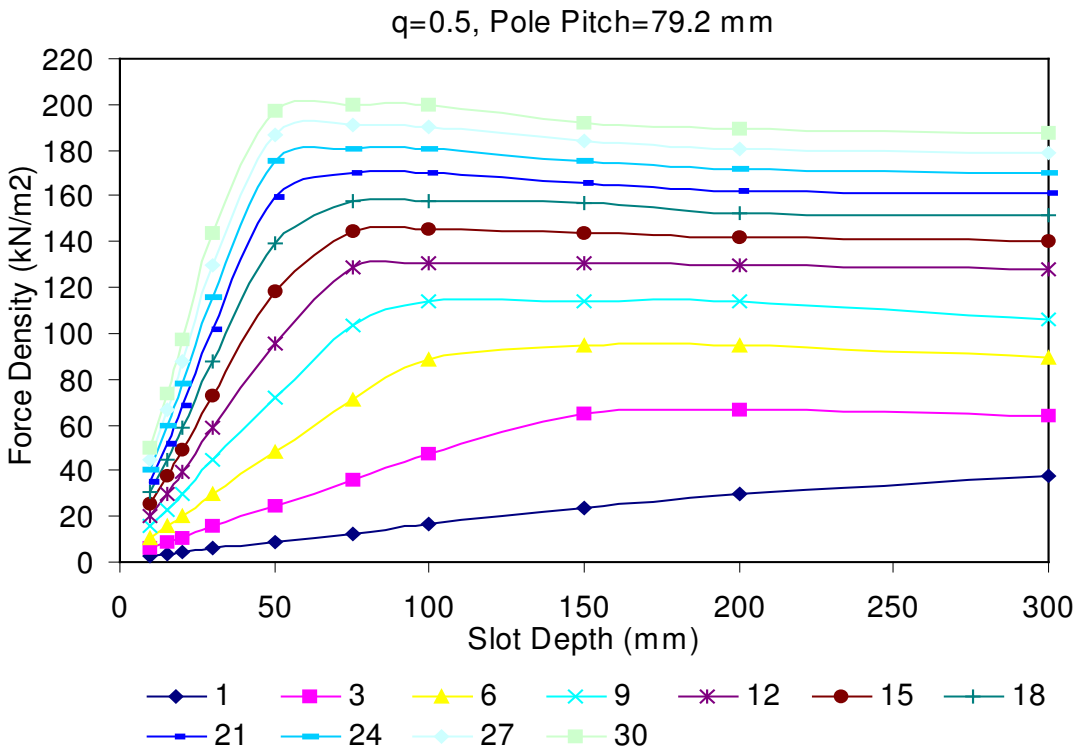
q=0.5, Pole Pitch=79.2 mm
Force Density (kN/m2)
220
200
180
160
140
120
100
80
60
40
20
0
0
50
100
150
200
250
300
Slot Depth (mm)
1
3
6
9
12
15
18
21
24
27
30

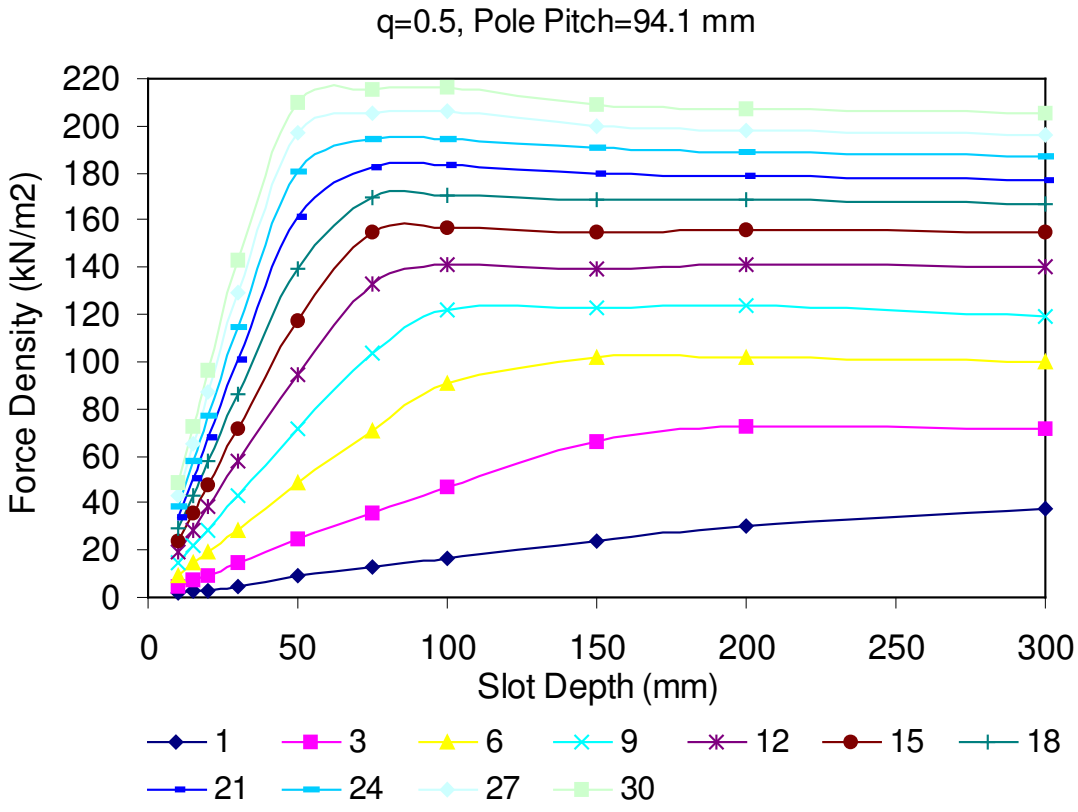
q=0.5, Pole Pitch=94.1 mm
Force Density (kN/m2)
220
200
180
160
140
120
100
80
60
40
20
0
0
50
100
150
200
250
300
Slot Depth (mm)
1
3
6
9
12
15
18
21
24
27
30

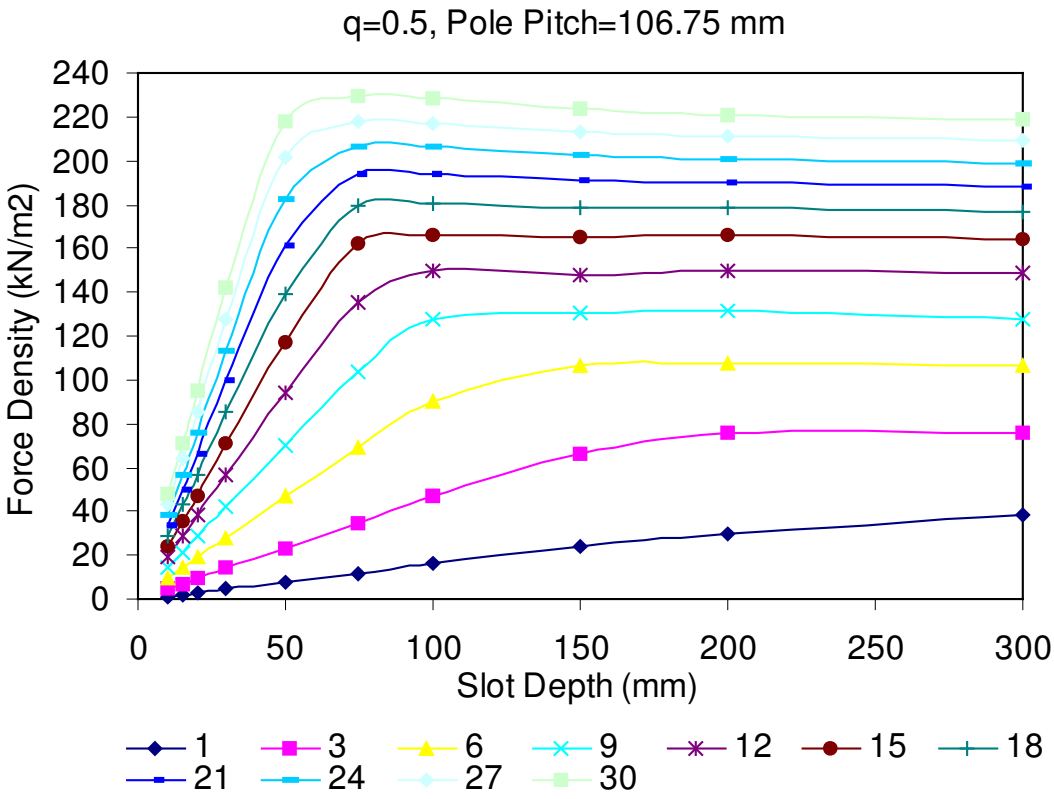
q=0.5, Pole Pitch=106.75 mm
Force Density (kN/m2)
240
220
200
180
160
140
120
100
80
60
40
20
0
0
50
100
150
200
250
300
Slot Depth (mm)
1
3
6
9
12
15
18
21
24
27
30

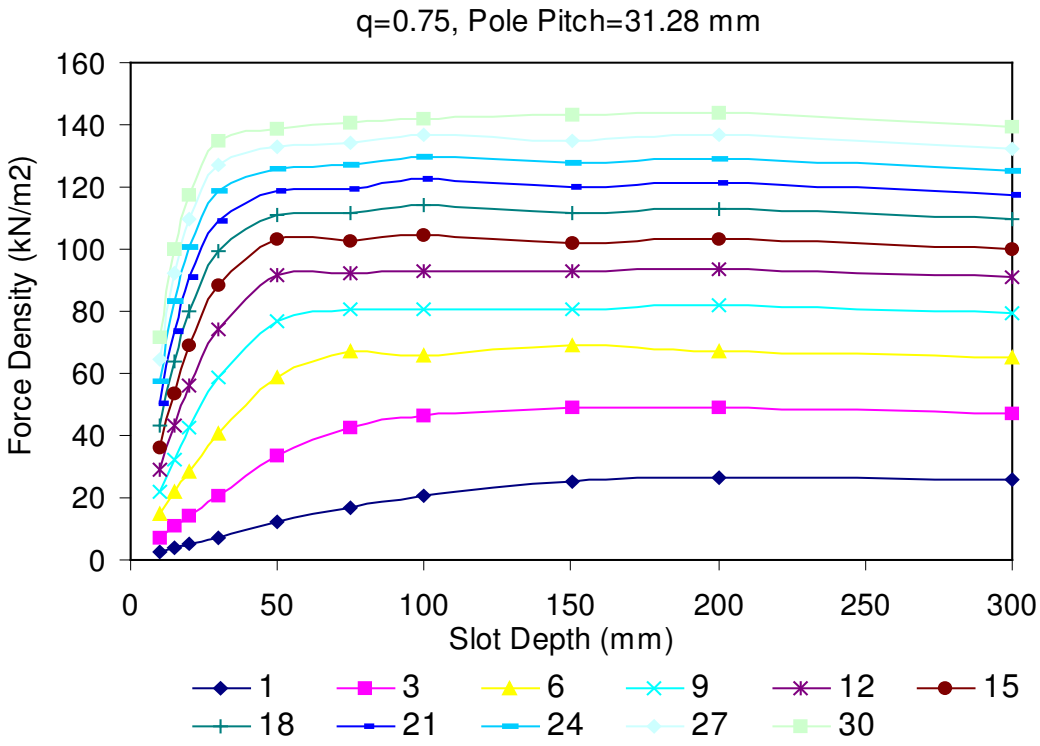
q=0.75, Pole Pitch=31.28 mm
Force Density (kN/m2)
Slot Depth (mm)
0
20
40
60
80
100
120
140
160
0
50
100
150
200
250
300
1
3
6
9
12
15
18
21
24
27
30

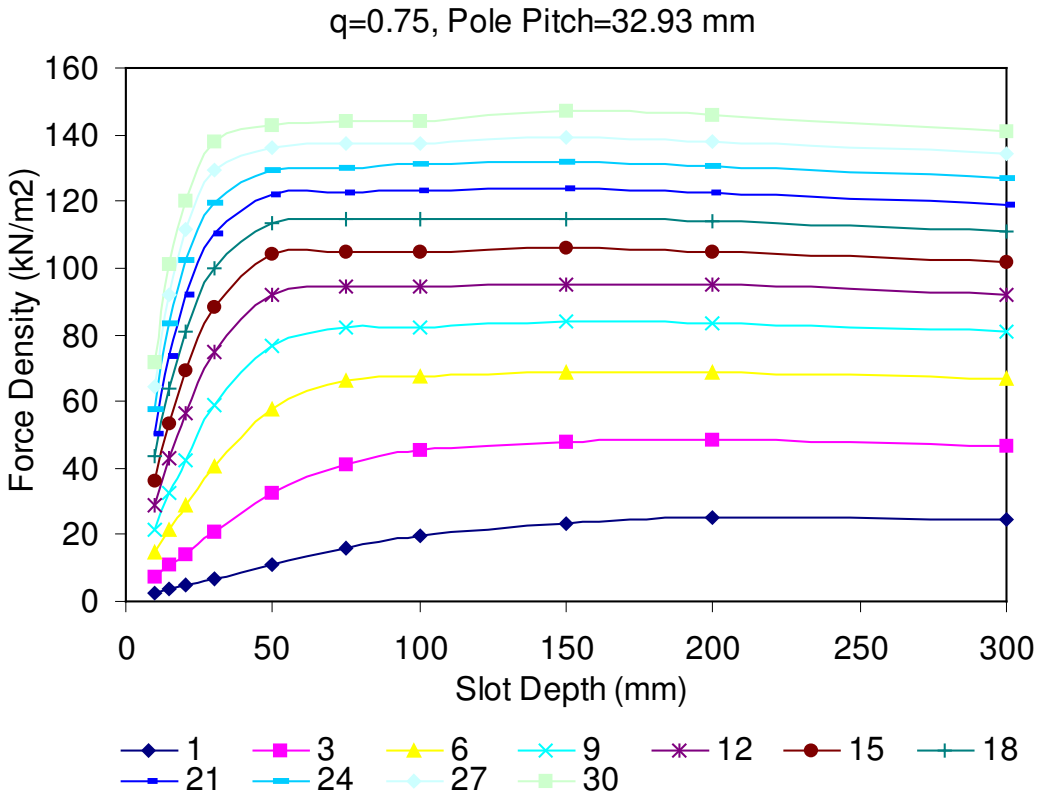
q=0.75, Pole Pitch=32.93 mm
Force Density (kN/m2)
Slot Depth (mm)
0
20
40
60
80
100
120
140
160
0
50
100
150
200
250
300
1
3
6
9
12
15
18
21
24
27
30

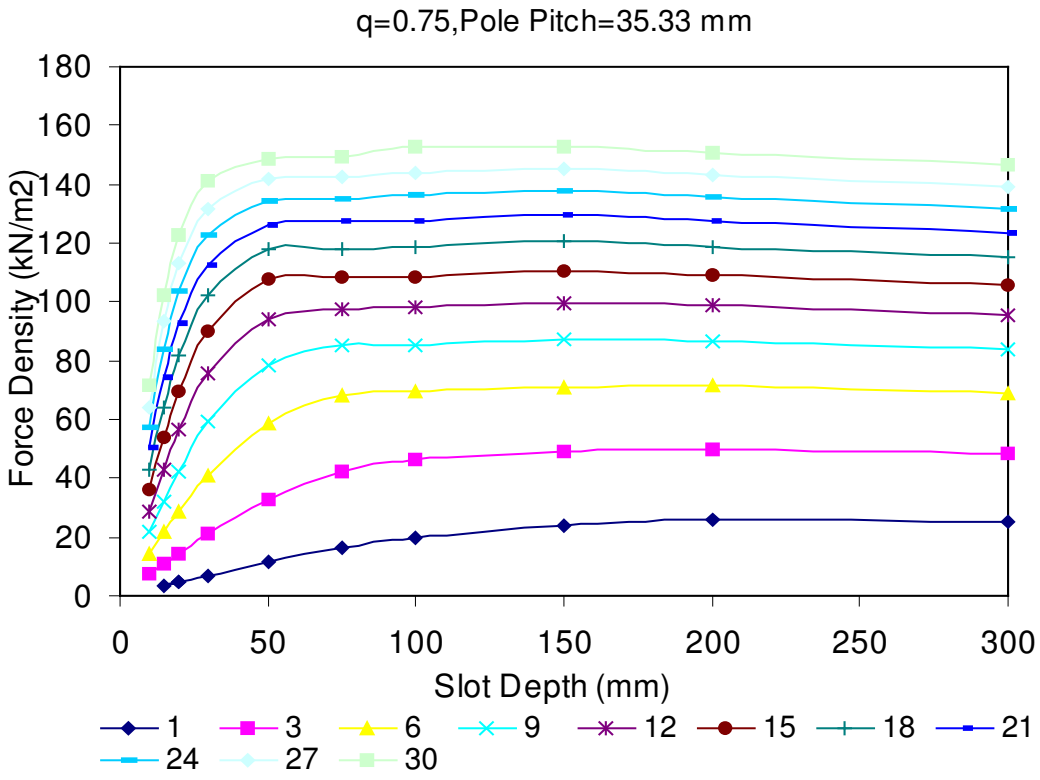
q=0.75,Pole Pitch=35.33 mm
Force Density (kN/m2)
180
160
140
120
100
80
60
40
20
0
0
50
100
150
200
250
300
Slot Depth (mm)
1
3
6
9
12
15
18
21
24
27
30

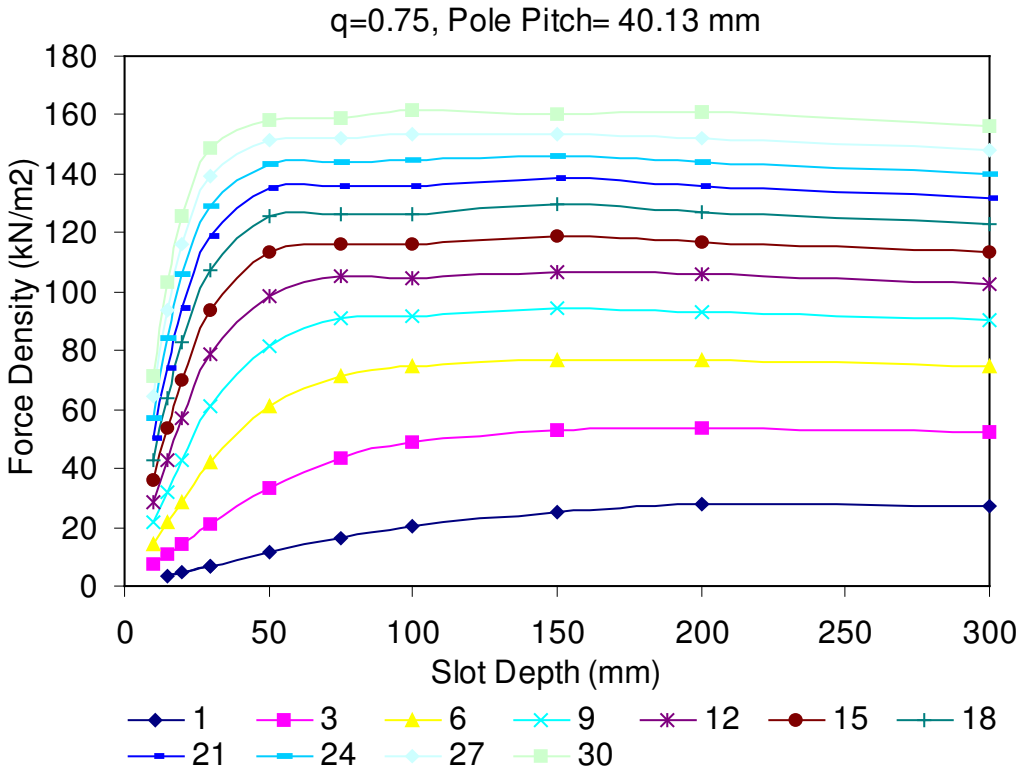
q=0.75, Pole Pitch= 40.13 mm
Force Density (kN/m2)
180
160
140
120
100
80
60
40
20
0
0
50
100
150
200
250
300
Slot Depth (mm)
1
3
6
9
12
15
18
21
24
27
30

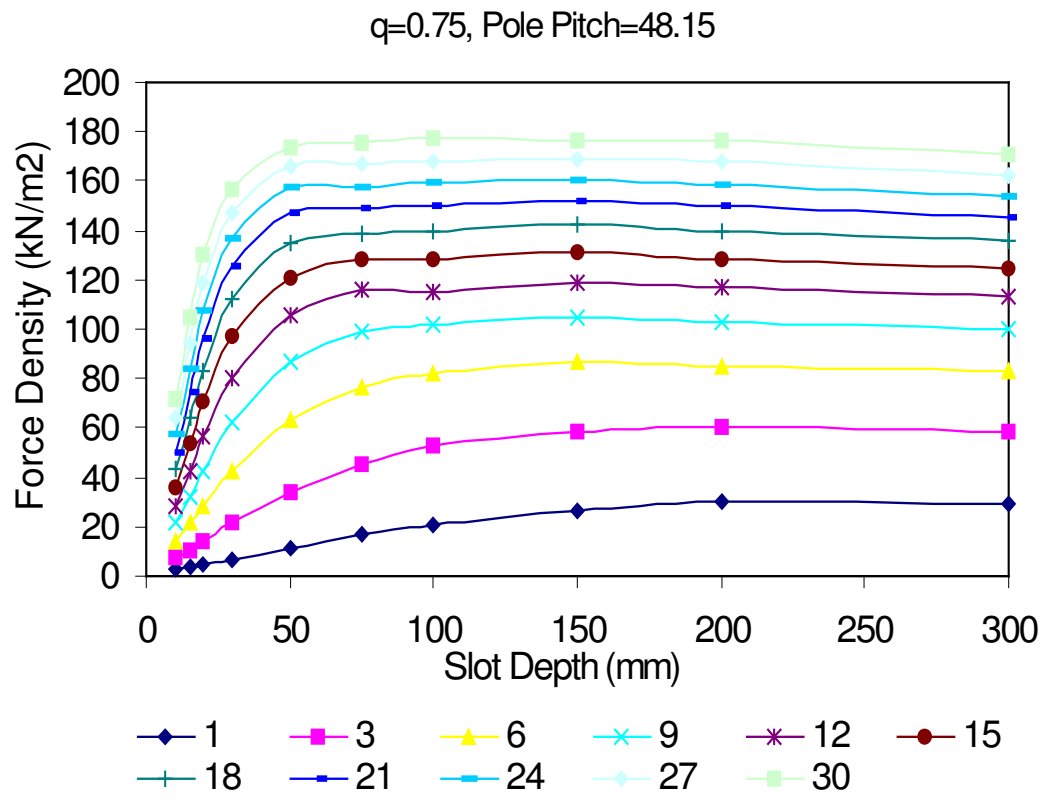
q=0.75, Pole Pitch=48.15
Force Density (kN/m2)
200
180
160
140
120
100
80
60
40
20
0
0
50
100
150
200
250
300
Slot Depth (mm)
1
3
6
9
12
15
18
21
24
27
30

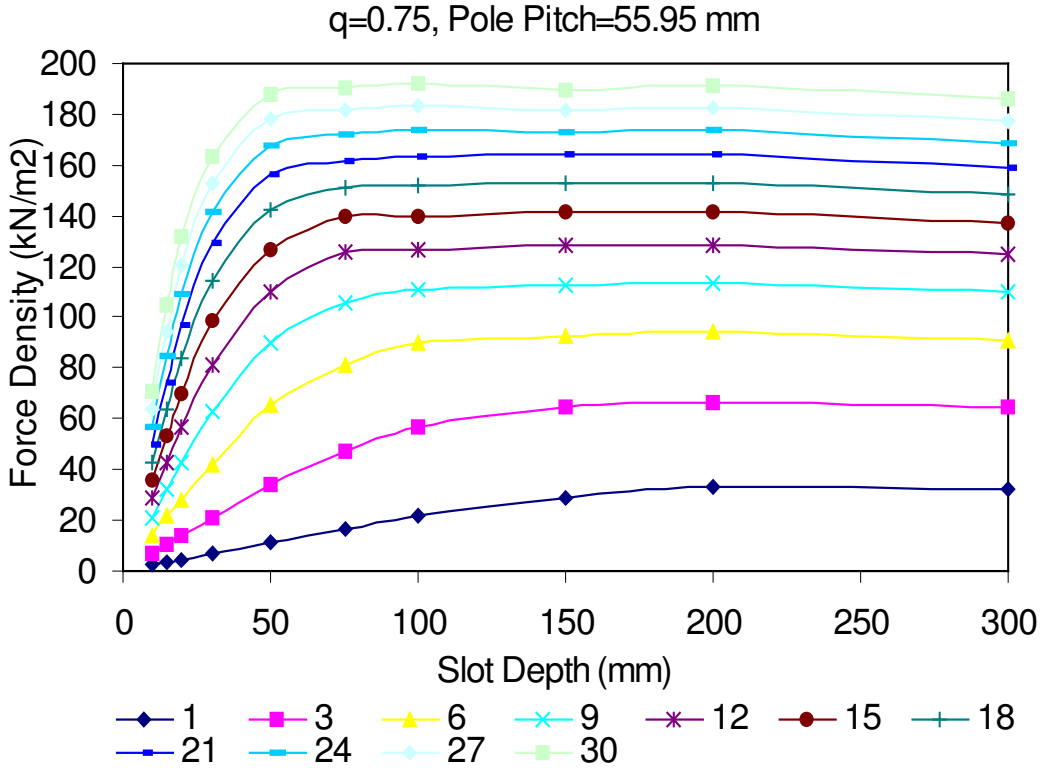
q=0.75, Pole Pitch=55.95 mm
Force Density (kN/m2)
200
180
160
140
120
100
80
60
40
20
0
0
50
100
150
200
250
300
Slot Depth (mm)
1
3
6
9
12
15
18
21
24
27
30

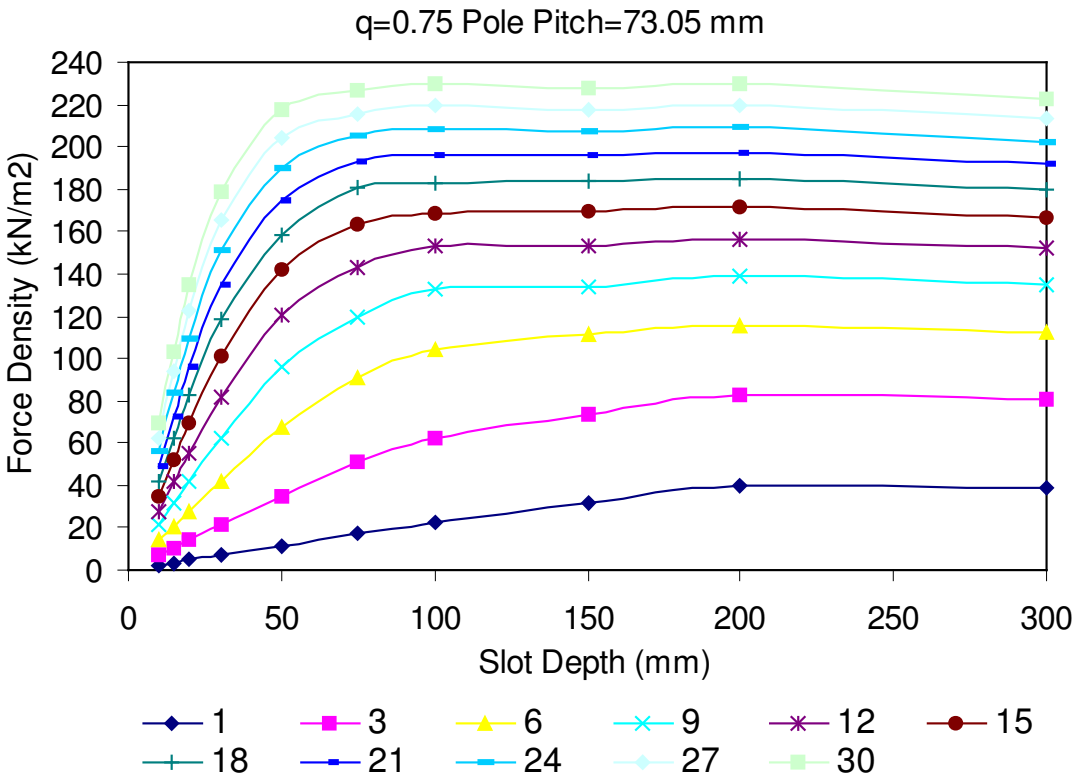
q=0.75 Pole Pitch=73.05 mm
Force Density (kN/m2)
240
220
200
180
160
140
120
100
80
60
40
20
0
0
50
100
150
200
250
300
Slot Depth (mm)
1
3
6
9
12
15
18
21
24
27
30

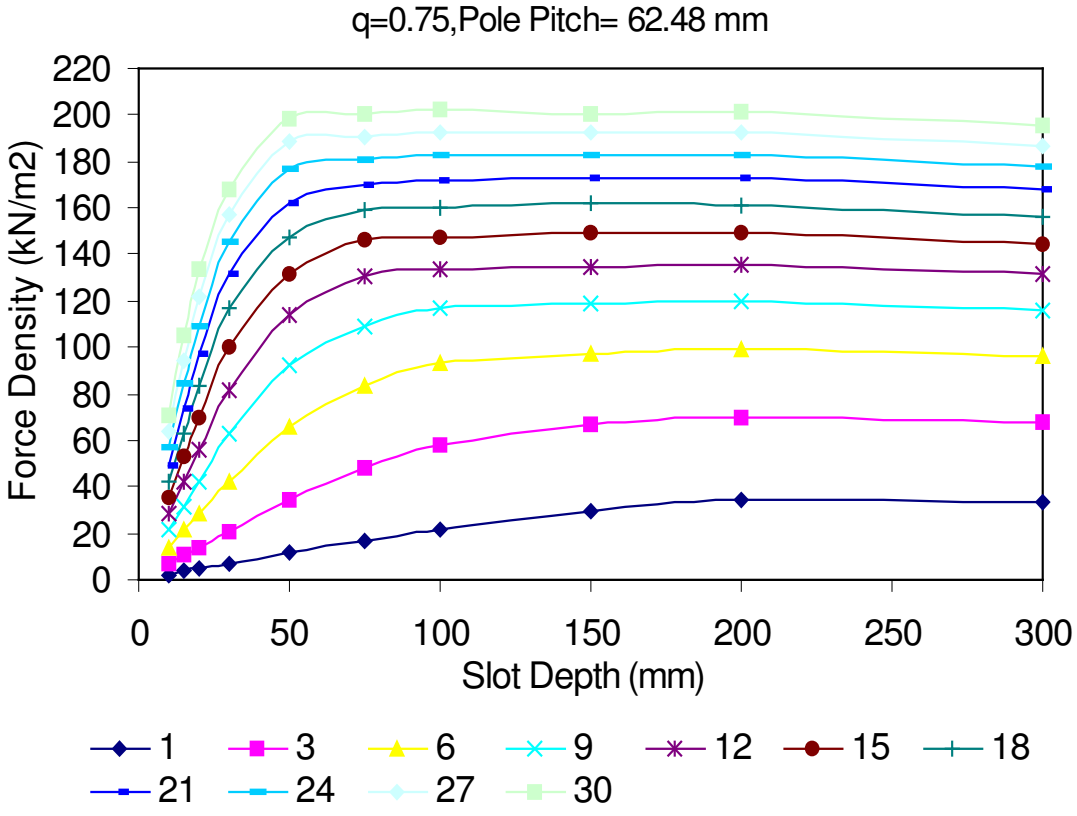
q=0.75,Pole Pitch= 62.48 mm
Force Density (kN/m2)
220
200
180
160
140
120
100
80
60
40
20
0
0
50
100
150
200
250
300
Slot Depth (mm)
1
3
6
9
12
15
18
21
24
27
30

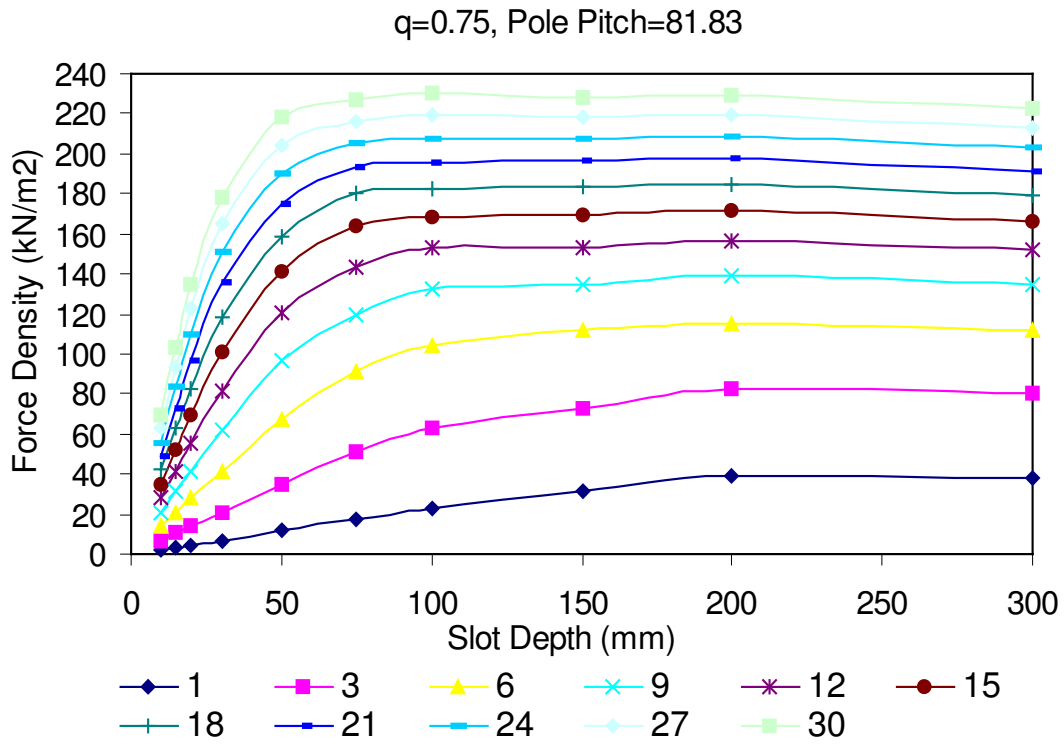
q=0.75, Pole Pitch=81.83
Force Density (kN/m2)
240
220
200
180
160
140
120
100
80
60
40
20
0
0
50
100
150
200
250
300
Slot Depth (mm)
1
3
6
9
12
15
18
21
24
27
30

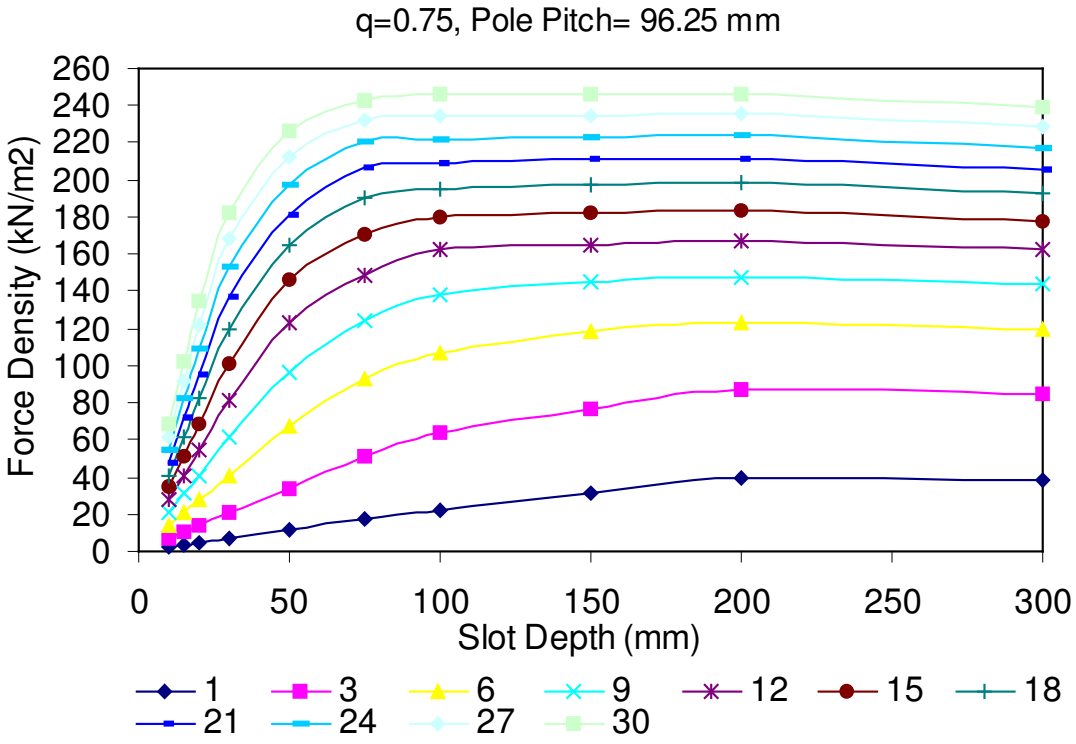
q=0.75, Pole Pitch= 96.25 mm
Force Density (kN/m2)
260
240
220
200
180
160
140
120
100
80
60
40
20
0
0
50
100
150
200
250
300
Slot Depth (mm)
1
3
6
9
12
15
18
21
24
27
30

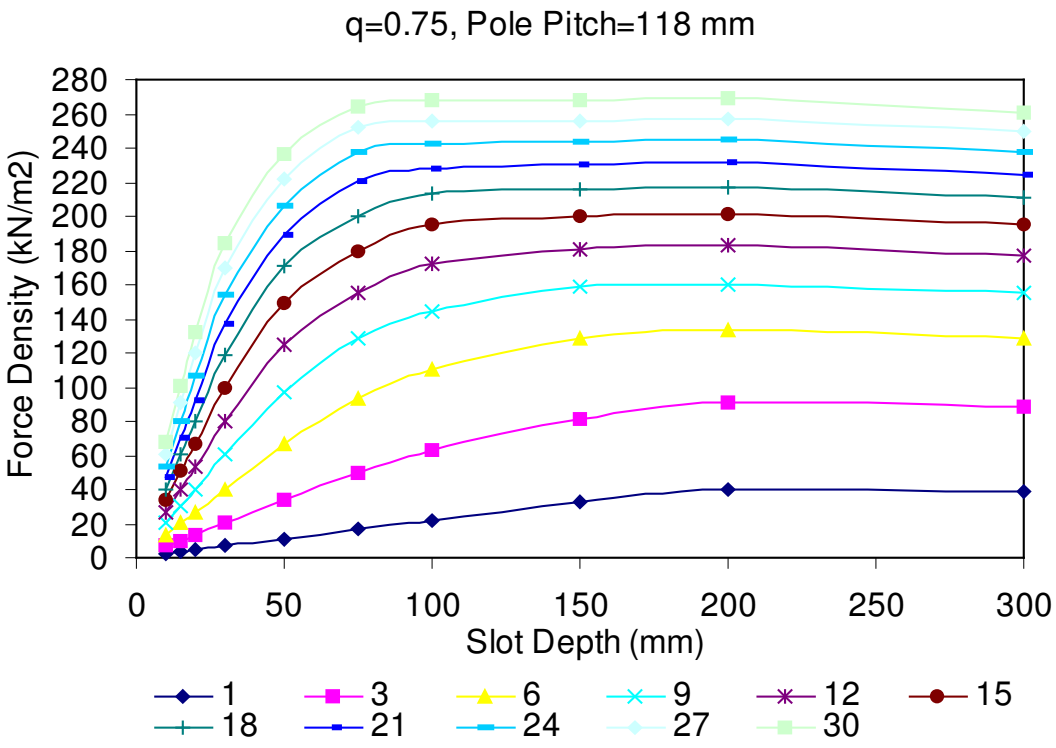
q=0.75, Pole Pitch=118 mm
Force Density (kN/m2)
0
20
40
60
80
100
120
140
160
180
200
220
240
260
280
0
50
100
150
200
250
300
Slot Depth (mm)
1
3
6
9
12
15
18
21
24
27
30

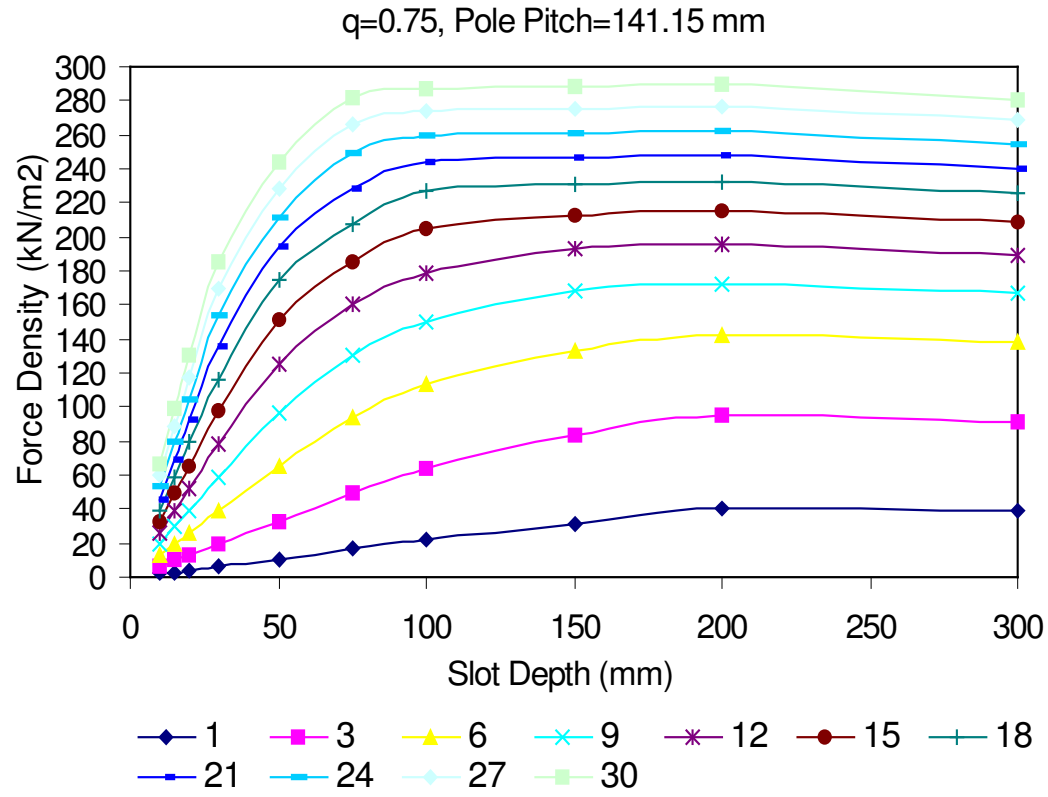
q=0.75, Pole Pitch=141.15 mm
Force Density (kN/m2)
0
20
40
60
80
100
120
140
160
180
200
220
240
260
280
300
0
50
100
150
200
250
300
Slot Depth (mm)
1
3
6
9
12
15
18
21
24
27
30

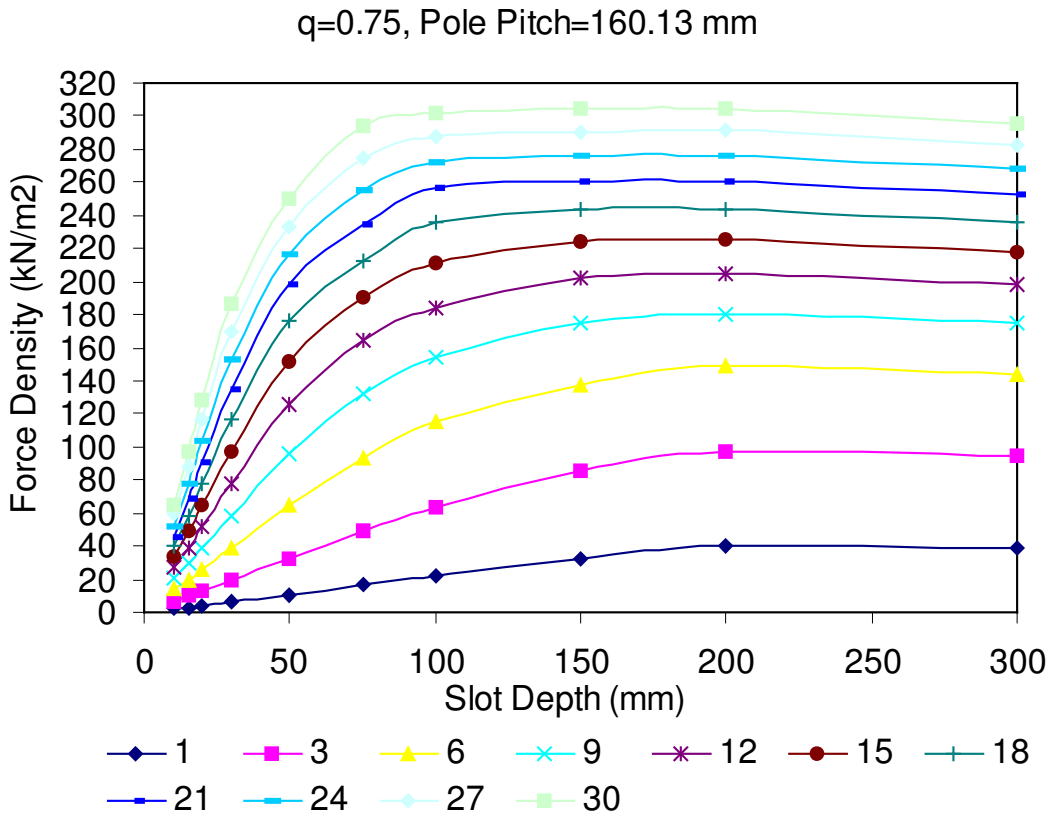
q=0.75, Pole Pitch=160.13 mm
Force Density (kN/m2)
320
300
280
260
240
220
200
180
160
140
120
100
80
60
40
20
0
0
50
100
150
200
250
300
Slot Depth (mm)
1
3
6
9
12
15
18
21
24
27
30

References

1. Hamdi, E.S. “Permanent magnet and variable reluctance drive systems”, ETI Press,Gothenburg, Sweden, 2003.
2. Essam S. Hamdi. “Design Of Small Electrical Machines”, John Wiley & Sons Ltd.
3. A Grauers, "Design of Direct-driven Permanent-magnet Generators for Wind Turbines", Ph.D. dissertation, Dept. Electric Power Eng., Chalmers Univ. of Technology, Göteborg, Sweden, 1996.
4. P. Kasinathan, A Grauers and E Hamdi "Force Density in Low-speed PM Machines: Saturation limits”, Proc. 2002 IEEE Power Engineering Society, Submitted.
5. A.Grauers, P.Kasinathan, “Force Density in Low-speed PM: “Temperature and Inductance limits”, Proc. 2002 IEEE Power Engineering Society, Submitted.
6. Murugesen, S: “An overview of electric motors for space applications”, IEEE Transcations On Industrial, Electronics And Control Instrumentation, Vol. IECI-28, No. 4, November 1981, pp261-265
7. S. K. Pal, "Direct drive high energy permanent magnet brush and brushless DC motors for robotic applications, ” in Robot Actuators, IEE Colloquium on, 1991, pp. 12/1-12/4.
8. L. M. C. Mhango, “Brushless DC machines with rare-earth magnets for high speed aerospace drives, ” presented at,6-7 Nov. 1990, Birmingham, UK, 1990.
9. L. M. C. Mhango and R. Perryman, “An assessment of high power density brushless DC motor technology with neodymium-iron-boron excitation”, presented at 1994 Universities Power Engineering Conference (UPEC),14-16 Sept. 1994, Galway, Ireland, 1994.
10. L. M. C. Mhango, “Design ideas for low-inertia high-speed electronically commutated PM motors for special applications”, in Variable Speed Drives and Motion Control, IEE Colloquium on, 1992, pp. 9/1-9/5.
11. S. K. Pal, “Comparative study of the design and development of direct drive brushed and brushless DC motors with samarium cobalt, neodymium-iron-boron and ceramic magnets”, in Permanent Magnet Machines and Drives, IEE Colloquium on, 1993, pp. 7/1-7/7.
12. S. K. Pal, “Comparative study of the design and manufacturing processes of electrical motors with low and high energy permanent magnets”, in Electrical Machines and Drives, 1993. Sixth International Conference on (Conf. Publ. No. 376), 1993, pp. 339-346.

13. Fink, R.A.: "The brushless motor-types and sources", Control Engineering, August 1970, pp.42-45.
14. Knights, D E: "Prospects for the printed motor", Design Engineering, March 1975, pp.199-202.
15. Hans Waagen: "Motors with printed circuit armatures", Design Engineering, January 1970, pp.52-55.
16. Casanova D: " The permanent magnet dish motor an assessment of the quality of mechanical commutation", Motorcon Proceedings, September 1982, pp.446-450.
17. Werninck, E.H: "The methodology of motor selection", Second International Conference on Small and Special Electrical Machines, IEE Conference Publication No. 202, 22-24 September 1981, pp1-5.
18. Carl M. Fink and Dennis F. Brown: "The permanent magnet dc pancake motor-An assesment of the quality of mechanical commutation", Motorcon, March 1982, pp693-699.
19. Mazurkiewcz, J.: "Consider hollow-rotor motors", Electronic Design 11, May 24, 1975, pp.76-79.
20. Mazurkiewcz, J.: "The drive motor of a servo", Electronic Design 15, July 19, 1976, pp.110-113.
21. Theodore Wildi.: "Electrical machines, drives and power systems" pp.417-436.
22. Wang Zong-pei, Cheng Shu-Kang.: "Bipolar drive three phase variable reluctance step motor", Second International Conference on Small and Special Electrical Machines, IEE Conference Publication No. 202, 22-24 September 1981, pp50-54.
23. A Huges, D.J.MacLoed.: "Hybrid and variable reluctance small-angle stepping motors", Second International Conference on Small and Special Electrical Machines, IEE Conference Publication No. 202, 22-24 September 1981, pp50-54.
24. Acarnley, P.P.: "Stepping motor control techniques", Conference on Drives/Motors/Controls, 24-26 October 1984, Brighton,United Kingdom, pp106-112.
25. Bimbra, P.S.: "Generlized theory of electrical machines", Fifth Edition, Khanna Publishes,pp1034-1036.
26. Caricchi F., Crescimbini F., Honorati O., Di Napoli A., Santini E., "Compact Wheel Direct Drive for Evs", Industry Applications Magazine, IEEE, 1996
27. Spooner E., Chalmers B.J., "TORUS: A Slotless, Toroidal-Stator, Permanent Magnet Generator", Proceedings-B, IEE, Nov. 1992, Vol. 139, No.6
28. Caricchi F., Crescimbini F., Mezzeti F., Santini E., "Multistage Axial-Flux PM Machine for Wheel Direct Drive", Transaction on Industry Applications, IEEE, 1996, Vol. 32, No.4

29. Caricchi F., Crescimbini F., Honorati O.,“Modular Axial-Flux Permanent Magnet Motor for Ship Propulsion Drives”, Transaction on Energy Conservation, IEEE, 1999, Vol. 14, No.3
30. Caricchi F., Crescimbini F., Fedeli E., Noia G., “Design and Construction of a Wheel-Directly-Coupled Axial-Flux PM Motor Prototype for EVs”
31. J. G. W. West, “PM DC motors with series field characteristics”, in Permanent Magnet Machines, IEE Colloquium on, 1988, pp. 5/1-5/5.
32. J. G. W. West, “DC, induction, reluctance and PM motors for electric vehicles", in Power Engineering Journal, vol. 8, 1994, pp. 77-88.
33. J. G. W. West, “The present status of electrical machines in vehicles", Machines for Automotive Applications (Digest No. 1996/166), IEE Colloquium on, 1996, pp. 1/1-121.
34. J. G. W. West, “Propulsion systems for hybrid electric vehicles", Electrical Machine Design for All-Electric and Hybrid-Electric Vehicles (Ref. No. 1999/196), IEE Colloquium on, 1999, pp. 1/1-1/9.
35. J Hystad, "Transverse Flux Generators in Direct-driven Wind Energy Converters", Ph.D. dissertation, Dept. Electrical Power Eng., NTNU, Trondheim, Norway, 2000.
36. Hasan El Hinaoui, “Green Car, Traction Motors” PhD project.
37. D.A.Staton, R.P.Deodhar, W.L.Soong and T.J.E.Miller., “Torque Prediction Using the Flux-Mmf Diagram in AC, DC, and Reluctance Motors.”, Transactions on Industry Application, IEEE, vol.32, no 1, Jan/Feb 1996
38. SGM Magnets Limited Catalogue, Sussex, United Kingdom
39. Magnet Application Catalogue, United Kingdom